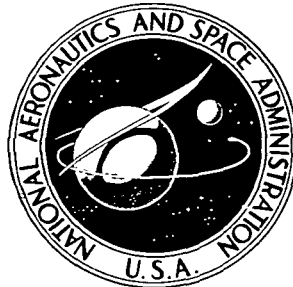


NASA TECHNICAL  
MEMORANDUM

NASA TM X-3398



NASA TM X-3398

CASE F  
100

EFFECT OF DROOPED-NOSE FLAPS  
ON THE EXPERIMENTAL FORCE  
AND MOMENT CHARACTERISTICS  
OF AN OBLIQUE WING

*Edward J. Hopkins and George H. Lovette*

*Ames Research Center*

*Moffett Field, Calif. 94035*



NATIONAL AERONAUTICS AND SPACE ADMINISTRATION • WASHINGTON, D. C. • NOVEMBER 1976

1. Report No. NASA TM X - 3398	2. Government Accession No.	3. Recipient's Catalog No.	
4. Title and Subtitle  EFFECT OF DROOPED-NOSE FLAPS ON THE EXPERIMENTAL FORCE AND MOMENT CHARACTERISTICS OF AN OBLIQUE WING		5. Report Date November 1976	
7. Author(s)  Edward J. Hopkins and George H. Lovette*		6. Performing Organization Code	
9. Performing Organization Name and Address  Ames Research Center Moffett Field, California 94035		8. Performing Organization Report No. A-6461	
12. Sponsoring Agency Name and Address  National Aeronautics and Space Administration Washington, D. C. 20546		10. Work Unit No. 505-11-12	
15. Supplementary Notes  *Project Engineer, ARO, Inc., Moffett Field, Calif. 94035		11. Contract or Grant No.	
16. Abstract  Six-component experimental force and moment data are presented for a low aspect-ratio, oblique wing equipped with drooped-nose flaps and mounted on top of a body of revolution. These flaps were investigated on the downstream wing panel with the nose drooped 5°, 10°, 20°, and 30°, and on both wing panels with the nose drooped 30°. The purpose of the study was to determine if such flaps would make the moment curves more linear by controlling the flow separation on the downstream wing panel at high lift coefficients. The wing was elliptical in planform and had an aspect ratio of 6.0 (based on the unswept wing span). The wing was tested at sweep angles of 45° and 50° throughout the Mach number range from 0.25 to 0.95. The drooped-nose flaps alone were not effective in making the moment curves more linear; however, a previous study showed that Krüger nose flaps improved the linearity of the moment curves when the Krüger flaps were used on only the downstream wing panel equipped with drooped-nose flaps deflected 5°.			
17. Key Words (Suggested by Author(s))  Leading-edge flaps Wing flaps Wing nose flaps Stability & control		18. Distribution Statement  Unlimited  STAR Category -08	
19. Security Classif. (of this report) Unclassified	20. Security Classif. (of this page) Unclassified	21. No. of Pages 142	22. Price* \$5.75

\* For sale by the National Technical Information Service, Springfield, Virginia 22161

## NOMENCLATURE

The axes systems and sign conventions are presented in figure 1. Lift and drag are presented about the wind axes; side force, pitching moments, rolling moments and yawing moments are presented about the body axes.

$b$	wing span
$C_D$	drag coefficient, $\frac{\text{drag}}{qS}$
$C_I$	rolling-moment coefficient about the body axes, $\frac{\text{rolling moment}}{qSb}$
$C_L$	lift coefficient, $\frac{\text{lift}}{qS}$
$C_m$	pitching-moment coefficient (see fig. 2(a) for moment-center location), $\frac{\text{pitching moment}}{qS\bar{c}}$
$C_n$	yawing-moment coefficient about the body axes, $\frac{\text{yawing moment}}{qSb}$
$C_Y$	side-force coefficient about the body axes, $\frac{\text{side force}}{qS}$
$c$	wing chord
$c_{aft}$	portion of wing chord aft of the $0.25c$ line
$c_{fwd}$	portion of wing chord forward of the $0.25c$ line
$c_{root}$	wing root chord
$\bar{c}$	wing mean aerodynamic chord
$H$	vertical distance from wing reference plane to base line (see fig. (2b))
$M$	Mach number
$q$	free-stream dynamic pressure
$RN/L$	unit Reynolds number per meter times $10^6$
$r$	body radius
$S$	wing area
$(t/c)_{max}$	maximum thickness-to-chord ratio
$V$	free-stream velocity
$x$	chordwise distance along airfoil

$x_1$  axial distance along body from the 57.45 cm longitudinal station

$Y$  distance along wing span (see fig. 2(b))

$z$  vertical distance above the wing-chord plane

$\alpha$  angle of attack, deg

$\delta_n$  nose flap deflection (positive with nose down), deg

$\Lambda$  sweep angle measured between a perpendicular to the body axis and the  $0.25c$  line of the wing in a horizontal plane (the right wing tip is forward for positive  $\Lambda$ 's), deg

180  
100  
50

# EFFECT OF DROOPED-NOSE FLAPS ON THE EXPERIMENTAL FORCE AND MOMENT CHARACTERISTICS OF AN OBLIQUE WING

Edward J. Hopkins and George H. Lovette\*

Ames Research Center

## SUMMARY

Six-component experimental force and moment data are presented for a low aspect-ratio, oblique wing equipped with drooped-nose flaps and mounted on top of a body of revolution. These flaps were investigated on the downstream wing panel with the nose drooped 5°, 10°, 20°, and 30°, and on both wing panels with the nose drooped 30°. The purpose of the study was to determine if such flaps would make the moment curves more linear by controlling the flow separation on the downstream wing panel at high lift coefficients. The wing was elliptical in planform and had an aspect ratio of 6.0 (based on the unswept wing span). The wing was tested at sweep angles of 45° and 50° throughout the Mach number range from 0.25 to 0.95. The drooped-nose flaps alone were not effective in making the moment curves more linear; however, a previous study showed that Krüger nose flaps improved the linearity of the moment curves when the Krüger flaps were used on only the downstream wing panel equipped with drooped-nose flaps deflected 5°.

## INTRODUCTION

It was shown experimentally in references 1 and 2 that the low aspect-ratio, oblique wing (suitable for a highly maneuverable vehicle) is more efficient and has considerably higher maximum lift-to-drag ratios at transonic Mach numbers than a conventional swept wing of the same aspect ratio. At high lift coefficients, however, there is flow separation on the downstream wing panel of oblique wings; this separation results in very nonlinear pitching-, rolling-, and yawing-moment curves. In references 1 and 2, an attempt was made to alleviate the asymmetrical spanwise wing stall associated with oblique wings by bending the wing panels upward to produce washout on the downstream wing panel and washin on the upstream wing panel. It was found that although wing bending might produce more linear moment curves, an impractical wing pivot location would be required to eliminate the rolling moments at low lift coefficients. For this reason, two types of nose flaps (Krüger and drooped-nose flaps) were investigated as a possible means of delaying the flow separation on the trailing wing panel of oblique wings at high lift coefficients. In the previous investigation (ref. 3), it was found that Krüger nose flaps mounted only on the downstream wing panel with a nose flap deflected 5° was the most effective arrangement for delaying the flow separation and making the moment curves more linear.

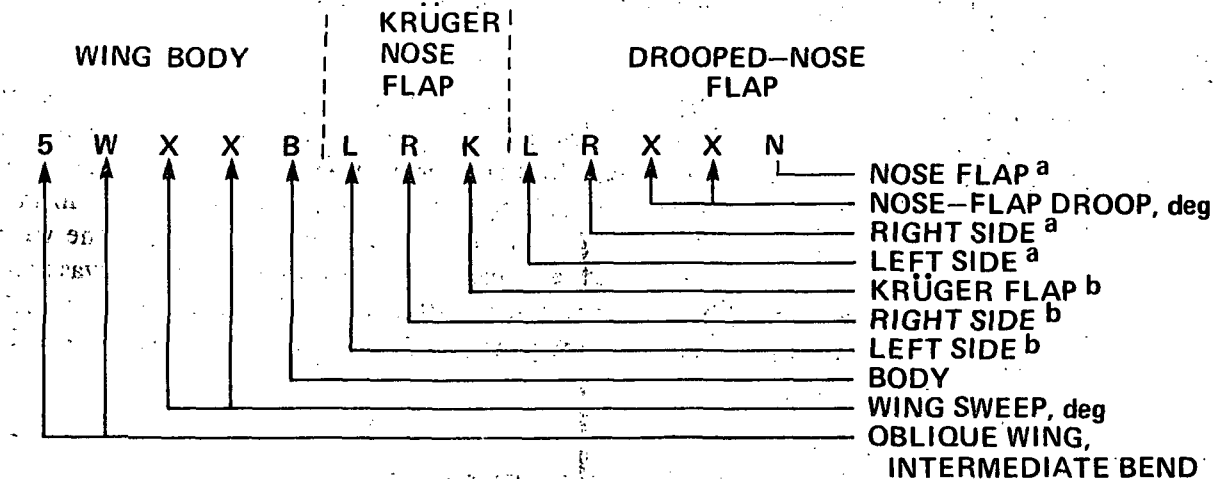
The present investigation was undertaken to study the effectiveness of drooped-nose flaps alone, mounted on the same low aspect-ratio oblique wing of reference 3, for controlling the flow

---

\*Project Engineer, ARO, Inc., Moffett Field, Calif. 94035

separation on the downstream wing panel and making the moment curves more linear at high lift coefficients. The effects of the drooped-nose flaps were studied with the flaps (1) mounted on the downstream panel only (nose drooped successively from  $5^\circ$  to  $30^\circ$ ) and (2) with the flaps mounted on both panels (nose drooped  $30^\circ$  only). The wing was investigated at sweep angles of  $45^\circ$  and  $50^\circ$ . The use of nose flaps on both wing panels might eliminate the rolling and yawing moments at low lift without loss in effectiveness of the nose flaps at high lift. A limited comparison between the effectiveness of the Krüger flaps (investigated in ref. 3) and the drooped-nose flaps of the present investigation in making the moment curves more linear is also presented.

### CONFIGURATION CODE



<sup>a</sup>WHEN SYMBOL IS DELETED, DROOPED-NOSE FLAP IS UNDEFLECTED

<sup>b</sup>WHEN SYMBOL IS DELETED, KRÜGER NOSE FLAP IS REMOVED

### TEST FACILITY

The Ames 6- by 6-Foot Wind Tunnel is a variable pressure, continuous flow, closed return-type facility. The nozzle ahead of the test section consists of an asymmetric sliding block which permits a continuous variation of Mach number from 0.25 to 2.3. The test section has a perforated floor and ceiling for boundary-layer removal to permit transonic testing.

### MODEL DESCRIPTION

The model consisted of an oblique wing mounted on top of a Sears-Haack body of revolution designed to have minimum wave drag for a given length and volume. By installing different fairing blocks under the wing, as shown in figure 2(a), the wing could be swept  $45^\circ$  and  $50^\circ$ . Details of the body and of the fairing blocks are given in table 3 of reference 4. Also, note in figure 2(a) that the wing pivot point and the moment center are located at  $0.40 c_{root}$  ( $\Lambda = 0$ ). The wing planform consisted of two semiellipses having the same major axis but different minor axes in the ratio of 3:1

so that the major axis is the quarter chord line. Effective geometric twist was accomplished by bending the wing panels upward so that the chord lines perpendicular to the quarter chord line remained in horizontal planes. This type of bending results in wing twist when the oblique wing is swept; that is, washout on the downstream panel and washin on the upstream panel. Equations for the bend lines of the wing with the intermediate bend of the present investigation, and the wing planform are shown in figure 2(b). Additional geometric details of the wing and body are presented in table 1.

A subcritical Garabedian profile with a design lift coefficient of 1.3 at  $M = 0.6$ ,  $(t/c)_{max} = 0.1016$ , was used perpendicular to the quarter chord line. This profile, shown in figure 2(c), varied in maximum thickness from  $0.11c$  at the wing root to  $0.06c$  at the wing tip according to the elliptical equation given in figure 2(b). Coordinates for the Garabedian profile are given in table 2.

The drooped-nose flaps with which the model was equipped had a span that was 67 percent that of the wing and were segmented as shown in figure 2(d). The drooped-nose flaps were tested when mounted on both wing panels and deflected  $30^\circ$ , and when mounted on the downstream panel only and deflected  $5^\circ$ ,  $10^\circ$ ,  $20^\circ$ , and  $30^\circ$ . The drooped-nose flaps were pivoted about an axis located on the lower surface of the wing at about 15 percent of the wing chord behind the wing leading edge. All gaps between the nose segments were sealed and a radius fairing of wax was used on the upper wing surface between the main wing and the nose flap when the flap was deflected. A sketch of the Krüger nose flaps mounted on the nose flaps with a deflection of  $5^\circ$ , as investigated in reference 3, is also shown in figure 2(d).

#### DATA REDUCTION AND TEST PROCEDURE

The model was sting-supported through the base of the model on a six-component electrical strain-gage balance as shown in figure 3. Measured drag forces were corrected to a condition corresponding to that of having the free-stream static pressure on the base of the fuselage. Moment data are presented about a moment center located on the body axis at  $0.4c_{root}$  of the unswept oblique wing (see fig. 2(a)). Reference lengths and the wing area used in the reduction of the data are given in table 1.

Boundary-layer transition strips (0.1905 cm wide) consisting of a random distribution of glass spheres (0.01905 cm diameter) were placed 0.762 cm downstream of the wing leading edge on both the upper and lower surfaces of the wing, and 2.54 cm downstream of the body tip. Sublimation studies made on the plain wing (with no leading-edge flaps) at wing sweep angles of 0 and  $45^\circ$  indicate that the boundary layer was tripped by the 0.01905 cm diameter spheres near the roughness strips at  $\alpha = 0$  and  $10^\circ$  at Mach numbers of 0.6 and 0.9.

The unit Reynolds number was held constant at  $8.2 \times 10^6 / m$  throughout the test except at the Mach number of 0.25; for  $M = 0.25$ , the unit Reynolds number was reduced to  $5.7 \times 10^6 / m$ , because of the dynamic overload restrictions of the balance. The model was mounted on a sting that was bent  $10^\circ$  to increase the maximum angle of attack; the resulting angle-of-attack range was from  $-1^\circ$  to  $31^\circ$ . Data were obtained at Mach numbers of 0.25, 0.4, 0.6, 0.8, 0.9, 0.95. Angle of attack was

indicated by an electrical dangleometer mounted in the model support located downstream of the sting. Corrections were applied to the indicated angle of attack for balance and sting deflections.

## RESULTS AND DISCUSSION

Experimental results for the oblique wing equipped with drooped-nose flaps on only the downstream wing panel are shown in figures 4-9 for a sweep angle of  $45^\circ$ , and in figures 10-15 for a sweep angle of  $50^\circ$ . Results for the case when the drooped-nose flaps were used on both wing panels are shown in figures 16-21 for a wing sweep angle of  $45^\circ$ , and in figures 22-27 for a sweep angle of  $50^\circ$ . A limited comparison of the drooped-nose flap results and the Krüger nose flap results of reference 3 is presented in figure 28.

### Drooped-Nose Flaps on the Downstream Wing Panel

With the oblique wing swept either  $45^\circ$  or  $50^\circ$ , drooping the nose flap on the downstream wing panel successively from  $5^\circ$  to  $30^\circ$  had little effect on controlling the flow separation on the downstream panel. This result is shown by the highly nonlinear pitching-, rolling-, or yawing-moment curves in figures 9(b), 9(e), 15(b), and 15(e). It can also be observed that deflecting the nose flaps had a progressively detrimental effect on the lift/drag ratio as the deflection angle was increased (see figs. 9(d) and 15(d)).

### Drooped-Nose Flaps on Both Wing Panels

With the oblique wing swept either  $45^\circ$  or  $50^\circ$ , deflecting the nose flap  $30^\circ$  on both wing panels did not improve the linearity of the moment curves at either high or low lift coefficients (see figs. 21(b), 21(e), 27(b) and 27(e)). Again, the lift/drag ratios for the oblique wing with drooped-nose flaps were generally lower than for the plain wing (see figs. 21(d) and 27(d)).

### A Comparison of the Drooped-Nose Flap Results and Previous Krüger Nose Flap Results

The effects of mounting Krüger nose flaps on the drooped-nose flaps, which were deflected  $5^\circ$  and mounted on the downstream wing panel only, are shown in figures 28(b) and 28(e) for a Mach number of 0.95 and a sweep angle of  $45^\circ$ . Results for the Krüger nose flaps at other Mach numbers and sweep angles are presented in reference 3. At low lift coefficients, the Krüger nose flaps produced increments of yawing moment (fig. 28(e)) and lower lift/drag ratios (fig. 28(d)).

As pointed out in reference 3, with no upward bending of the wing panels the rolling moment coefficients of  $-0.01$  to  $-0.02$  could be eliminated at low lift coefficients. Bending the wing panels upward to the so-called intermediate bend did not improve the linearity of the moment curves.

## CONCLUDING REMARKS

It was shown that drooped-nose flaps alone on a low-aspect ratio, oblique wing were not effective in making the pitching-, rolling-, and yawing-moment curves more linear at high lift coefficients. As previously reported, however, Krüger flaps were effective in producing more linear moment curves for the oblique wing when they were mounted on to downstream wing panel with the nose flap deflected 5°.

Ames Research Center

National Aeronautics and Space Administration  
Moffett Field, California 94035, March 15, 1976

## REFERENCES

1. Hopkins, Edward J.; and Levin, Alan D.: An Experimental and Theoretical Study of Low-Aspect Ratio Swept and Oblique Wings at Mach Numbers Between 0.6 and 1.4. AIAA Preprint 74-771, AIAA Mechanics and Control of Flight Conference, Anaheim, Calif. August 5-9, 1974.
2. Hopkins, Edward J.: Effects of Wing Bend on the Aerodynamic Characteristics of a Low Aspect Ratio Oblique Wing. AIAA Preprint 75-995, AIAA Aircraft Systems and Technology Meeting, Los Angeles, Calif. August 4-7, 1975.
3. Hopkins, Edward J.; and Lovette, George H.: Effect of Krüger Nose Flaps on the Experimental Force and Moment Characteristics of an Oblique Wing. NASA TM X-3372, 1976.
4. Hopkins, Edward J.; Meriwether, Frank D.; and Pena, Douglas F.: Experimental Aerodynamic Characteristics of Low Aspect-Ratio Swept and Oblique Wings at Mach Numbers Between 0.6 and 1.4. NASA TM X-62,317, 1973.

TABLE 1.— MODEL GEOMETRY

Body	
Radius	$r = 3.856[1 - (1 - 2x_1/114.91)^2]^{3/4}$ cm
Length	
Closed	114.91 cm
Cutoff	91.44 cm
Maximum diameter	7.71 cm
Wing	
Planform ellipticity about 0.25 $c$ line	4.7:1
Span	90.51 cm
Span (reference)	71.12 cm
Area (reference)	1365.09 cm <sup>2</sup>
Mean aerodynamic chord (reference), $\bar{c}$	20.88 cm
Root chord	19.20 cm
Aspect ratio ( $\Lambda = 0$ )	6.0
Aspect ratio ( $\Lambda = 45^\circ$ )	3.2
Incidence relative to body centerline	0
Profile perpendicular to 0.25 $c$ line	Garabedian, subcritical (see table 2)

TABLE 2.- COORDINATES FOR GARABEDIAN PROFILE  
 $[(t/c)_{max} = 0.1016, \text{design lift coefficient} = 1.3 \text{ at } M = 0.6]$

$x/c$	$z/c$	$x/c$	$z/c$
0	0	0	0
-.00045	.00079	.00048	-.00058
-.00073	.00146	.00104	-.00120
-.00086	.00191	.00165	-.00176
-.00097	.00244	.00257	-.00249
-.00103	.00290	.00343	-.00308
-.00106	.00345	.00467	-.00382
-.00104	.00403	.00592	-.00445
-.00098	.00463	.00674	-.00481
-.00077	.00572	.00774	-.00519
-.00052	.00653	.00943	-.00570
-.00021	.00732	.01149	-.00620
.00026	.00830	.01539	-.00694
.00073	.00909	.02583	-.00837
.00163	.01033	.03967	-.00970
.00276	.01161	.06022	-.01116
.00464	.01340	.09339	-.01288
.00709	.01538	.13965	-.01462
.01197	.01878	.19880	-.01601
.02179	.02443	.25034	-.01684
.03187	.02928	.31761	-.01738
.04250	.03373	.38597	-.01735
.06373	.04113	.45495	-.01657
.09353	.04969	.50010	-.01568
.13389	.05882	.54359	-.01456
.17545	.06597	.57465	-.01363
.22415	.07249	.61351	-.01232
.28227	.07822	.65330	-.01090
.34741	.08236	.68122	-.00988
.41444	.08434	.71655	-.00865
.48168	.08406	.74682	-.00771
.55738	.08094	.77611	-.00702
.62052	.07591	.82243	-.00642
.68276	.06852	.87054	-.00698
.72012	.06288	.89717	-.00810
.75413	.05684	.91595	-.00941
.82318	.04227	.94348	-.01235
.85663	.03370	.96854	-.01674
.89115	.02388	.98615	-.02126
.92448	.01327	.99596	-.02434
.95410	.00145	1.00000	-.02600
.97175	-.00538		
.99163	-.01450		
1.00000	-.01900		

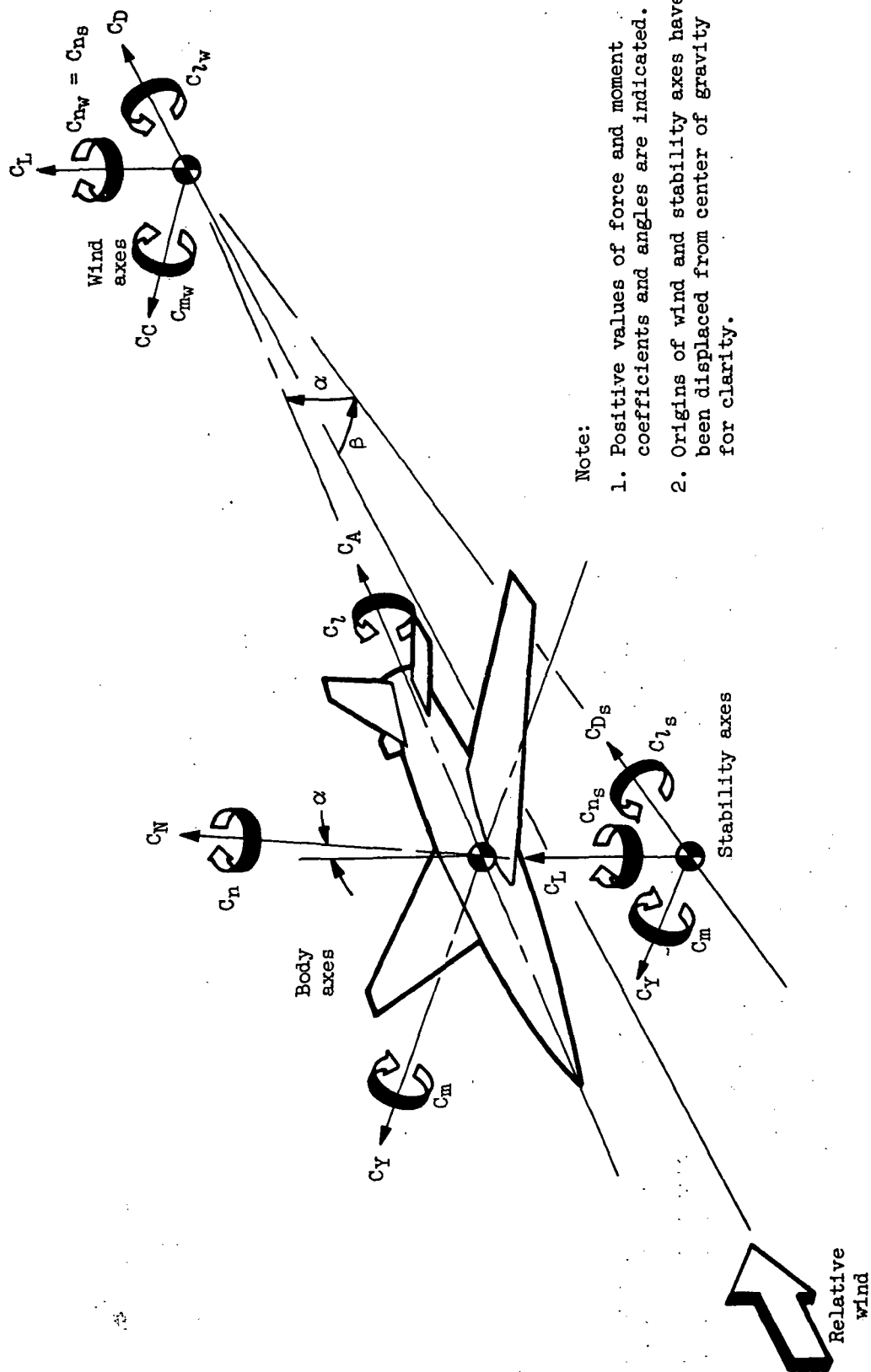
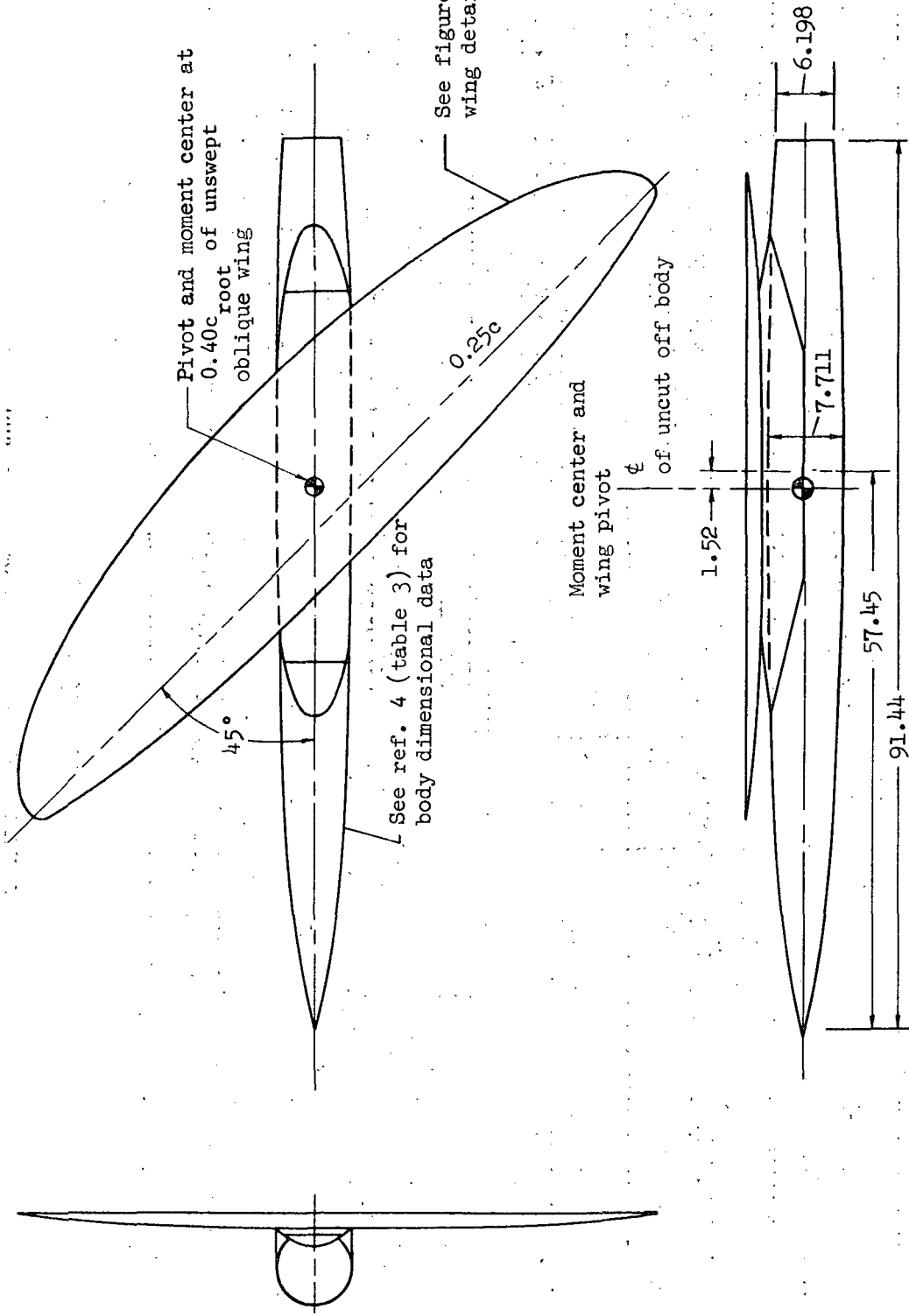


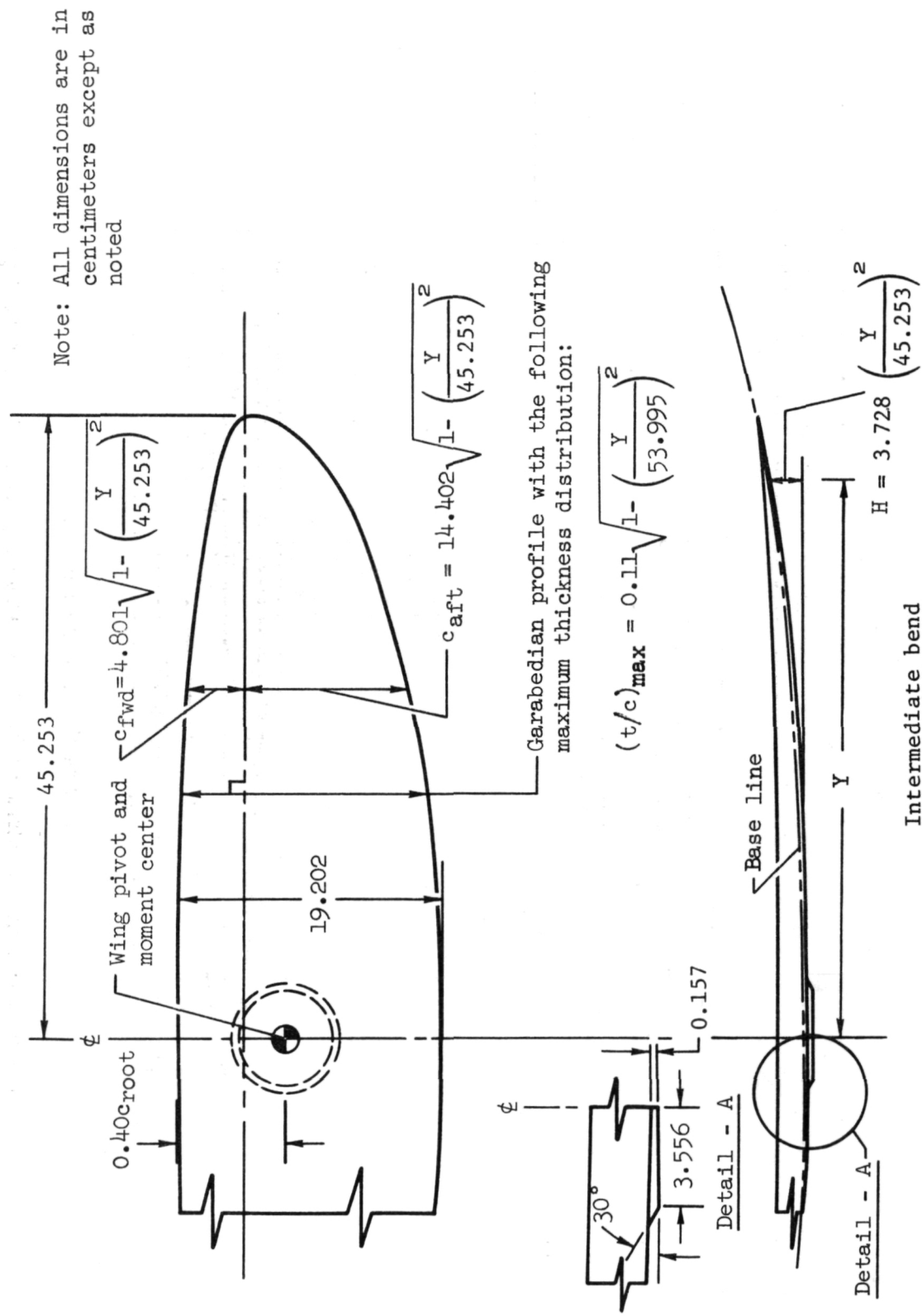
Figure 1.—Axes systems and sign conventions.

Note: All dimensions are in centimeters except as noted



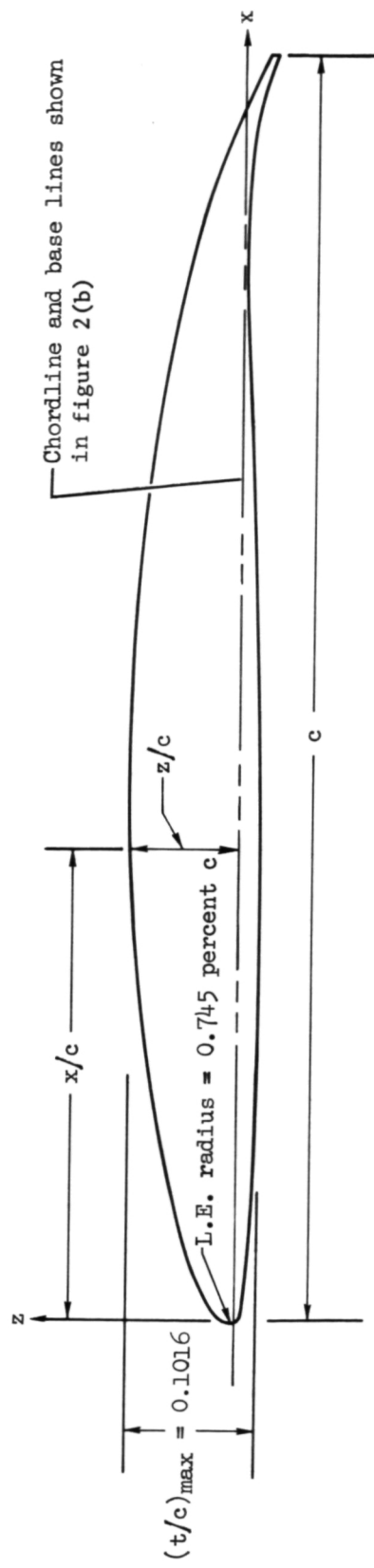
(a) Wing pivot and moment center.

Figure 2.— Geometric details for the oblique wing-body combination and the flaps.



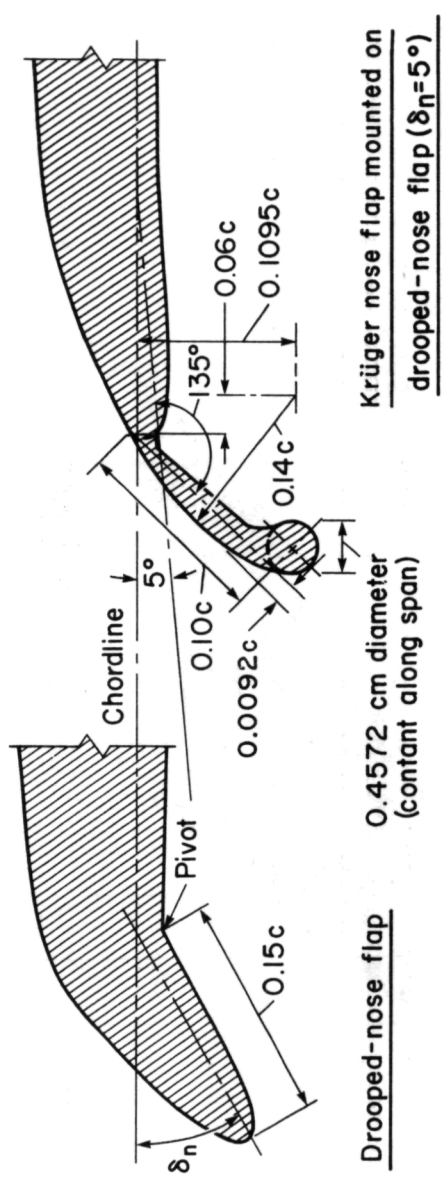
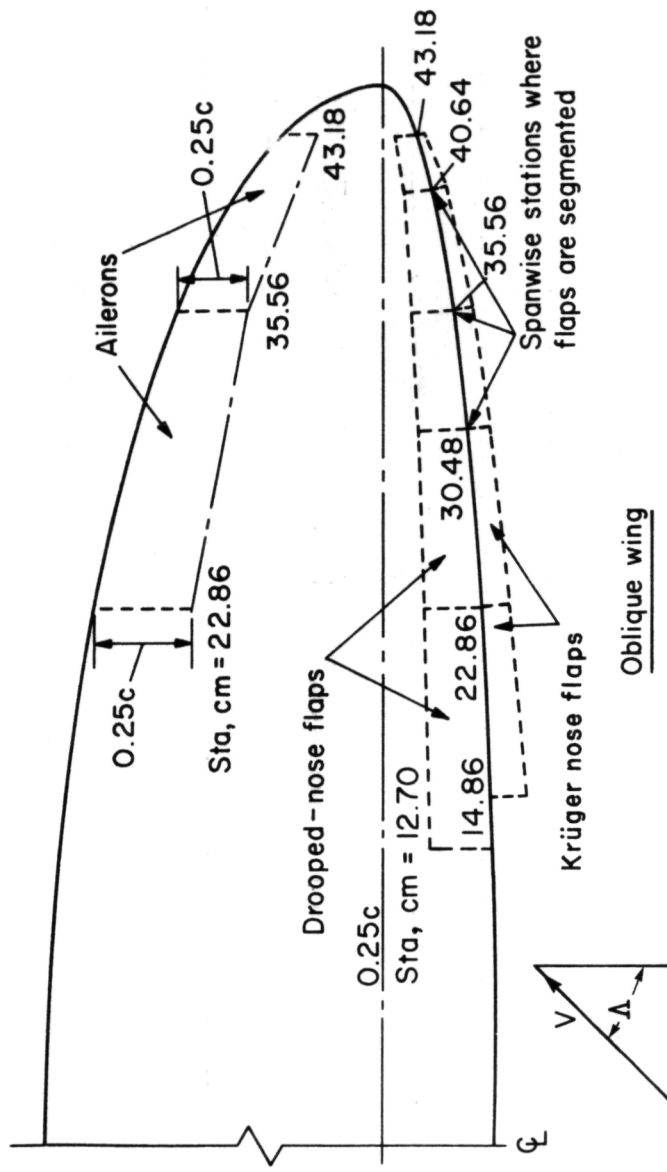
(b) Wing planform, thickness distribution and bend line.

Figure 2. – Continued.



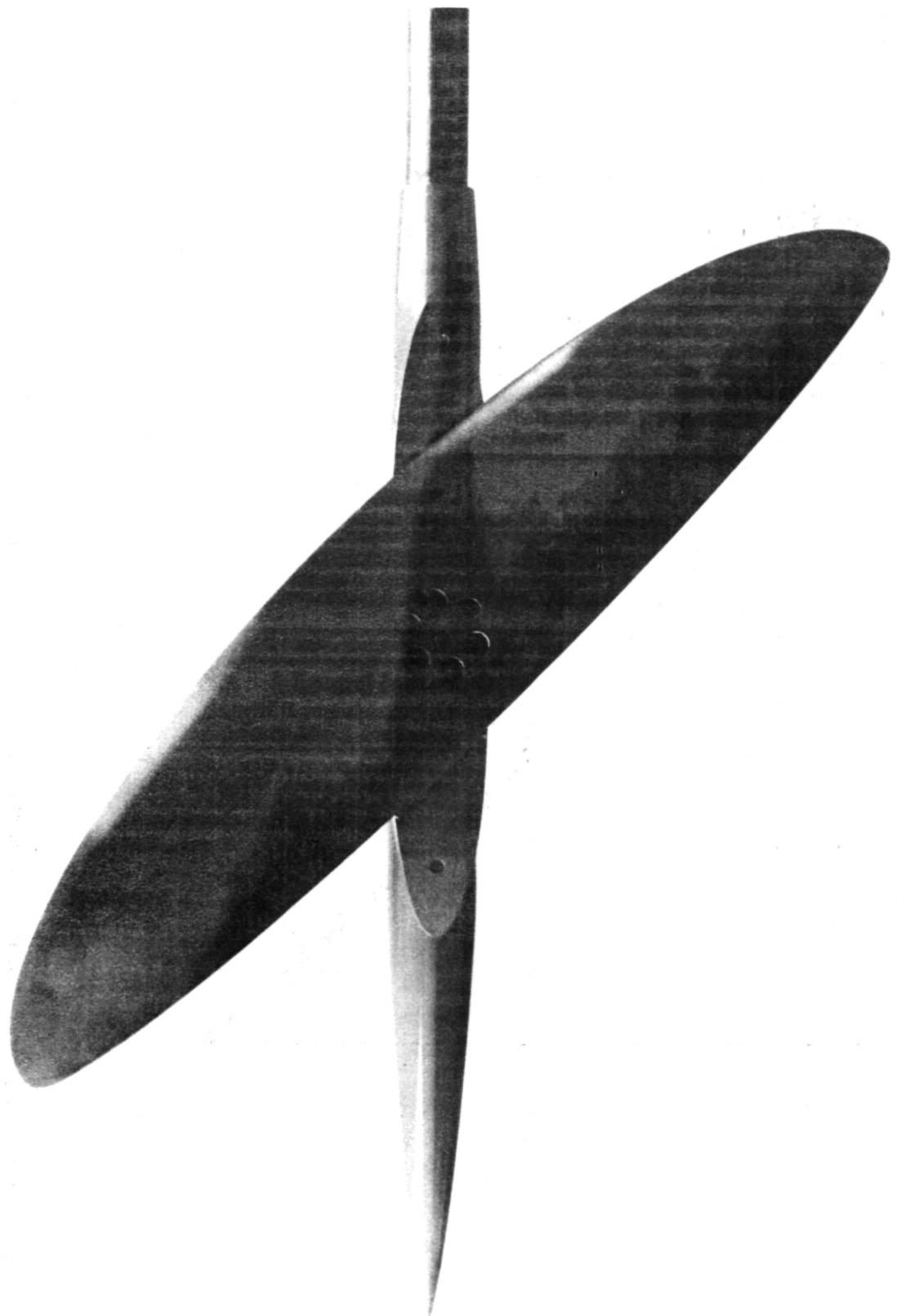
(c) Garabedian airfoil (designed for a section lift coefficient of 1.3 at  $M = 0.6$ ,  $(t/c)_{\max} = 0.1016$ ).

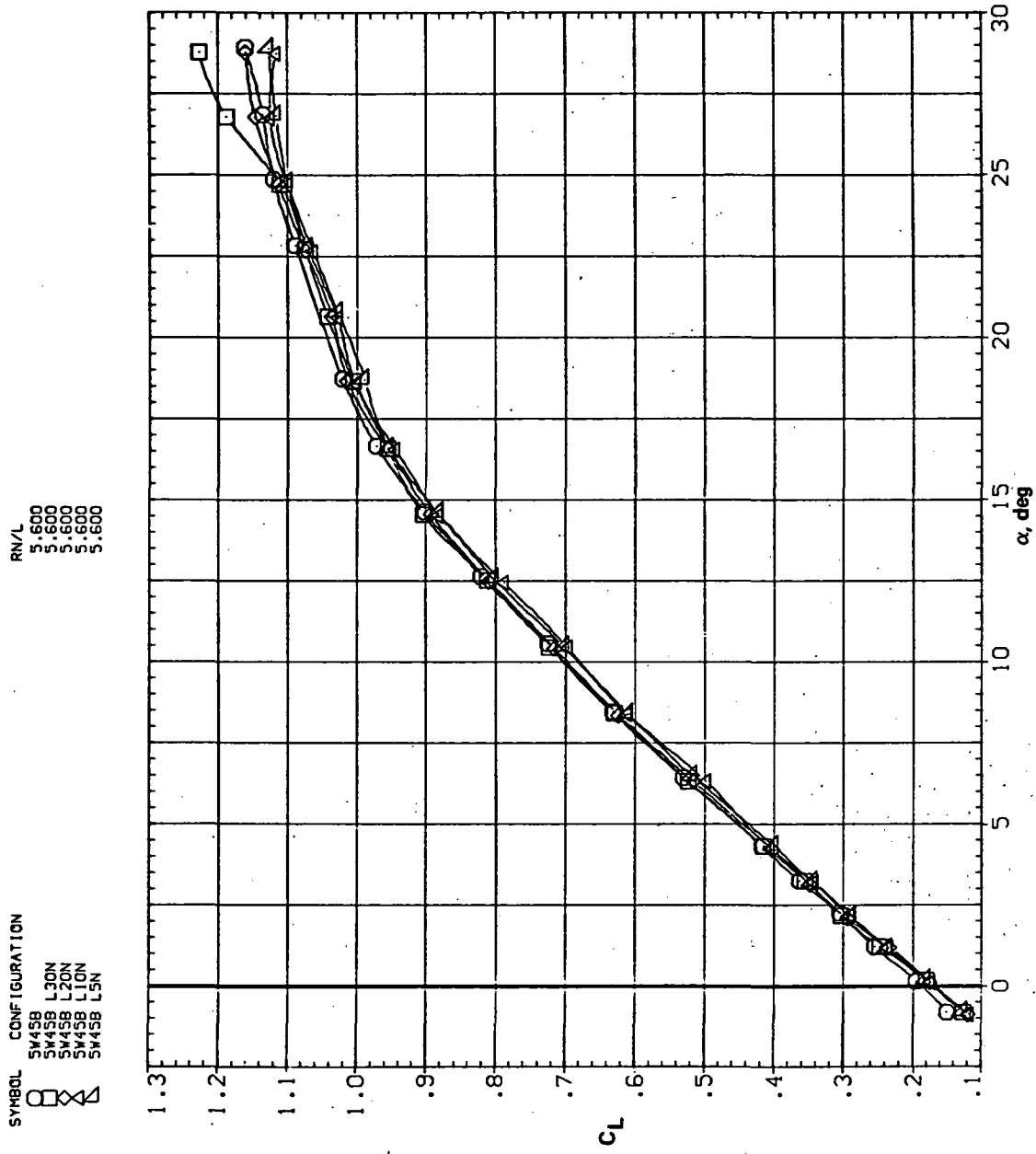
Figure 2.—Continued.



(d) Drooped-nose and Krüger nose flaps.

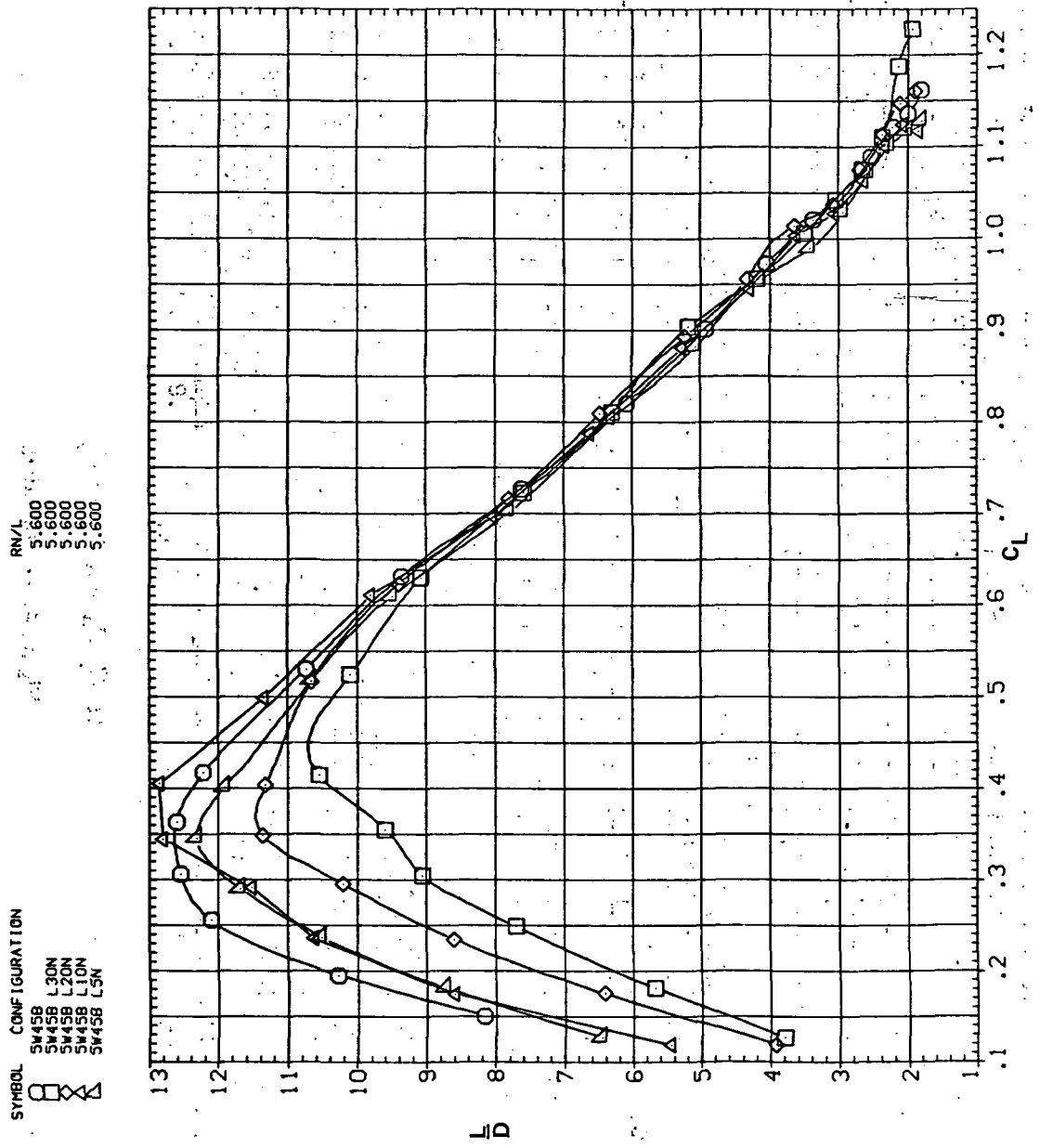
Figure 2.—Concluded.





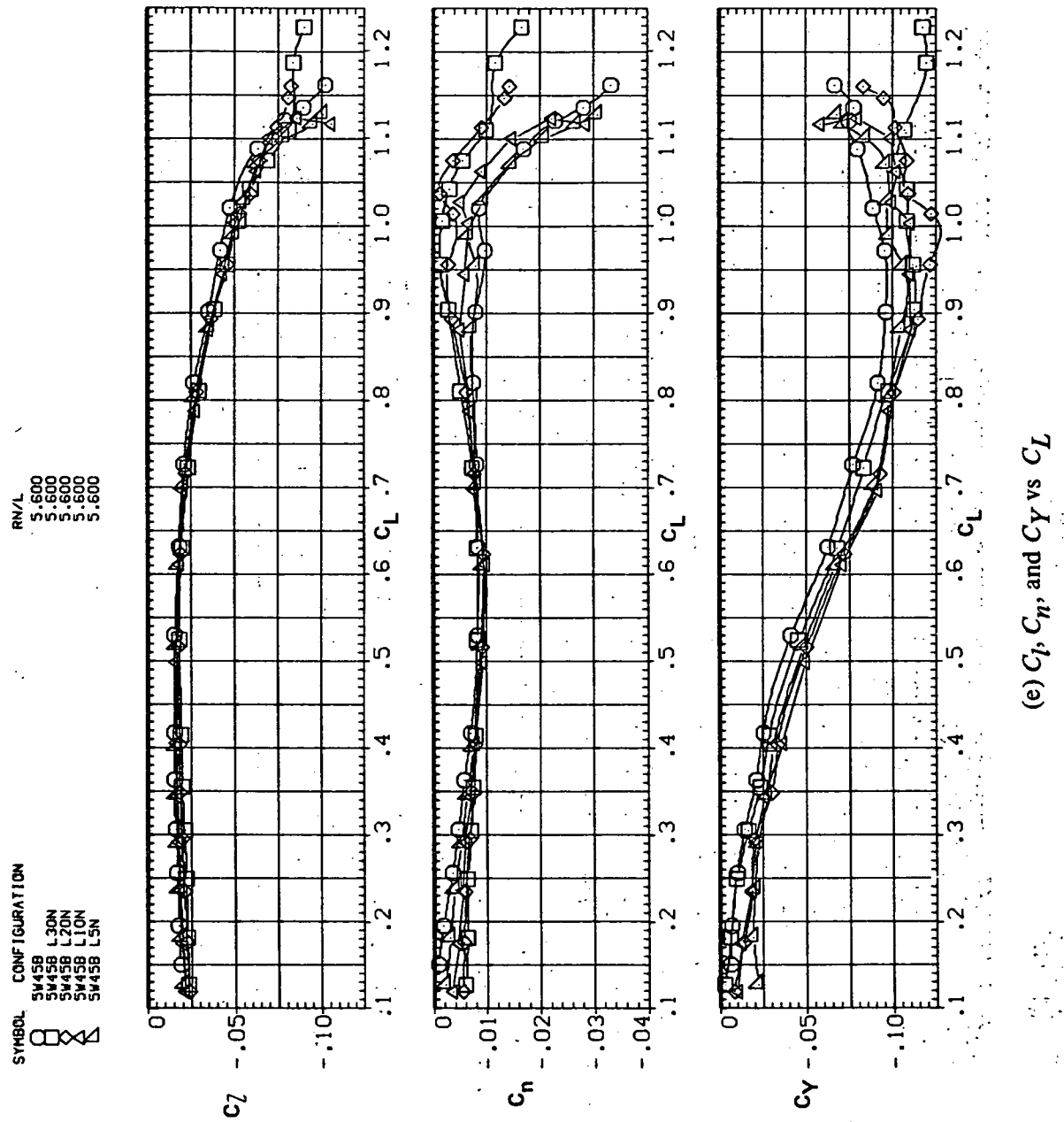
(a)  $C_L$  vs  $\alpha$

Figure 4.— Effect of drooped-nose flaps on the static longitudinal characteristics of the oblique wing: flaps on downstream wing panel only,  $\Lambda = 45^\circ$ ,  $M = 0.25$ .



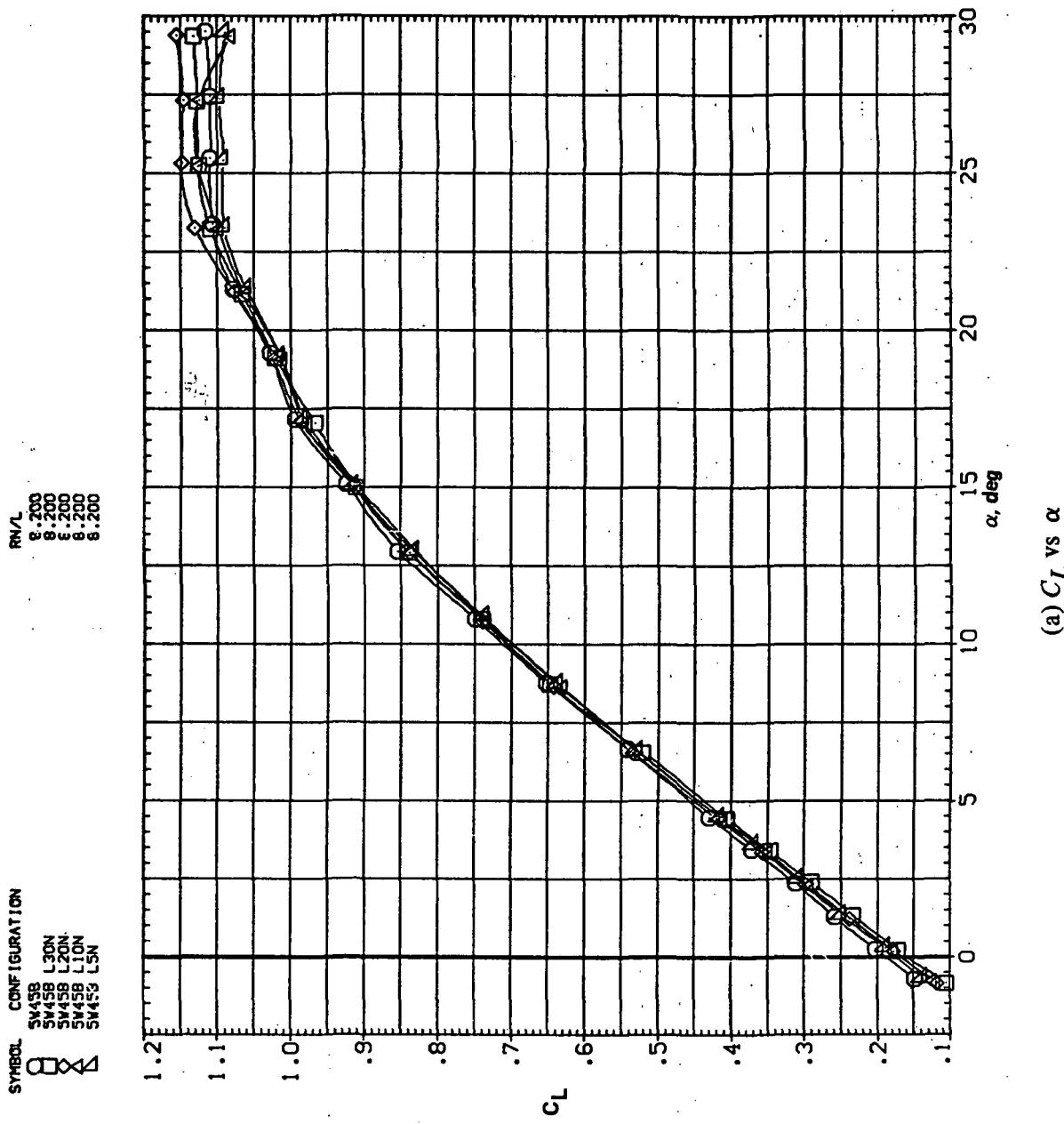
(d)  $L/D$  vs.  $C_L$

Figure 4.—Continued.



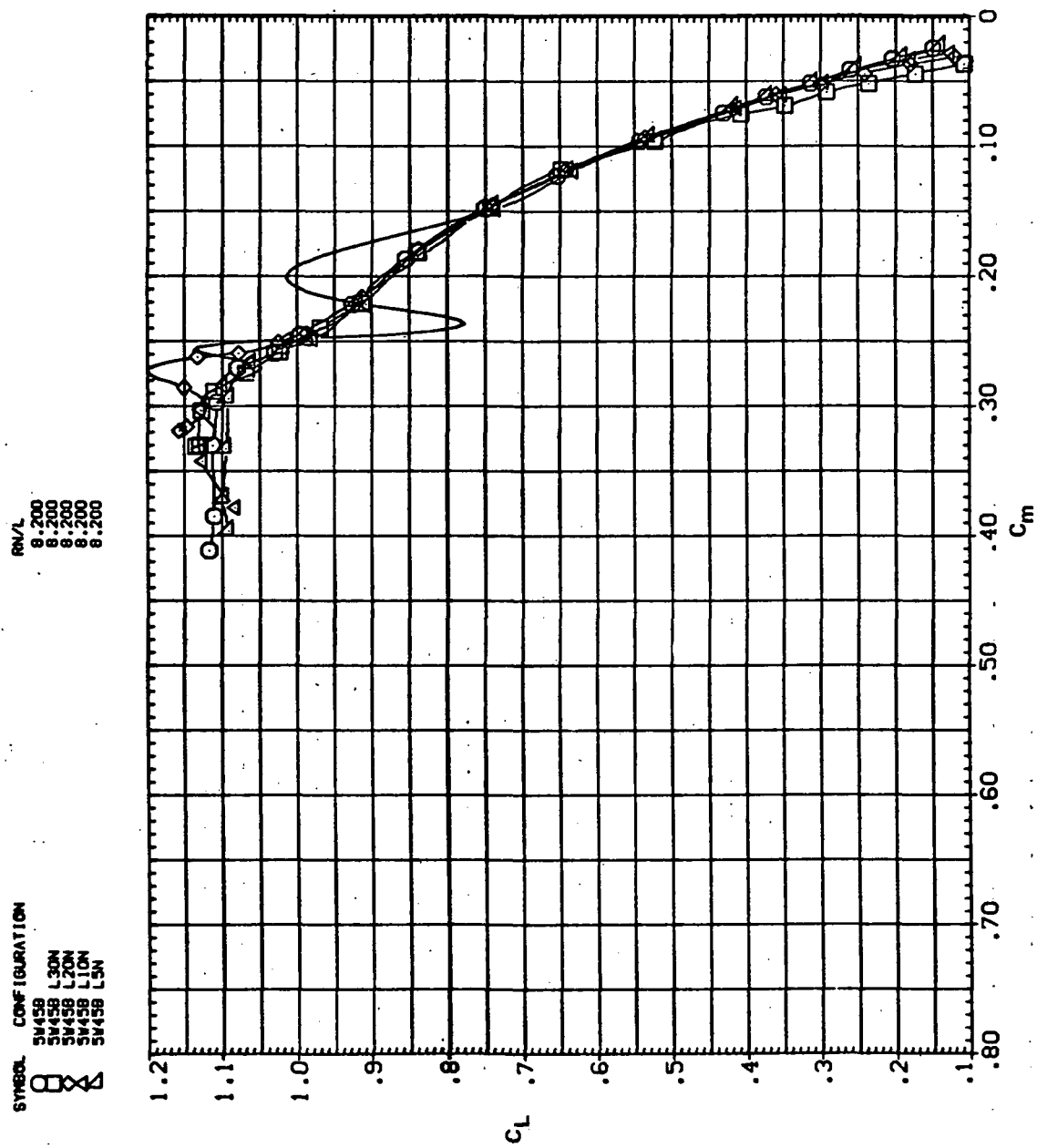
(e)  $C_D$ ,  $C_n$ , and  $C_Y$  vs  $C_L$

Figure 4.—Concluded.



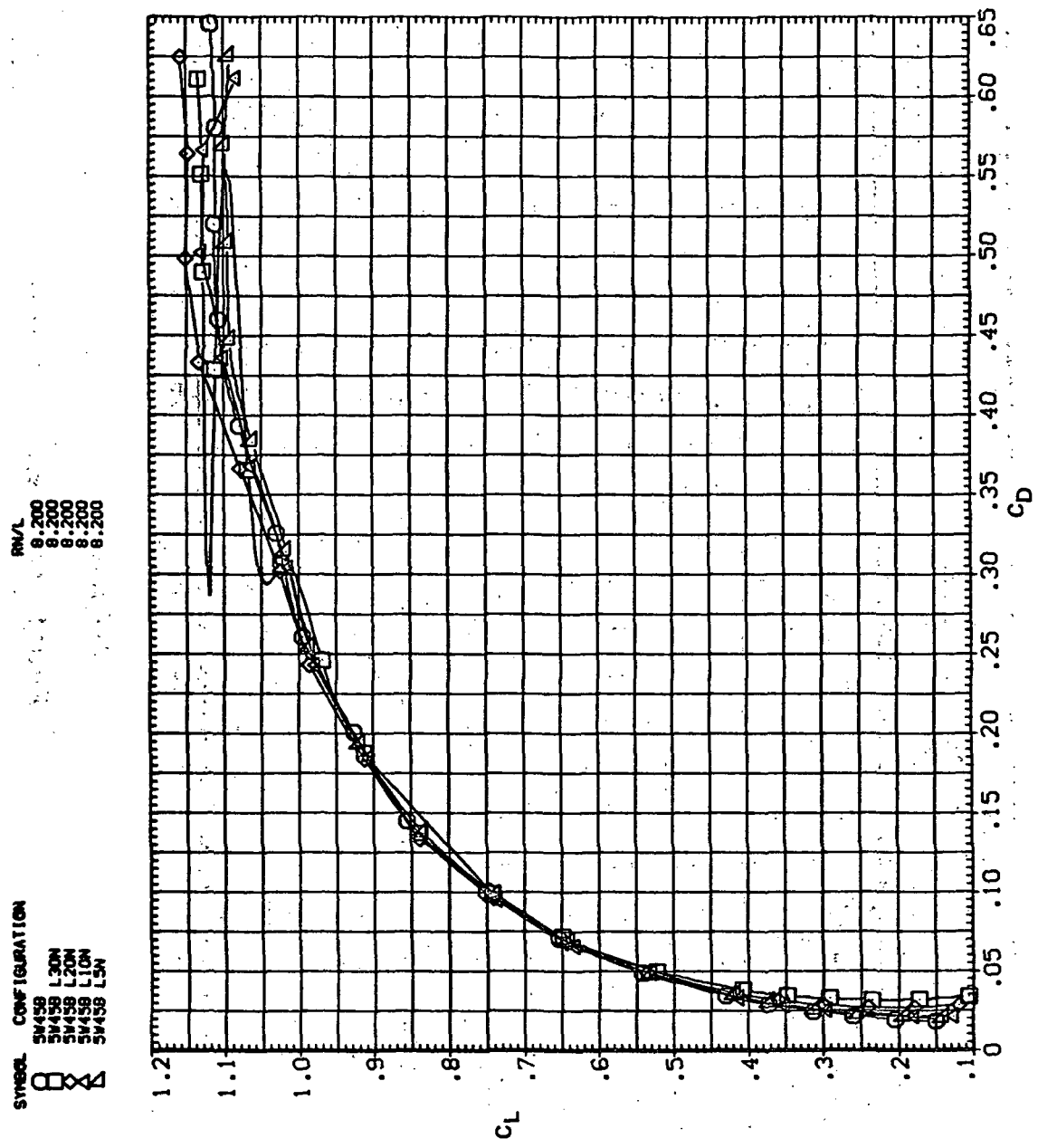
(a)  $C_L$  vs  $\alpha$

Figure 5.— Effect of drooped-nose flaps on the static longitudinal characteristics of the oblique wing: flaps on downstream wing panel only,  $\Lambda = 45^\circ$ ,  $M = 0.4$ .



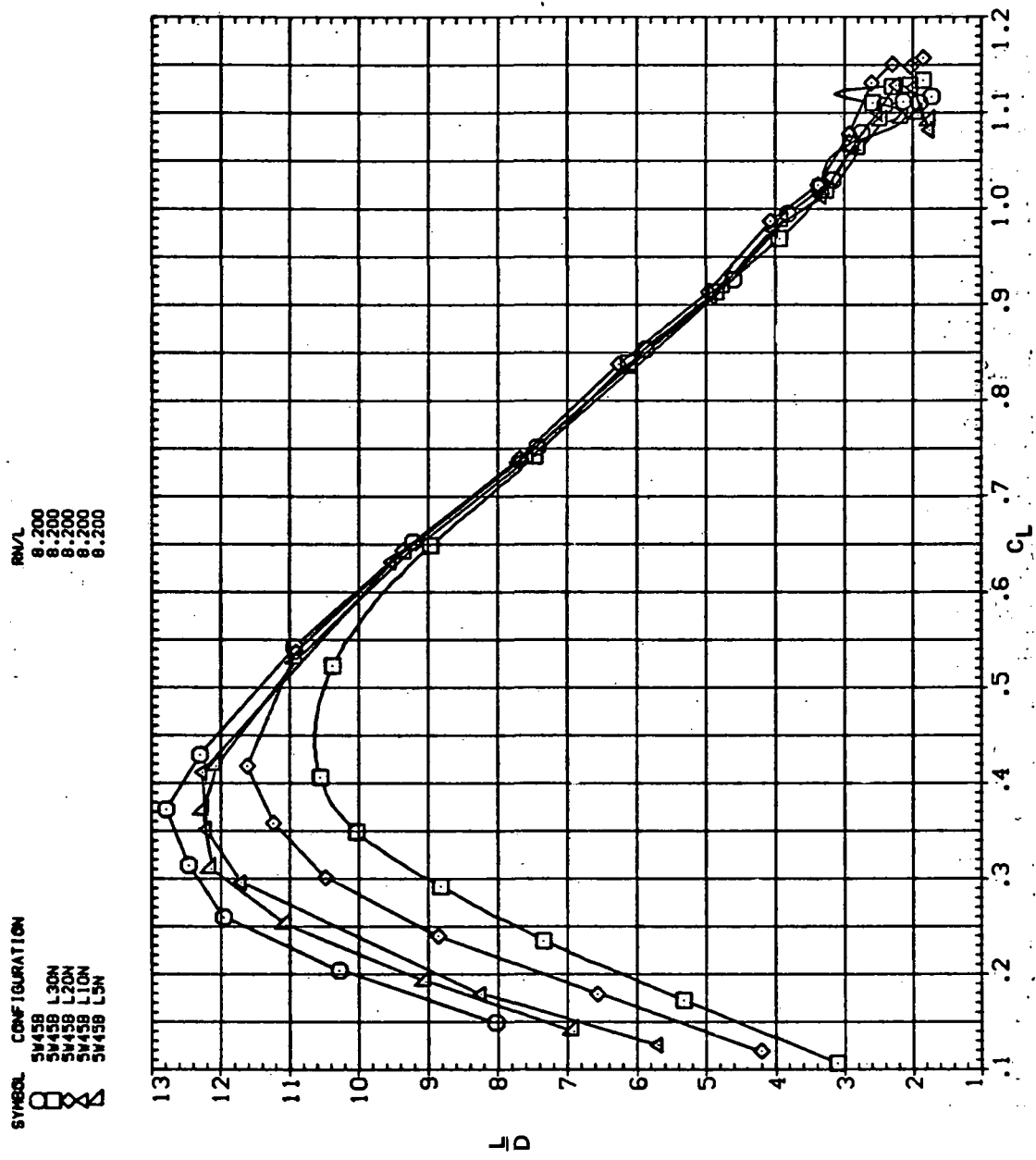
(b)  $C_L$  vs  $C_m$

Figure 5.—Continued.



(c)  $C_L$  vs  $C_D$

Figure 5.—Continued.

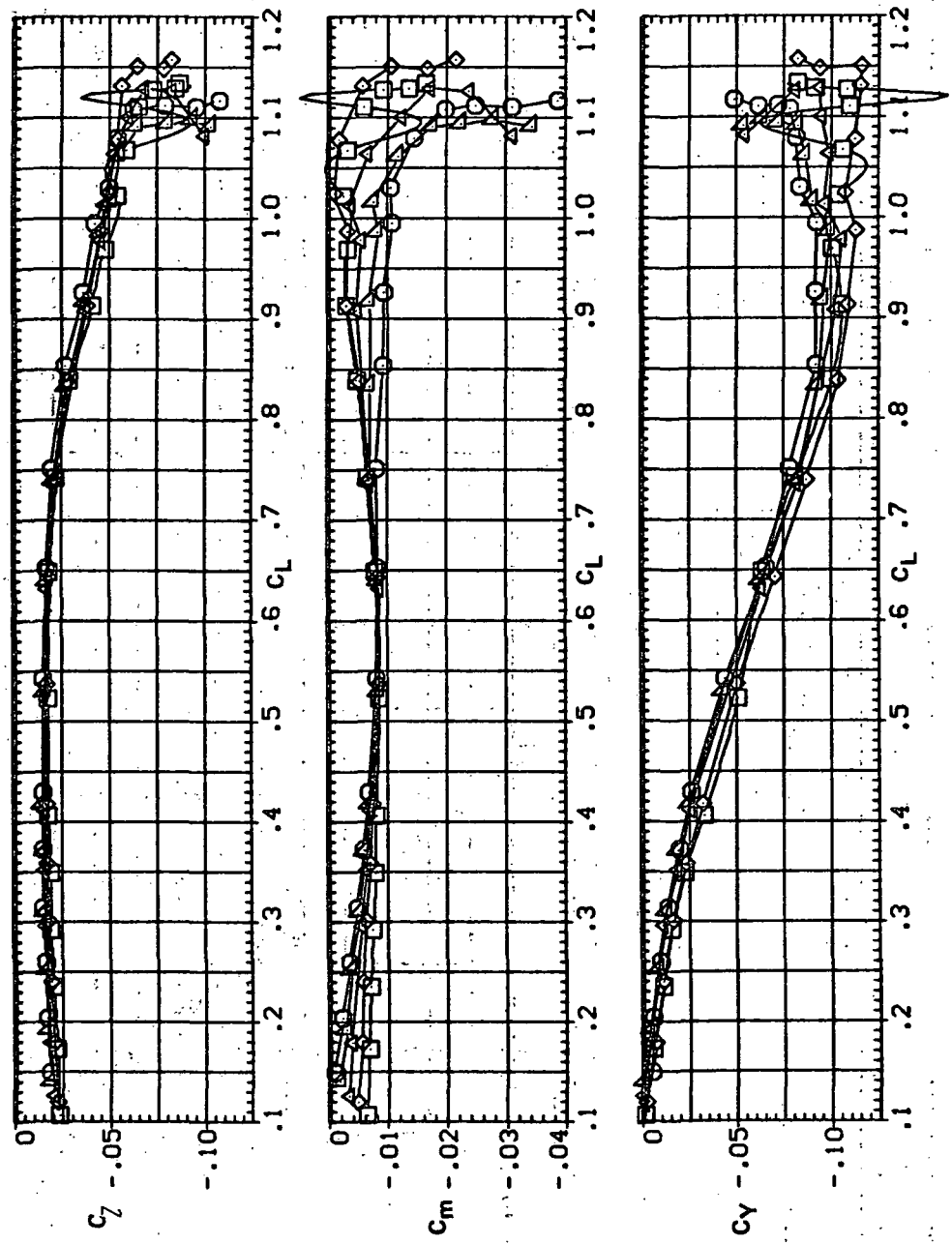


(d)  $L/D$  vs  $C_L$

Figure 5.—Continued.

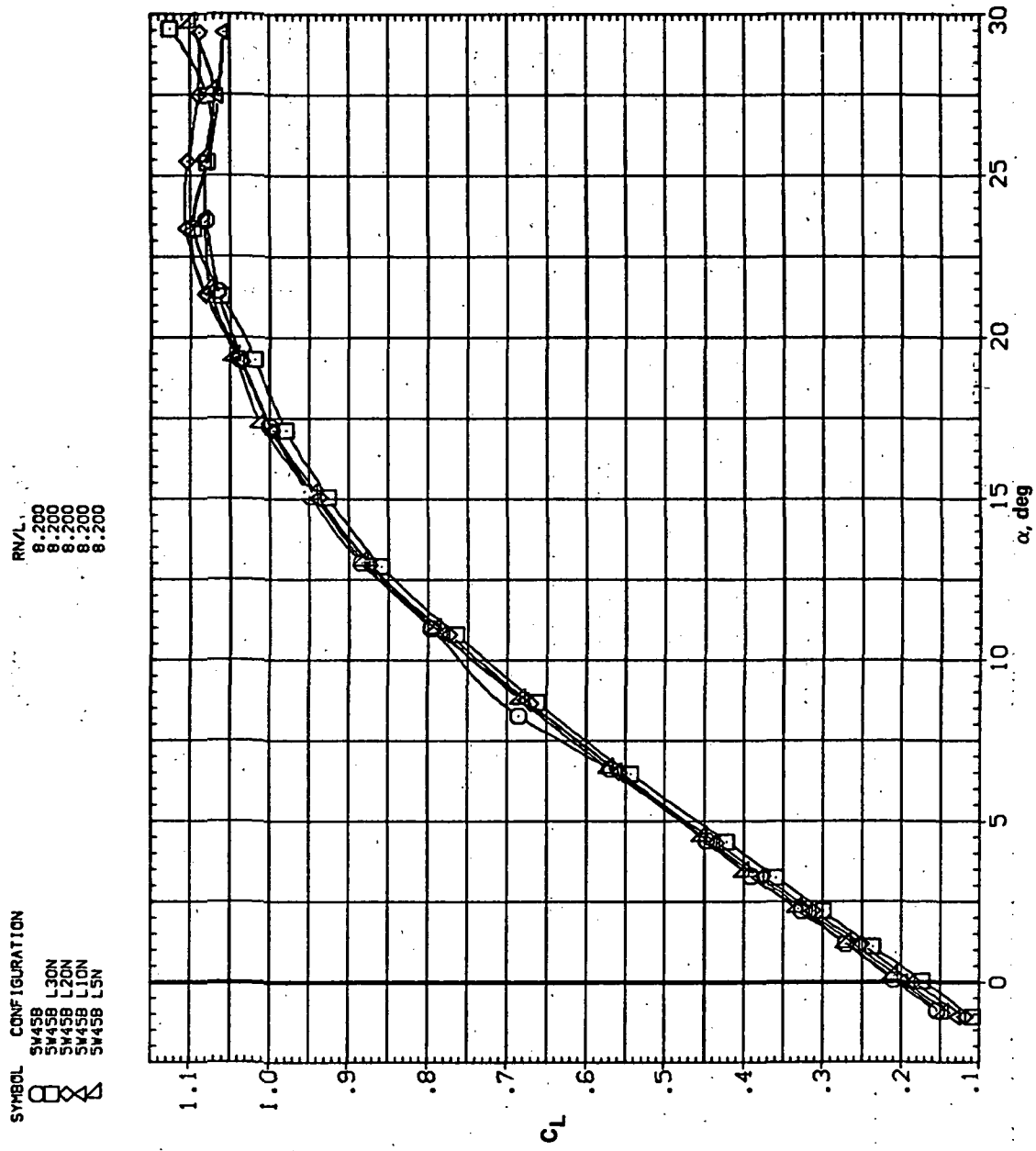
SYMBOL CONFIGURATION RV/L

3N458	L30N	8.200
SM458	L20N	8.200
SM458	L12N	8.200
SM458	L10N	8.200
SM458	L5N	8.200



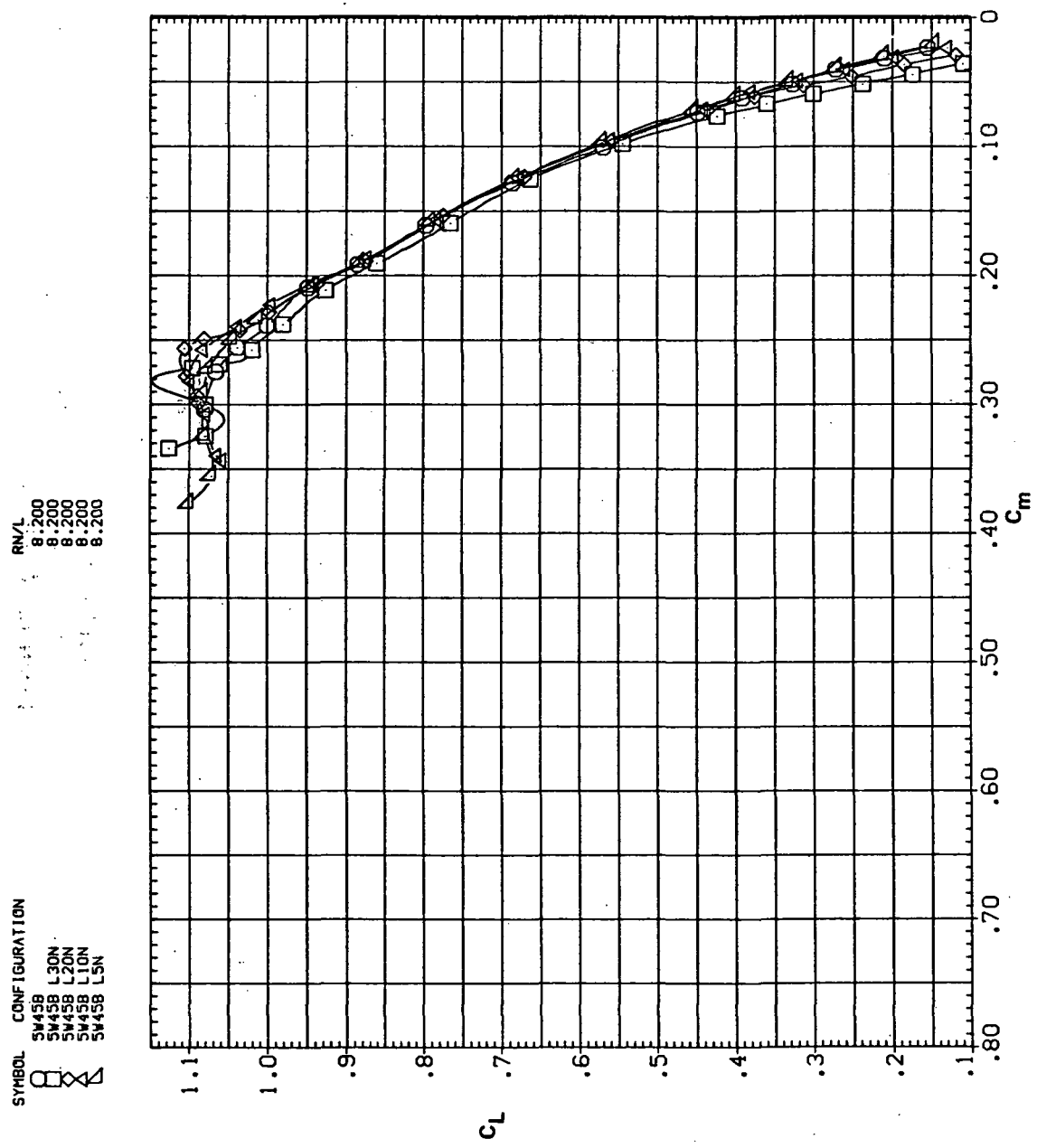
(e)  $C_D$ ,  $C_N$  and  $C_Y$  vs  $C_L$

Figure 5.— Concluded.



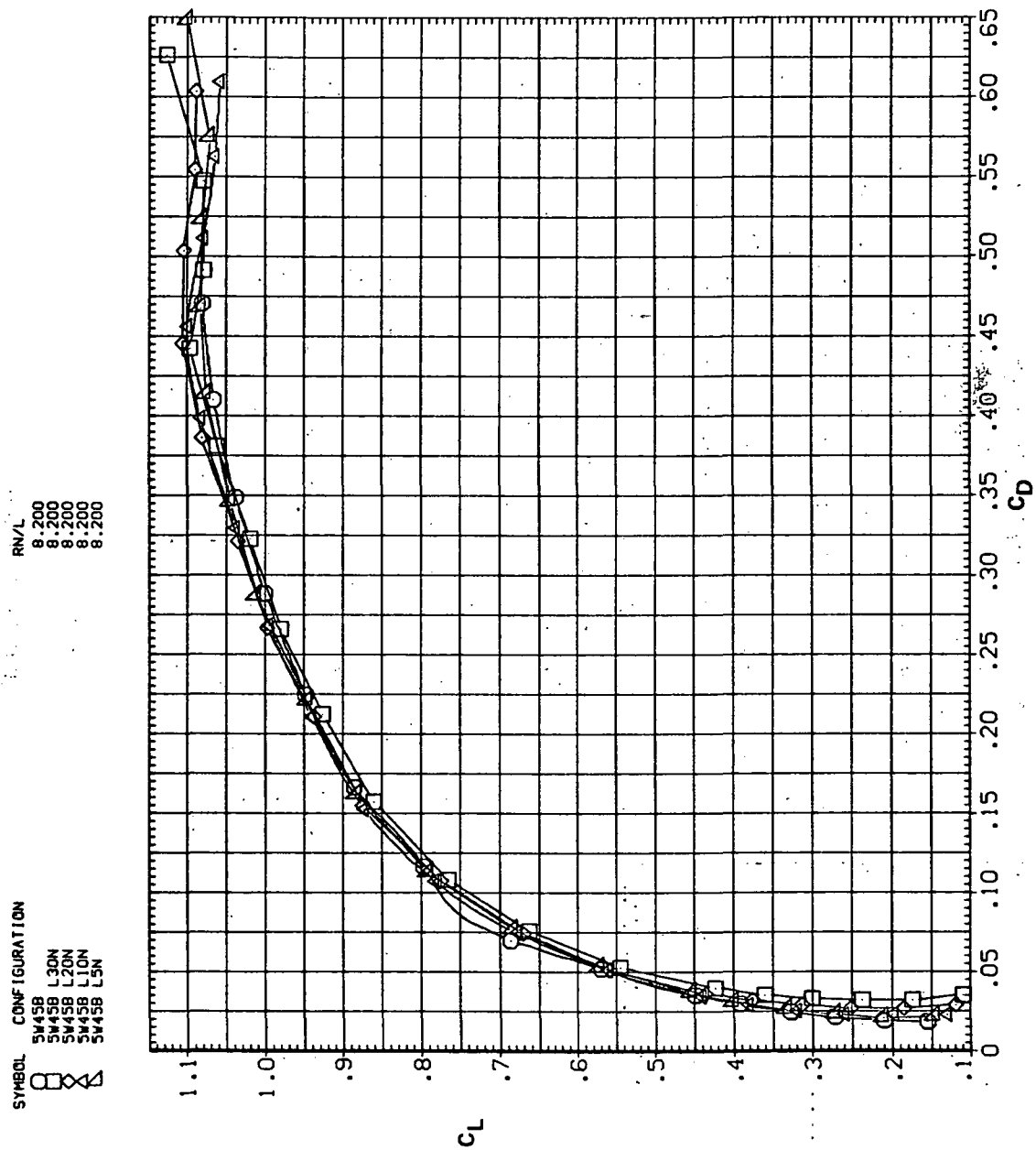
(a)  $C_L$  vs  $\alpha$

Figure 6.—Effect of drooped-nose flaps on the static longitudinal characteristics of the oblique wing: flaps on downstream wing panel only,  $\Lambda = 45^\circ$ ,  $M = 0.6$ .



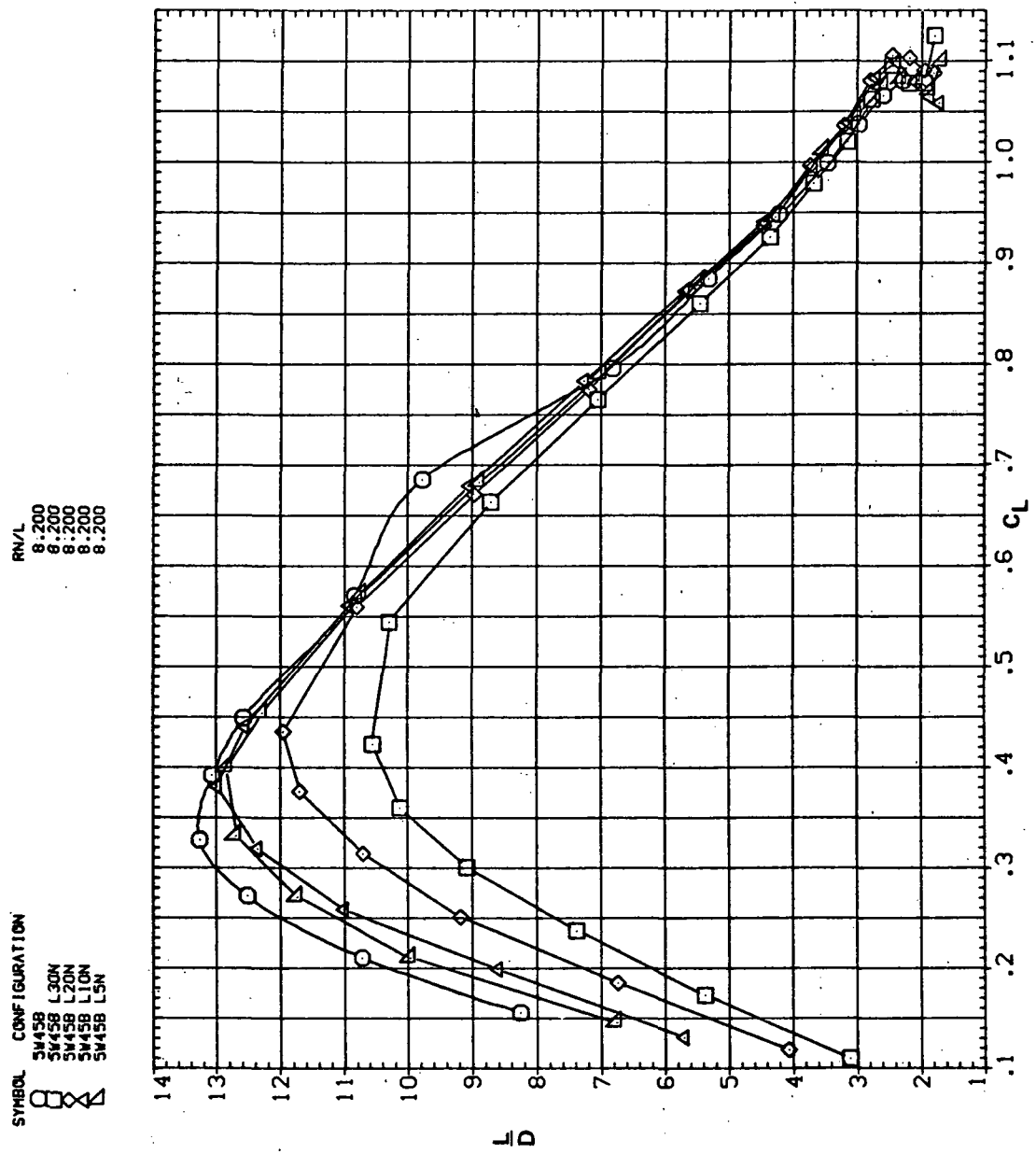
(b)  $C_L$  vs  $C_m$

Figure 6.—Continued.



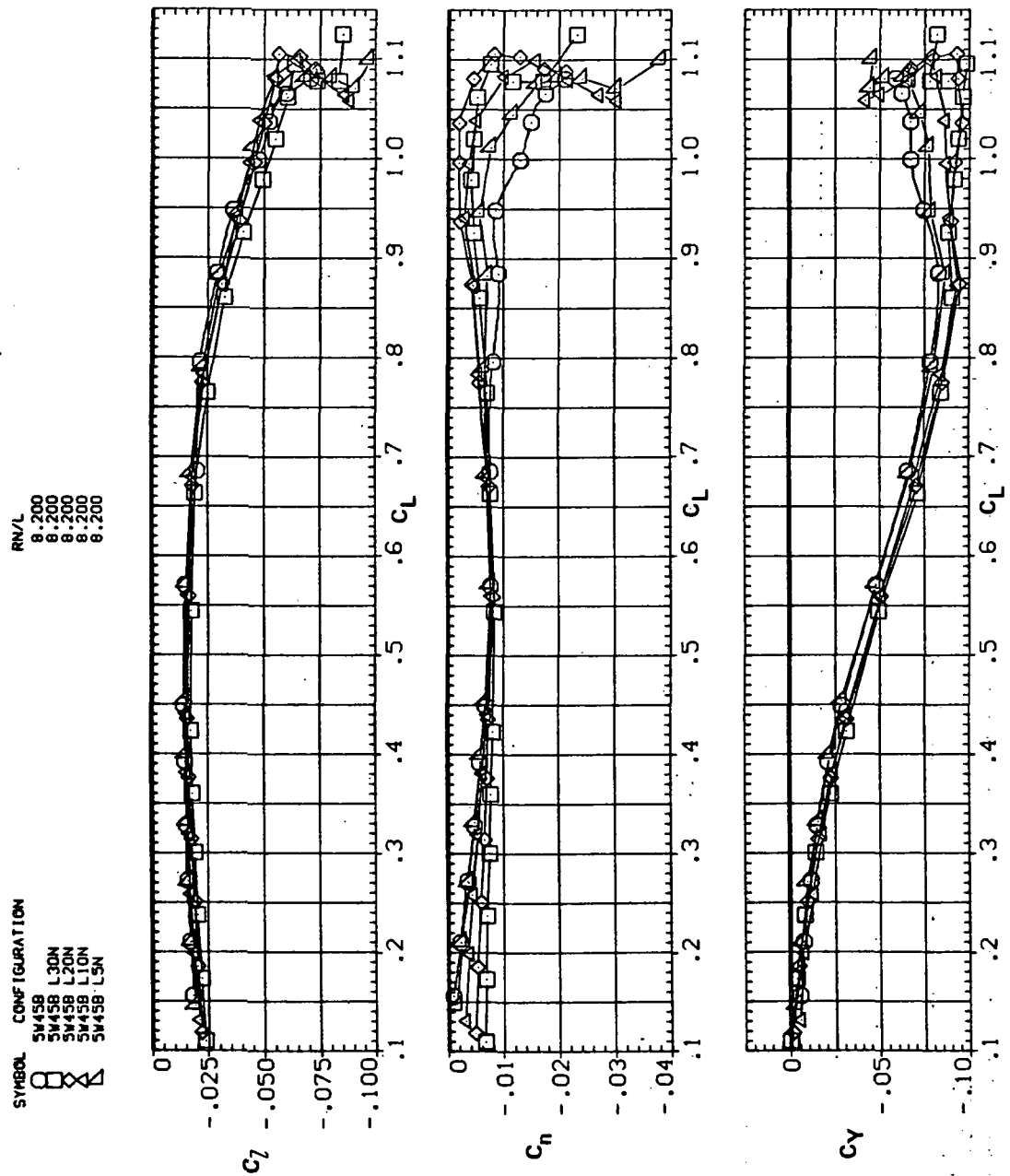
(c)  $C_L$  vs  $C_D$

Figure 6.— Continued.

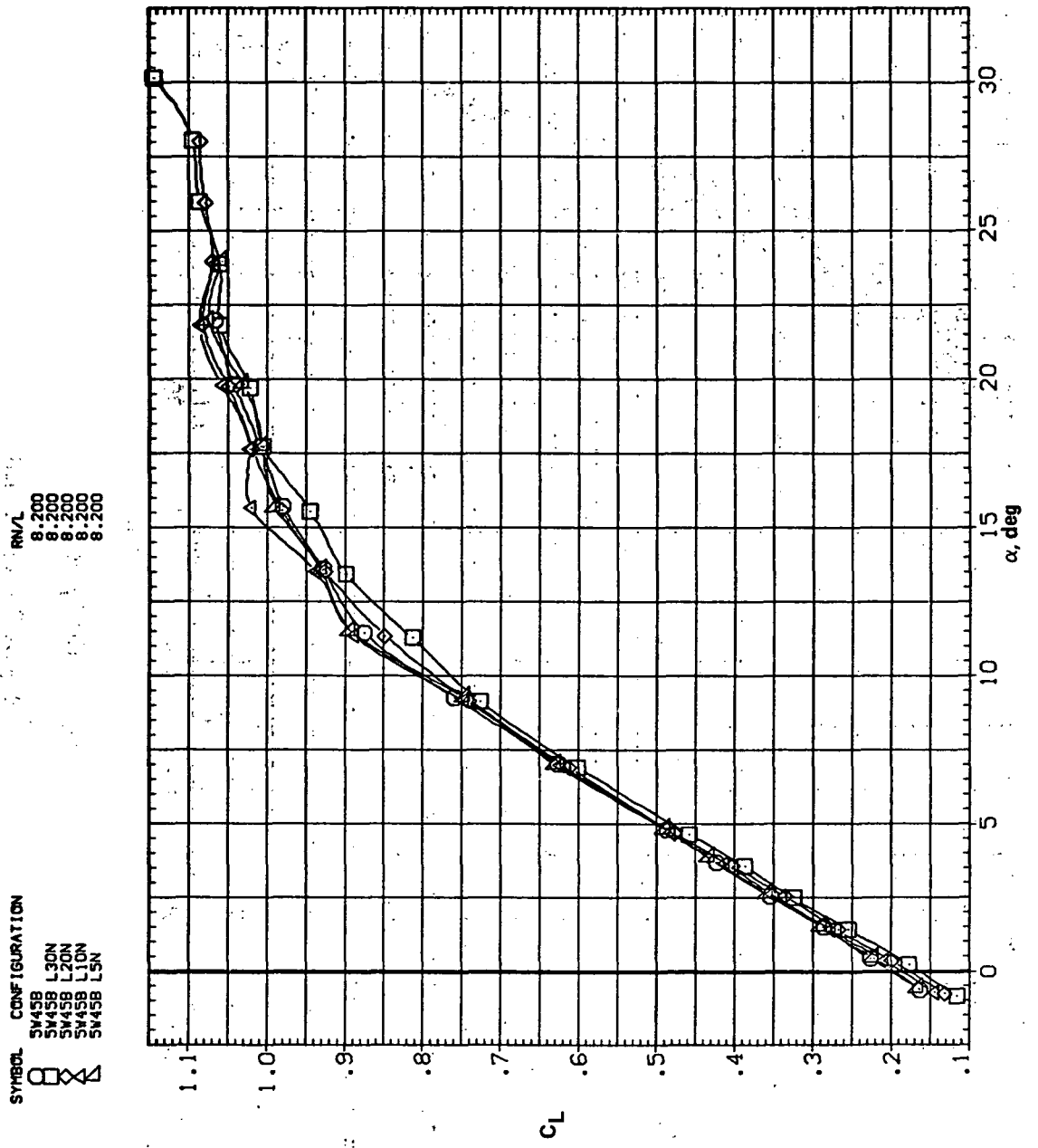


(d)  $L/D$  vs  $C_L$

Figure 6.— Continued.

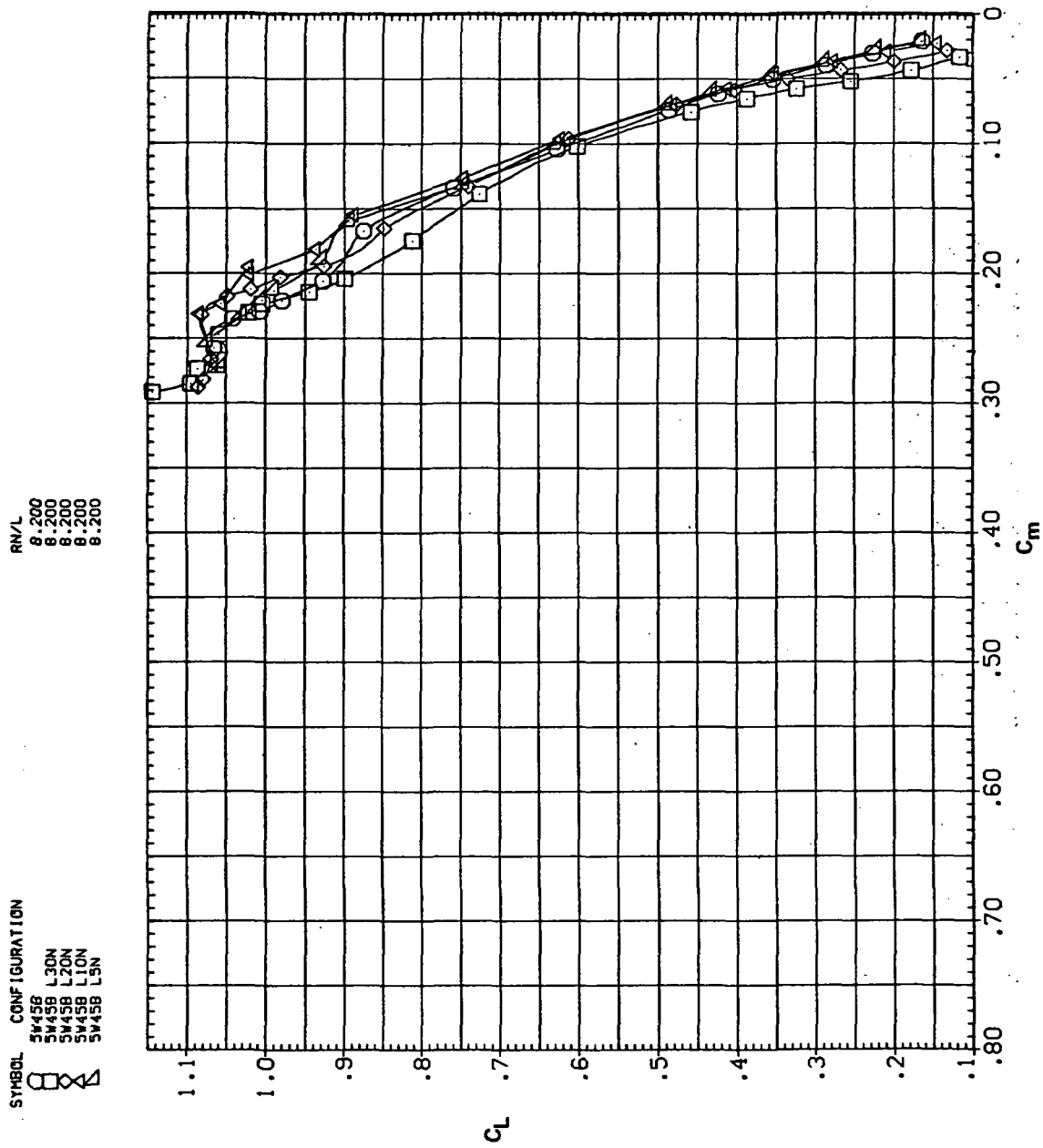


(e)  $C_l$ ,  $C_n$ , and  $C_Y$  vs  $C_L$   
Figure 6.— Concluded.



(a)  $C_L$  vs.  $\alpha$

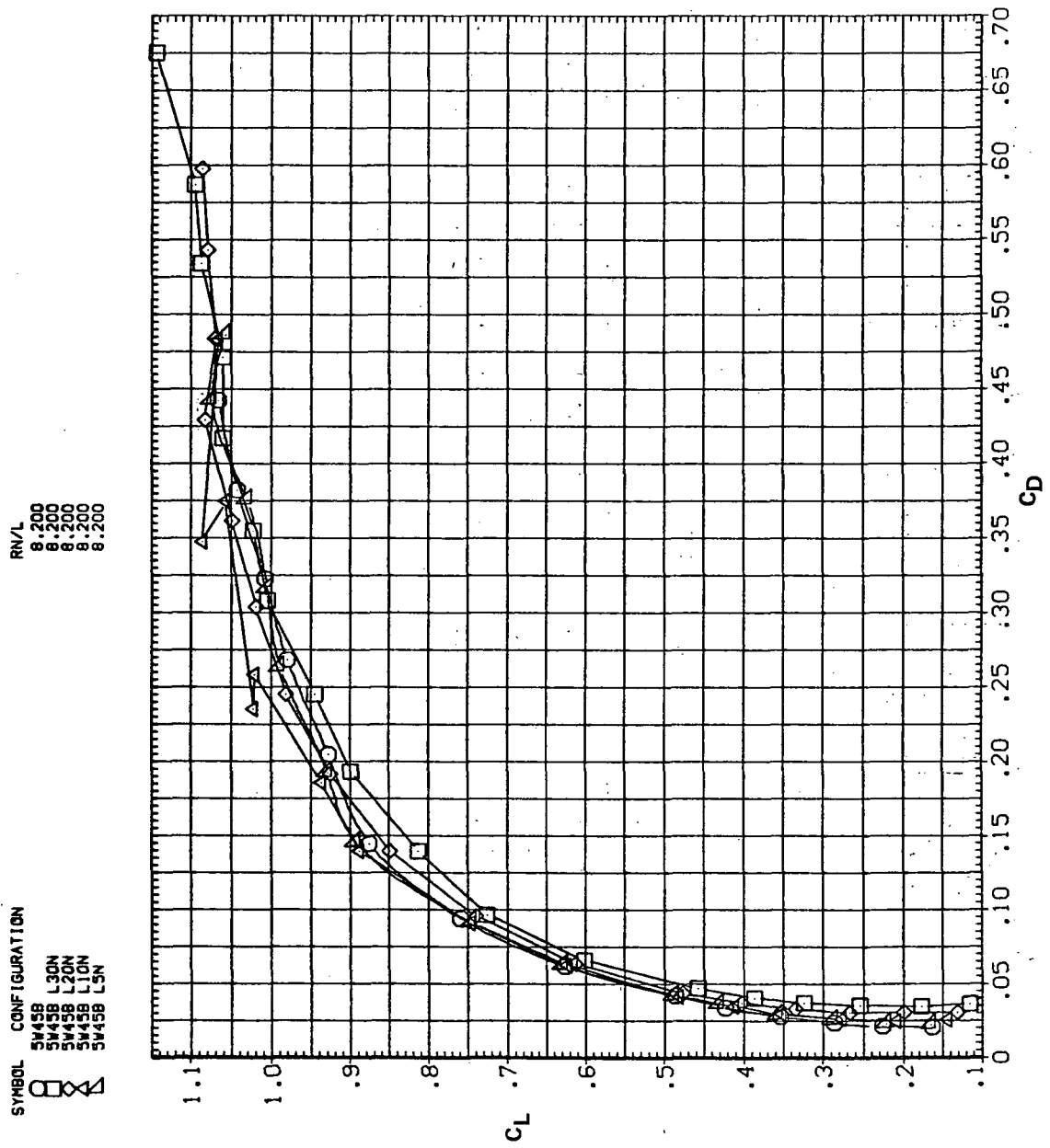
Figure 7.— Effect of drooped-nose flaps on the static longitudinal characteristics of the oblique wing: flaps on downstream wing panel only,  $\Lambda = 45^\circ$ ,  $M = 0.8$ .



(b)  $C_L$  vs  $C_m$

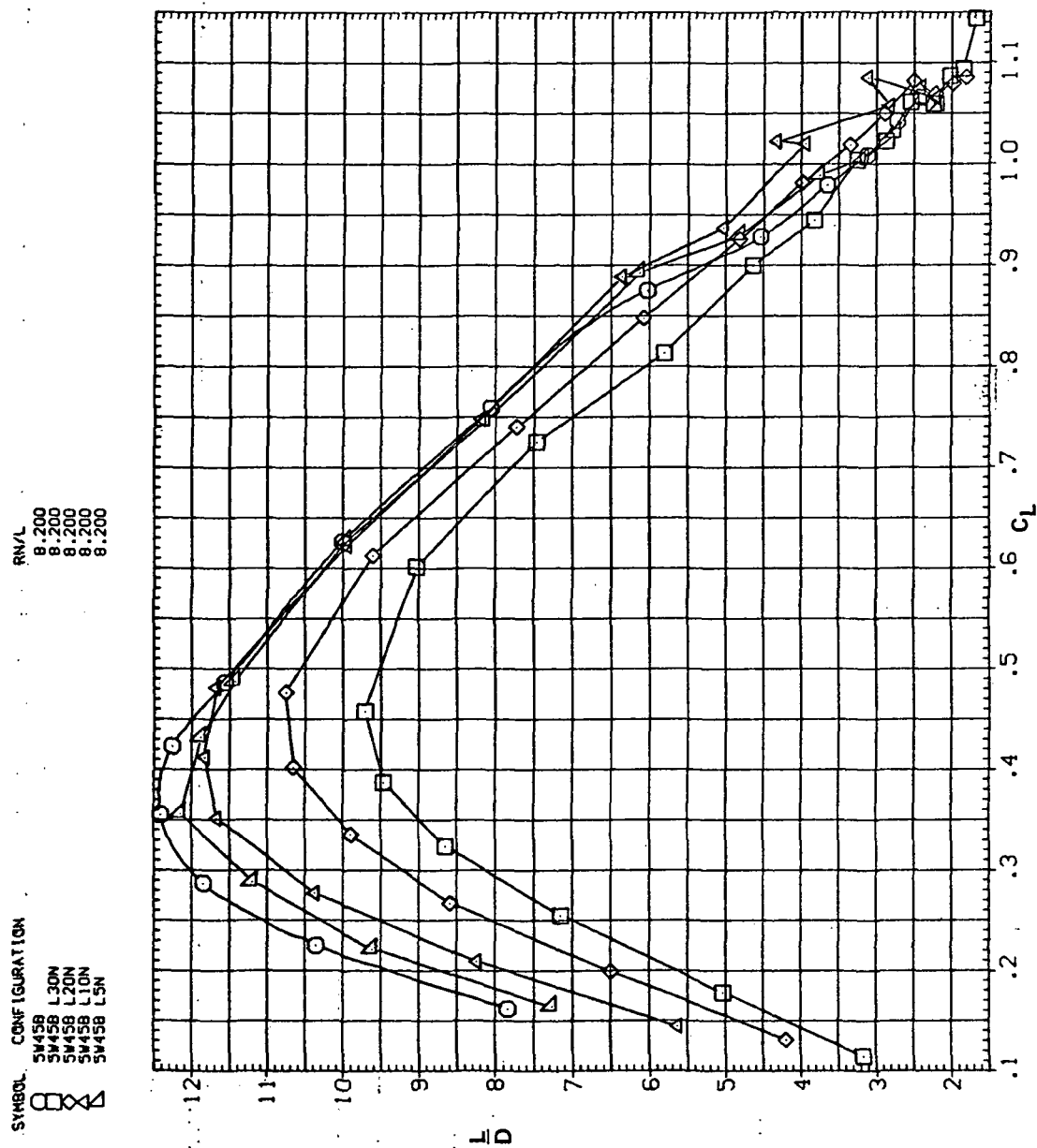
Figure 7.—Continued.

SYMBOL CONFIGURATION  
 SM458 L30N  
 SM458 L20N  
 SM458 L10N  
 SM458 L5N



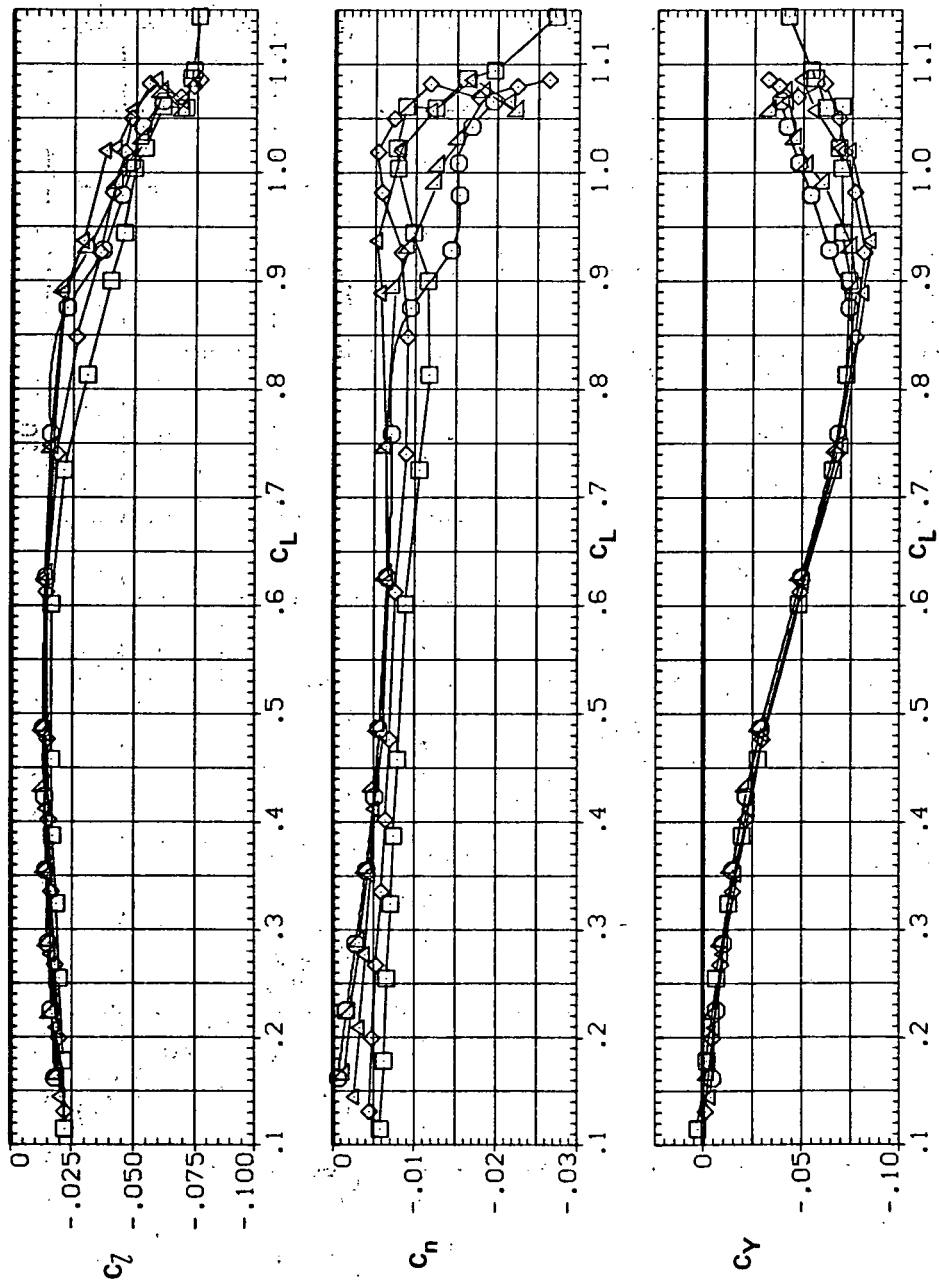
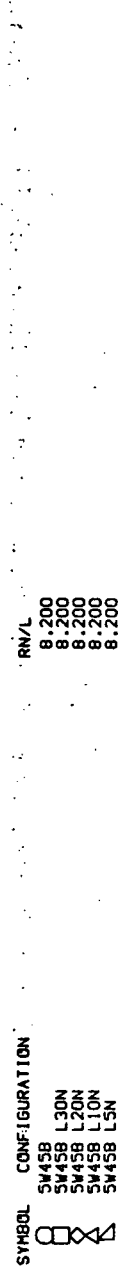
(c)  $C_L$  vs.  $C_D$

Figure 7.—Continued.



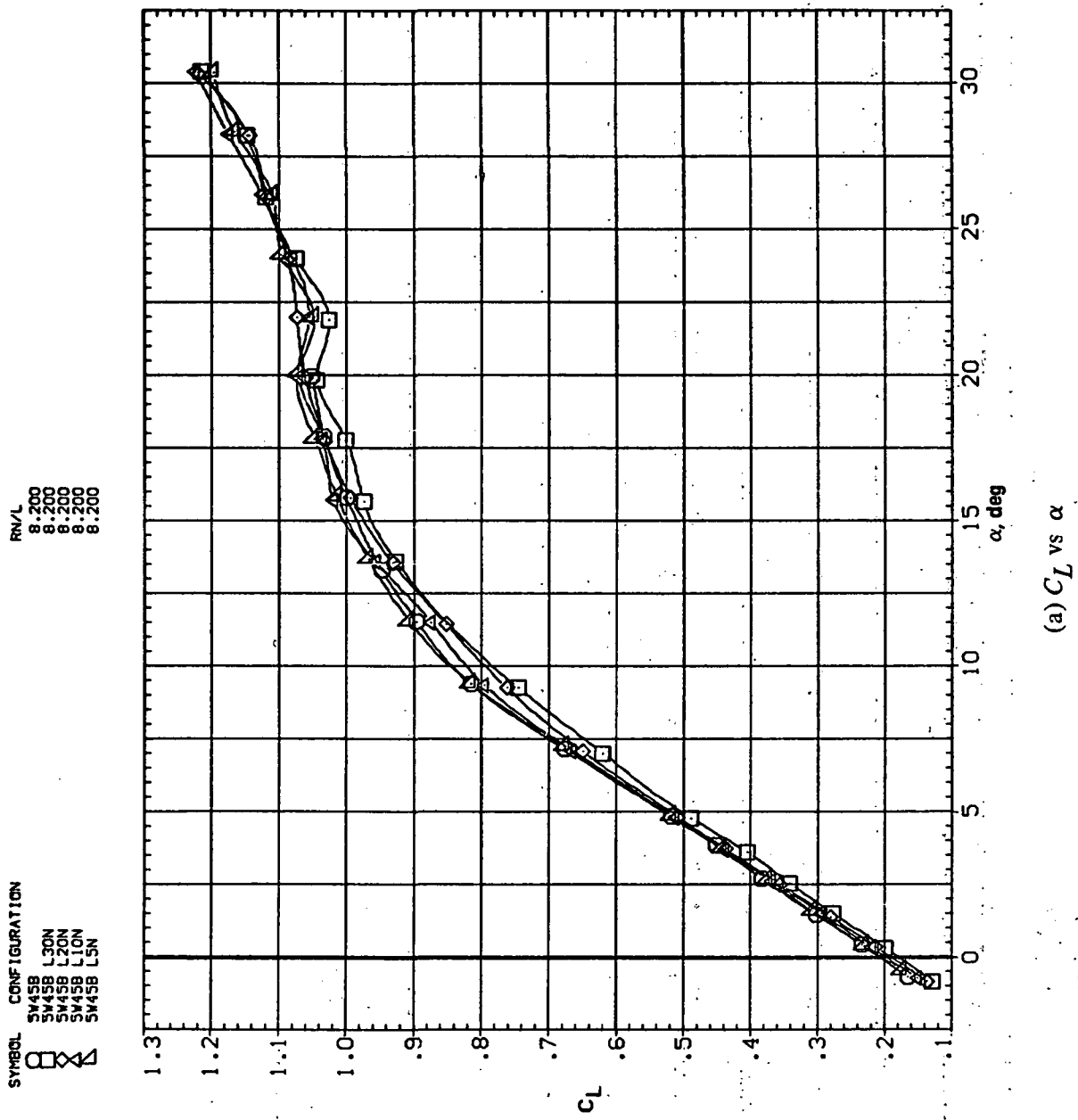
(d)  $L/D$  vs  $C_L$

Figure 7.—Continued.



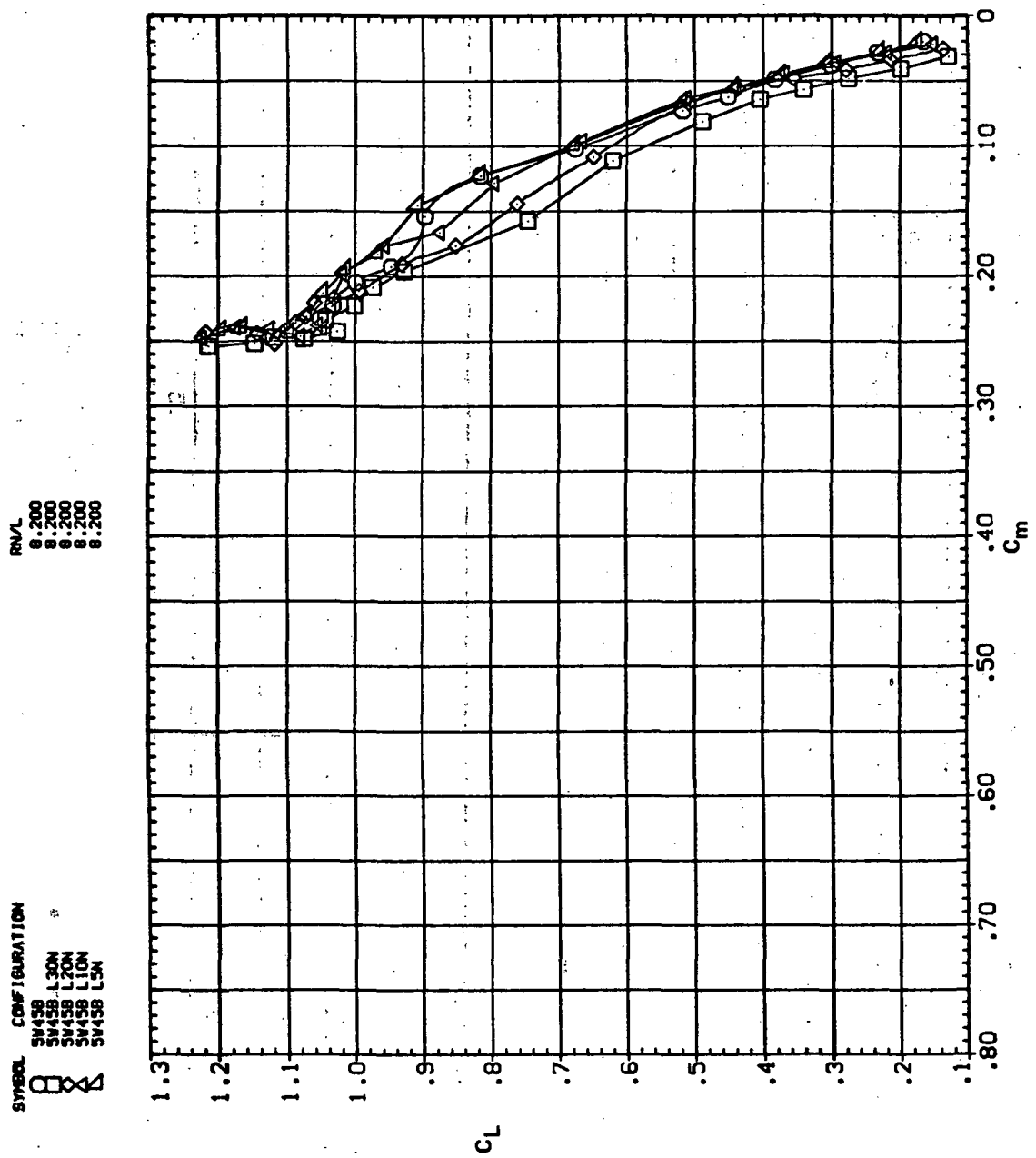
(e)  $C_L$ ,  $C_n$ , and  $C_Y$  vs  $C_L$

Figure 7.— Concluded.



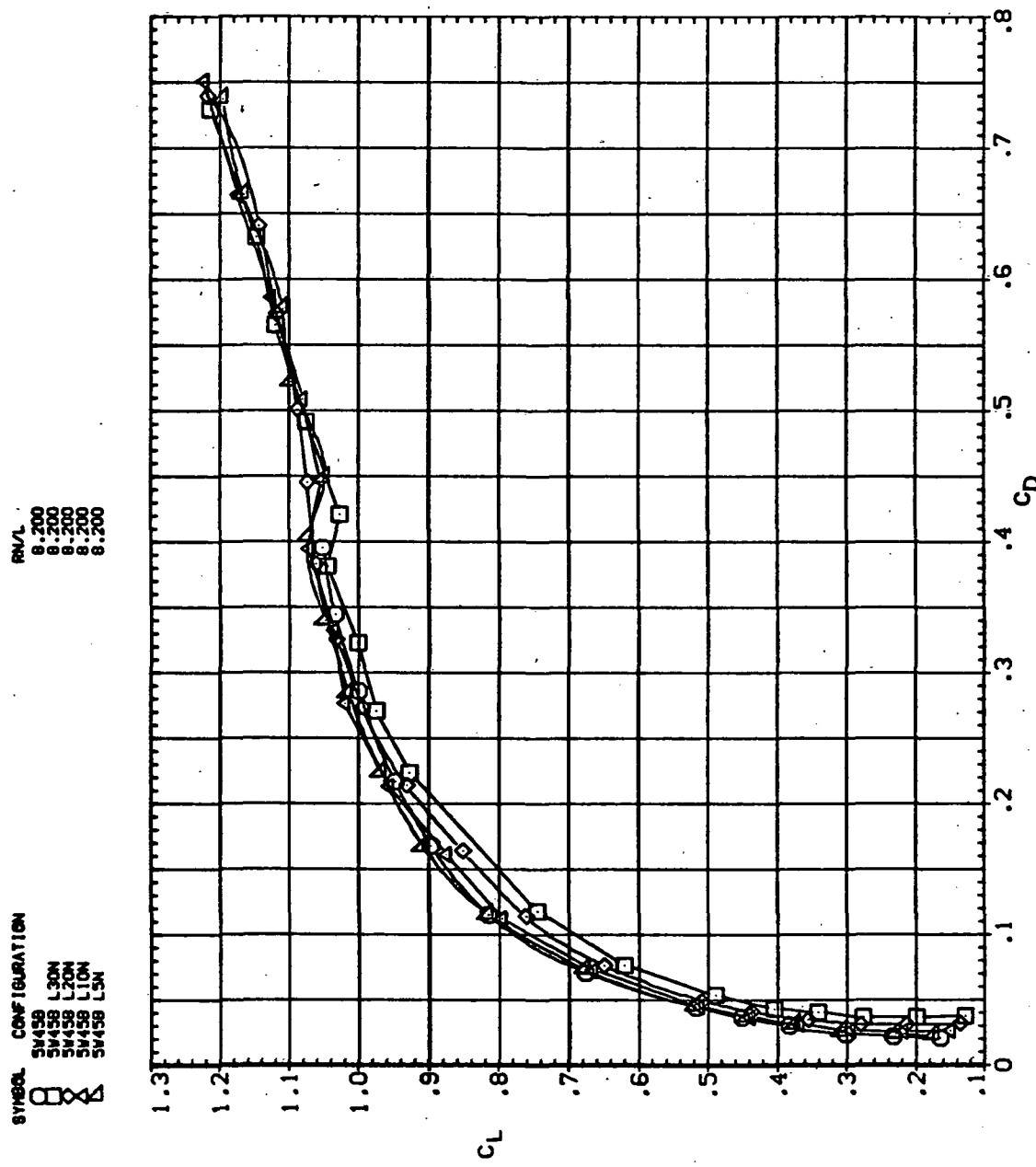
(a)  $C_L$  vs  $\alpha$

Figure 8.— Effect of drooped-nose flaps on the static longitudinal characteristics of the oblique wing: flaps on downstream wing panel only,  $\Lambda = 45^\circ$ ,  $M = 0.9$ .

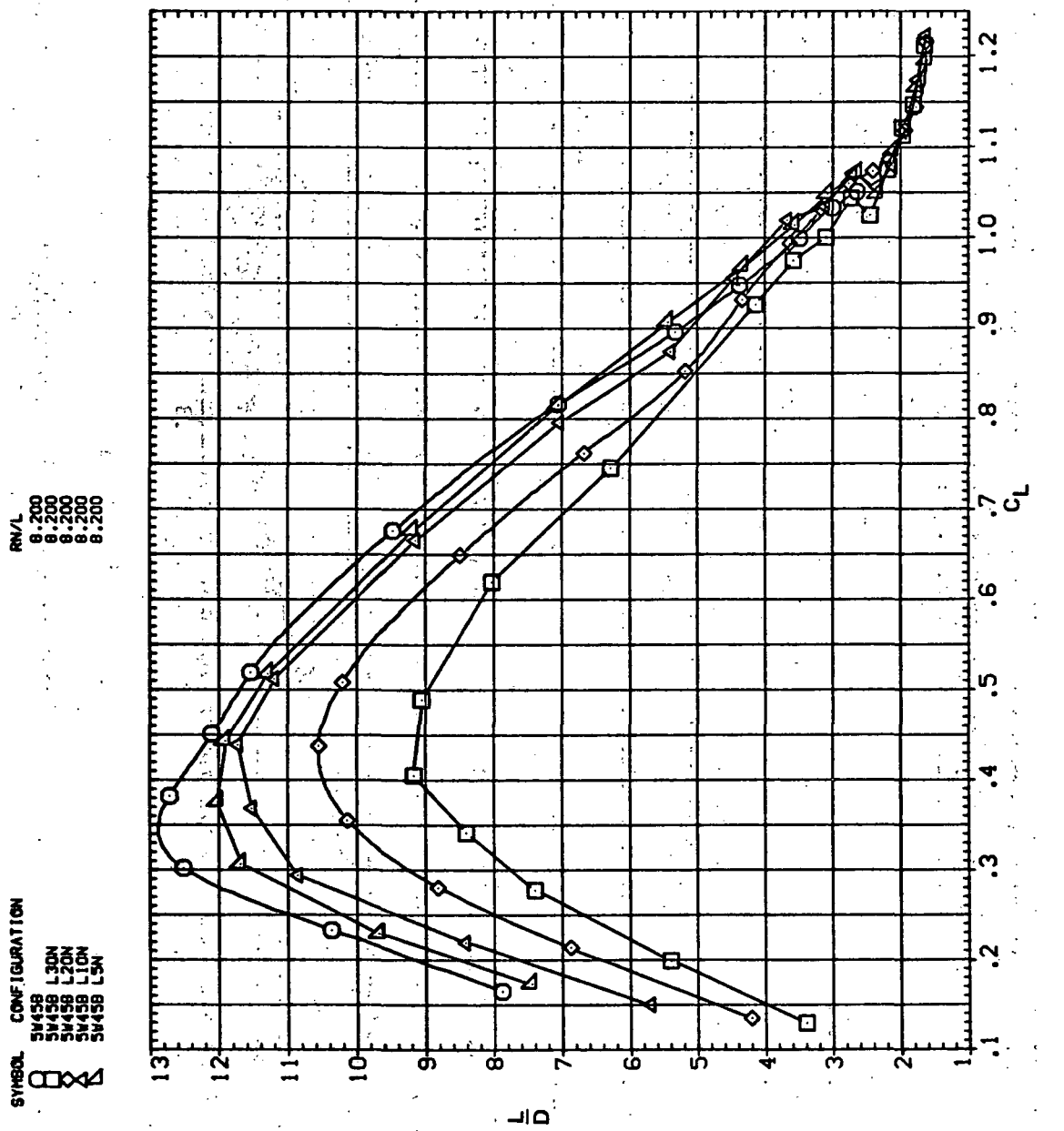


(b)  $C_L$  vs  $C_D$

Figure 8.—Continued.

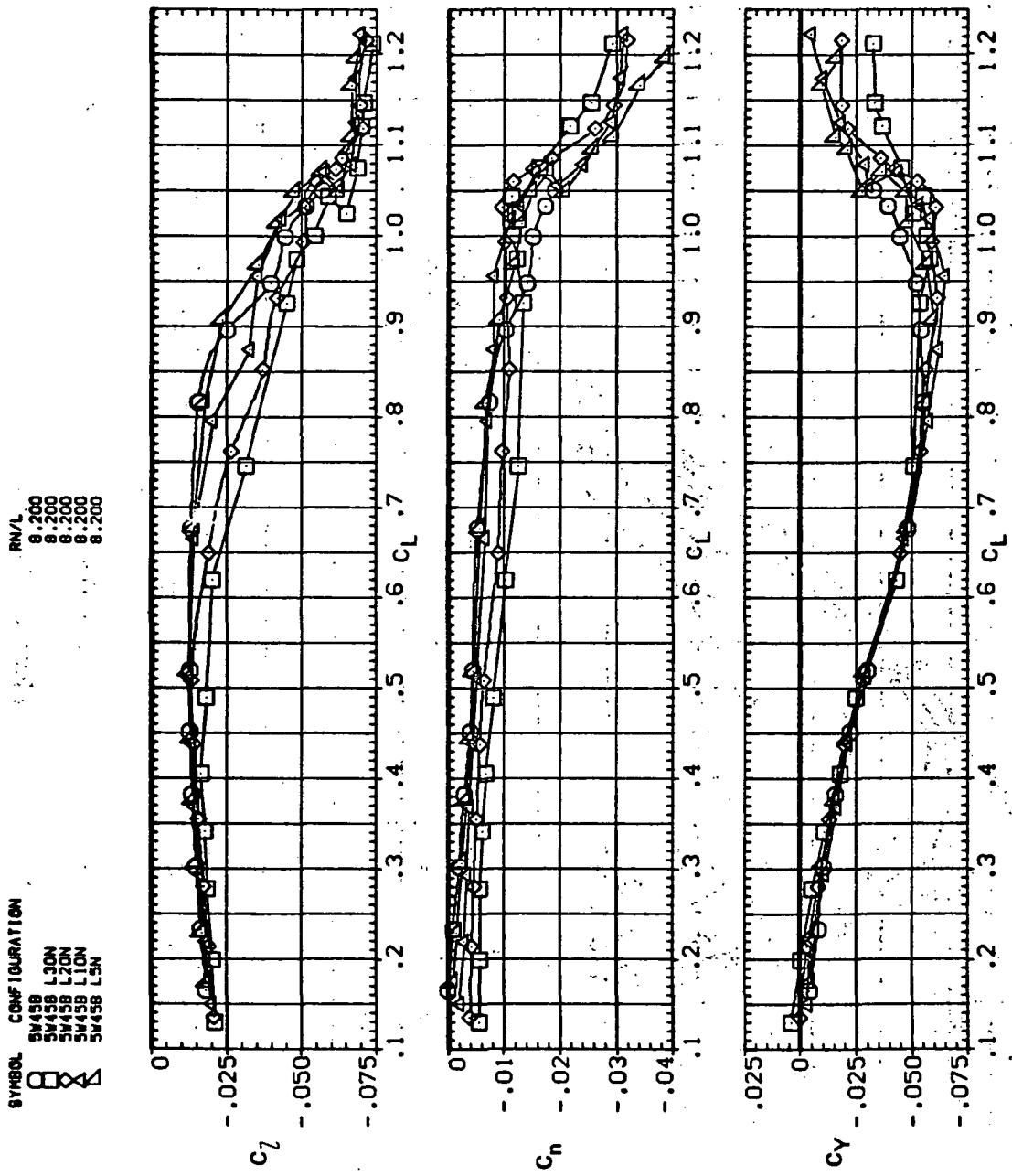


(c)  $C_L$  vs  $C_D$   
Figure 8.—Continued.



(d)  $L/D$  vs  $C_L$

Figure 8.—Continued.



(e)  $C_l$ ,  $C_n$ , and  $C_y$  vs  $C_l$

Figure 8.—Concluded.

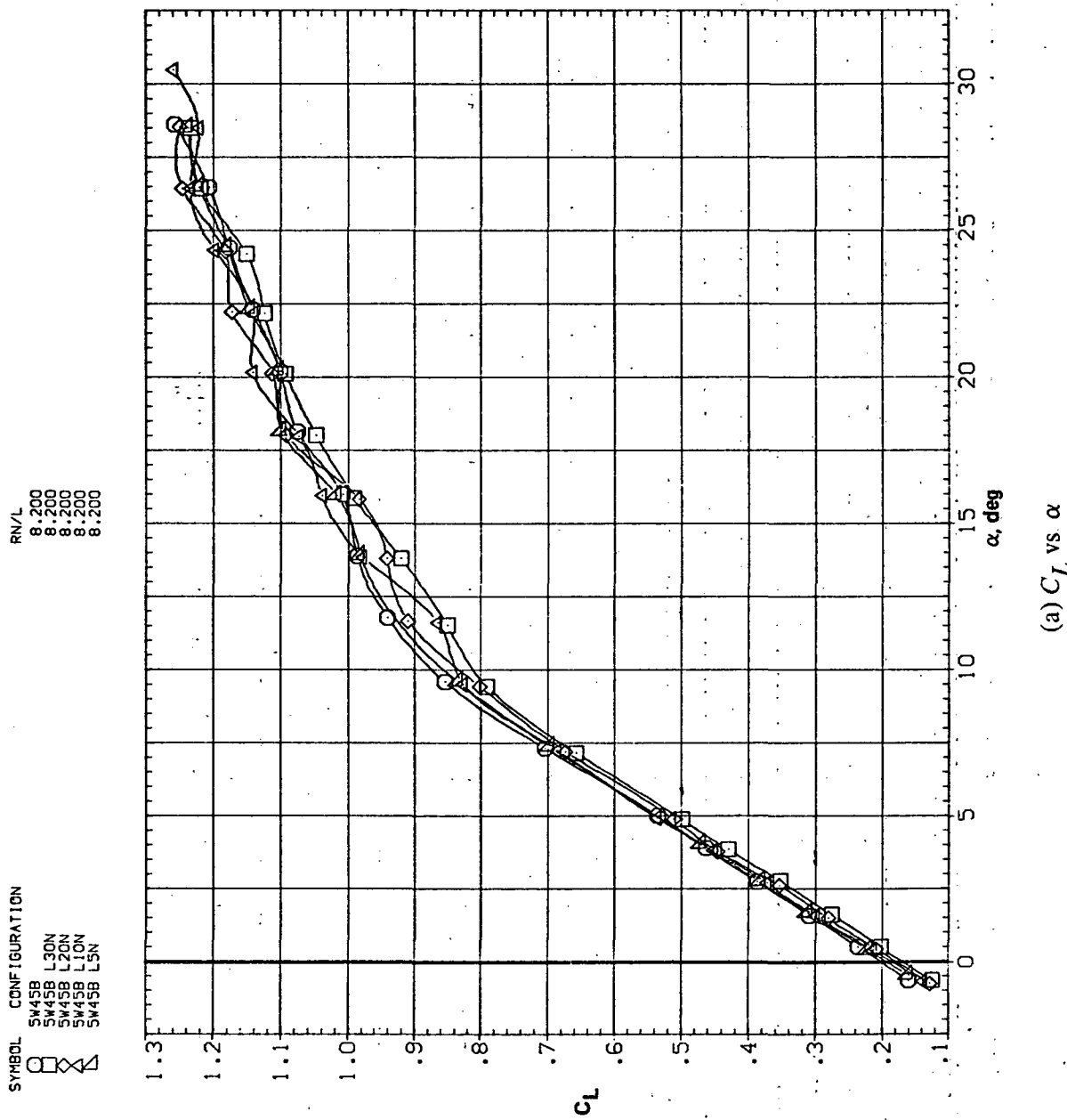
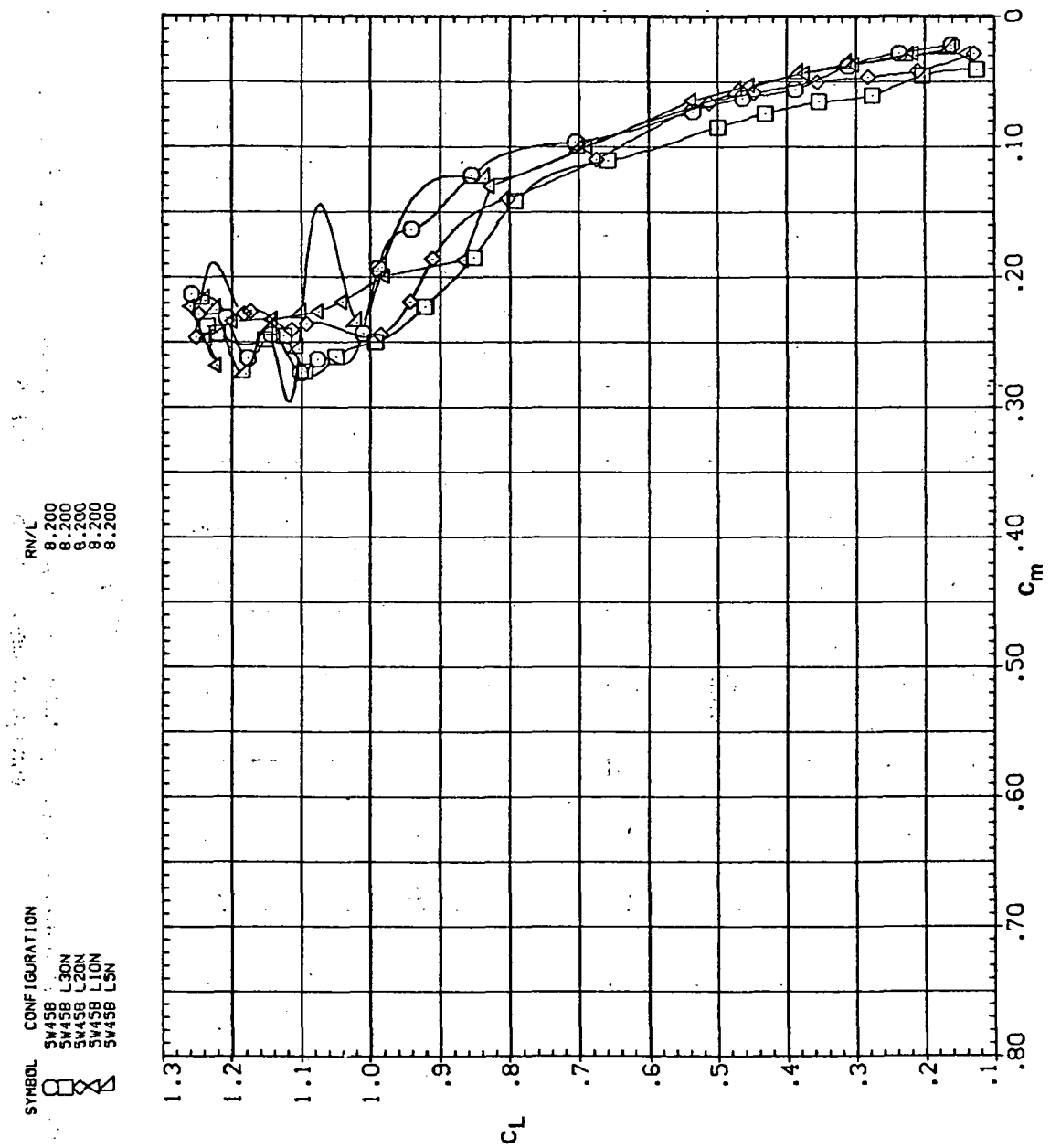
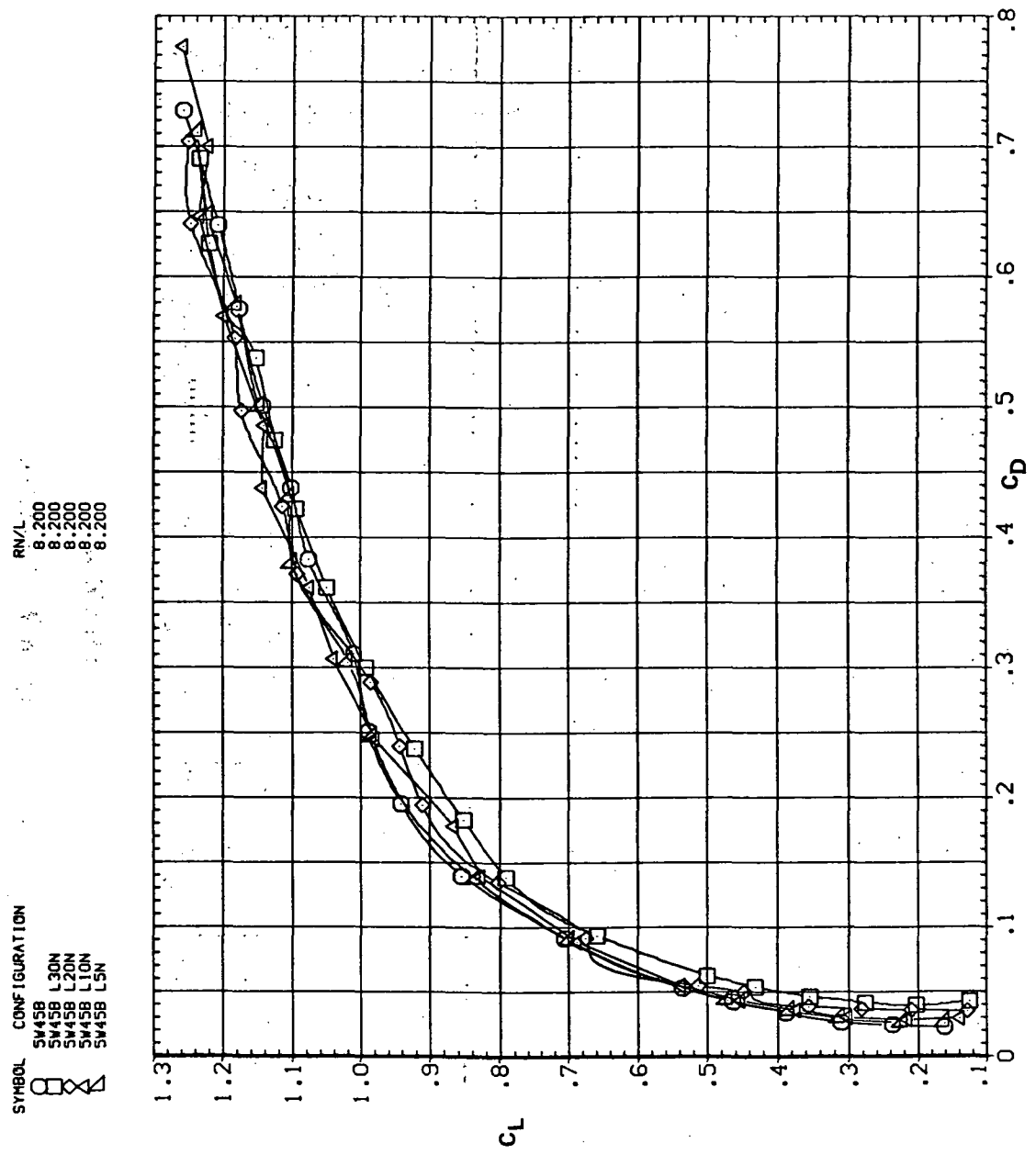
(a)  $C_L$  vs.  $\alpha$ 

Figure 9.— Effect of drooped-nose flaps on the static longitudinal characteristics of the oblique wing: flaps on downstream wing panel only,  $\Lambda = 45^\circ$ ,  $M = 0.95$ .



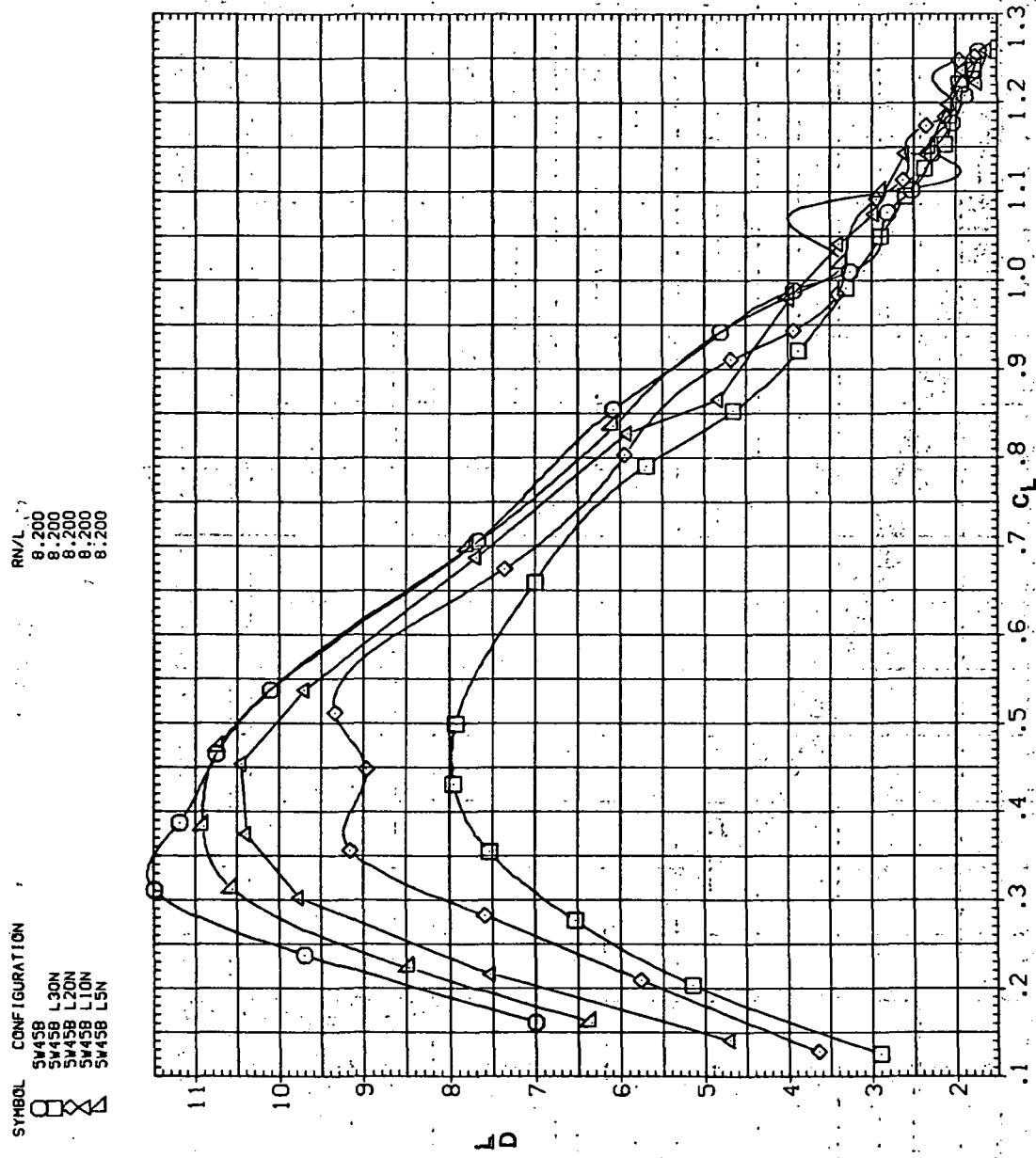
(b)  $C_L$  vs  $C_m$

Figure 9.—Continued.



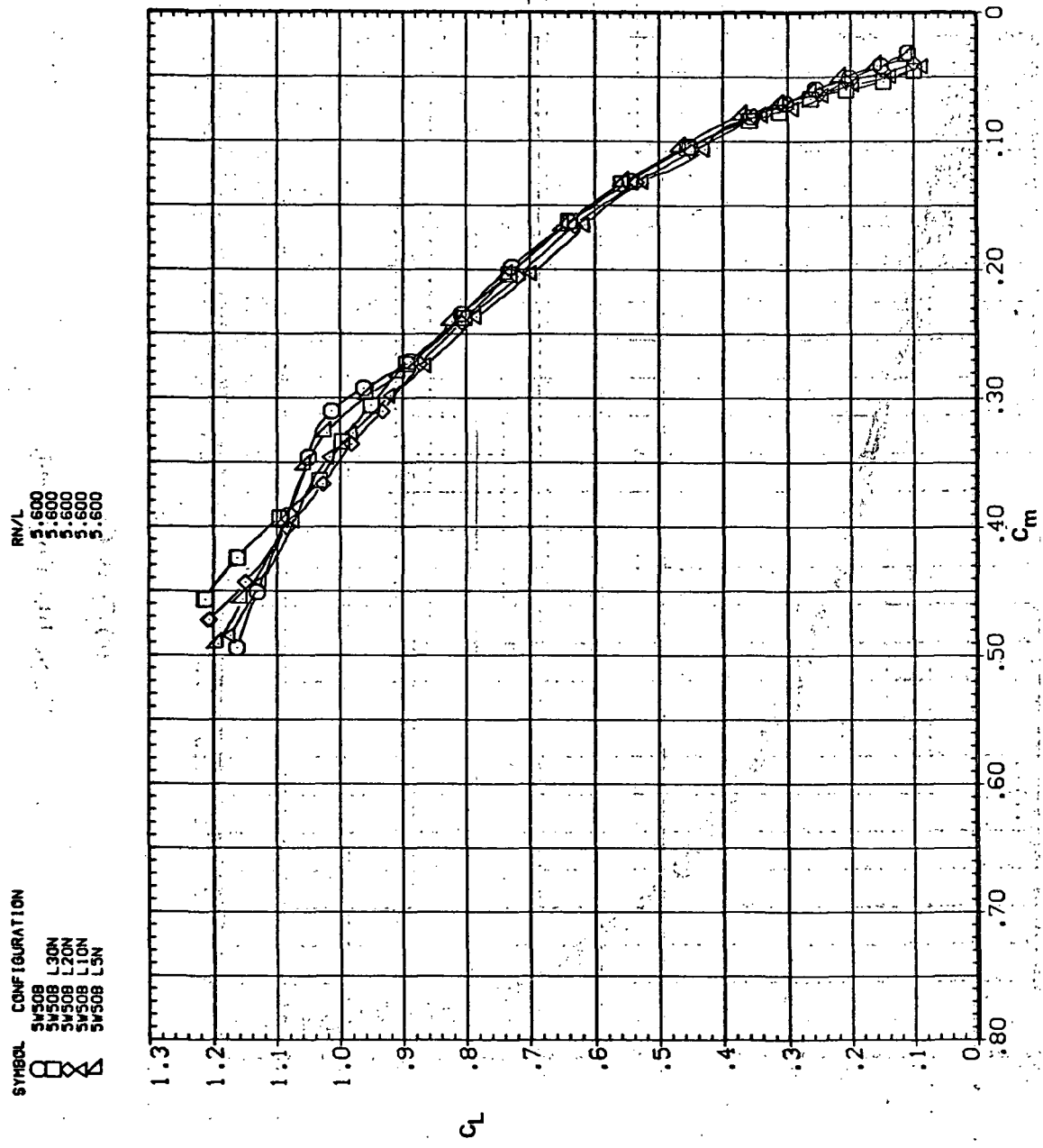
(c)  $C_L$  vs  $C_D$

Figure 9.—Continued.



(d)  $L/D$  vs  $C_L$

Figure 9.—Continued.



(b)  $C_L$  vs.  $C_m$

Figure 10.—Continued.

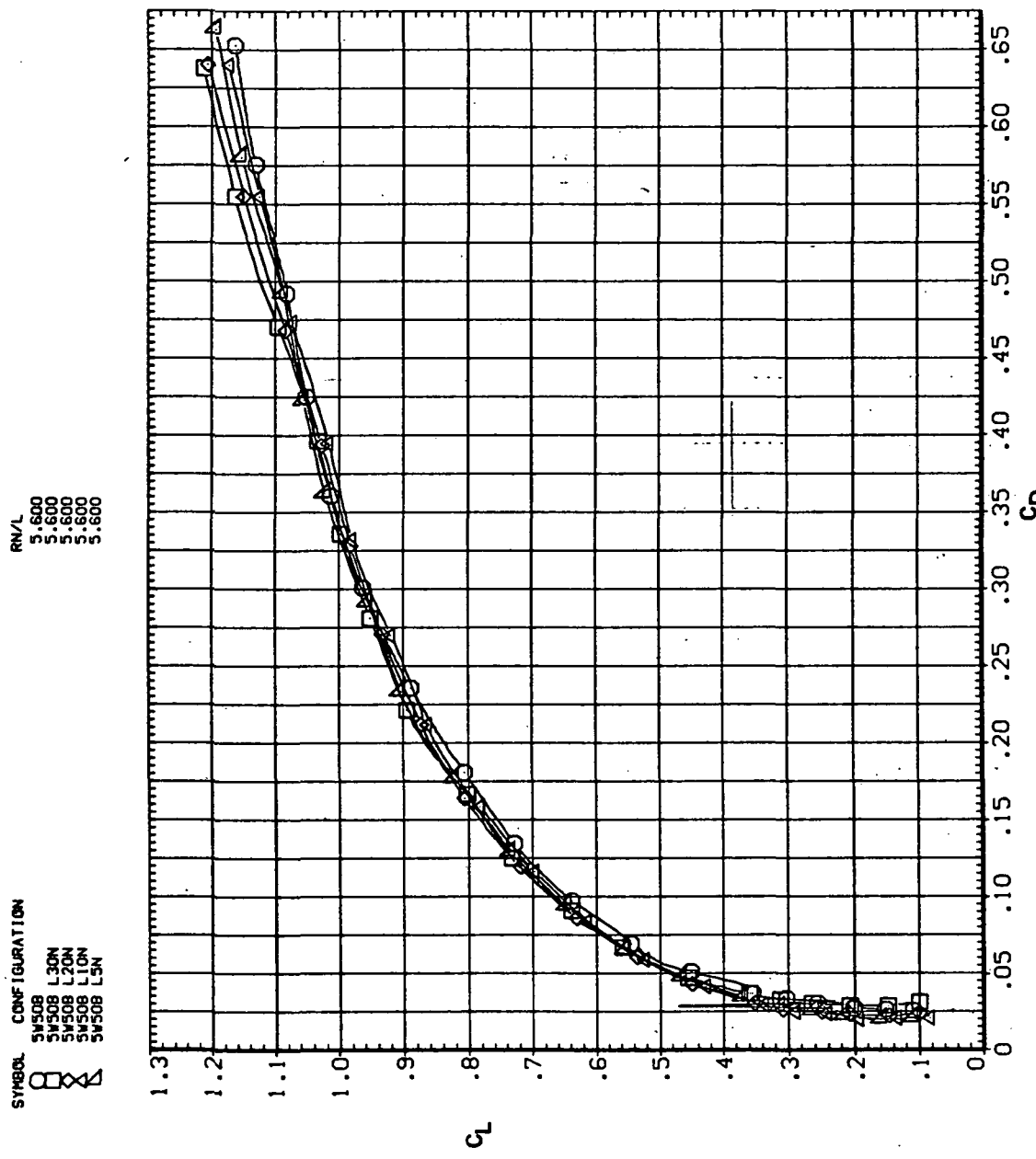


Figure 10(c) is a line graph showing the relationship between lift coefficient ( $C_L$ ) and drag coefficient ( $C_D$ ). The vertical axis ( $C_L$ ) ranges from 0 to 1.3 with increments of 0.1. The horizontal axis ( $C_D$ ) ranges from 0 to 0.65 with increments of 0.05. The graph displays five data series, each representing a different configuration of the aircraft. The configurations are: 5W08 (open square), 5W08 L30N (open circle), 5W08 L20N (cross), 5W08 L10N (x), and 5W08 L5N (open triangle). All series show a similar trend: a steep initial decrease in  $C_D$  as  $C_L$  increases from 1.0 to 0.9, followed by a more gradual, nearly linear decrease as  $C_L$  continues to decrease towards 0.3. The data points are connected by straight line segments.

SYMBOL	CONFIGURATION
○	5W08 L30N
×	5W08 L20N
△	5W08 L10N
△	5W08 L5N

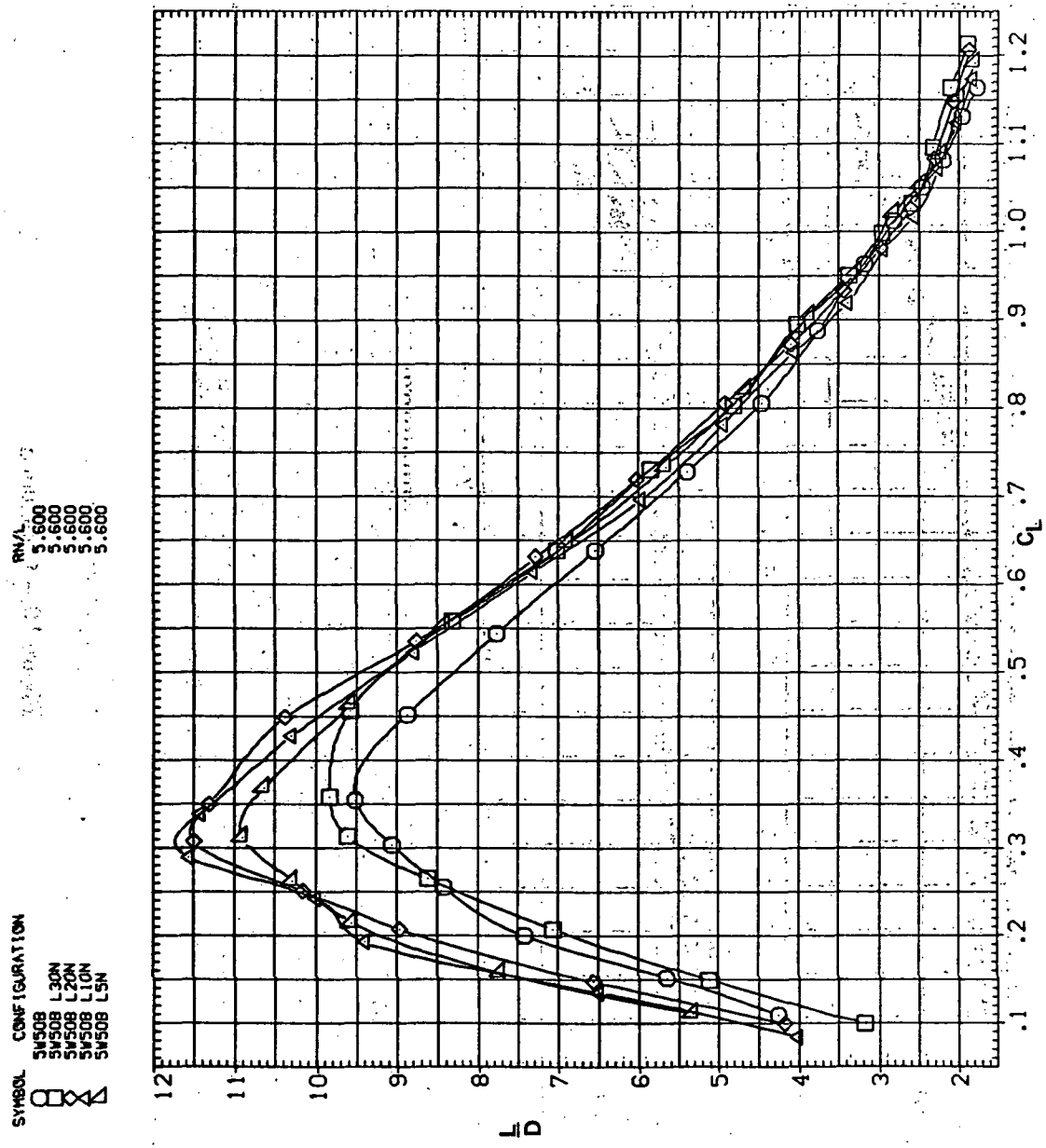
(d)  $L/D$  vs.  $C_L$ 

Figure 10.—Continued.

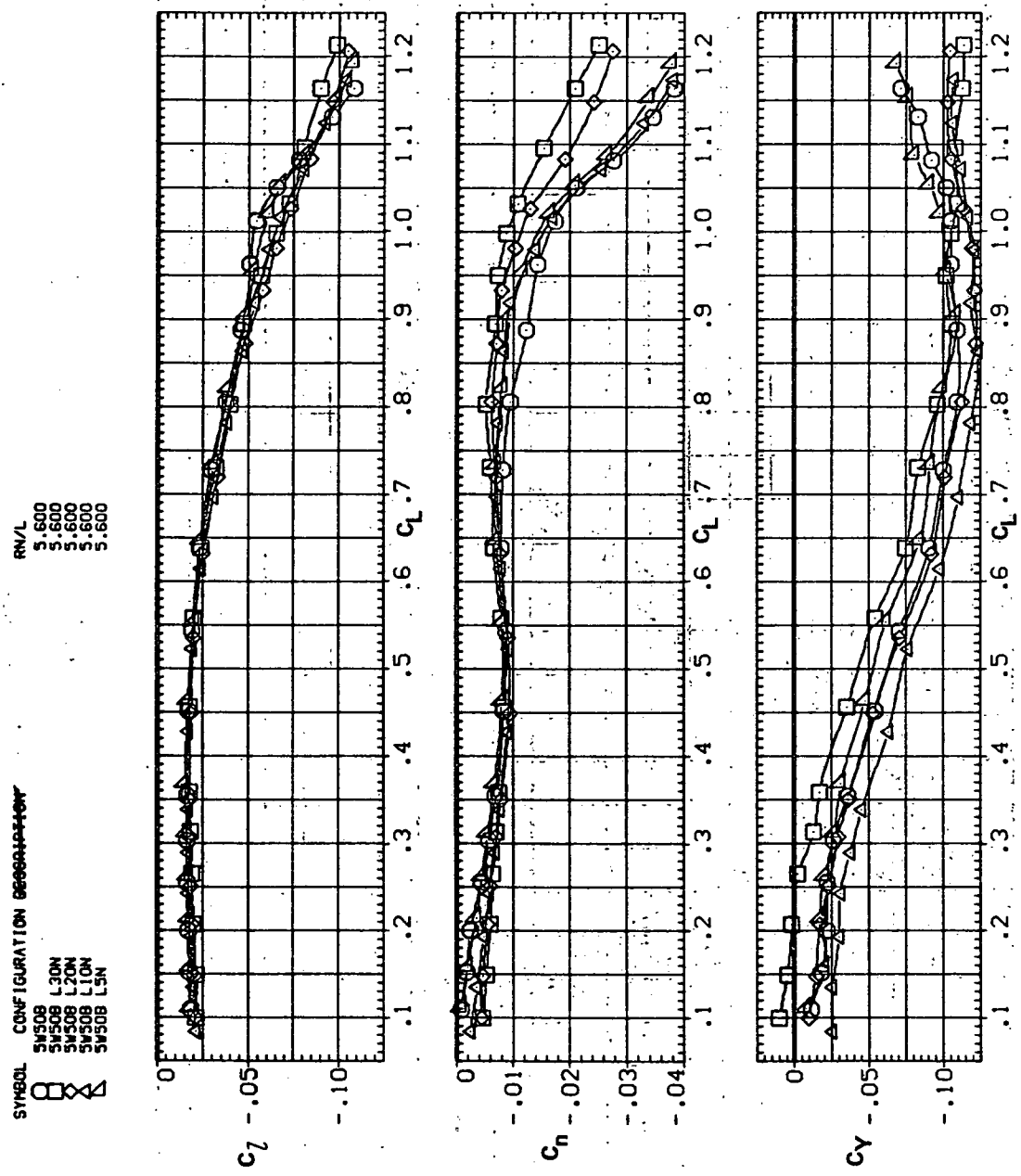


Figure 10.—Concluded.

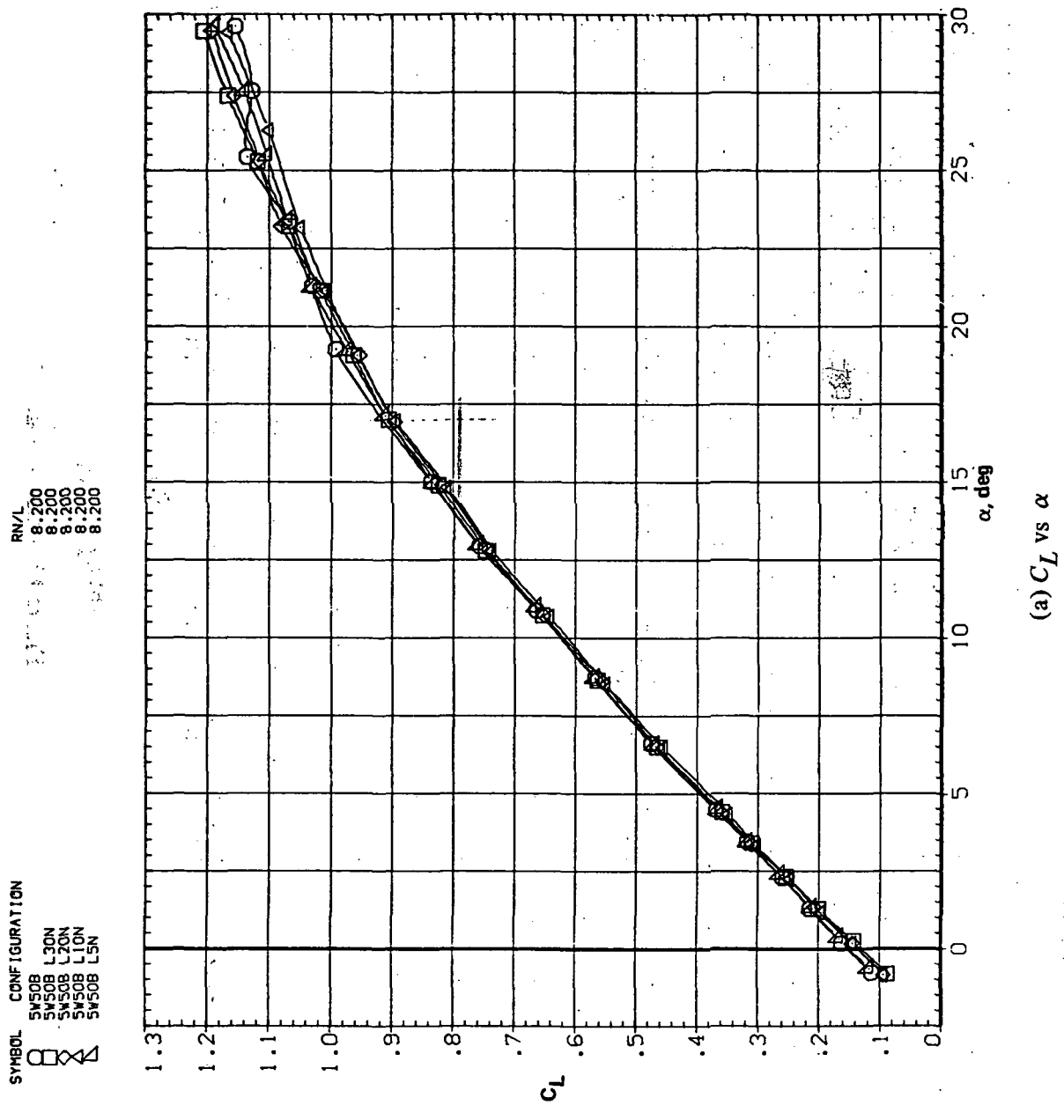
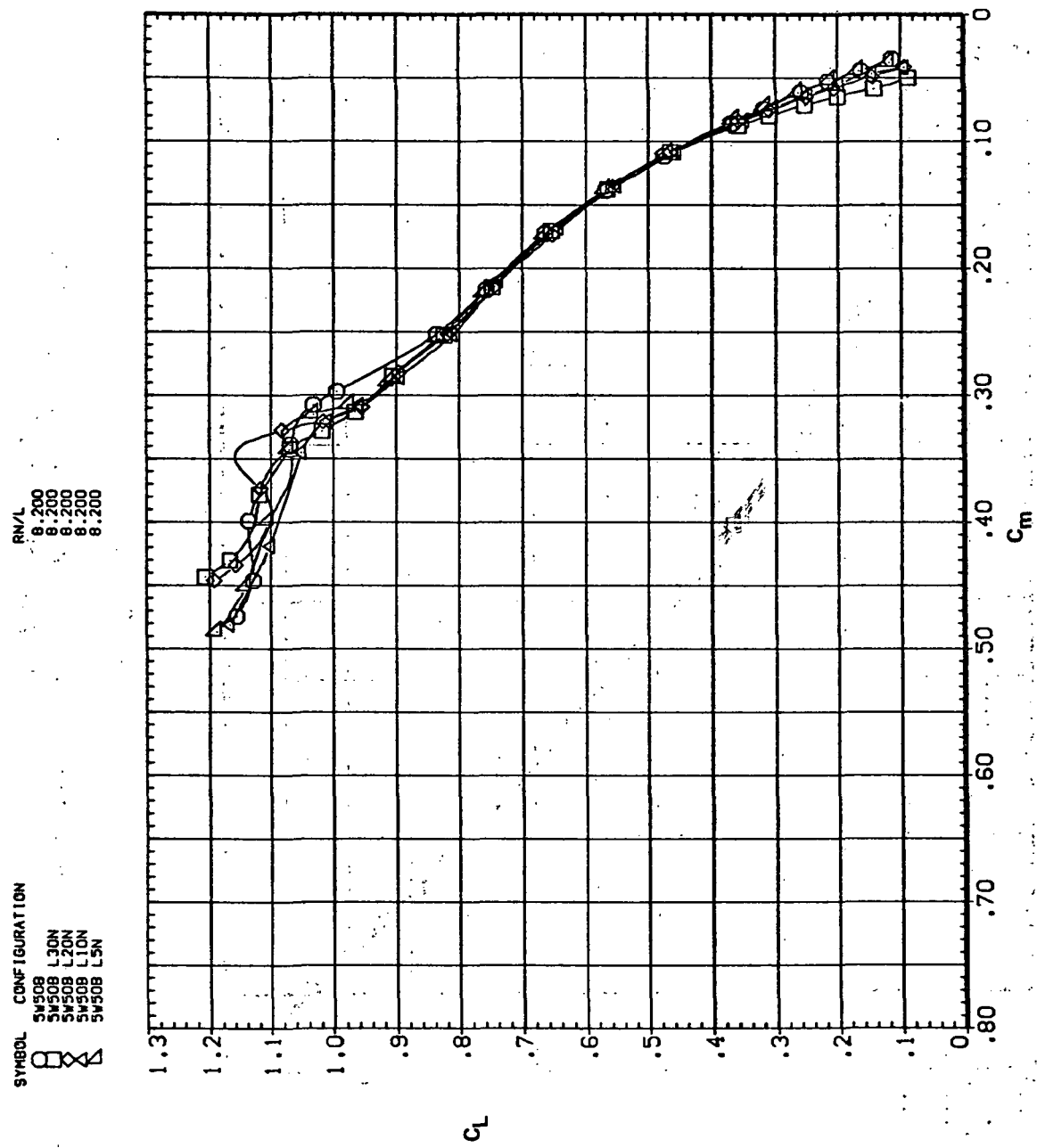


Figure 11.— Effect of drooped-nose flaps on the static longitudinal characteristics of the oblique wing: flaps on downstream wing panel only,  $\Lambda = 50^\circ$ ,  $M = 0.4$ .



(b)  $C_L$  vs  $C_m$

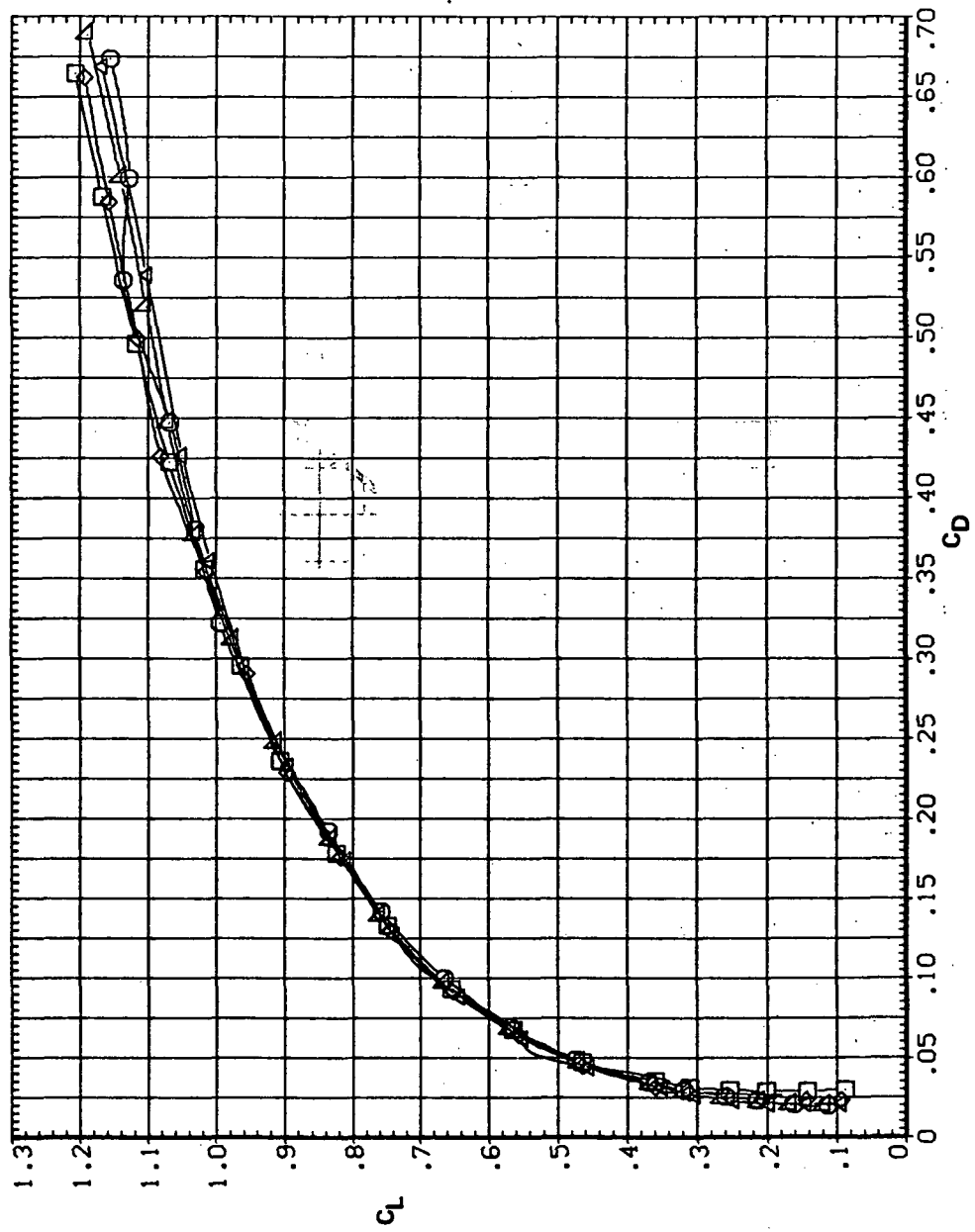
Figure 11.—Continued.

SYMBOL CONFIGURATION

○	SW508
◇	SW508 L3DN
△	SW508 L2DN
□	SW508 L1DN
△	SW508 LSN

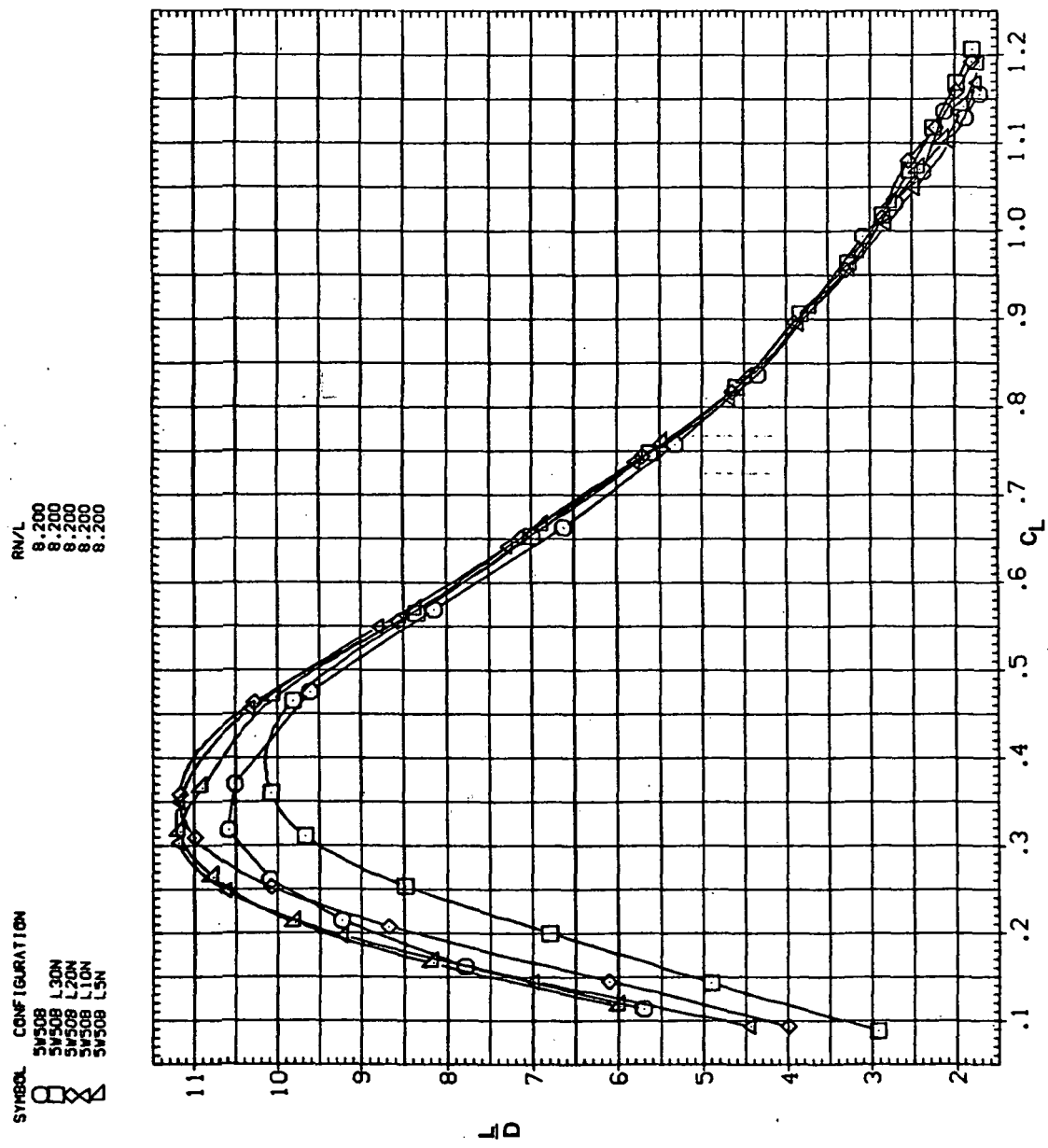
RN/L

8.200
8.200
8.200
8.200
8.200
8.200



(c)  $C_L$  vs  $C_D$

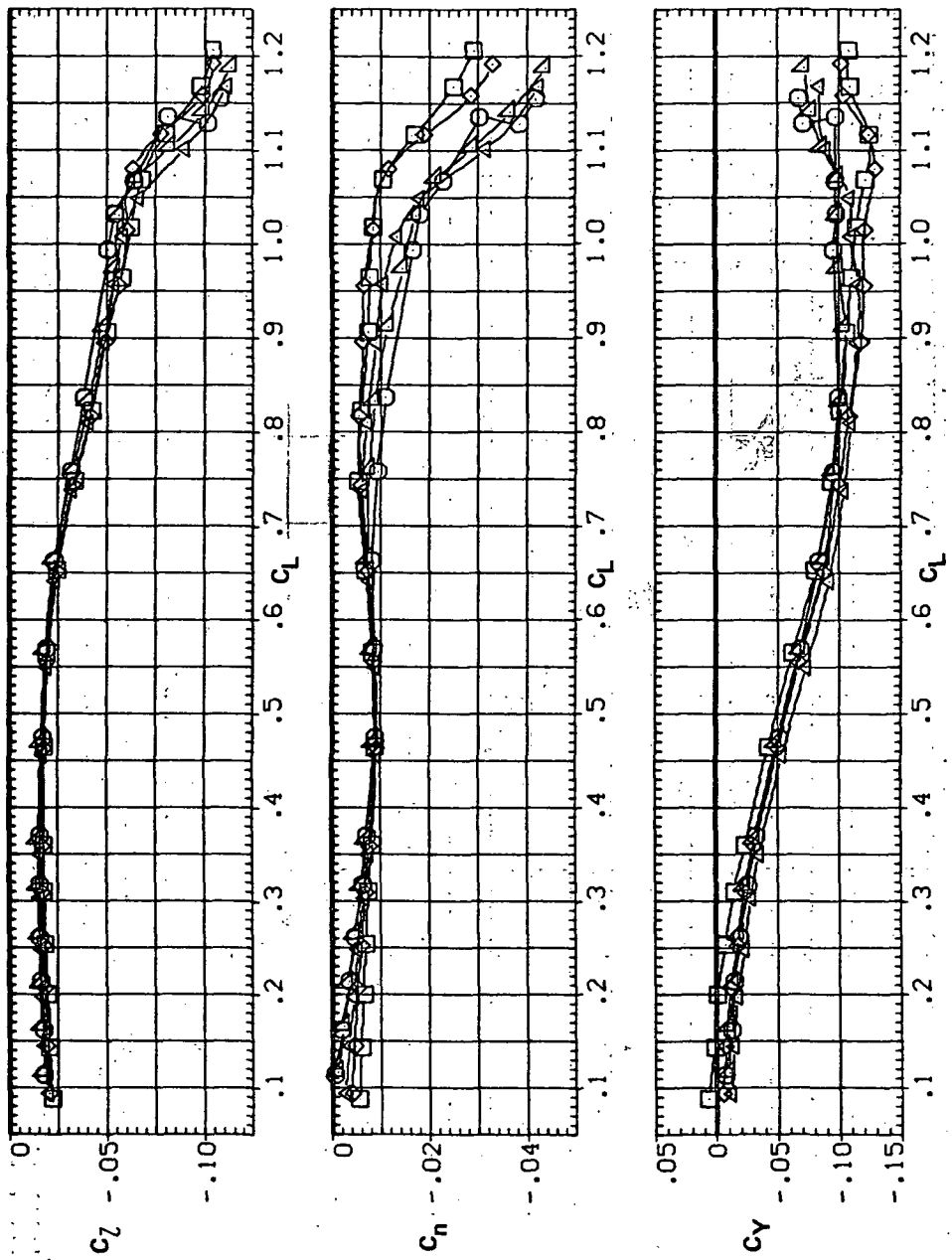
Figure 11.—Continued.



(d)  $L/D$  vs  $C_L$

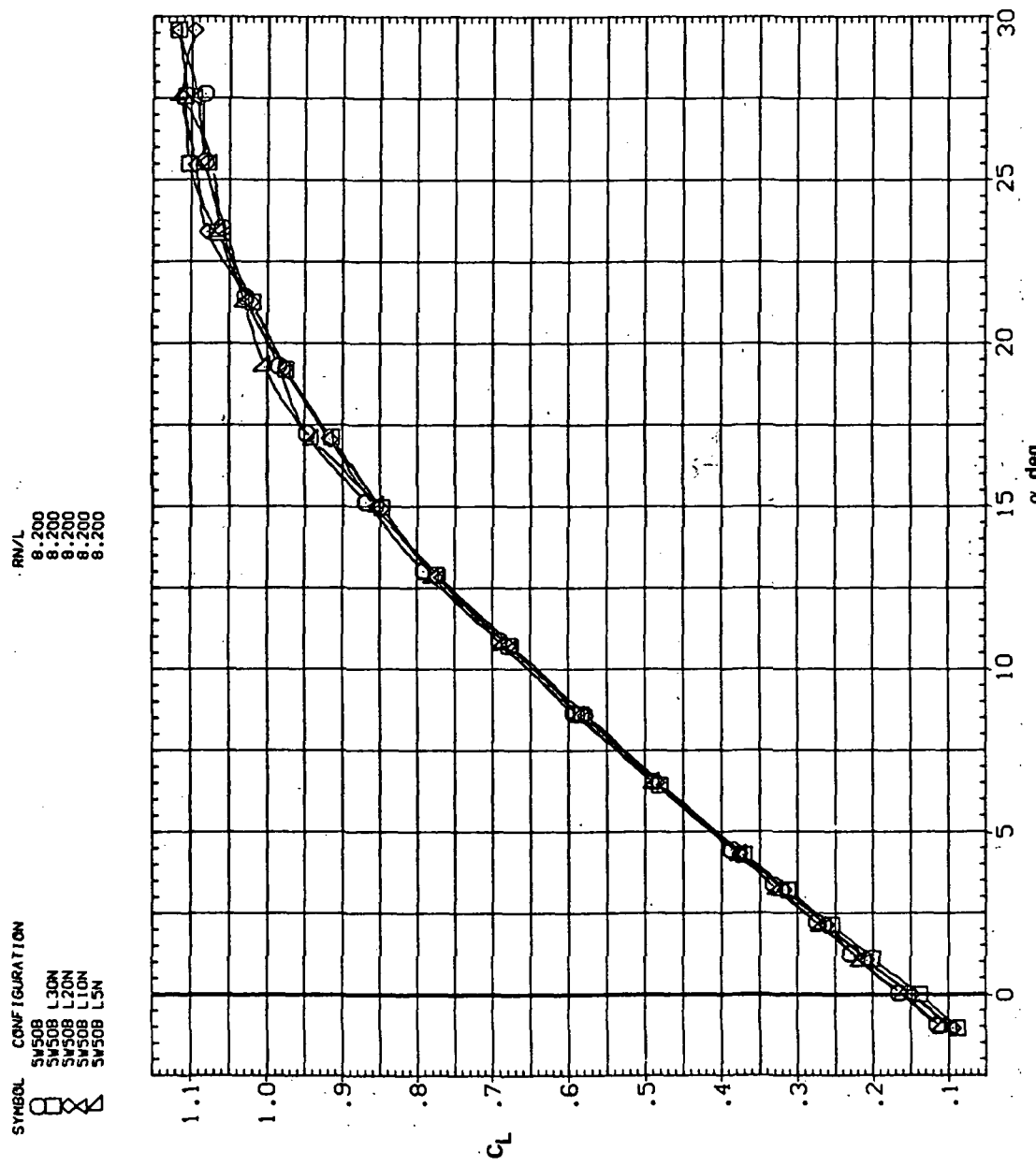
Figure 11.— Continued.

SYMBOL CONFIGURATION  
 5W50B 5W50B 5W50B 5W50B  
 5W50B L30N 5W50B L20N 5W50B L10N 5W50B L5N  
 8.200 8.200 8.200 8.200



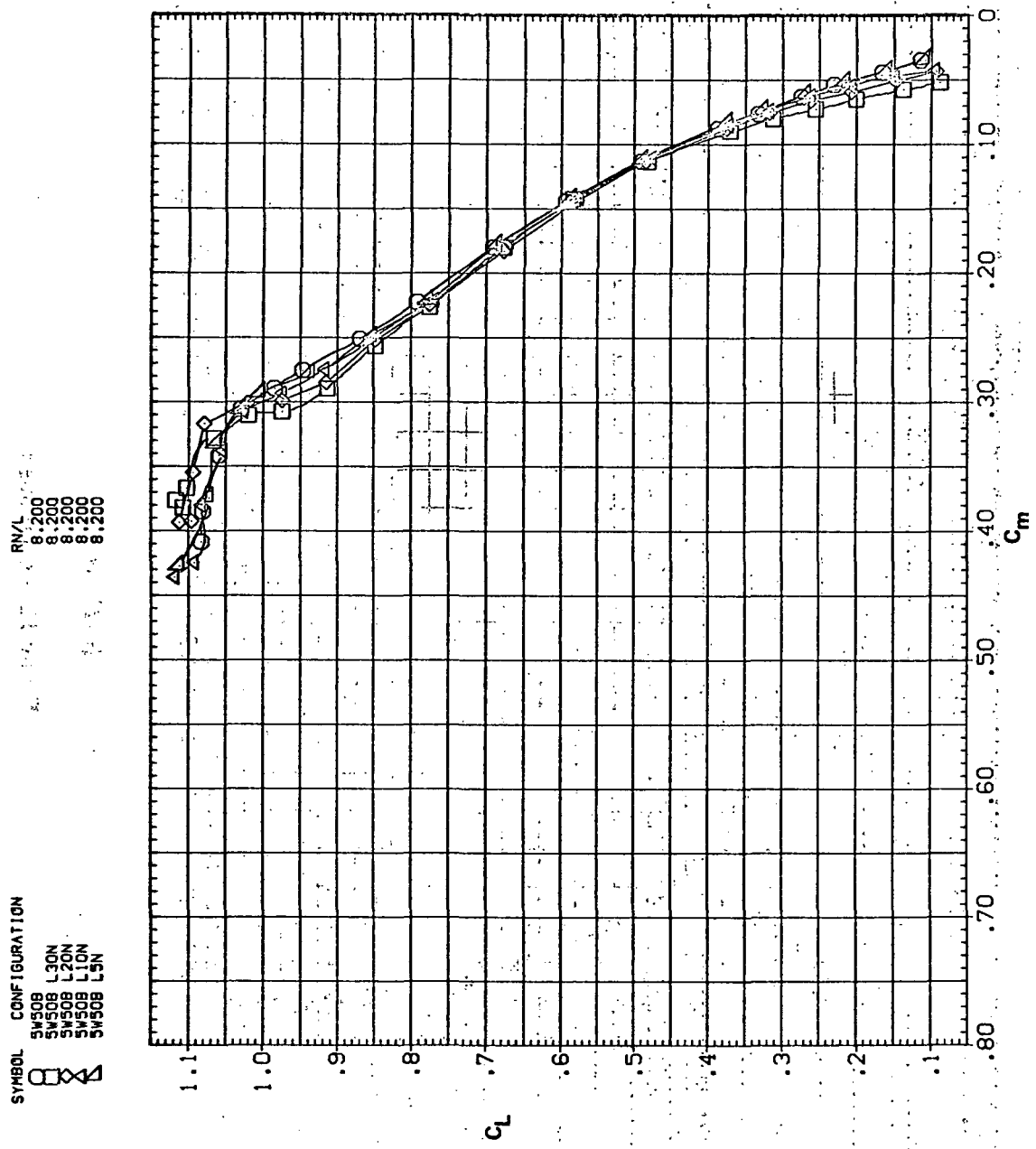
(e)  $C_l$ ,  $C_n$ , and  $C_Y$  vs  $C_L$

Figure 11.—Concluded.



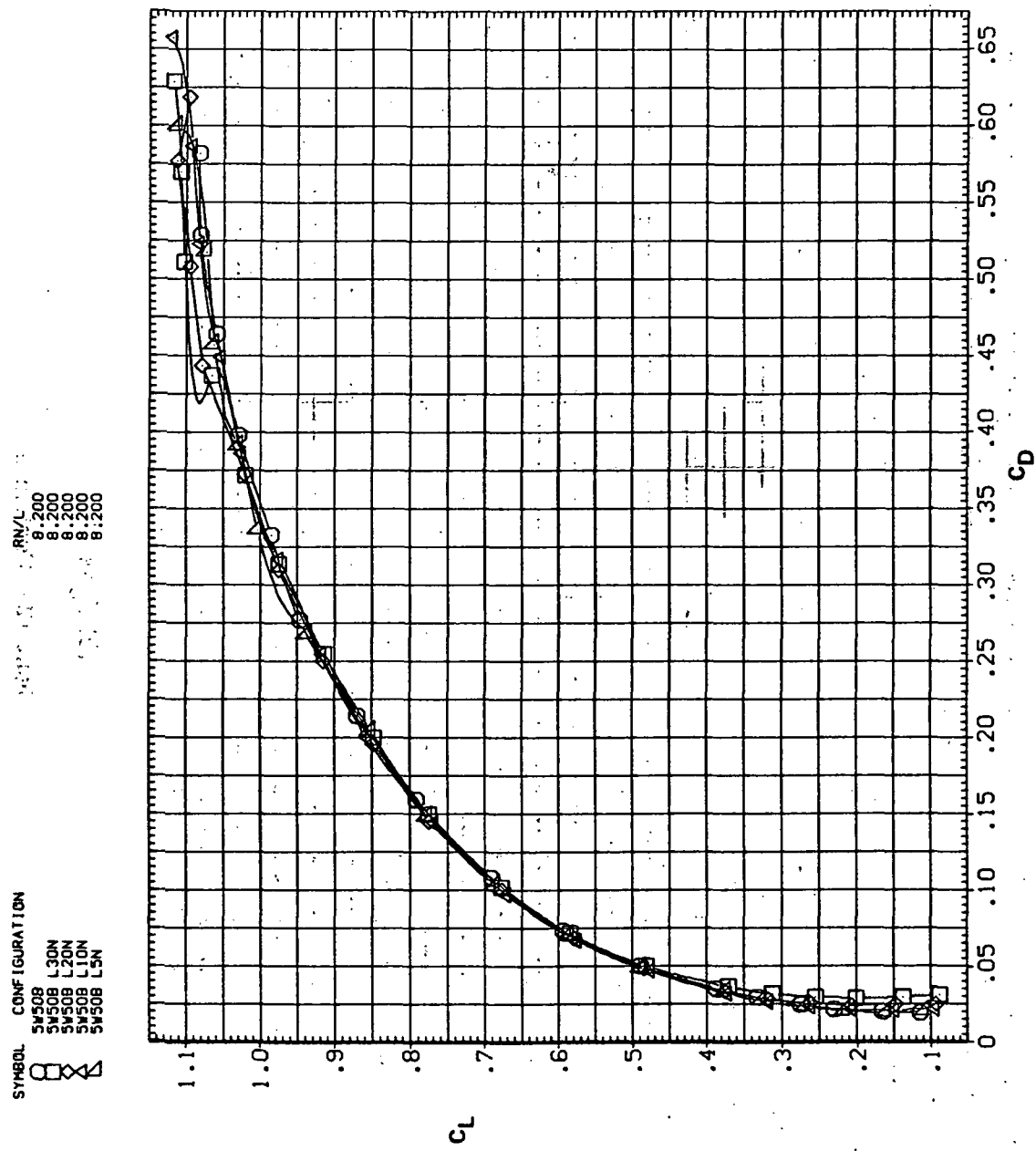
(a)  $C_L$  vs.  $\alpha$

Figure 12.— Effect of drooped-nose flaps on the static longitudinal characteristics of the oblique wing: flaps on downstream wing panel only,  $\Lambda = 50^\circ, M = 0.6$ .



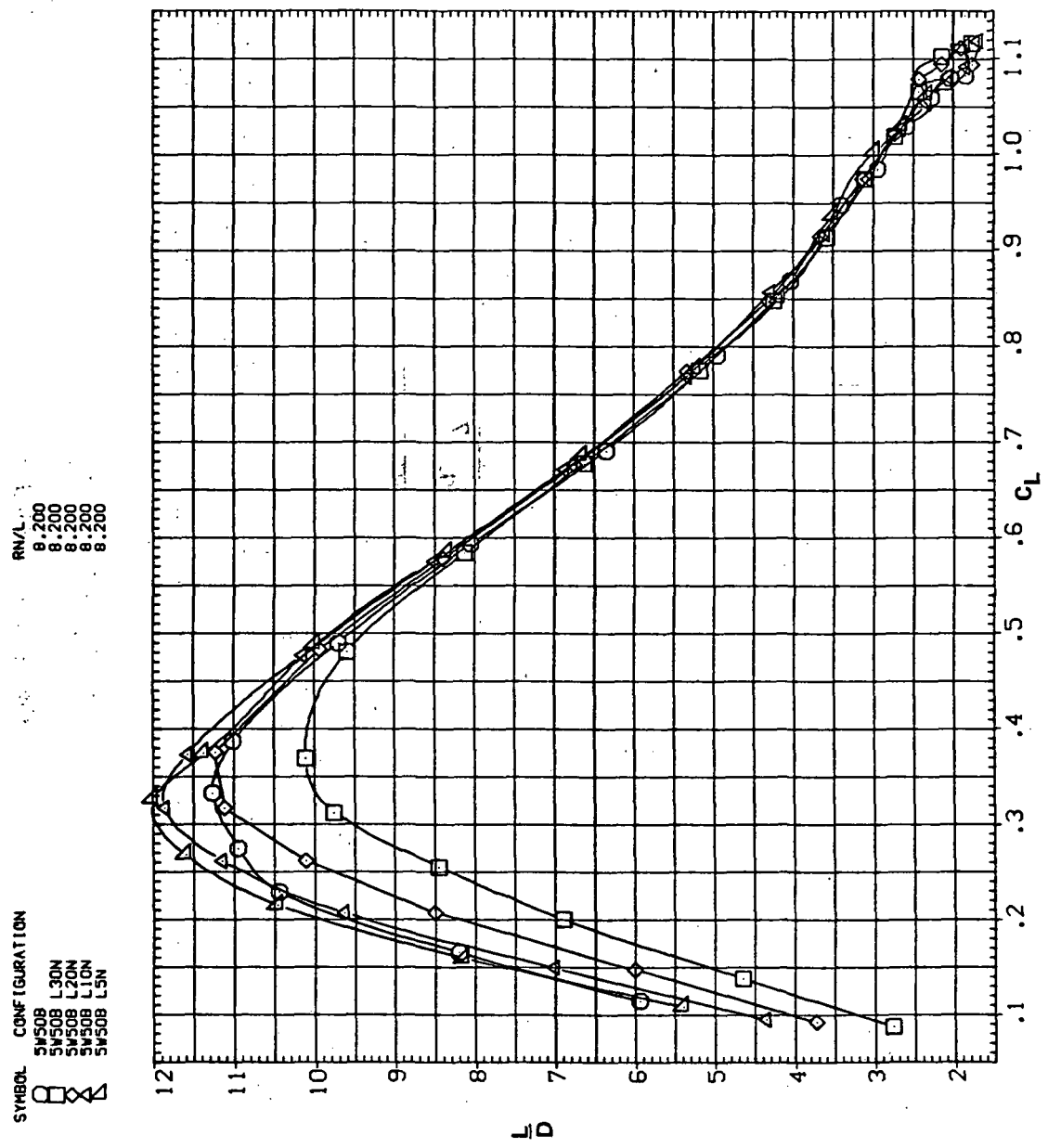
(b)  $C_L$  vs  $C_m$

Figure 12.—Continued.



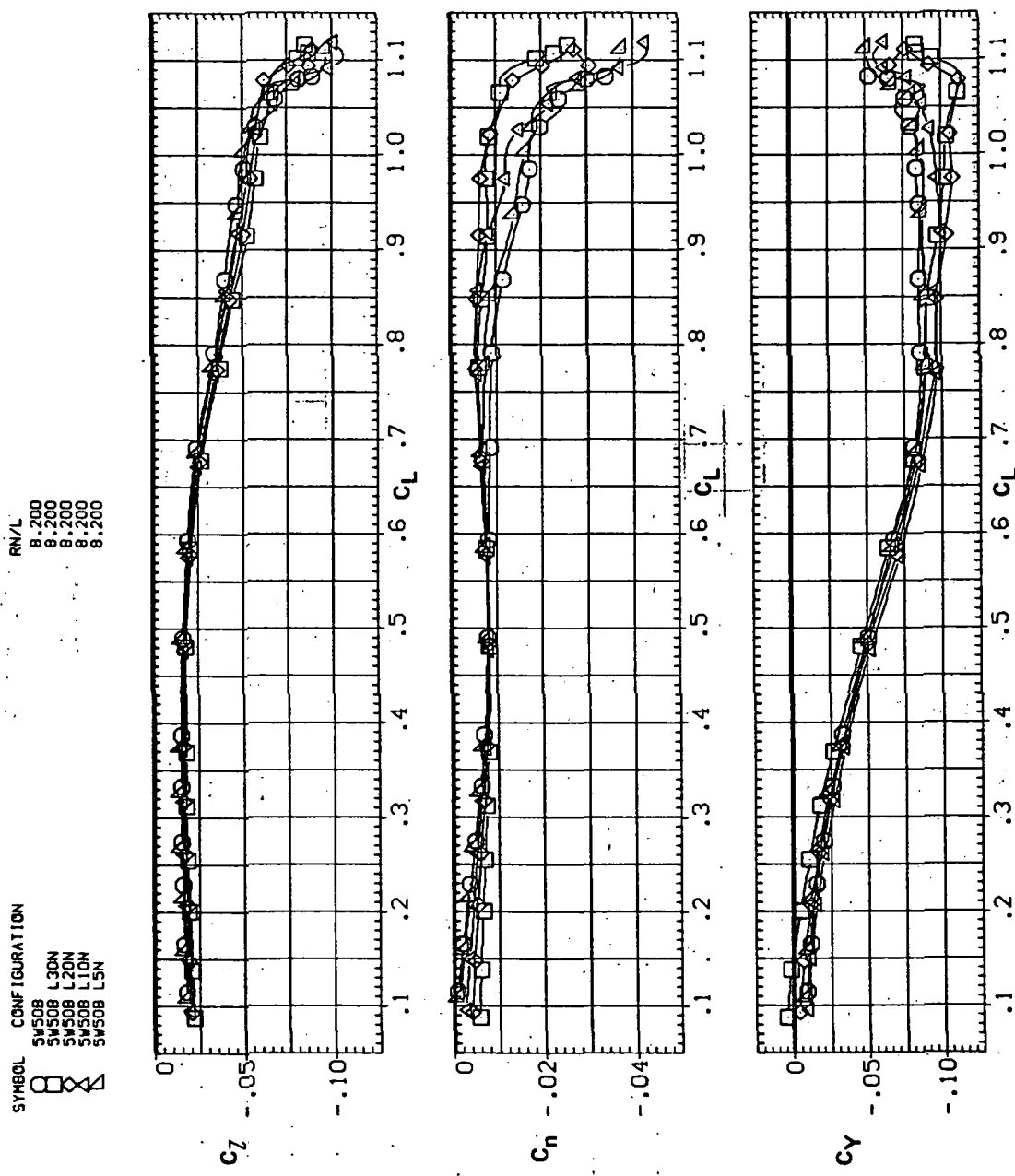
(c)  $C_L$  vs  $C_D$

Figure 12.—Continued.



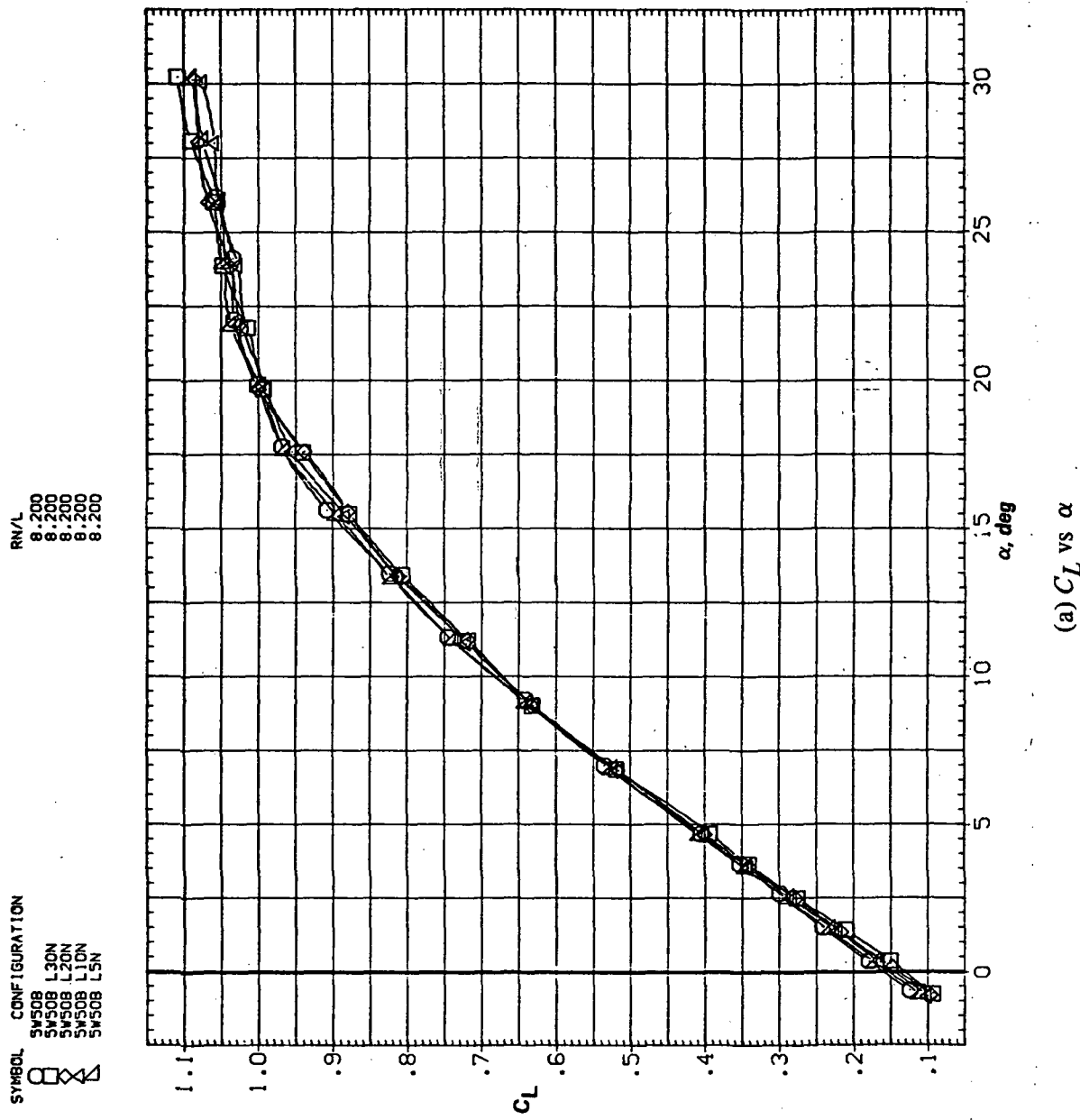
(d)  $L/D$  vs  $C_L$

Figure 12.—Continued.



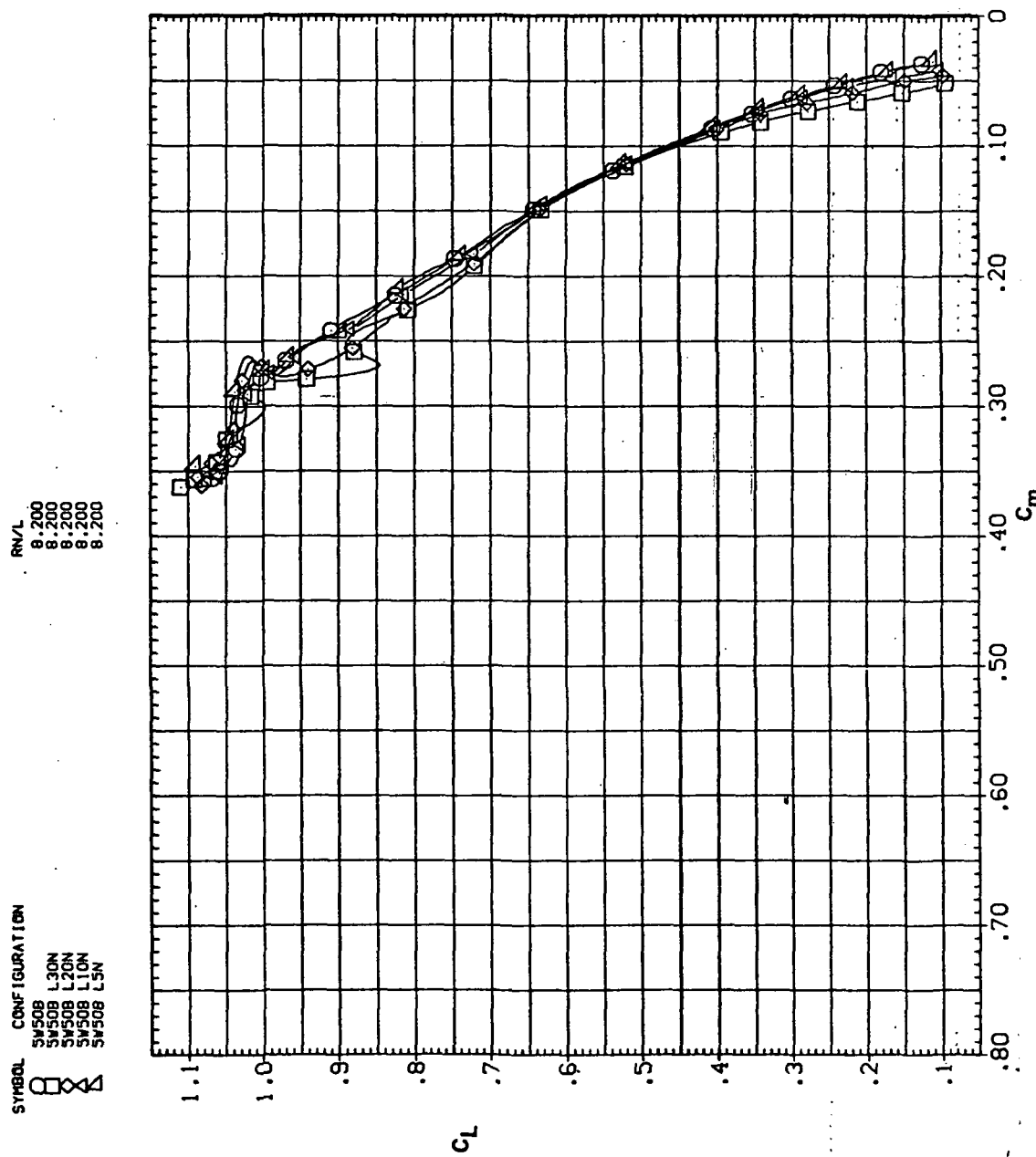
(e)  $C_l$ ,  $C_n$ , and  $C_Y$  vs  $C_L$

Figure 12.— Concluded.

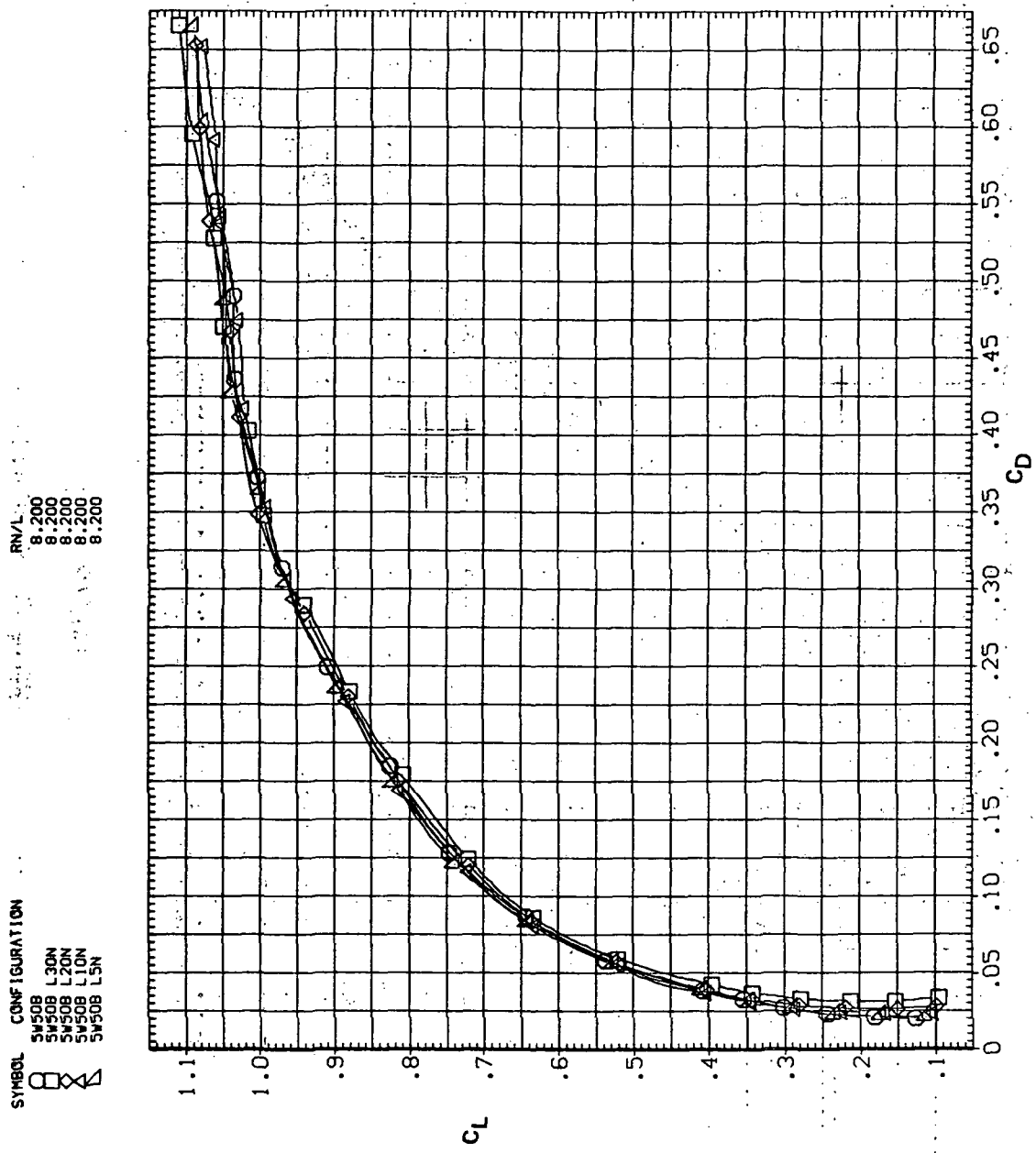


(a)  $C_L$  vs  $\alpha$

Figure 13.— Effect of drooped-nose flaps on the static longitudinal characteristics of the oblique wing: flaps on downstream wing panel only,  $\Lambda = 50^\circ$ ,  $M = 0.8$ .

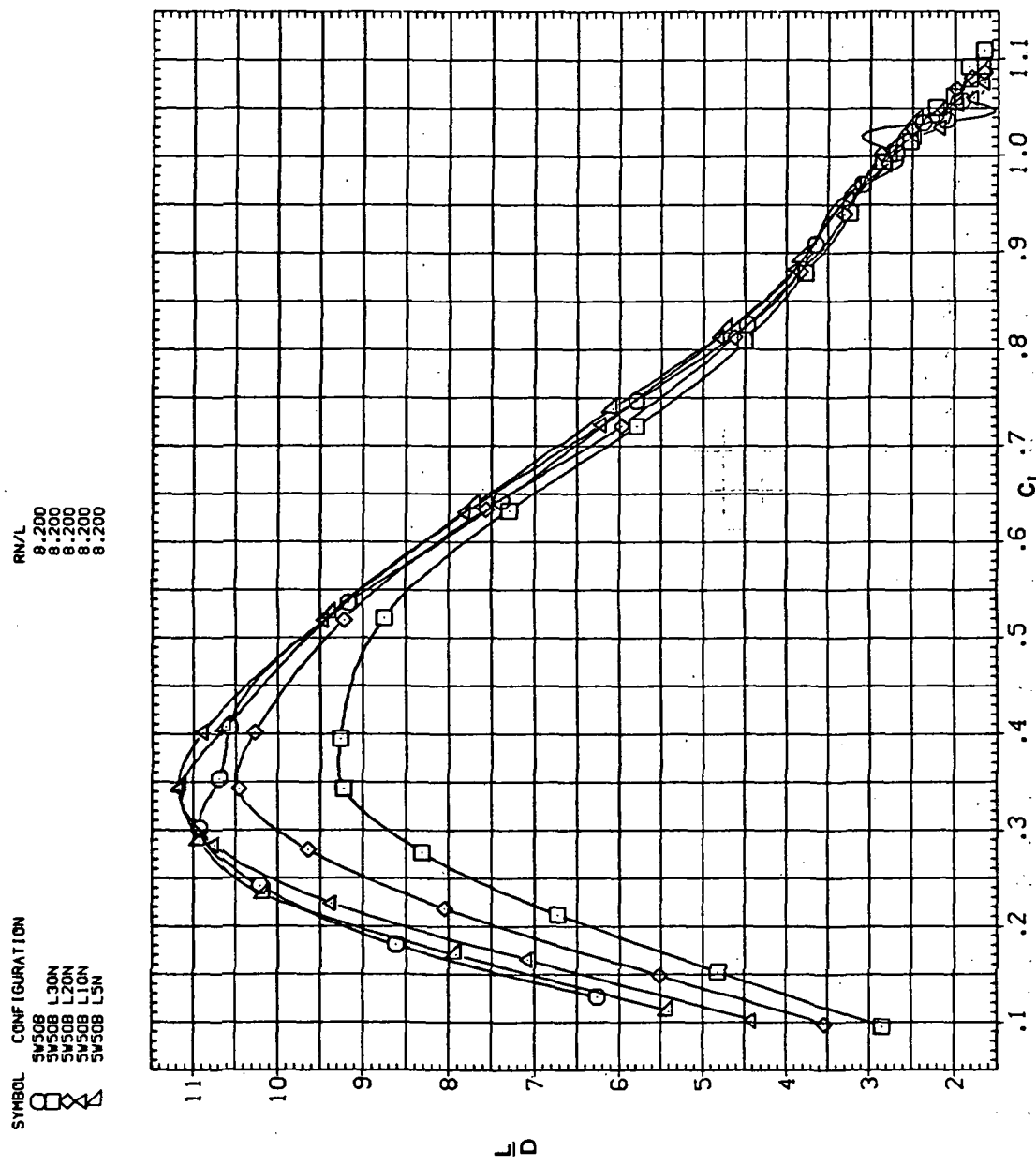


(b)  $C_L$  vs  $C_m$   
Figure 13.— Continued.



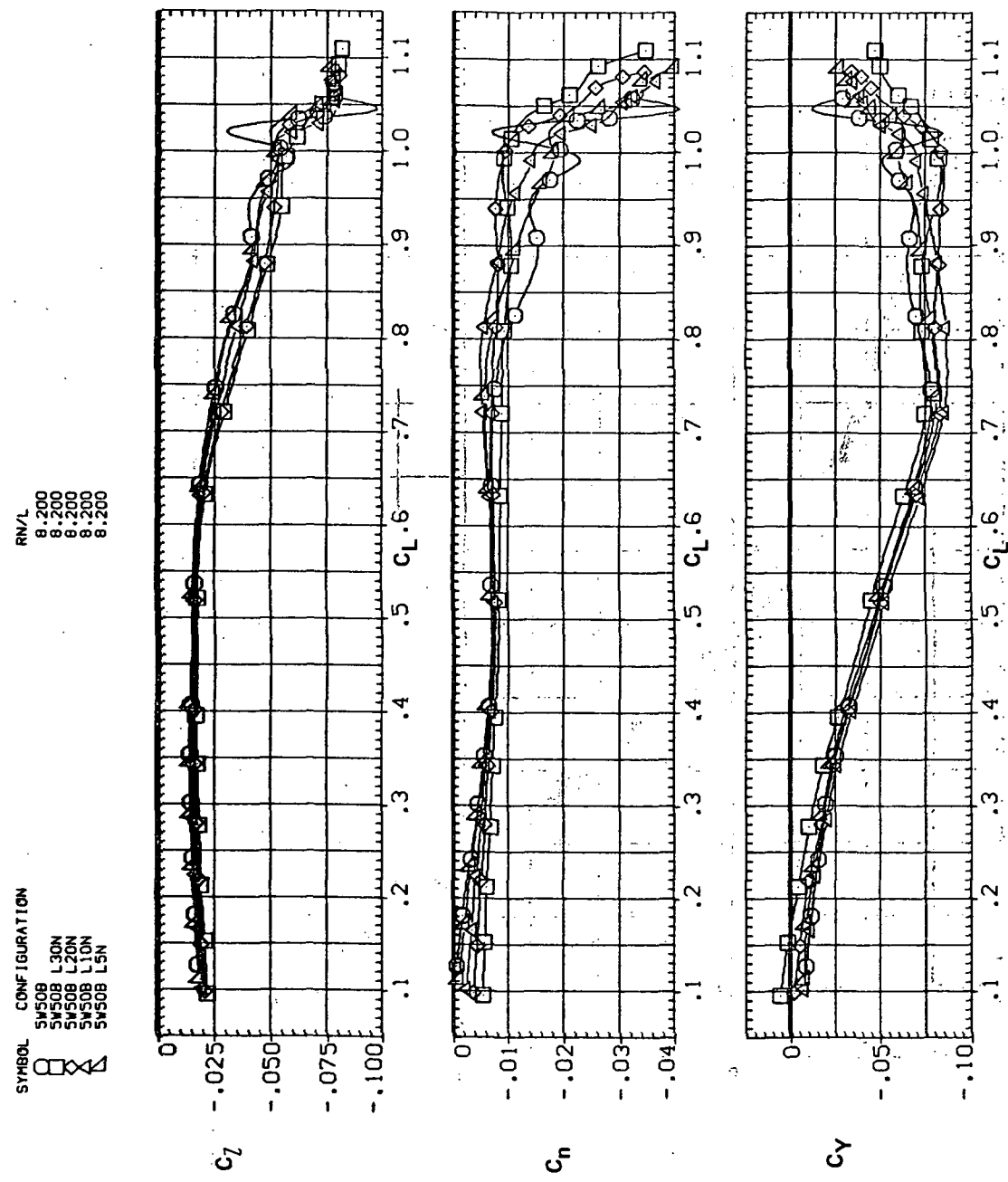
(c)  $C_L$  vs  $C_D$

Figure 13.—Continued.



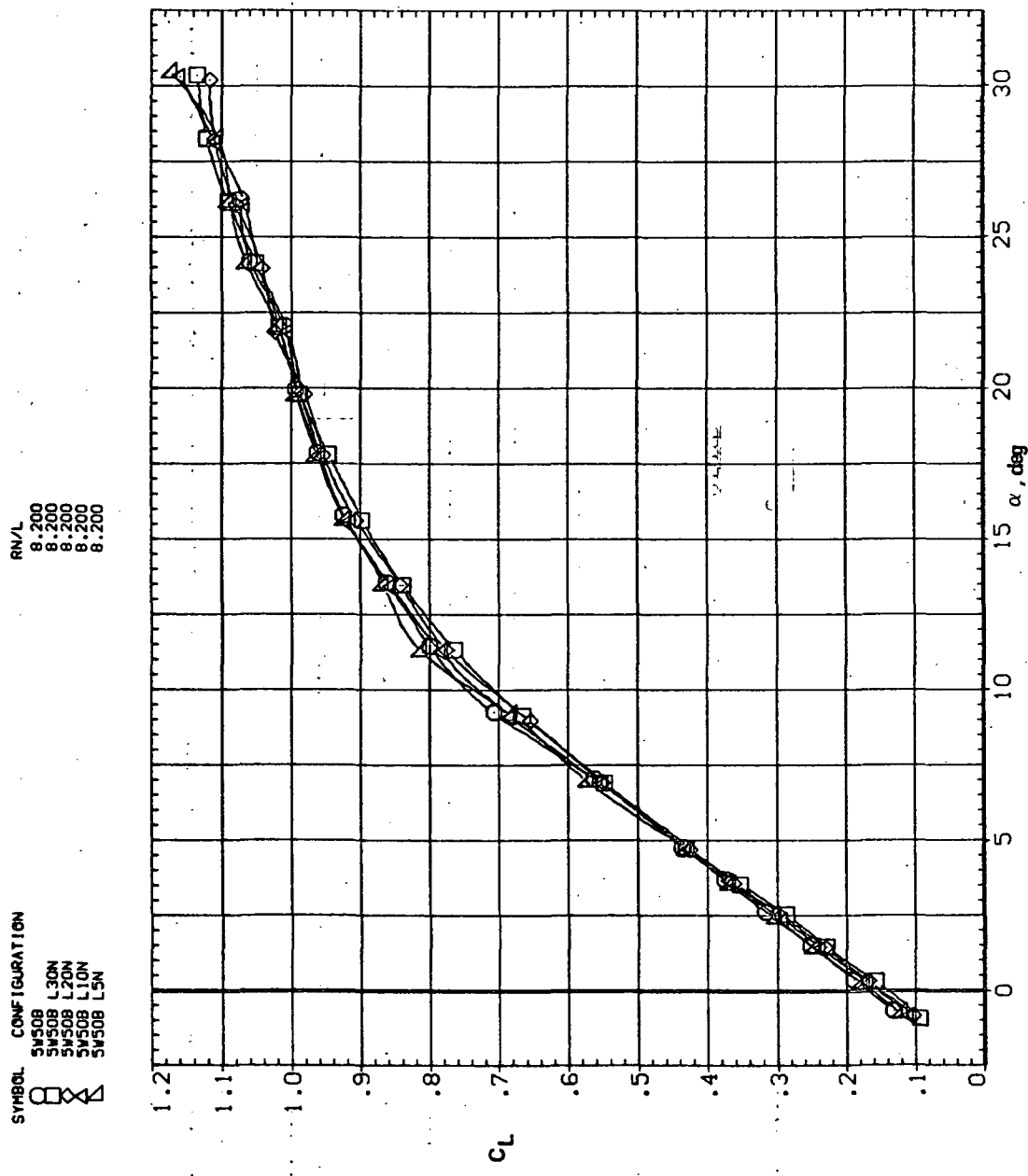
(d)  $L/D$  vs  $C_L$

Figure 13.— Continued.



(e)  $C_L$ ,  $C_n$ , and  $C_Y$  vs  $C_L$

Figure 13.— Concluded.



(a)  $C_L$  vs  $\alpha$

Figure 14.—Effect of drooped-nose flaps on the static longitudinal characteristics of the oblique wing: flaps on downstream wing panel only,  $\Lambda = 50^\circ, M = 0.9$ .

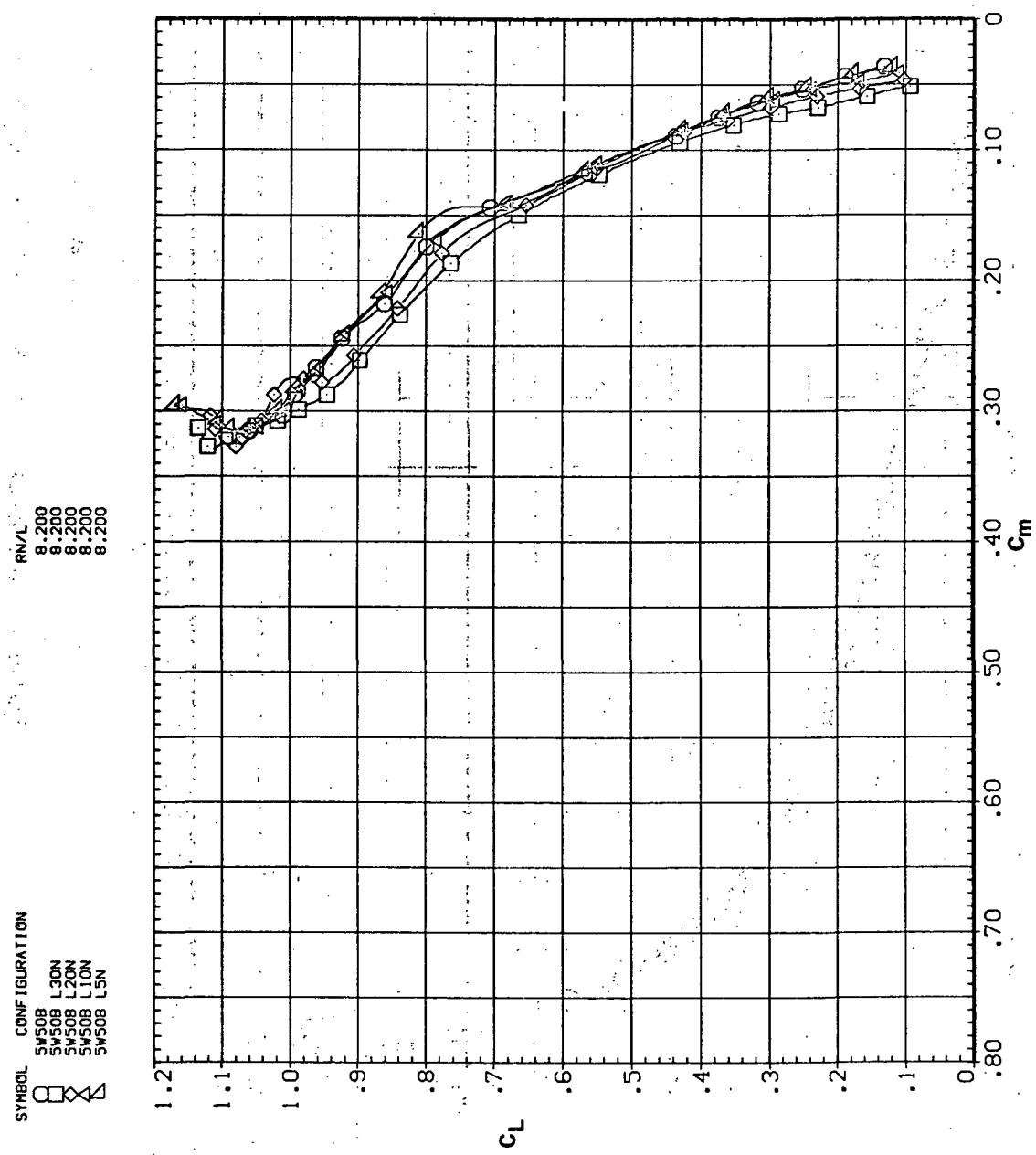
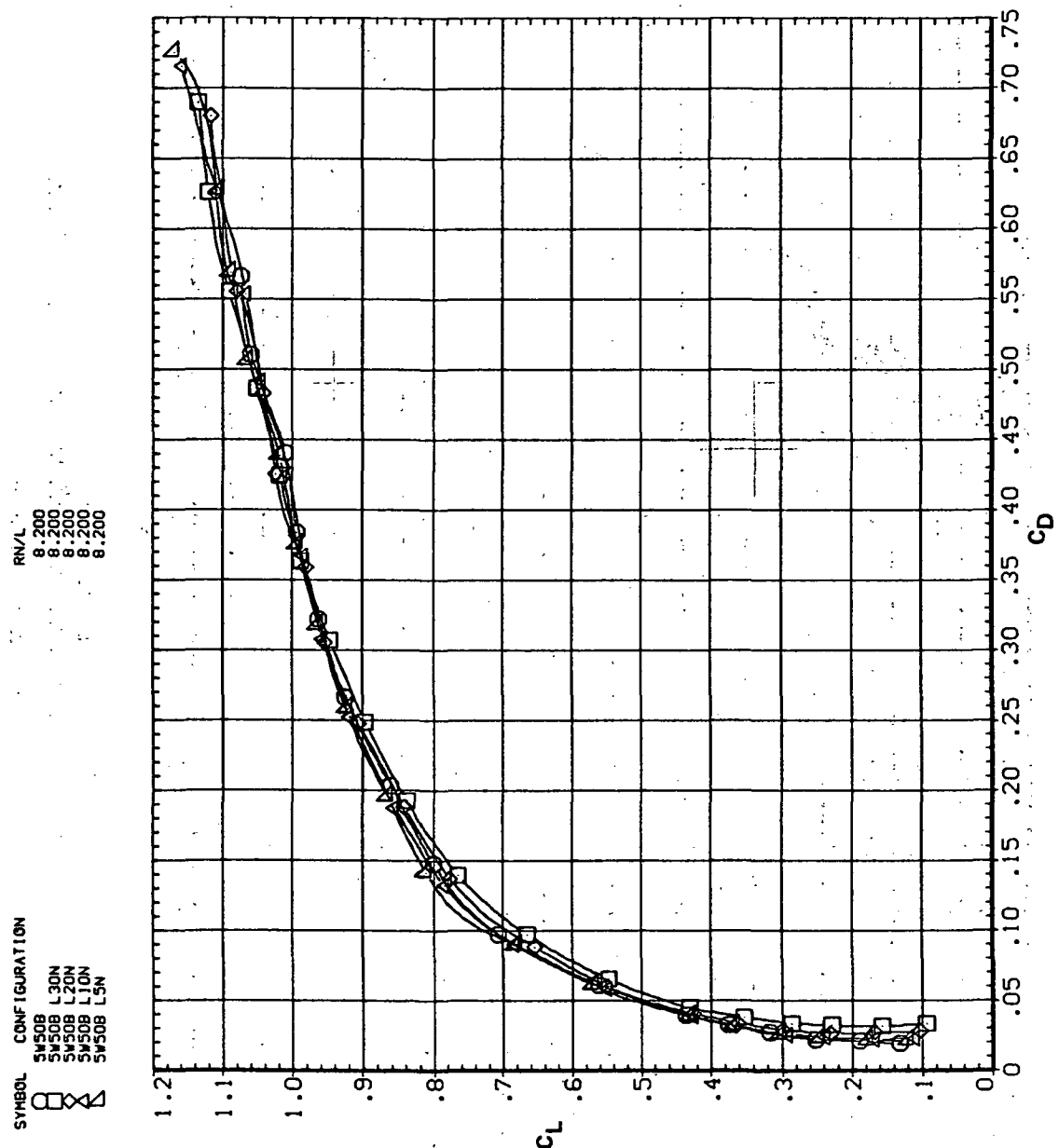
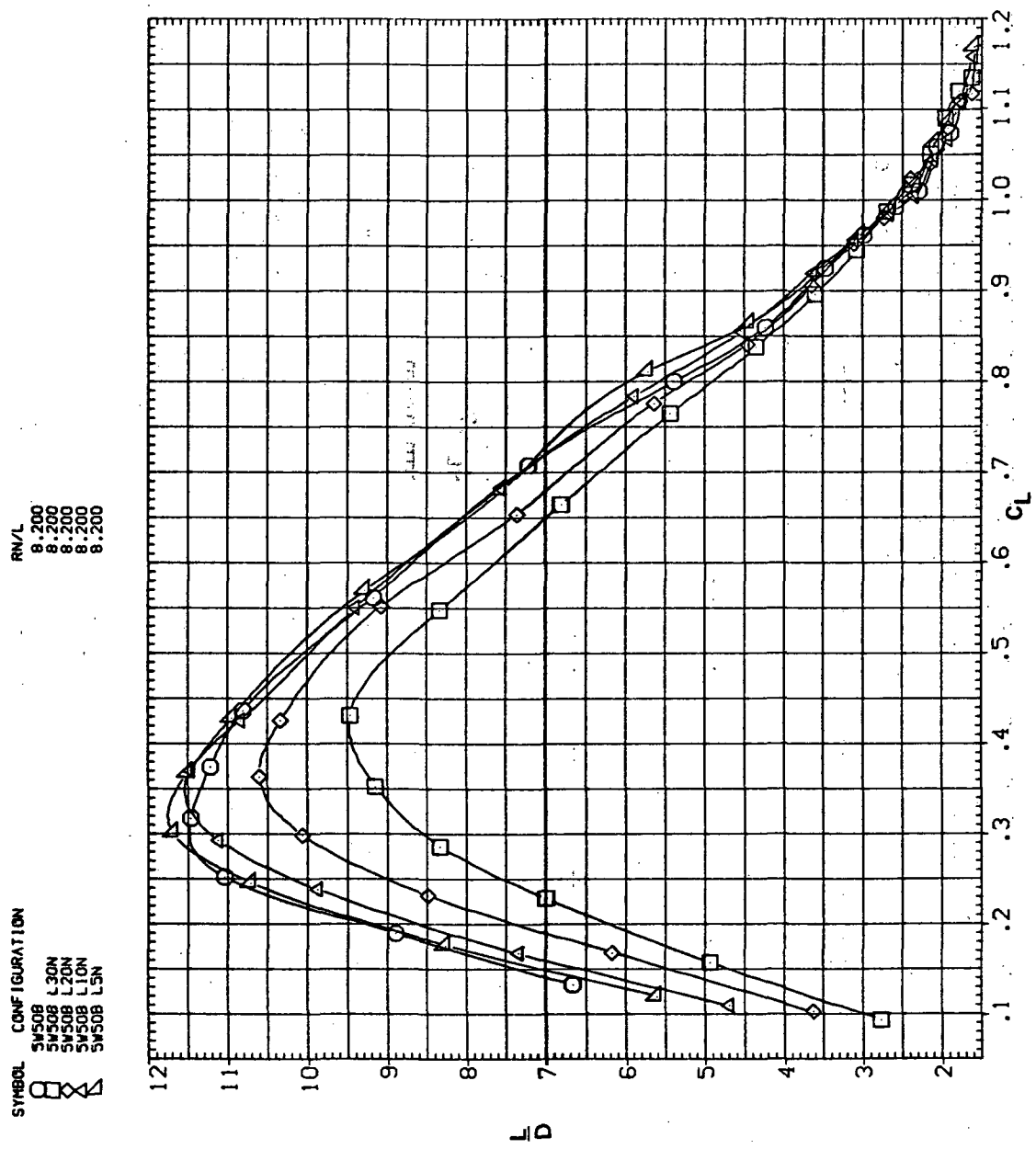
(b)  $C_L$  vs  $C_m$ 

Figure 14.—Continued.



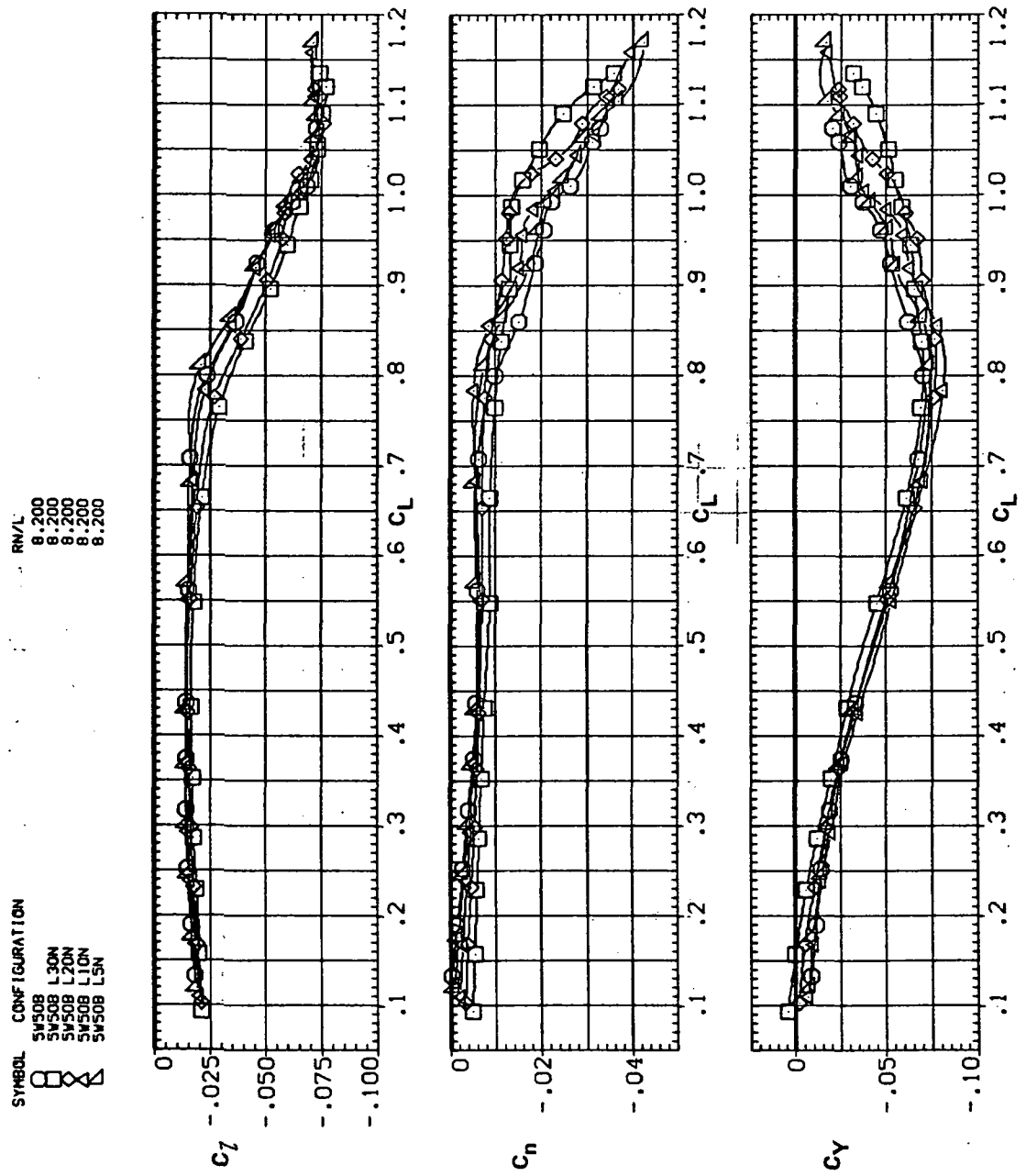
(c)  $C_L$  vs  $C_D$

Figure 14.— Continued.



(d)  $L/D$  vs  $C_L$

Figure 14.— Continued.



(e)  $C_l$ ,  $C_n$ , and  $C_Y$  vs  $C_L$

Figure 14.— Concluded.

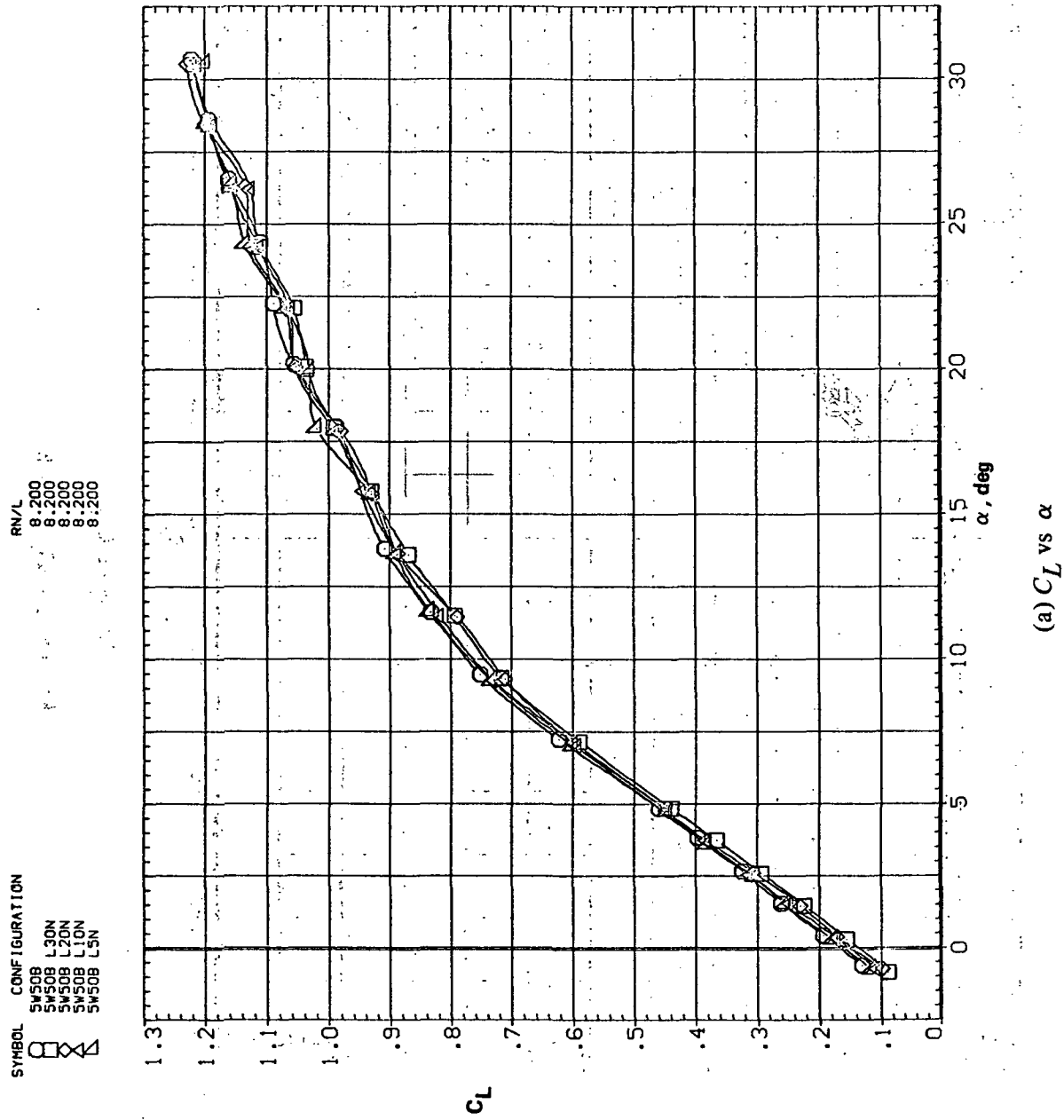
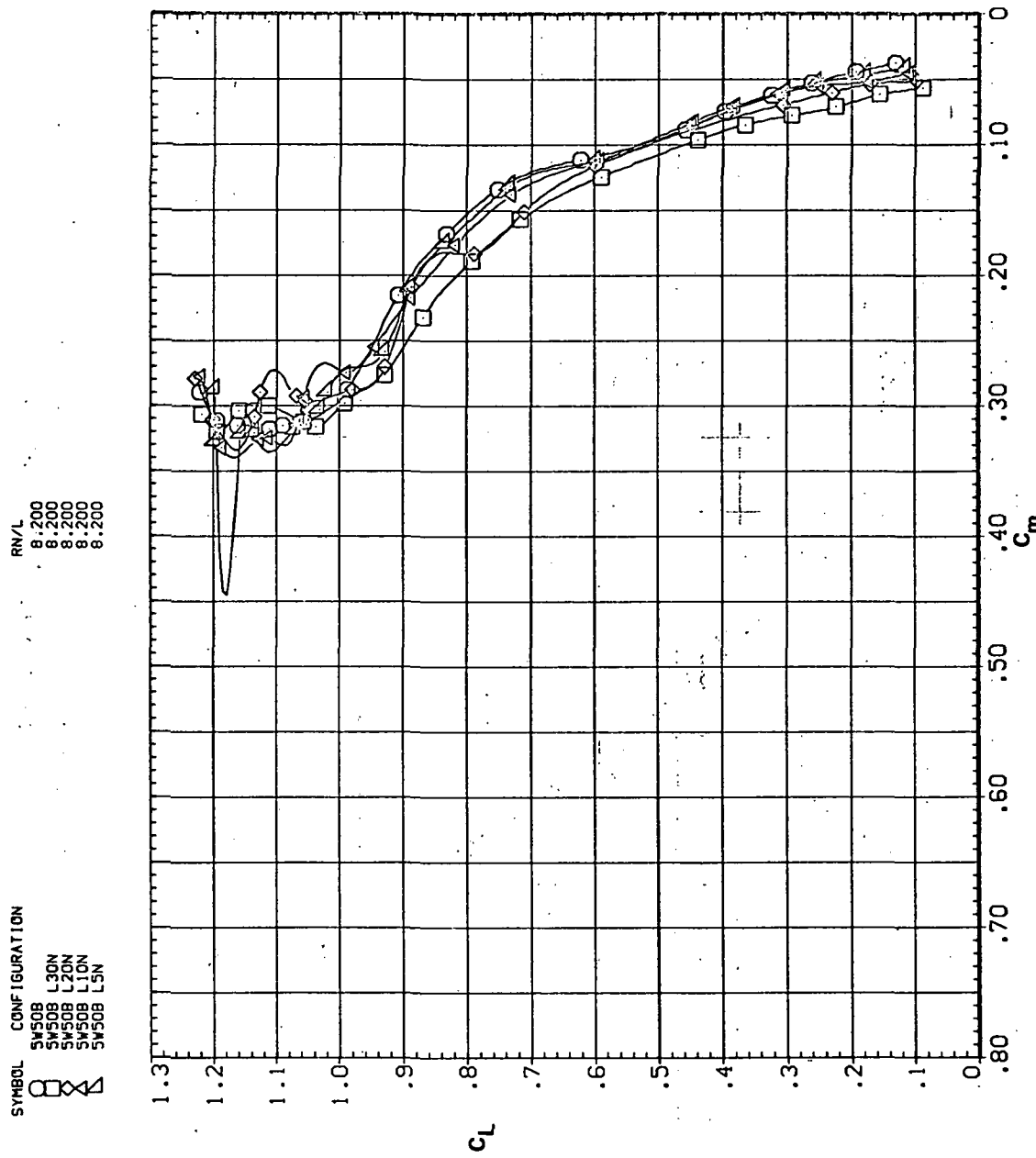
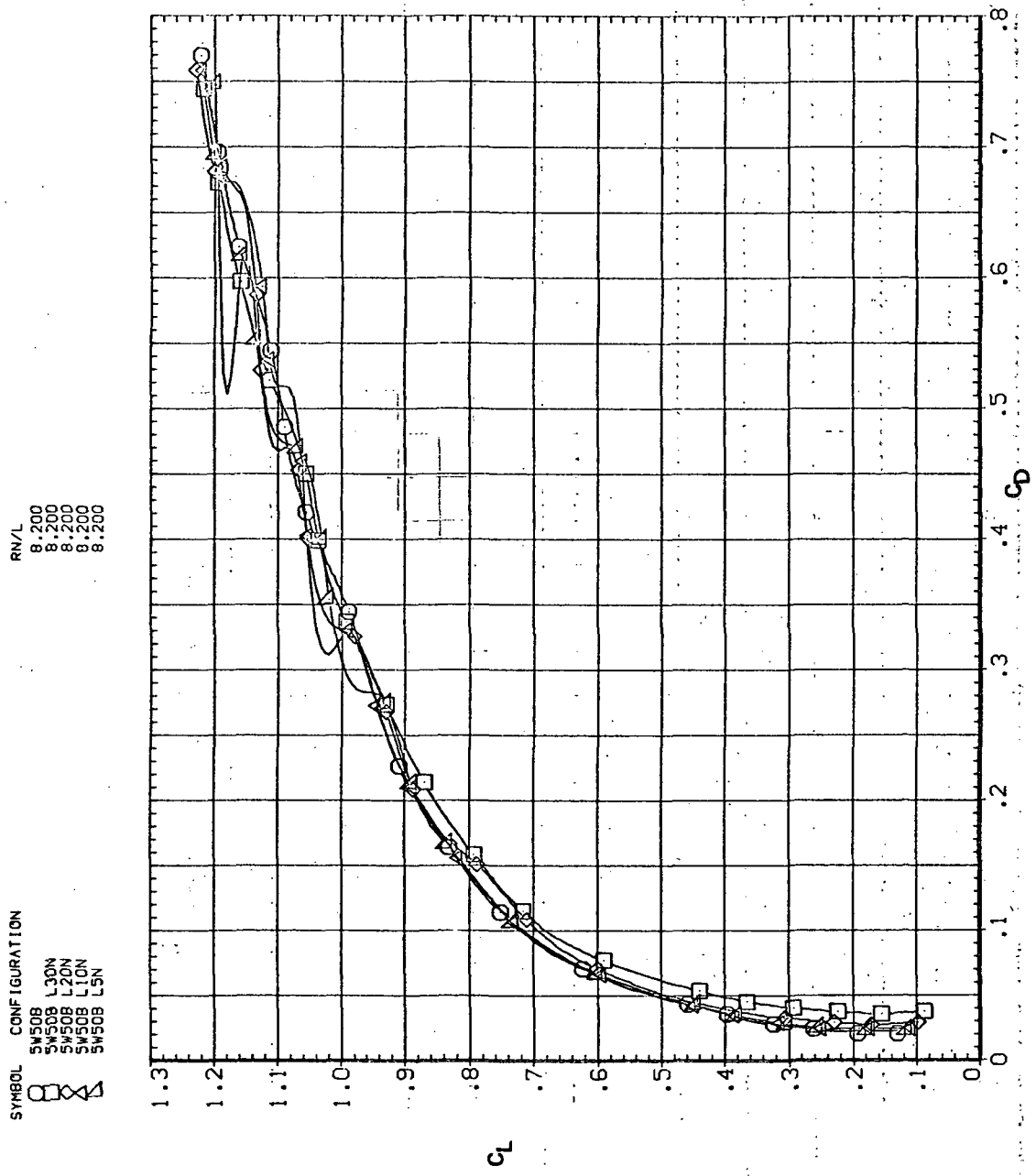


Figure 15.— Effect of drooped-nose flaps on the static longitudinal characteristics of the oblique wing: flaps on downstream wing panel only,  $\Lambda = 50^\circ, M = 0.95$ .



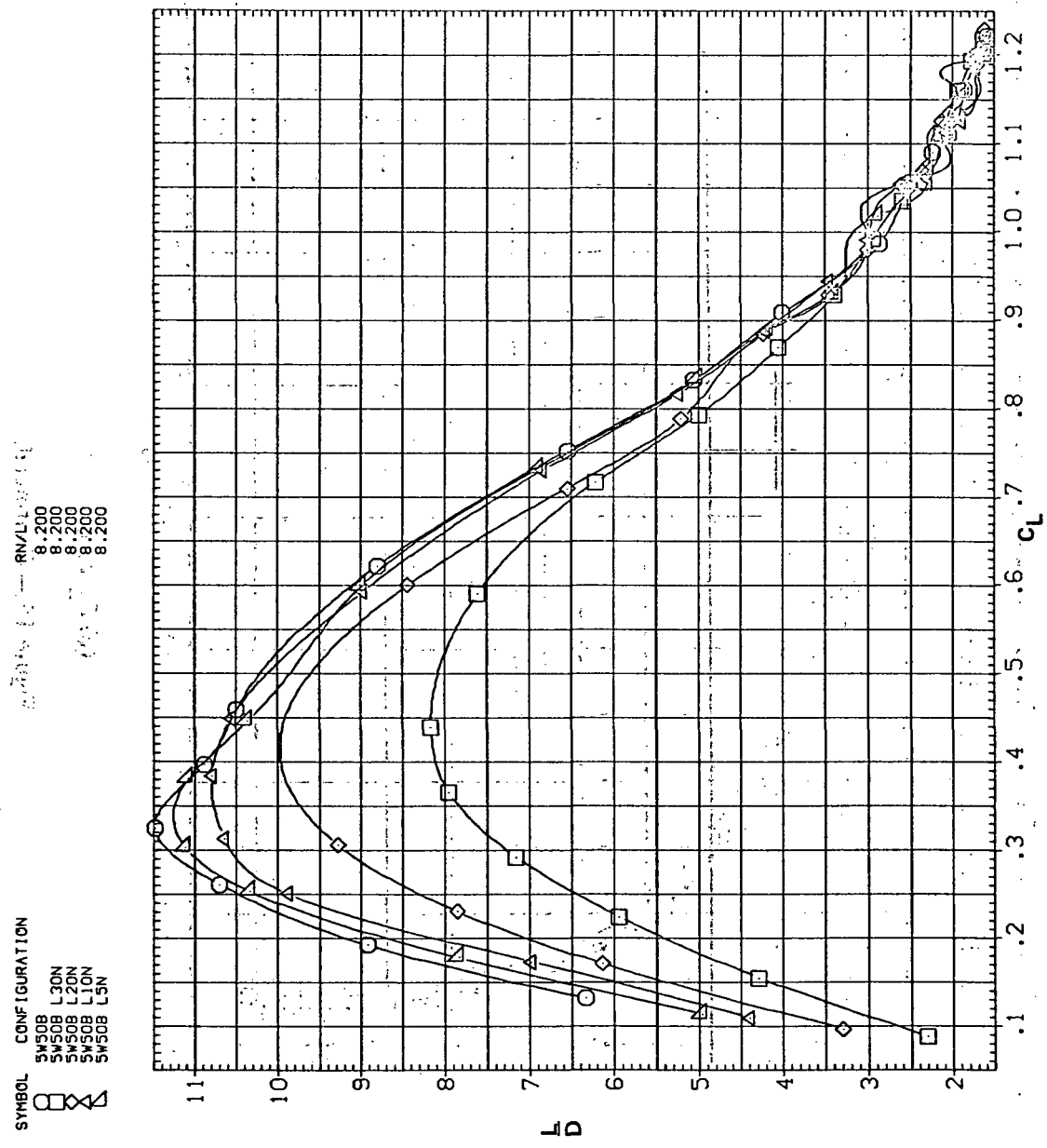
(b)  $C_L$  vs  $C_m$

Figure 15-5.—Continued.



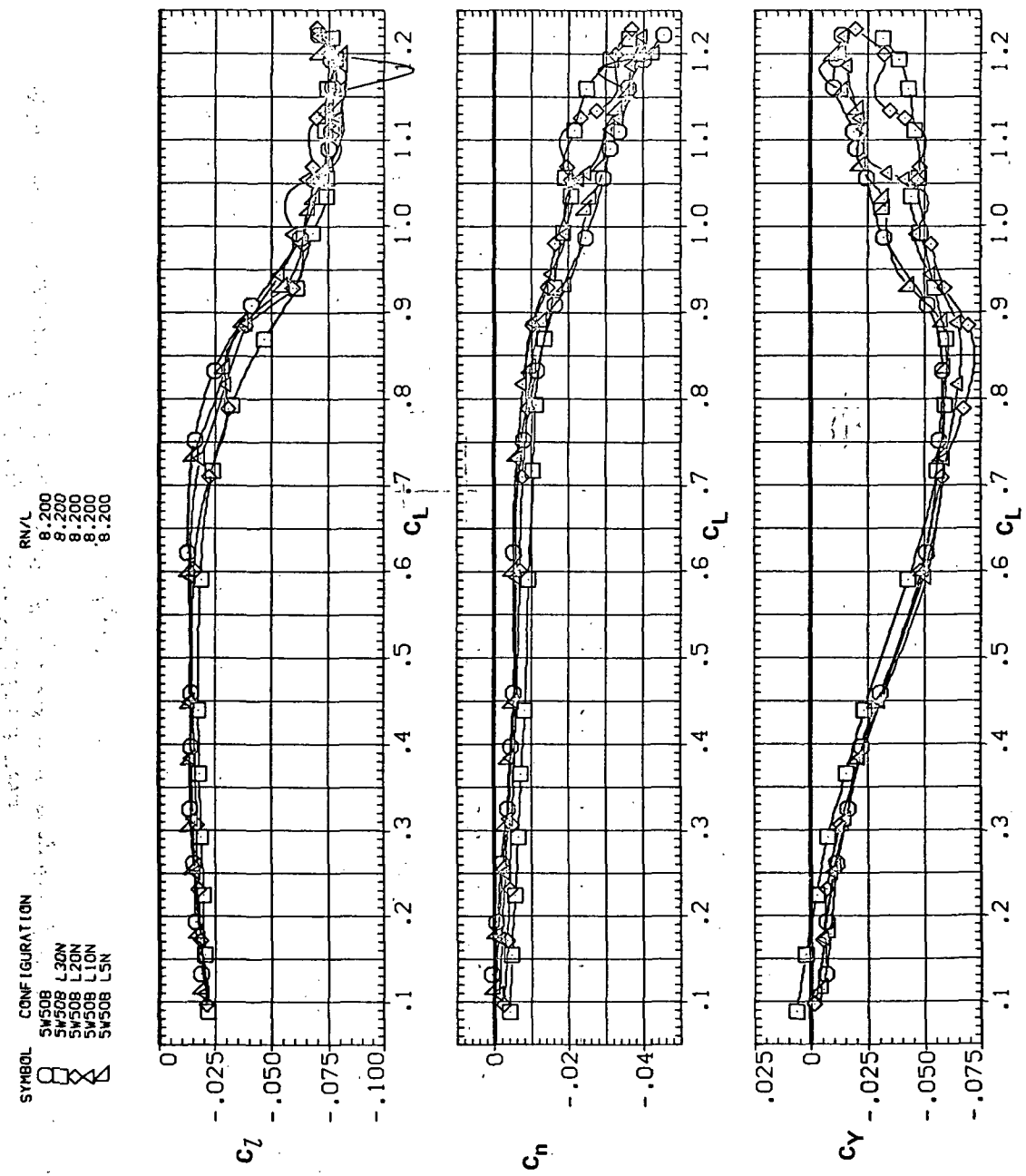
(c)  $C_L$  vs  $C_D$

Figure 15.—Continued.



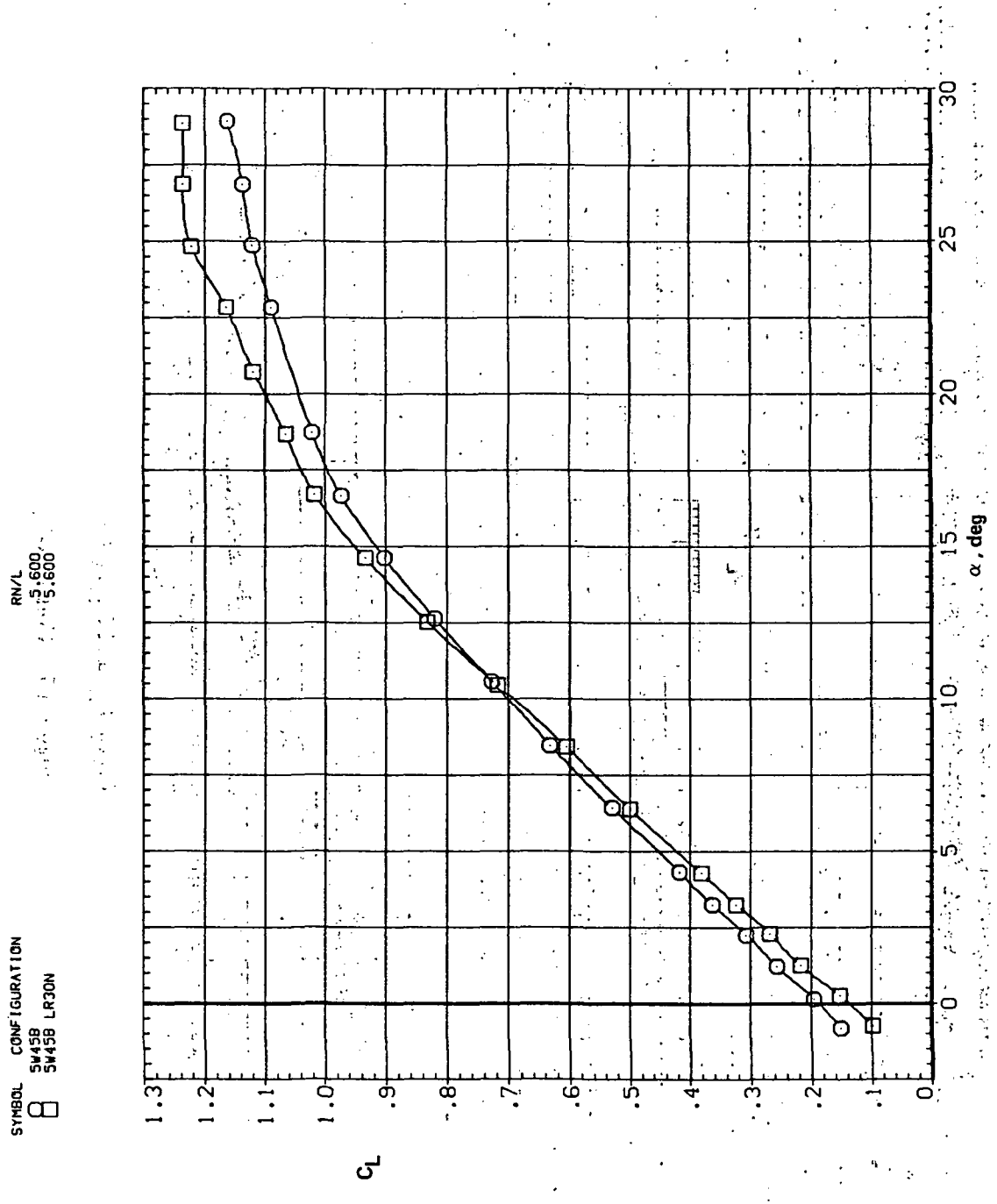
(d)  $L/D$  vs  $C_L$

Figure 15.— Continued.



(e)  $C_D$ ,  $C_n$ , and  $C_Y$  vs  $C_L$

Figure 15.— Concluded.

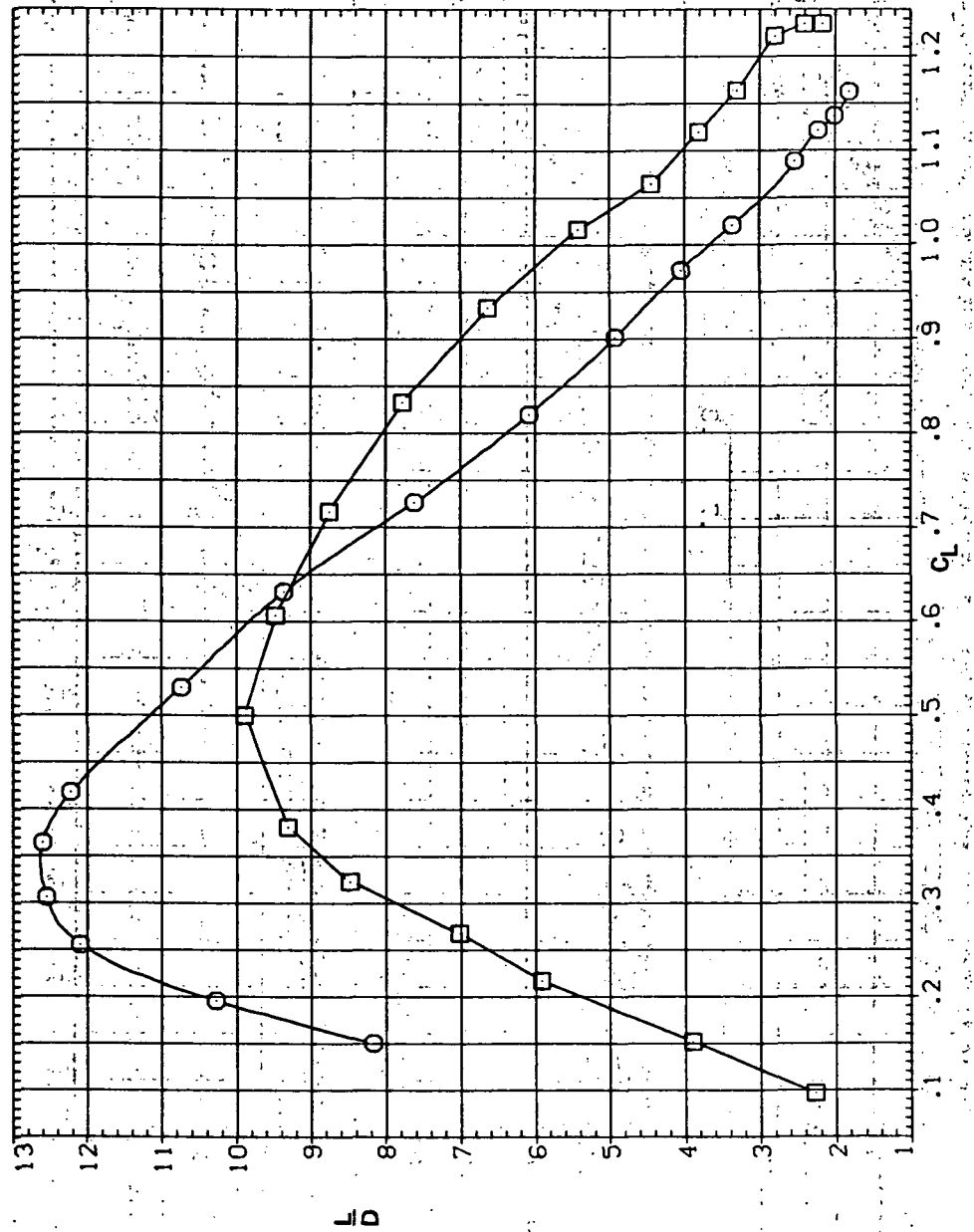


(a)  $C_L$  vs  $\alpha$

Figure 16.—Effect of drooped-nose flaps on the static longitudinal stability characteristics of the oblique wing: flaps on both wing panels,  $\Lambda = 45^\circ$ ,  $M = 0.25$ .

SYMBOL CONFIGURATION  
□ SW58  
□ SW458 LR30N

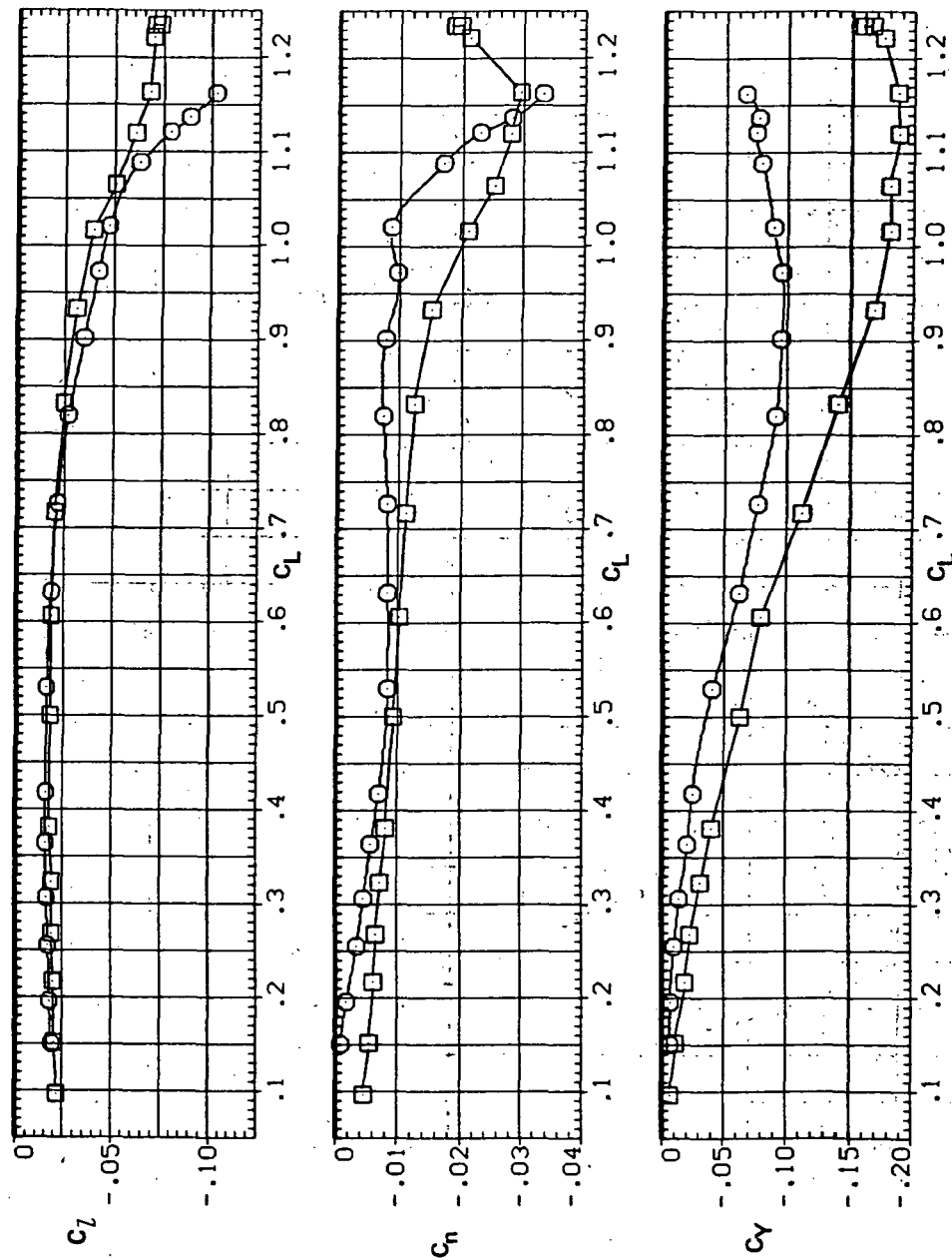
RN/L  
5.600  
5.8600



(d)  $L/D$  vs.  $C_L$

Figure 16.—Continued.

SYMBOL      CONFIGURATION  
□      SW58      SW458      LR30N  
RN/L      5.600      5.600



(e)  $C_L$ ,  $C_n$ , and  $C_Y$  vs  $C_L$

Figure 16.—Concluded.

SYMBOL CONFIGURATION  
□ RN/L  
○ SW45B  
■ SW45B LR30N

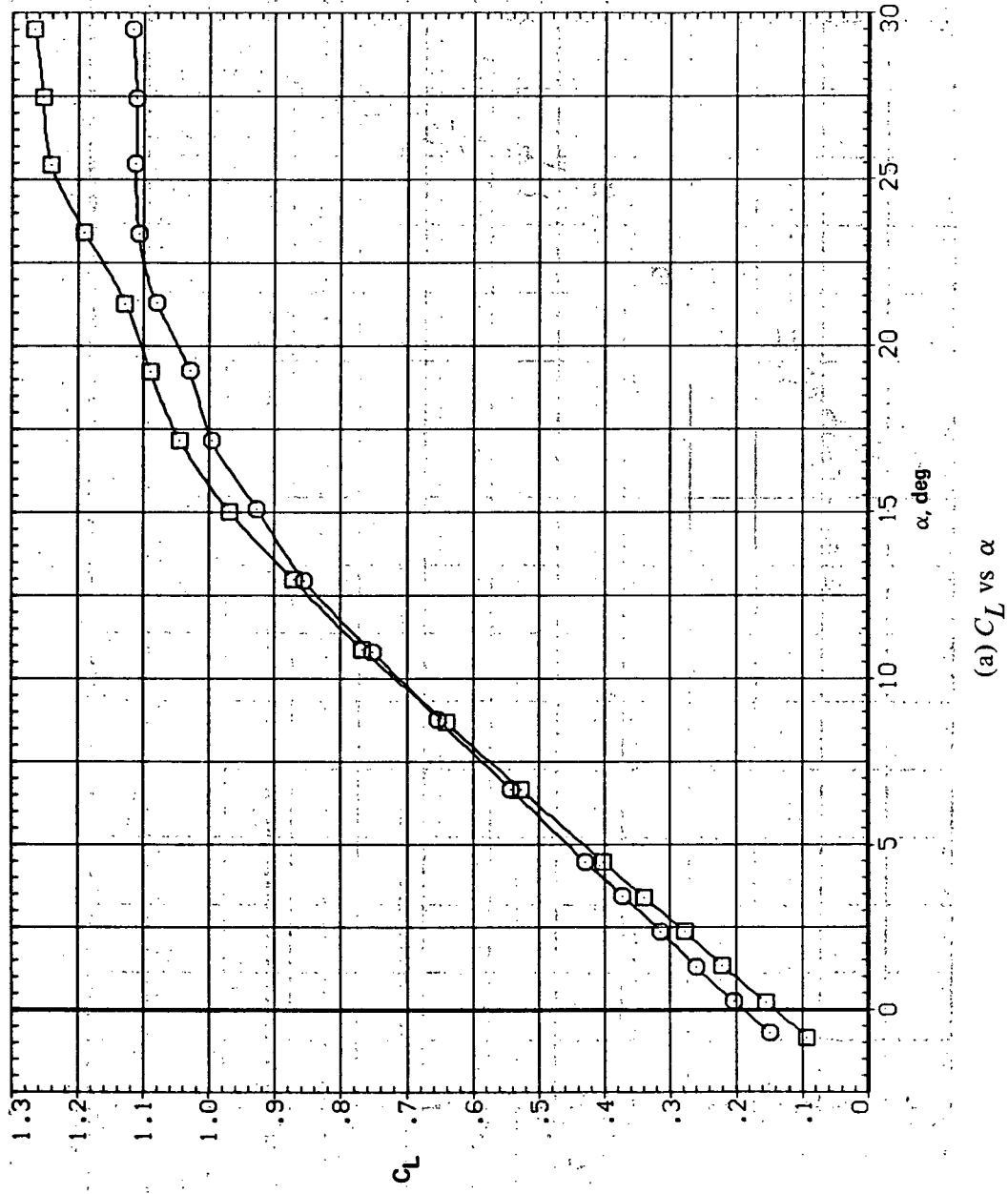
(a)  $C_L$  vs  $\alpha$ 

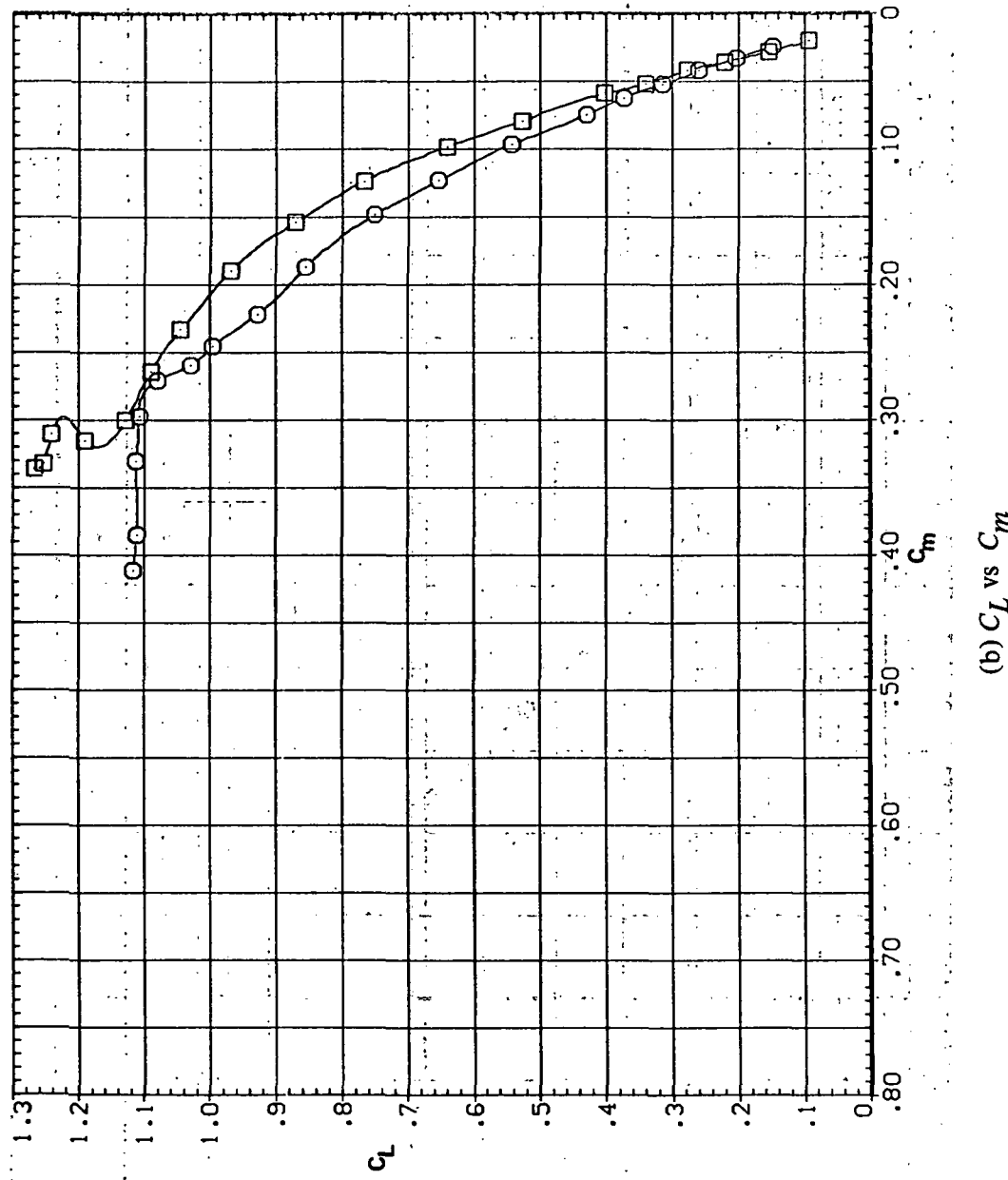
Figure 17.—Effect of drooped-nose flaps on the static longitudinal characteristics of the oblique wing: flaps on both wing panels,  $\Lambda = 45^\circ$ ,  $M = 0.4$ .

81

CONFIGURATION

SW458 SW458 LR30N

RN/L 8.200 8.200



(b)  $C_L$  vs  $C_m$

Figure 17.7—Continued.

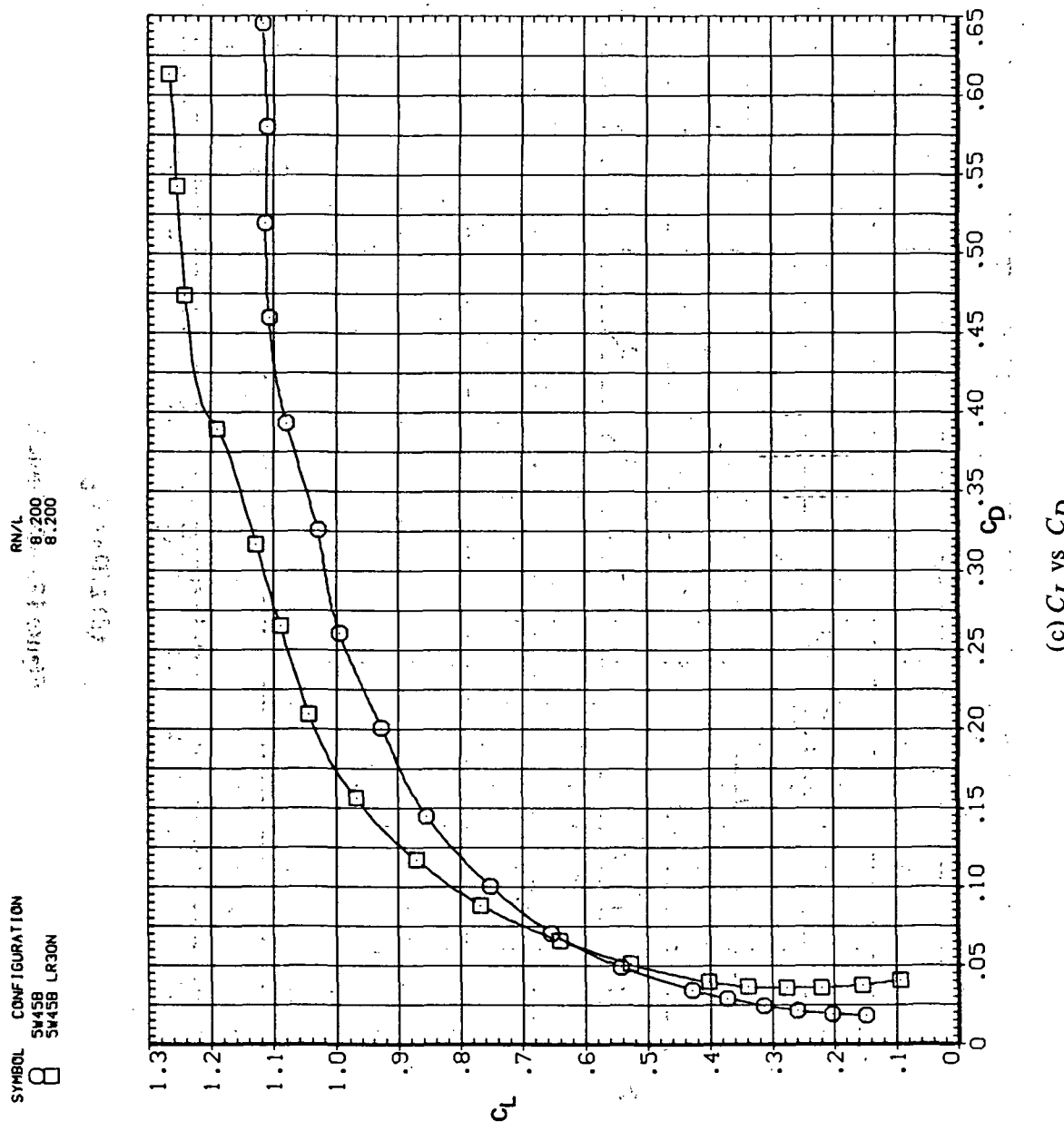
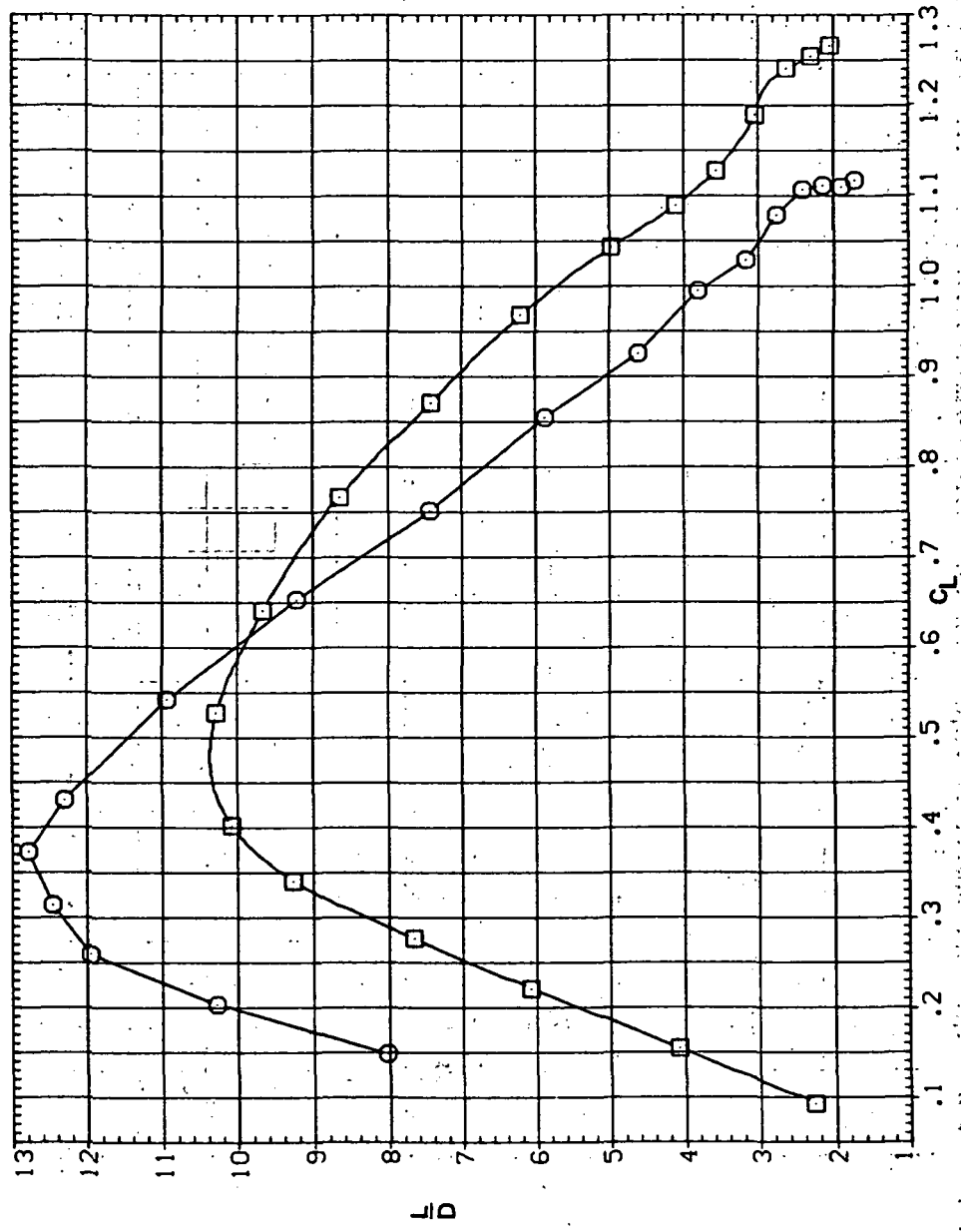


Figure 17.—Continued.

SYMBOL CONFIGURATION  
○ SW15B  
□ SW45B LR30N  
■ RNL  
 8.200  
 8.200



(d)  $L/D$  vs  $C_L$

Figure 17.—Continued.

SYMBOL CONFIGURATION  
□ SN45B  
□ SN45B LR30N

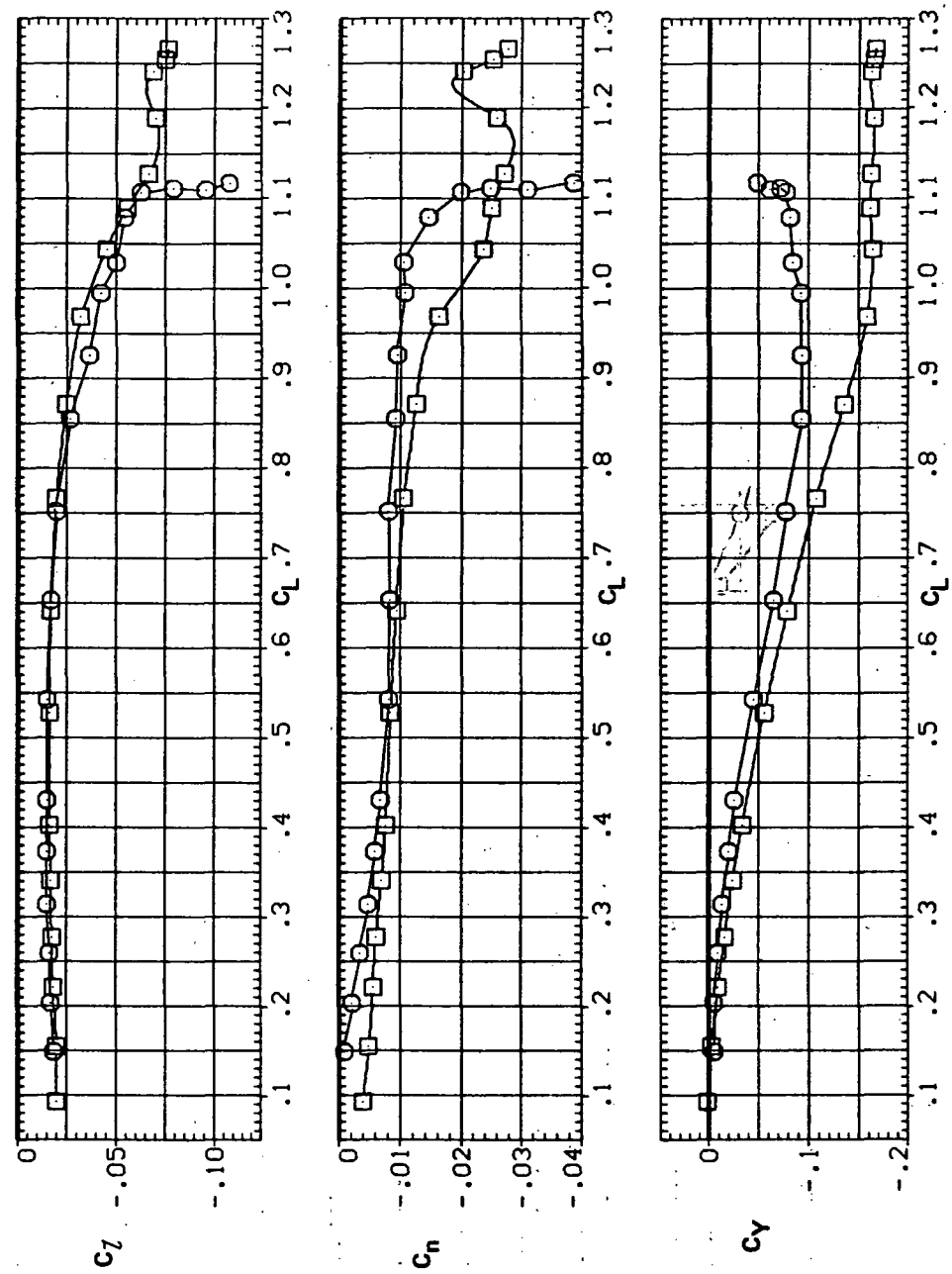
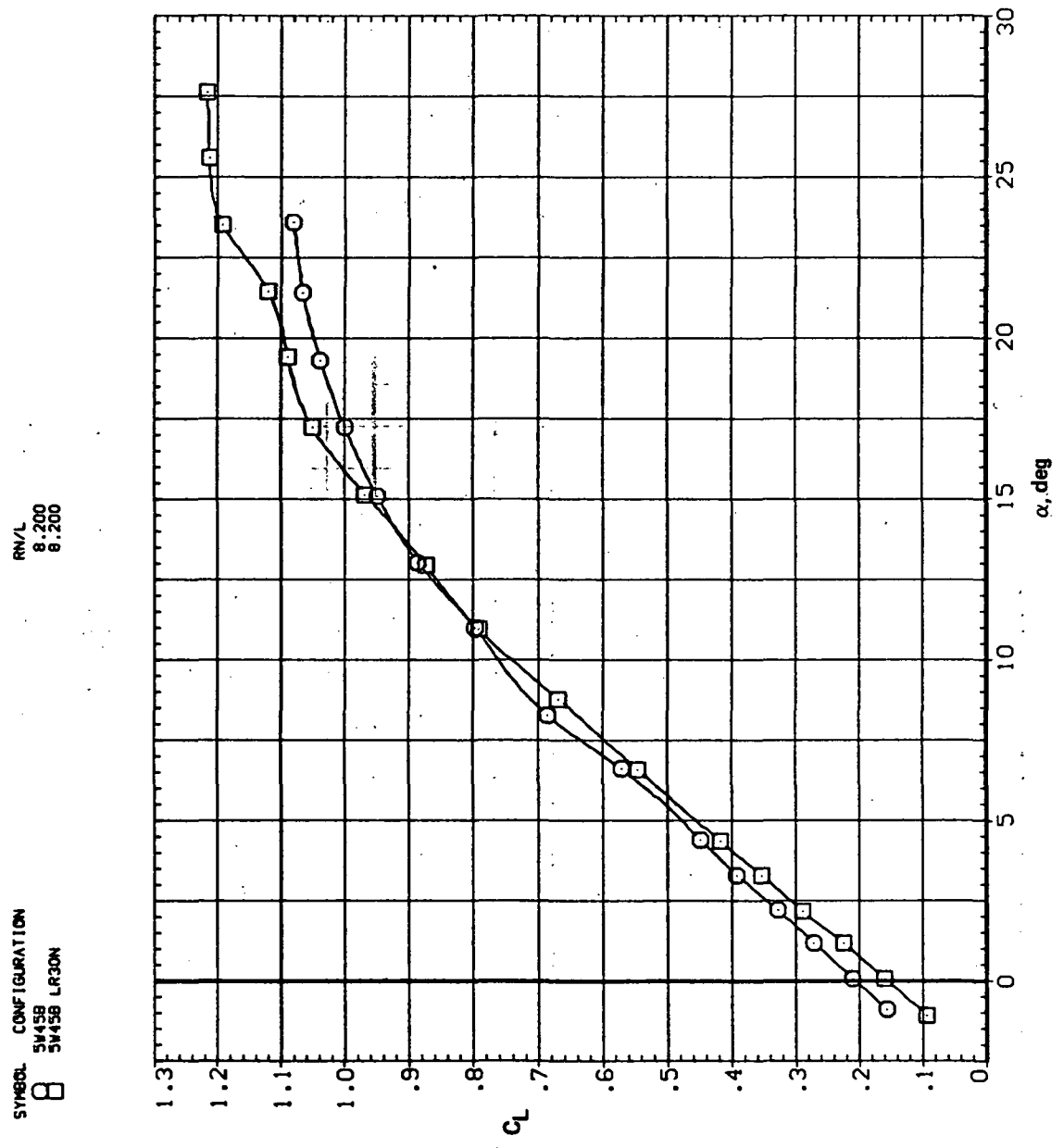
(e)  $C_L$ ,  $C_n$ , and  $C_Y$  vs  $C_L$ 

Figure 17.—Concluded.

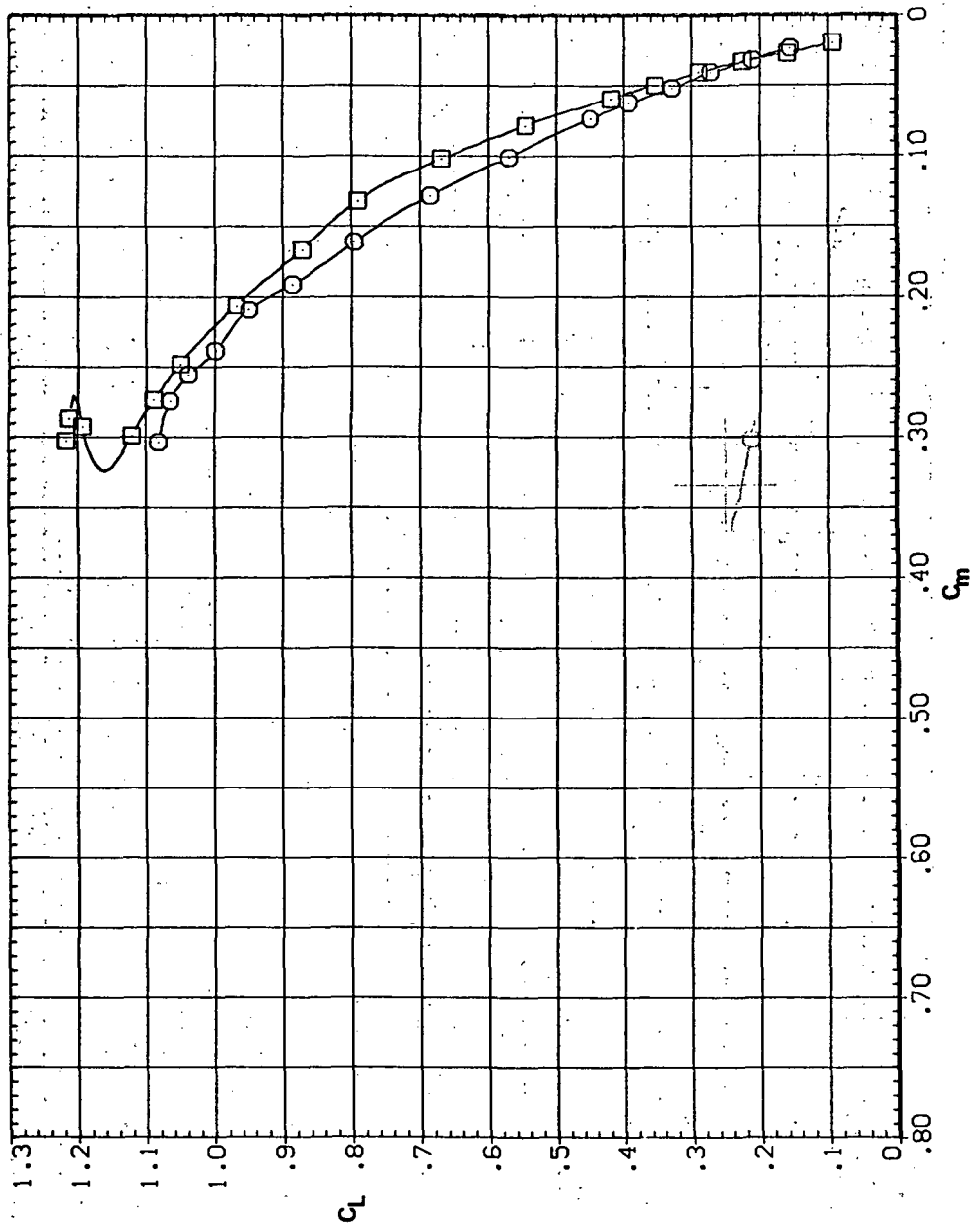


(a)  $C_L$  vs  $\alpha$

Figure 18.— Effect of drooped-nose flaps on the static longitudinal stability characteristics of the oblique wing: flaps on both wing panels,  $\Lambda = 45^\circ$ ,  $M = 0.6$ .

SYMBOL CONFIGURATION  
□ SW58 LR30N  
○ SW458 LR30N

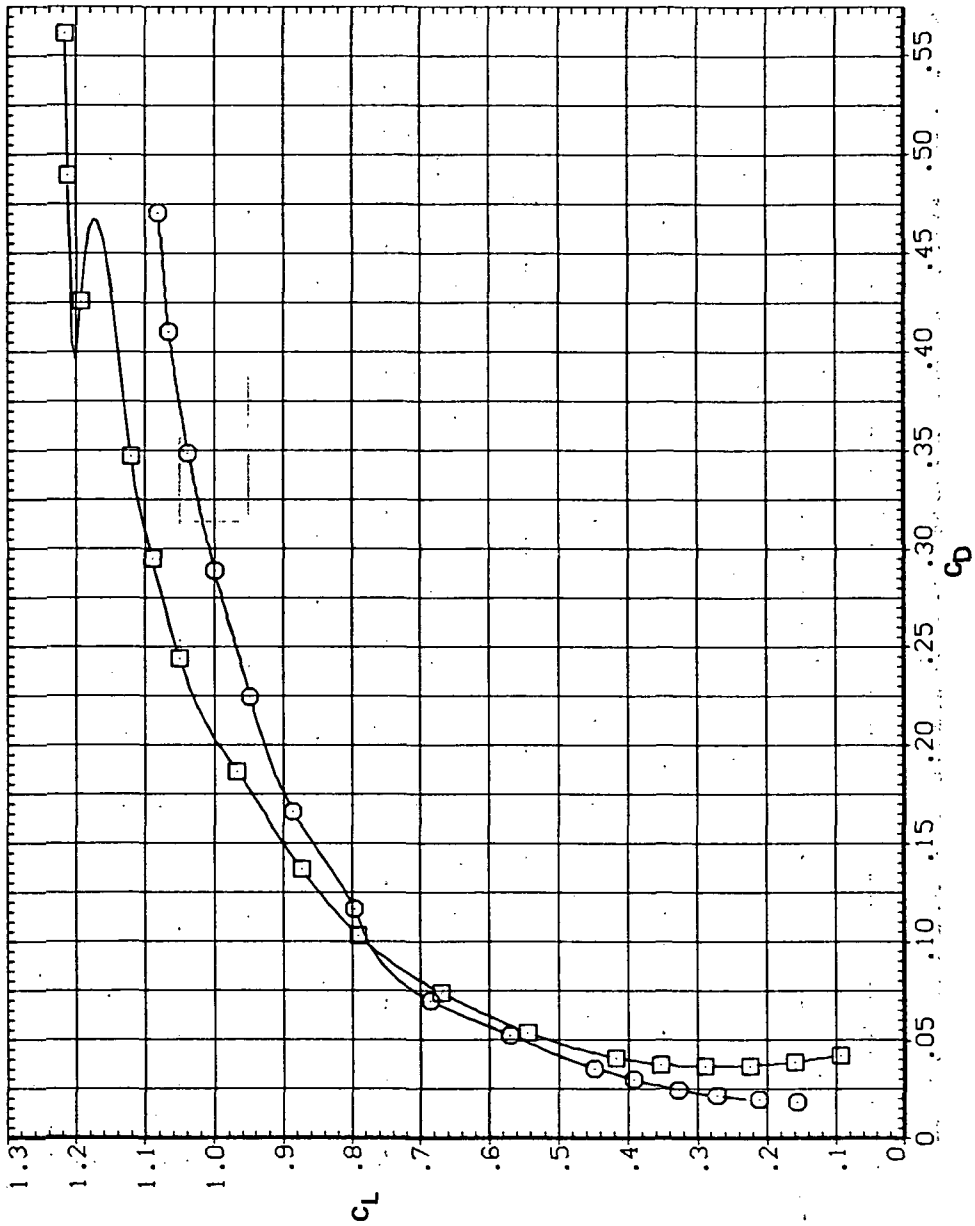
RN/L  
 8.200  
 8.200



(b)  $C_L$  vs  $C_m$

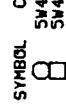
Figure 18.—Continued.

SYMBOL CONFIGURATION  
□ SM45B  
○ SM45B LR30N

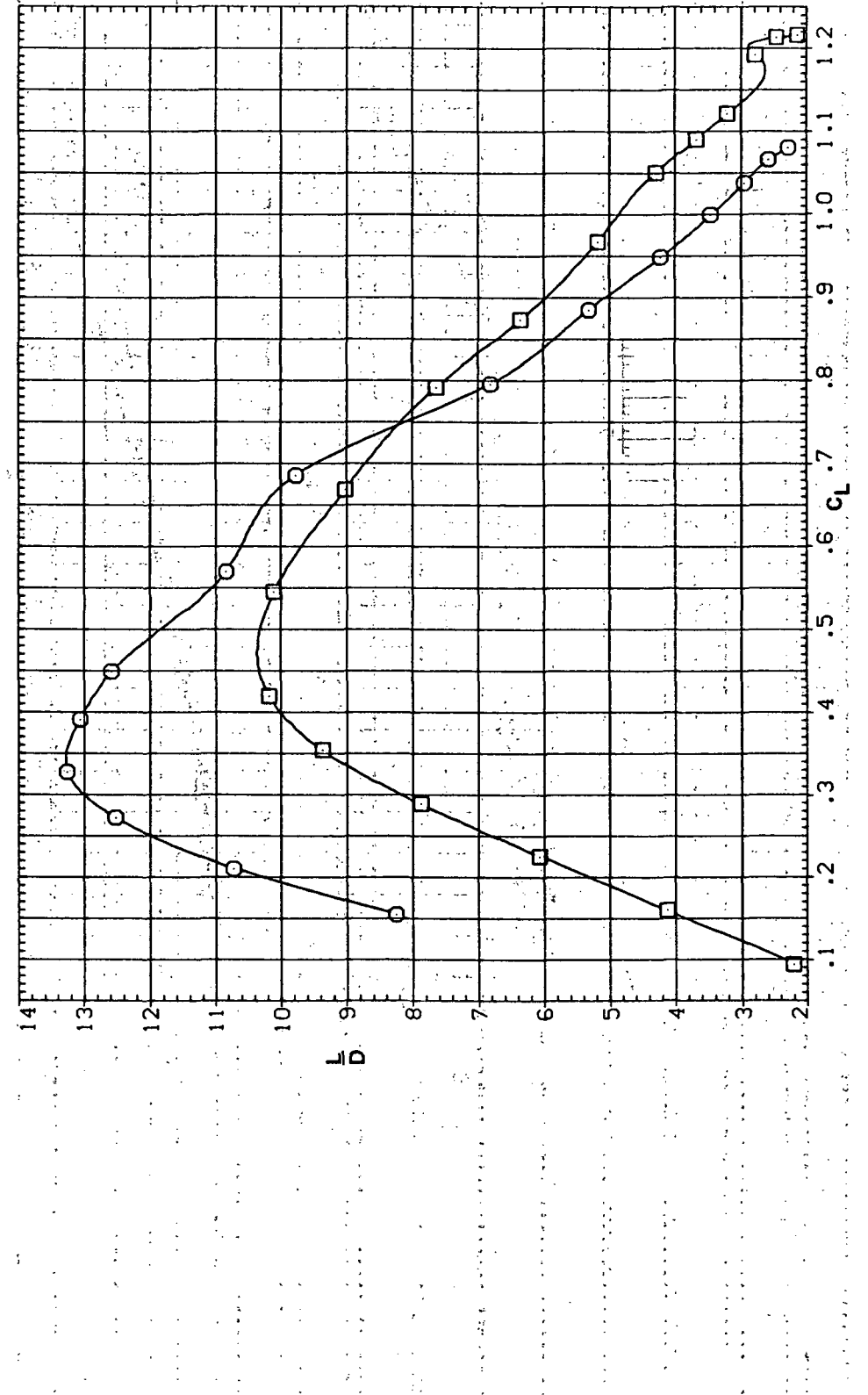


(c)  $C_L$  vs  $C_D$

Figure 18.—Continued.

SYMBOL CONFIGURATION  
 SR45B LR30N

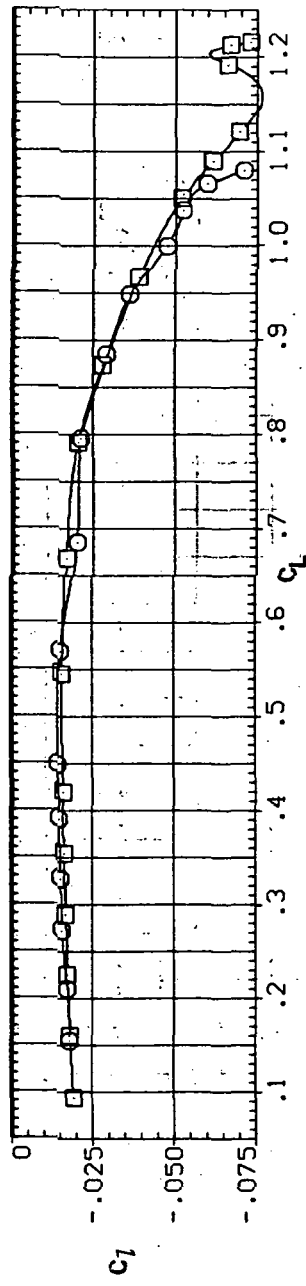
RN/L 8.200  
 8.200



(d)  $L/D$  vs  $C_L$

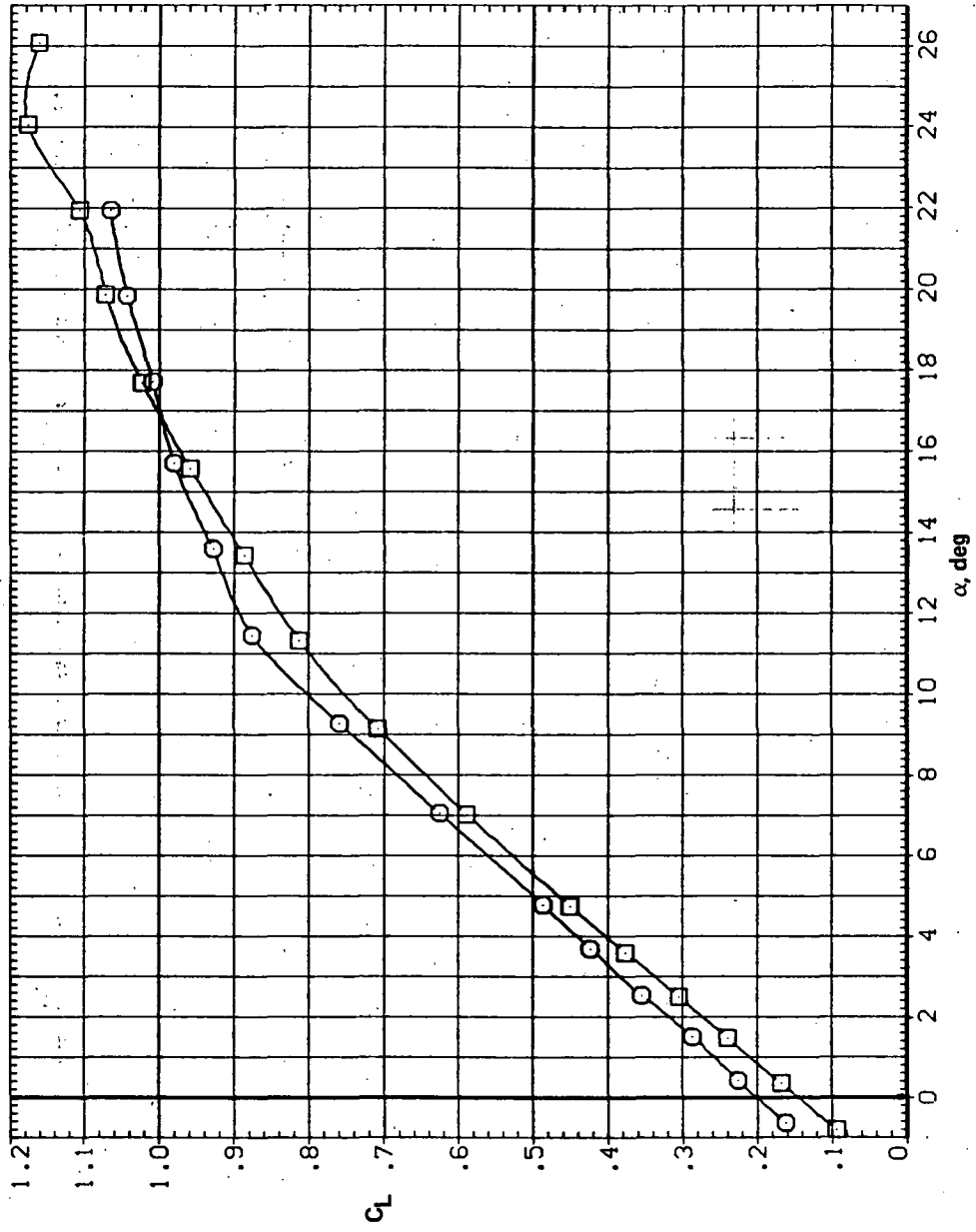
Figure 18.—Continued.

SYMBOL      CONFIGURATION  
□ SW58      SW458 LR30N  
RN/L  
8.200  
8.200



SYMBOL CONFIGURATION  
□ SW15B  
○ SW45B LR3DN

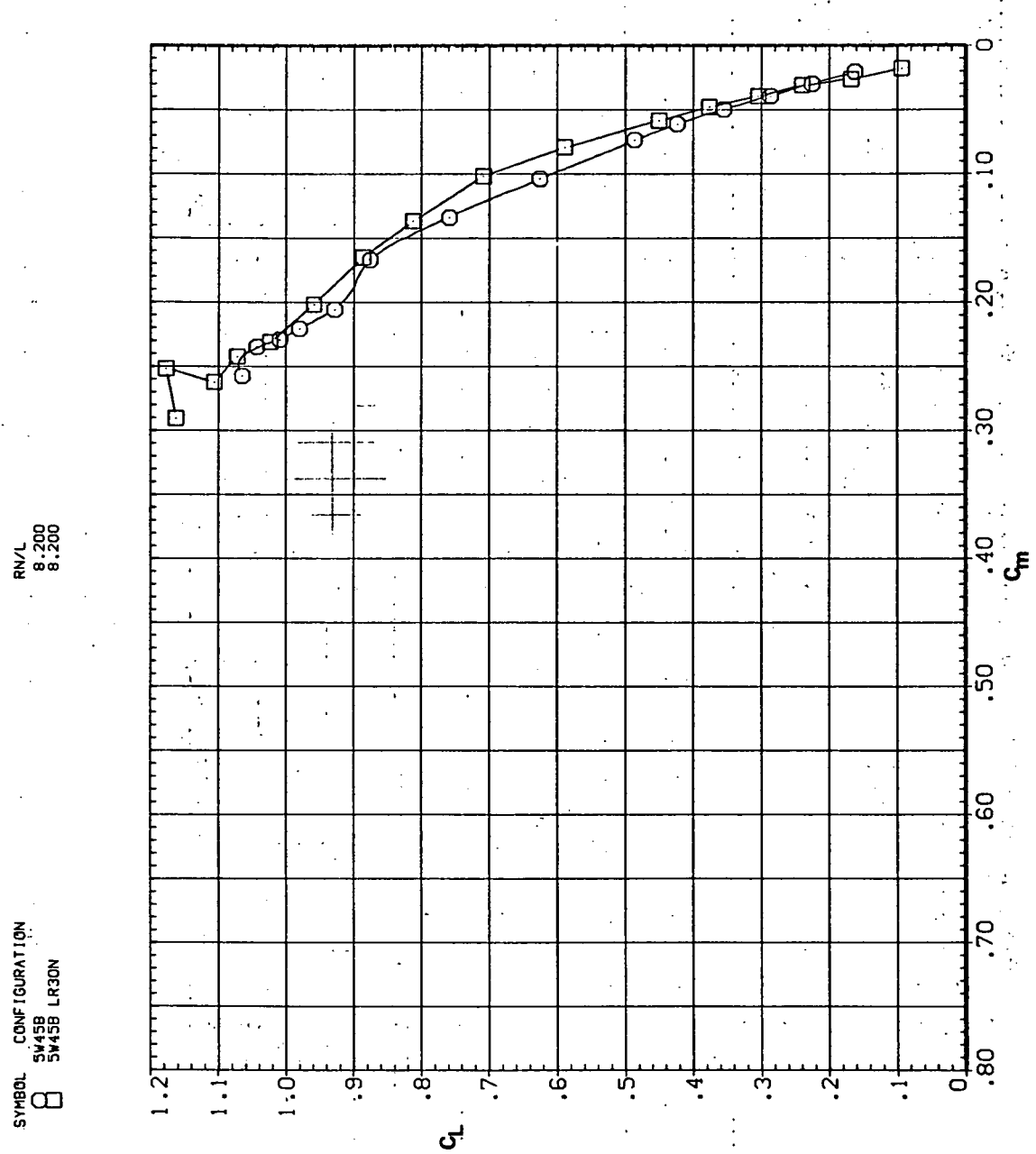
TRN/L  
8.200  
8.200



(a)  $C_L$  vs  $\alpha$

Figure 19.—Effect of drooped-nose flaps on the static longitudinal characteristics of the oblique wing: flaps on both wing panels,  $\Lambda = 45^\circ$ ,  $M = 0.8$ .

SYMBOL    CONFIGURATION  
□ SW5B    SW45B LR30N



(b)  $C_L$  vs  $C_m$

Figure 19.—Continued.

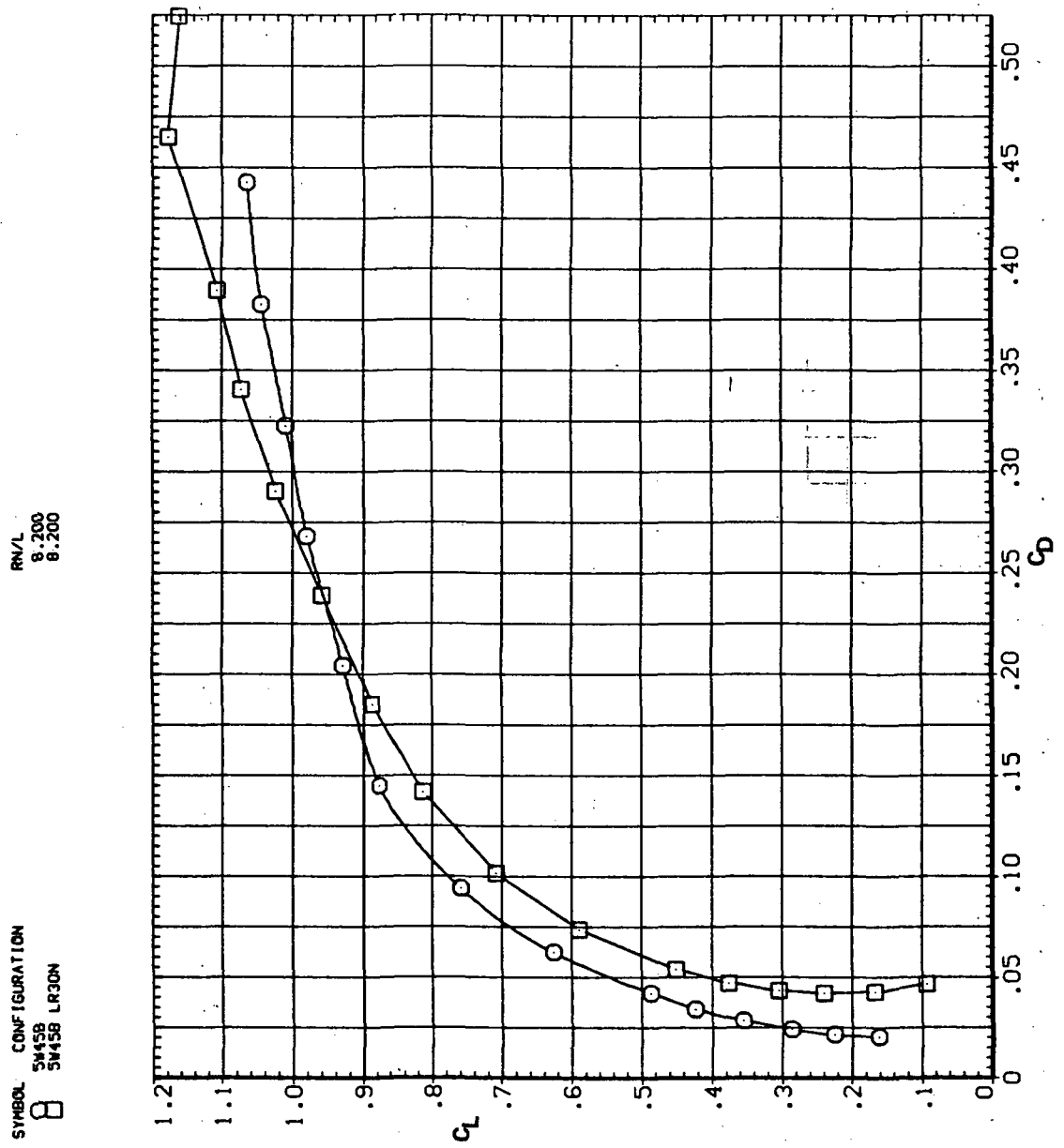
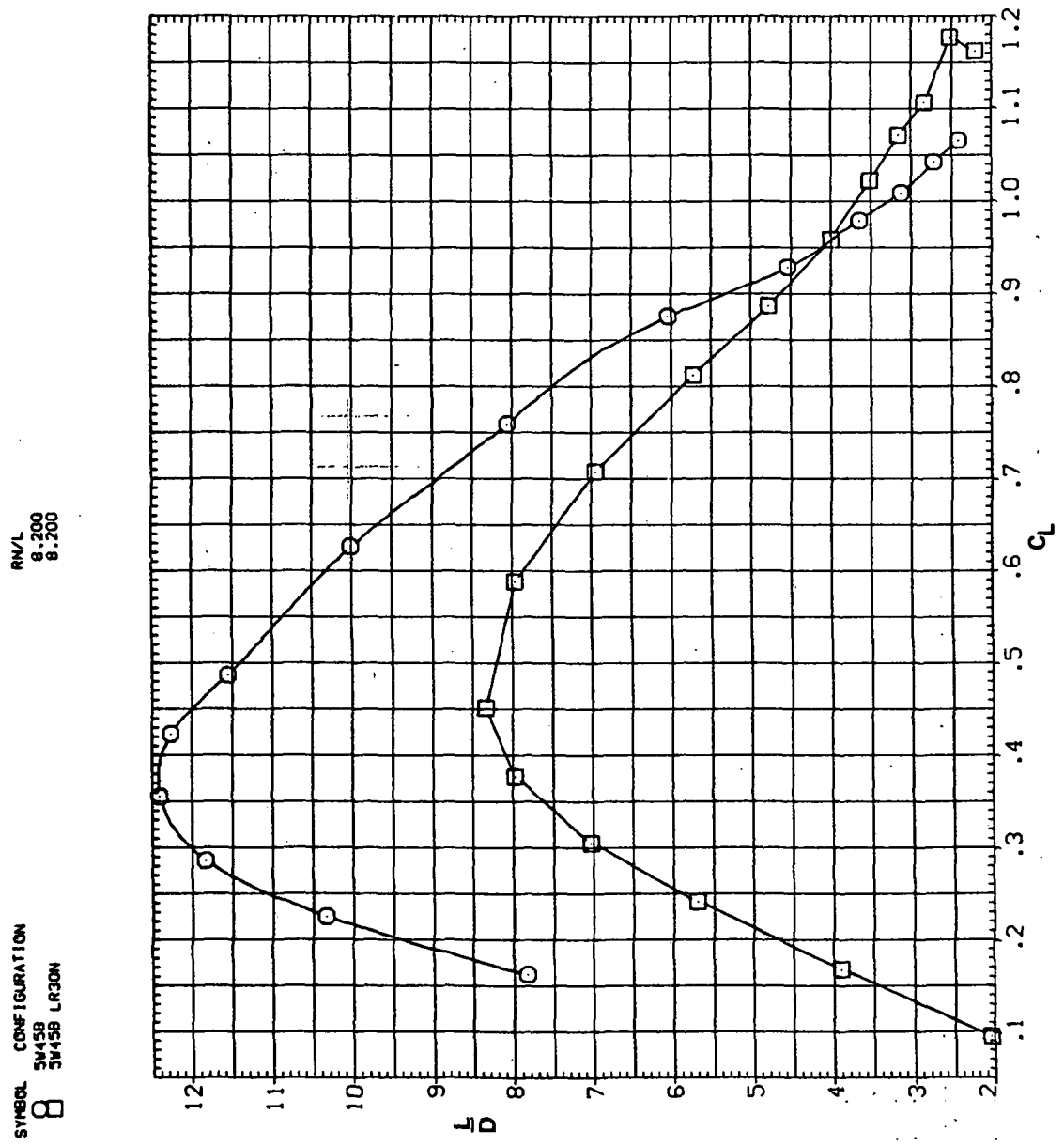
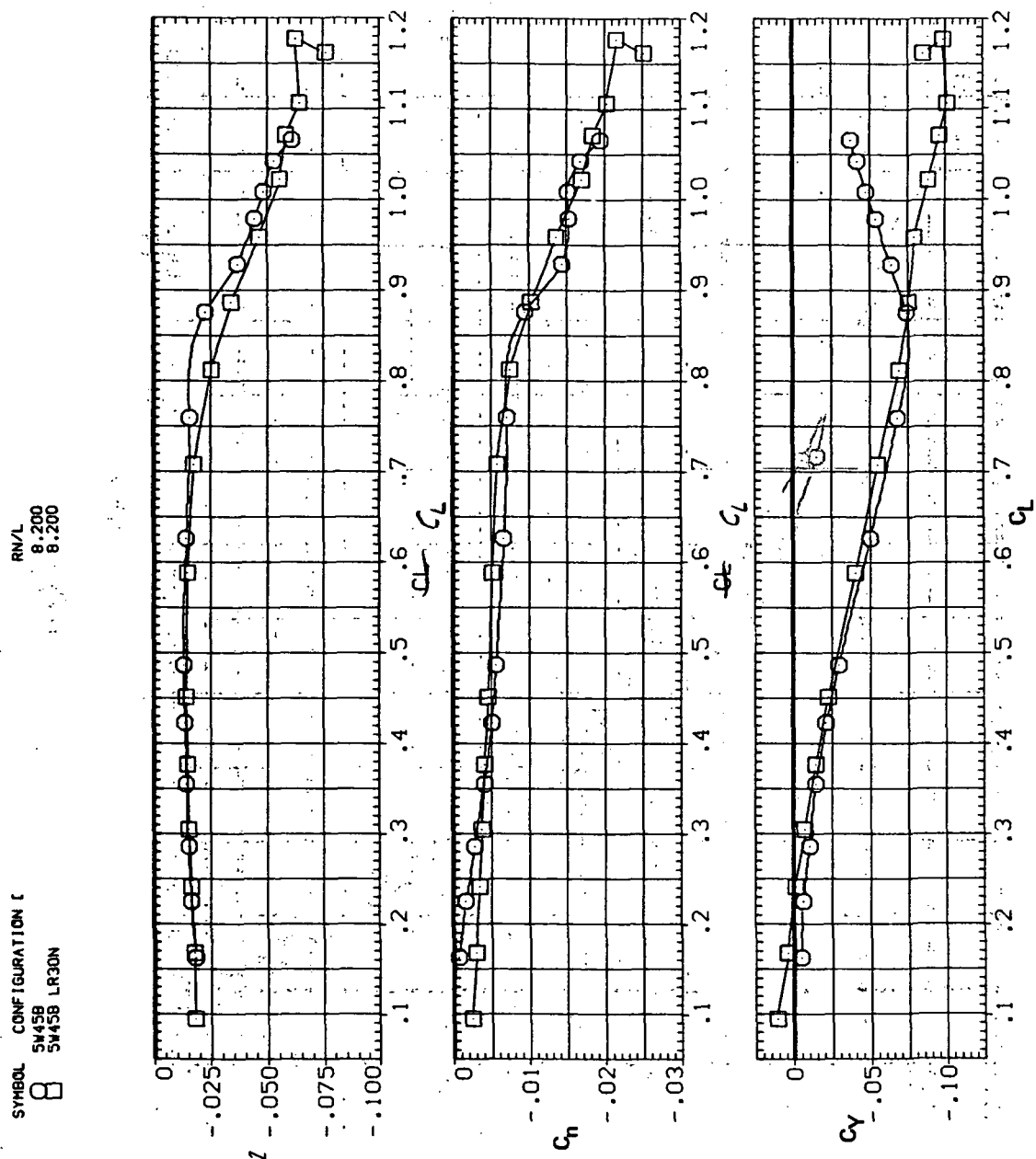


Figure 19.— Continued.



(d)  $L/D$  vs  $C_L$

Figure 19.— Continued.

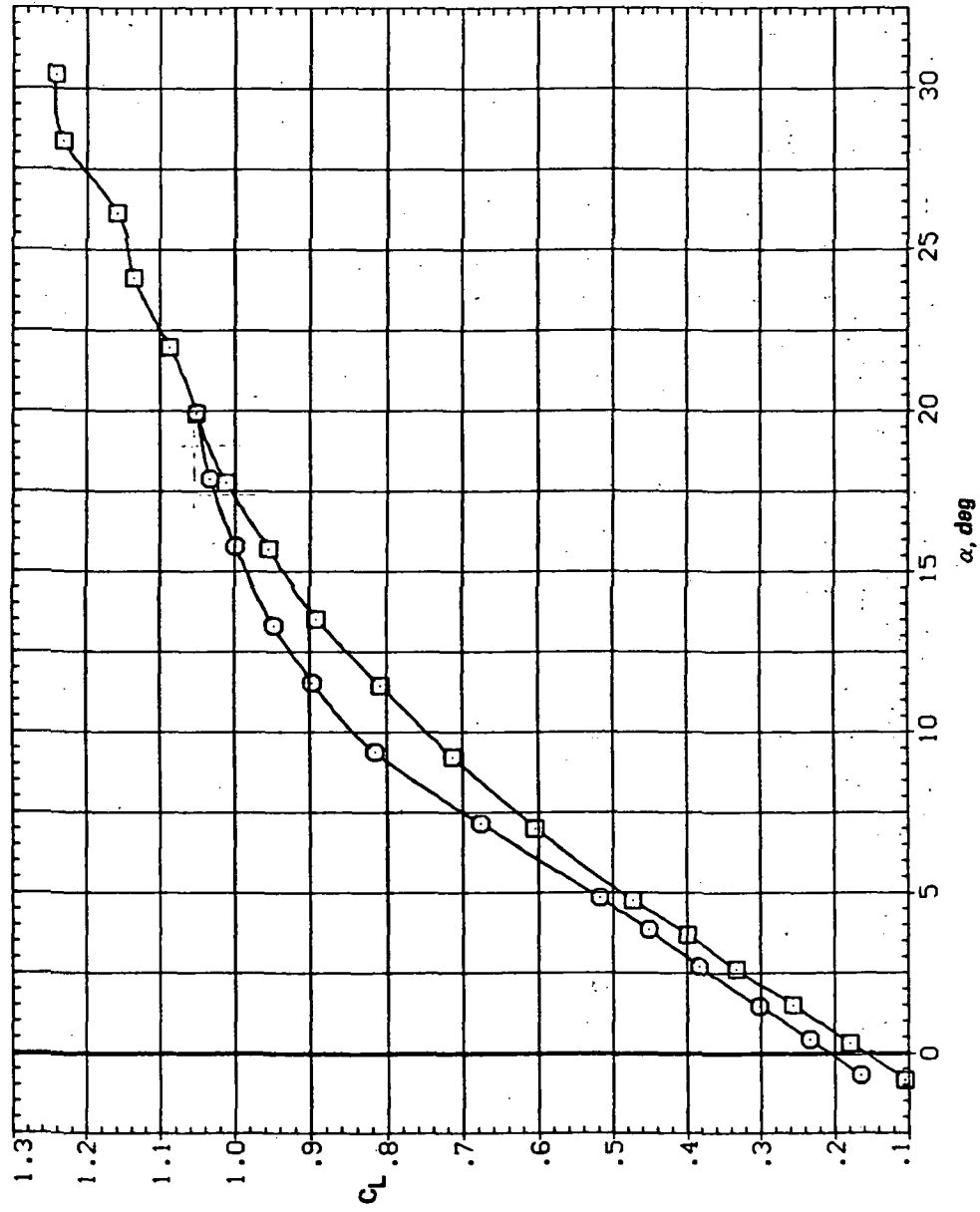


(e)  $C_L$ ,  $C_n$ , and  $C_Y$  vs  $C_L$

Figure 19.— Concluded.

SYMBOL    CONFIGURATION  
□ SW58    LR30N  
○ SW58    LR30N

RNL  
8.200  
8.200

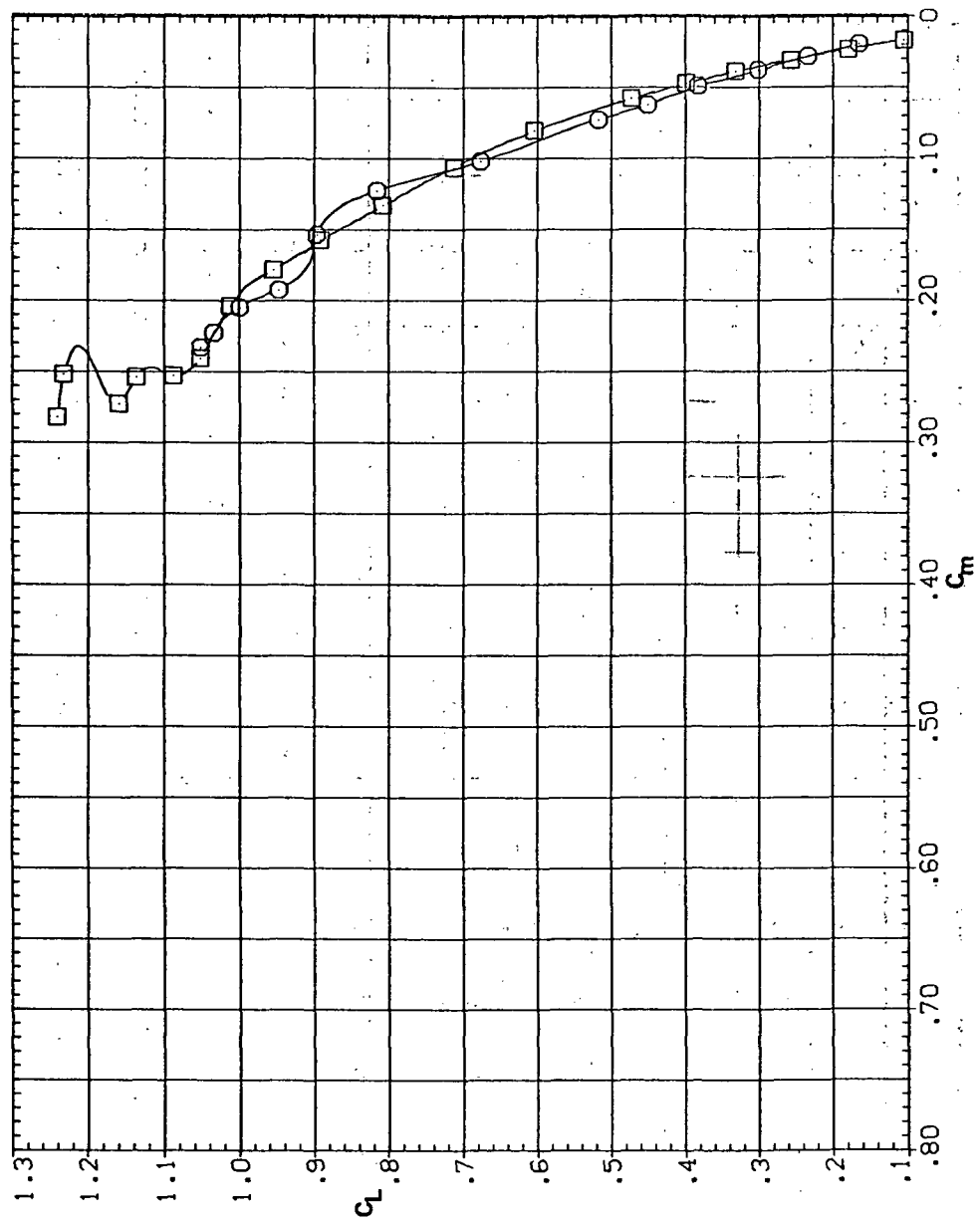


(a)  $C_L$  vs  $\alpha$

Figure 20.—Effect of drooped-nose flaps on the static longitudinal characteristics of the oblique wing: flaps on both wing panels,  $\Lambda = 45^\circ$ ,  $M = 0.9$ .

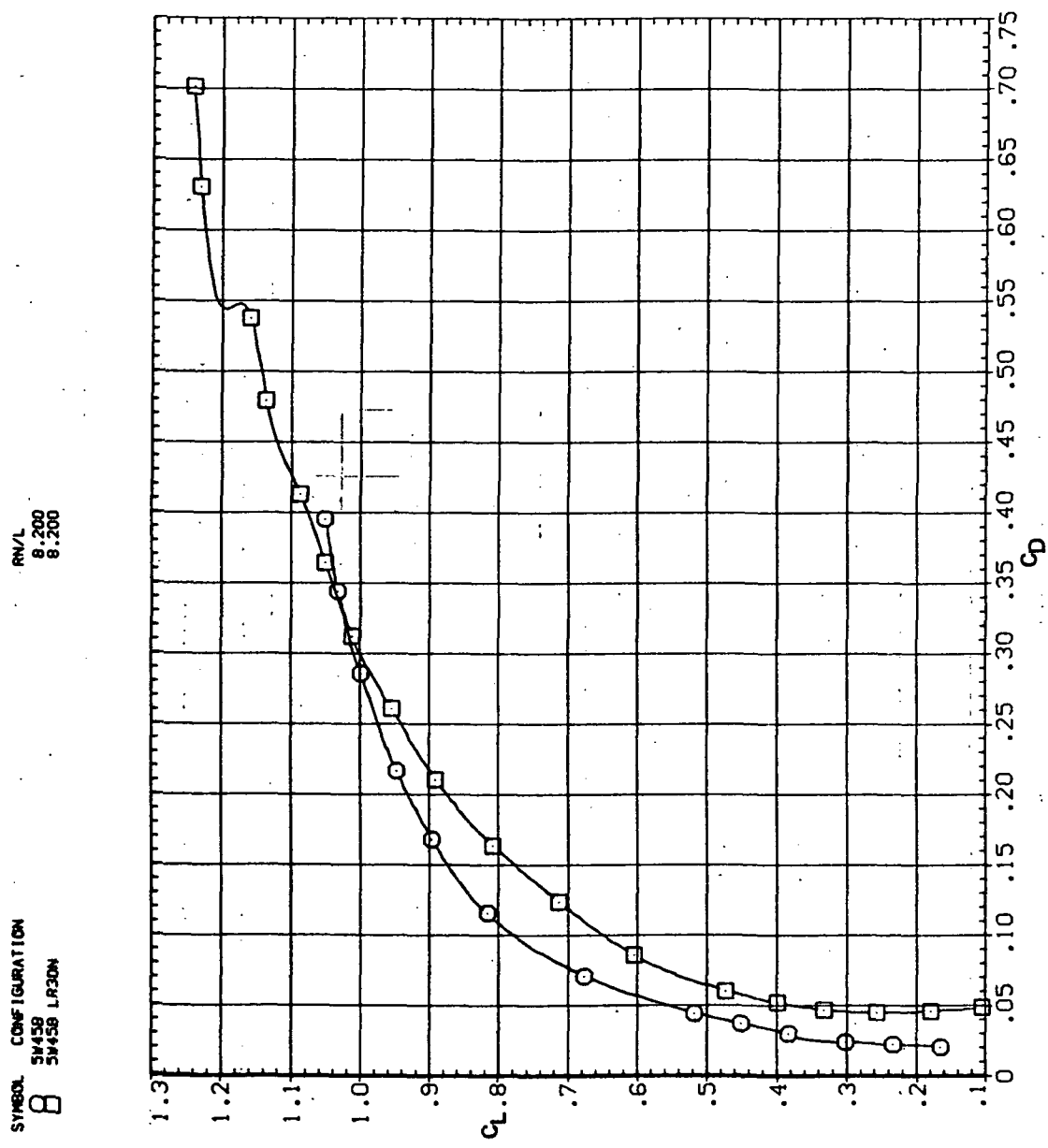
SYMBOL CONFIGURATION  
 5W45B  
 5W45B LR30N

RN/L  
 8.200  
 8.200



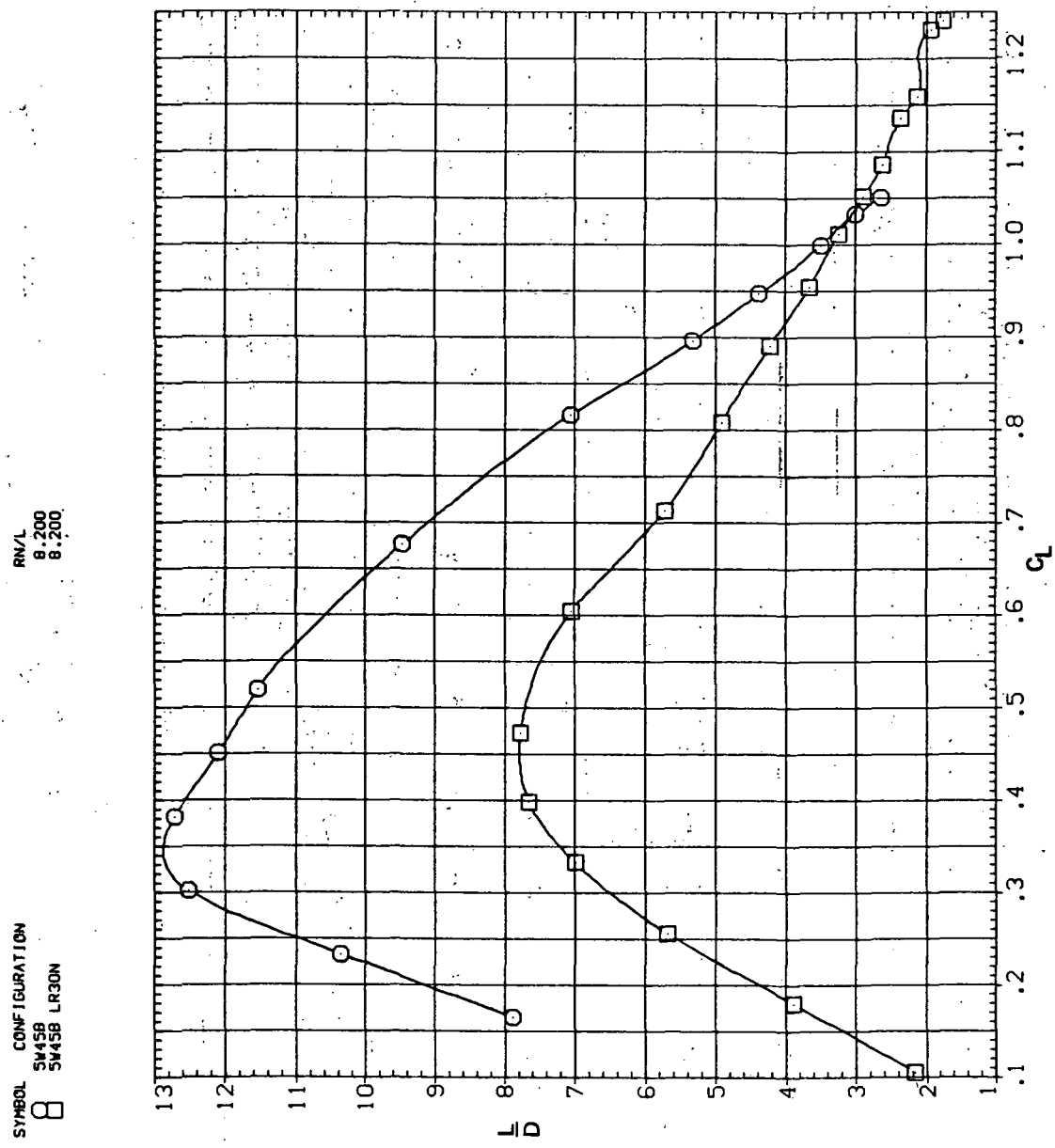
(b)  $C_L$  vs  $C_m$

Figure 20.—Continued.

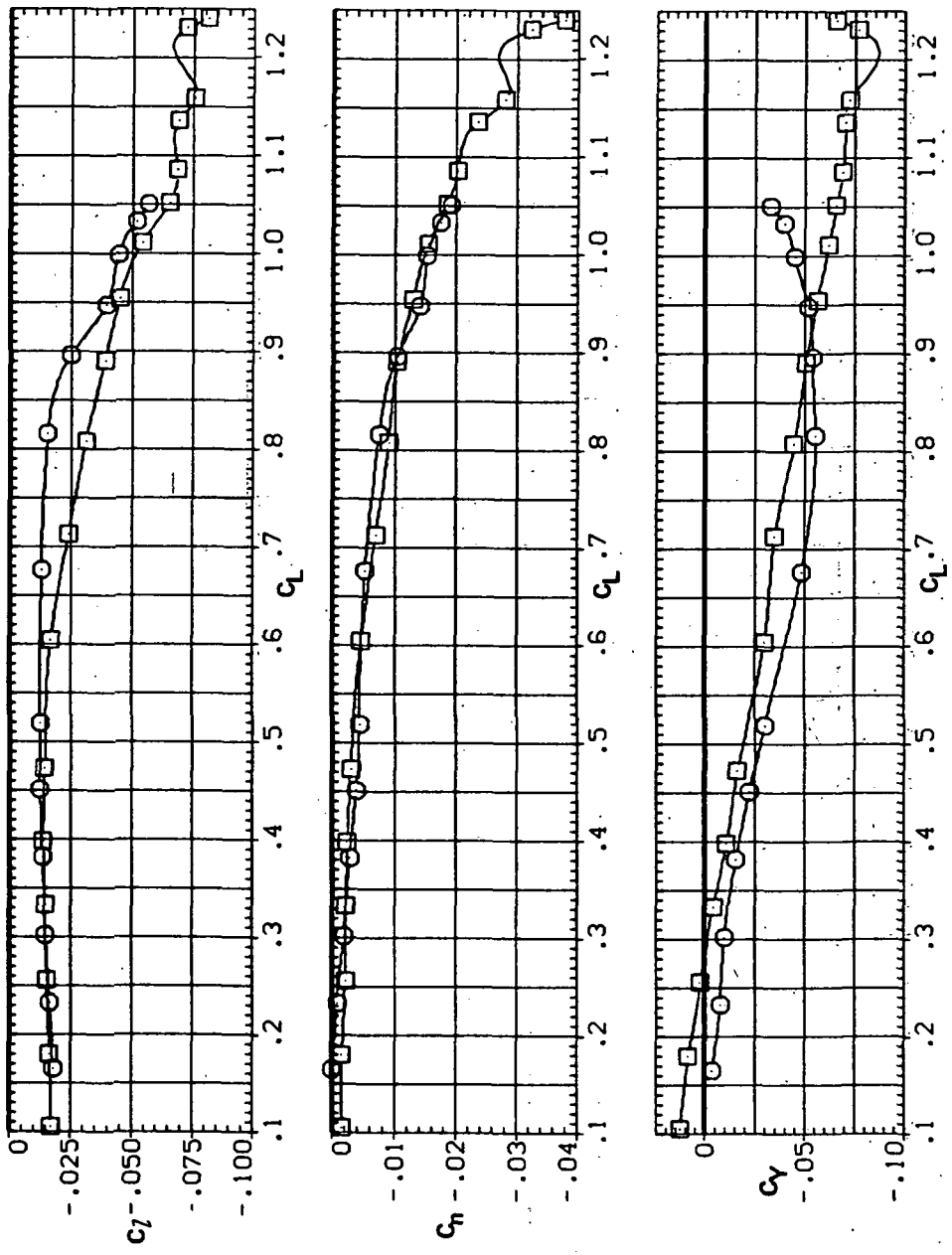


(c)  $C_L$  vs  $C_D$

Figure 20.—Continued.



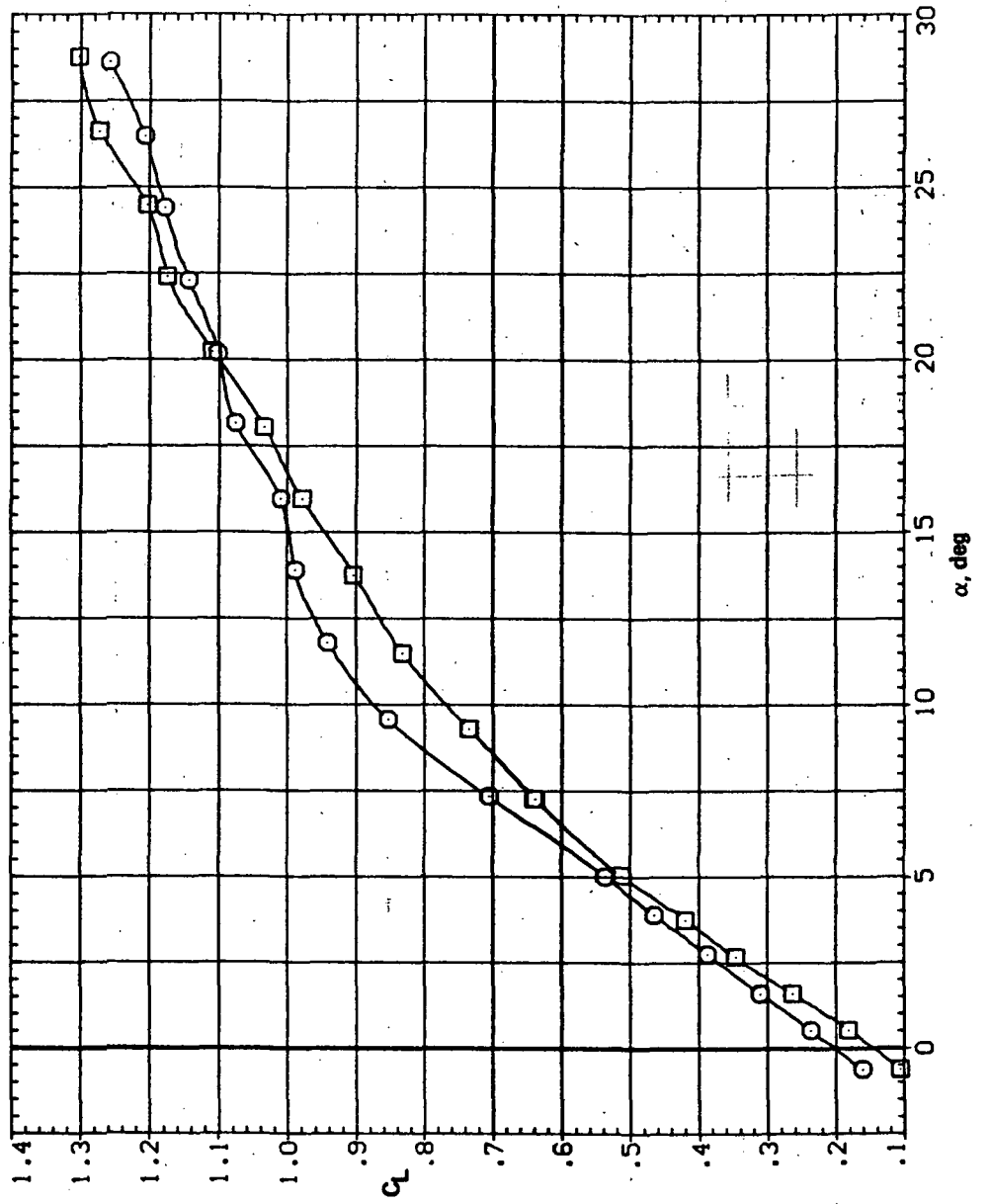
SYMBOL CONFIGURATION  
 8 SM45B SM45B LR30N  
 RNL 8.200  
 8.200



(e)  $C_l$ ,  $C_n$ , and  $C_Y$  vs  $C_L$

Figure 20.— Concluded.

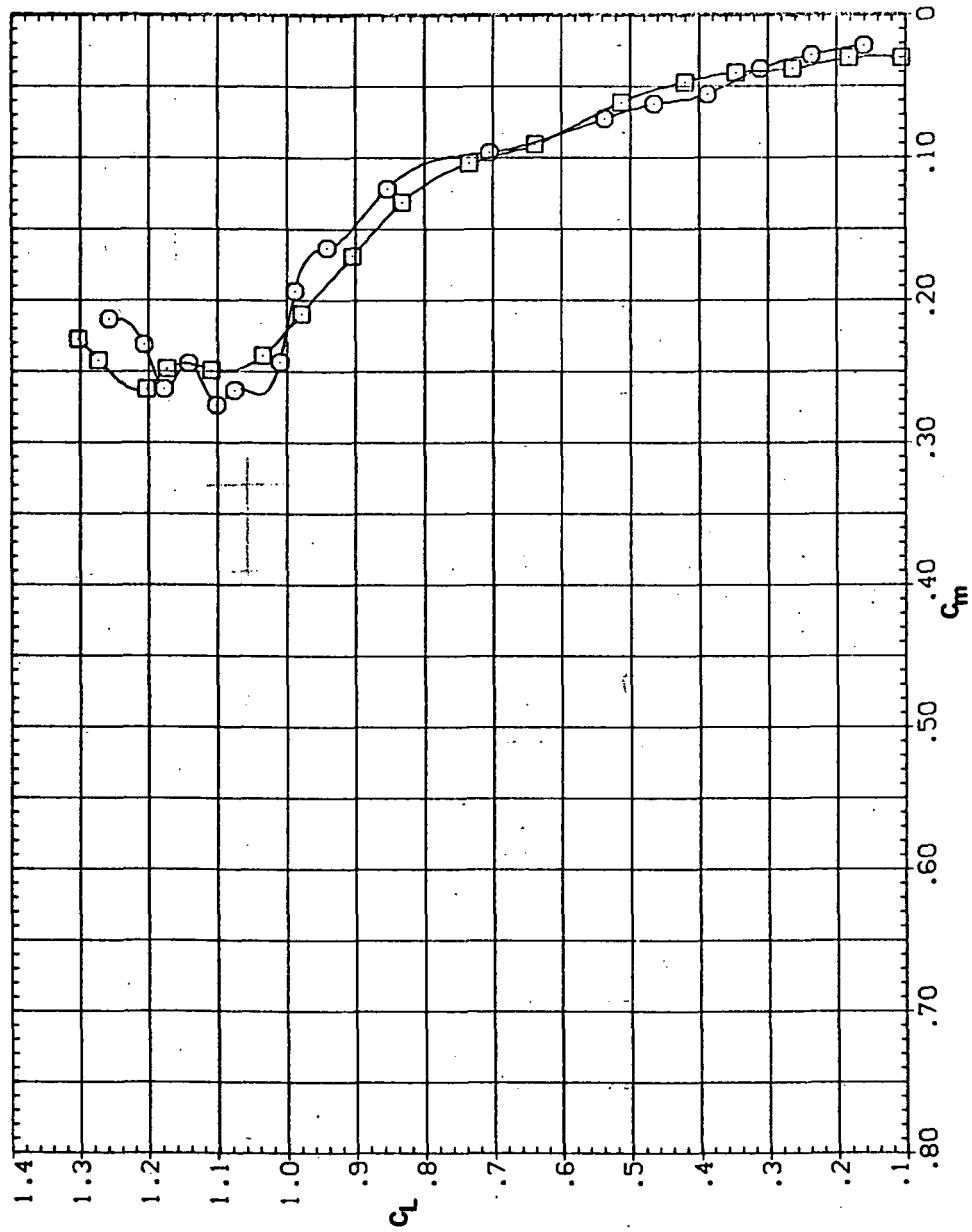
Symbol      CONFIGURATION  
□ SW458      8.2000  
○ SW458 LRDON      8.2000



(a)  $C_L$  vs  $\alpha$

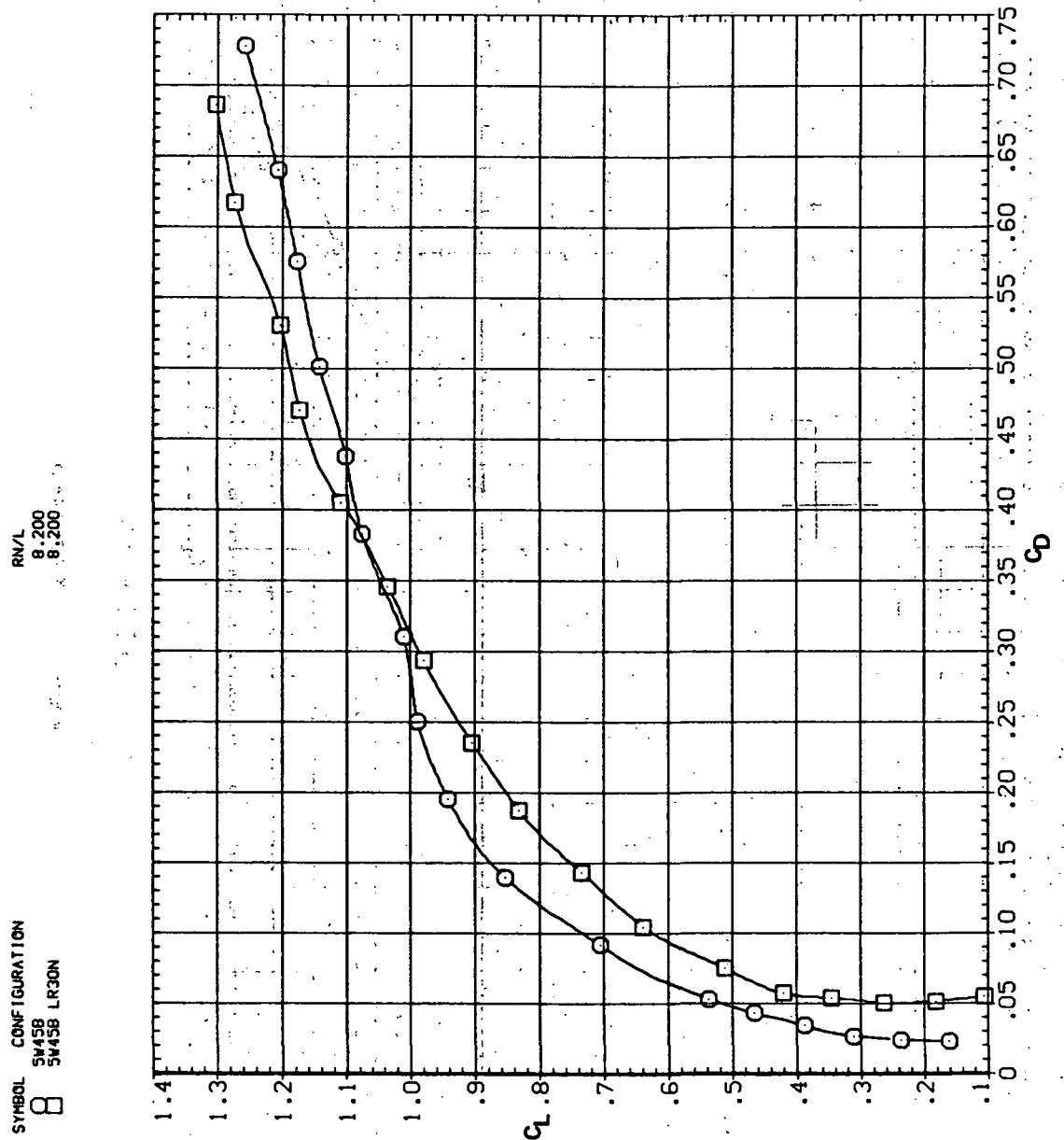
Figure 21.— Effect of drooped-nose flaps on the static longitudinal characteristics of the oblique wing: flaps on both wing panels,  $\Lambda = 45^\circ$ ,  $M = 0.95$ .

SYMBOL CONFIGURATION  
 8 SW458 SW458 LR30N



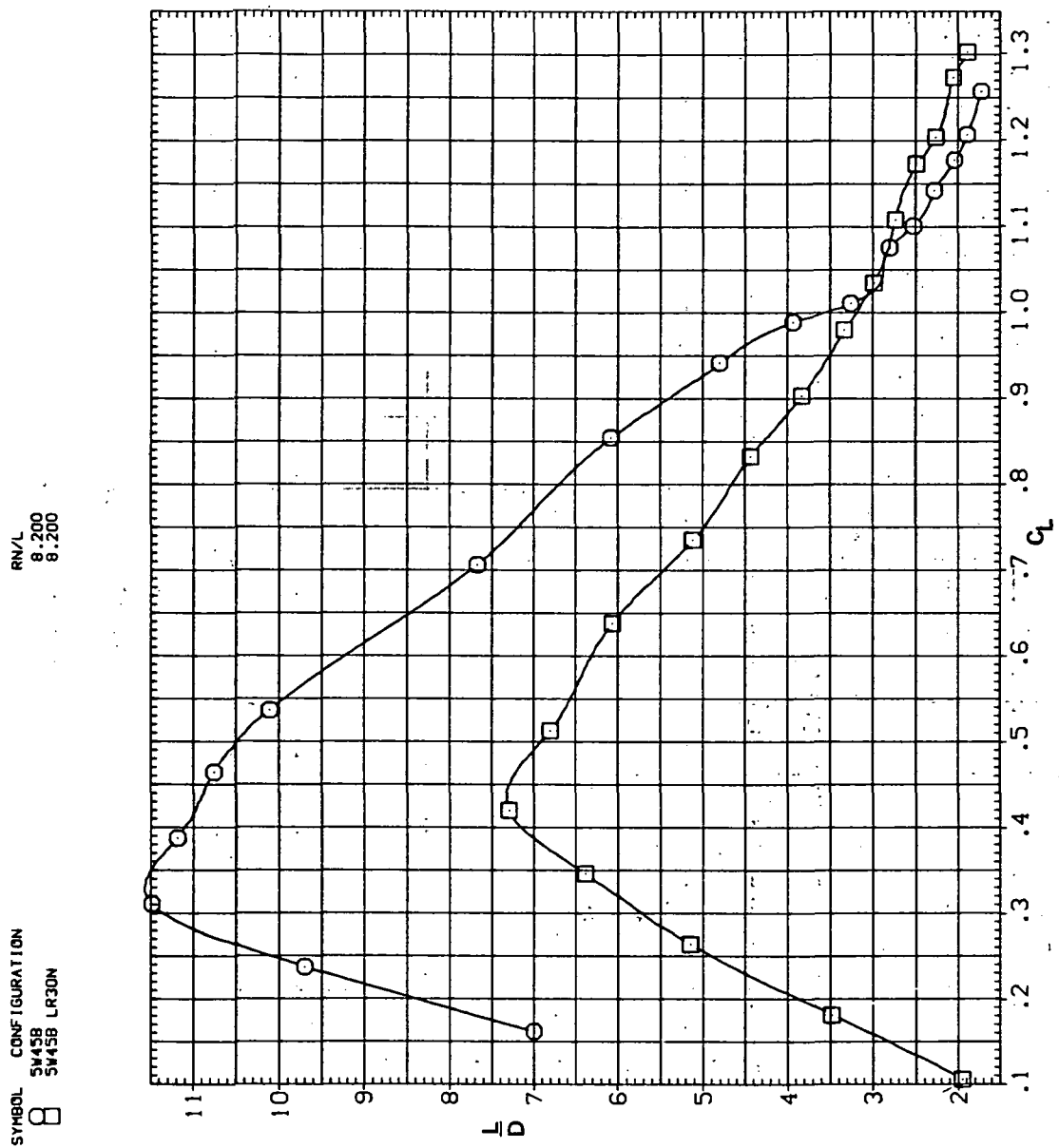
(b)  $C_L$  vs  $C_m$

Figure 21.—Continued.



(c)  $C_L$  vs  $C_D$

Figure 21.—Continued.

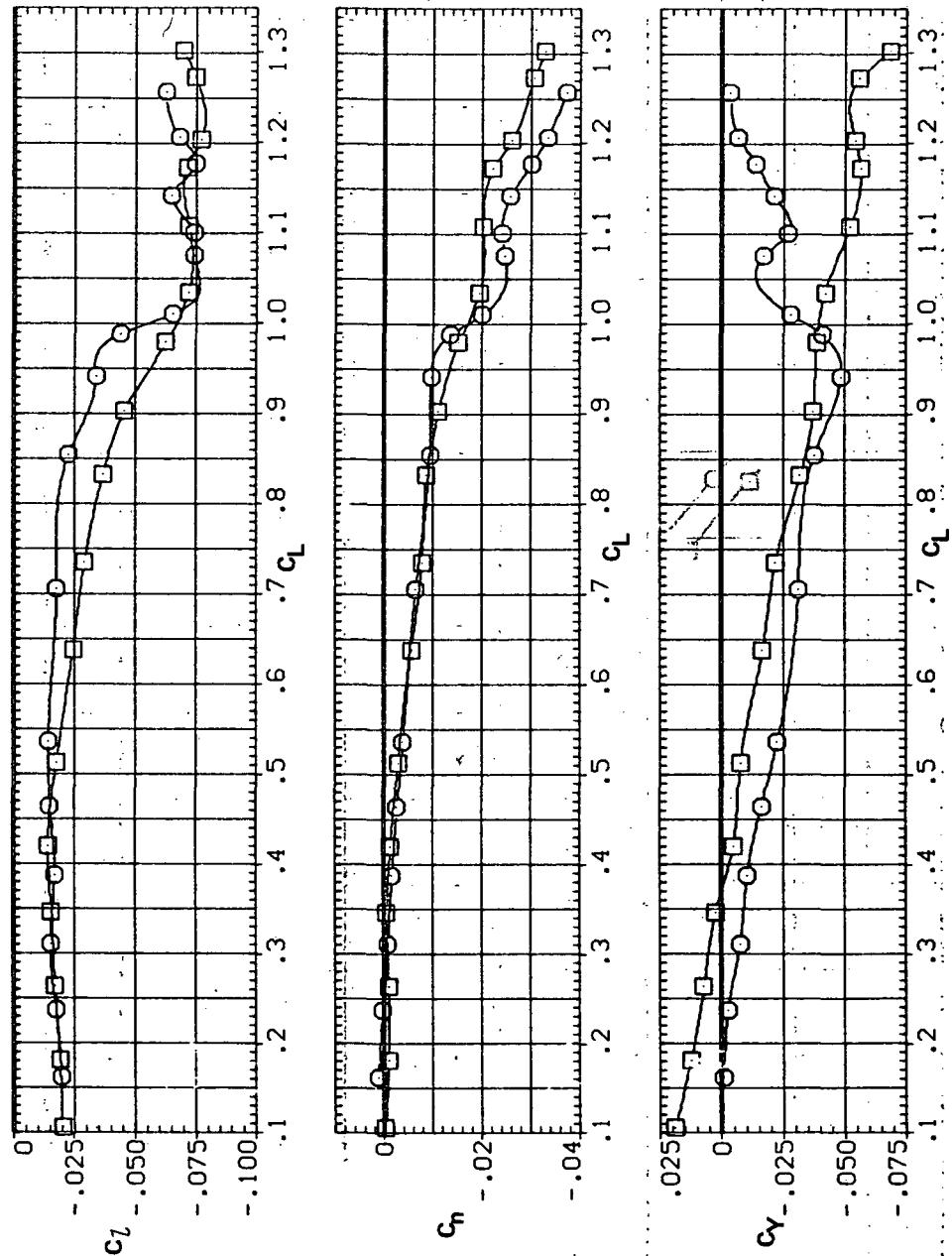


(d)  $L/D$  vs  $C_L$

Figure 21.—Continued.

SYMBOL CONFIGURATION  
□ SW45B LR3DN

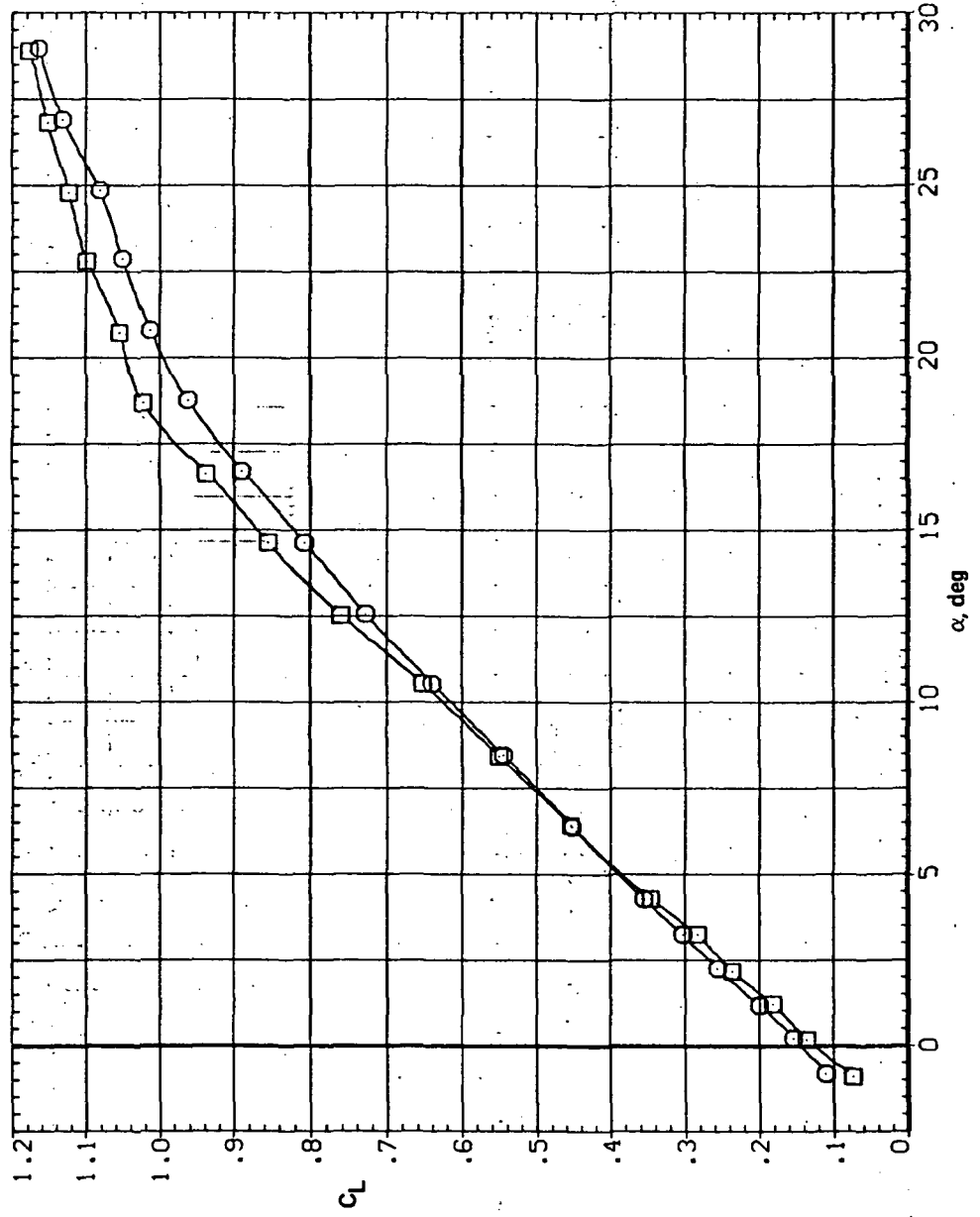
RN/L  
 8.200  
 8.200



(e)  $C_L$ ,  $C_n$ , and  $C_Y$  vs.  $C_L$

Figure 21.— Concluded.

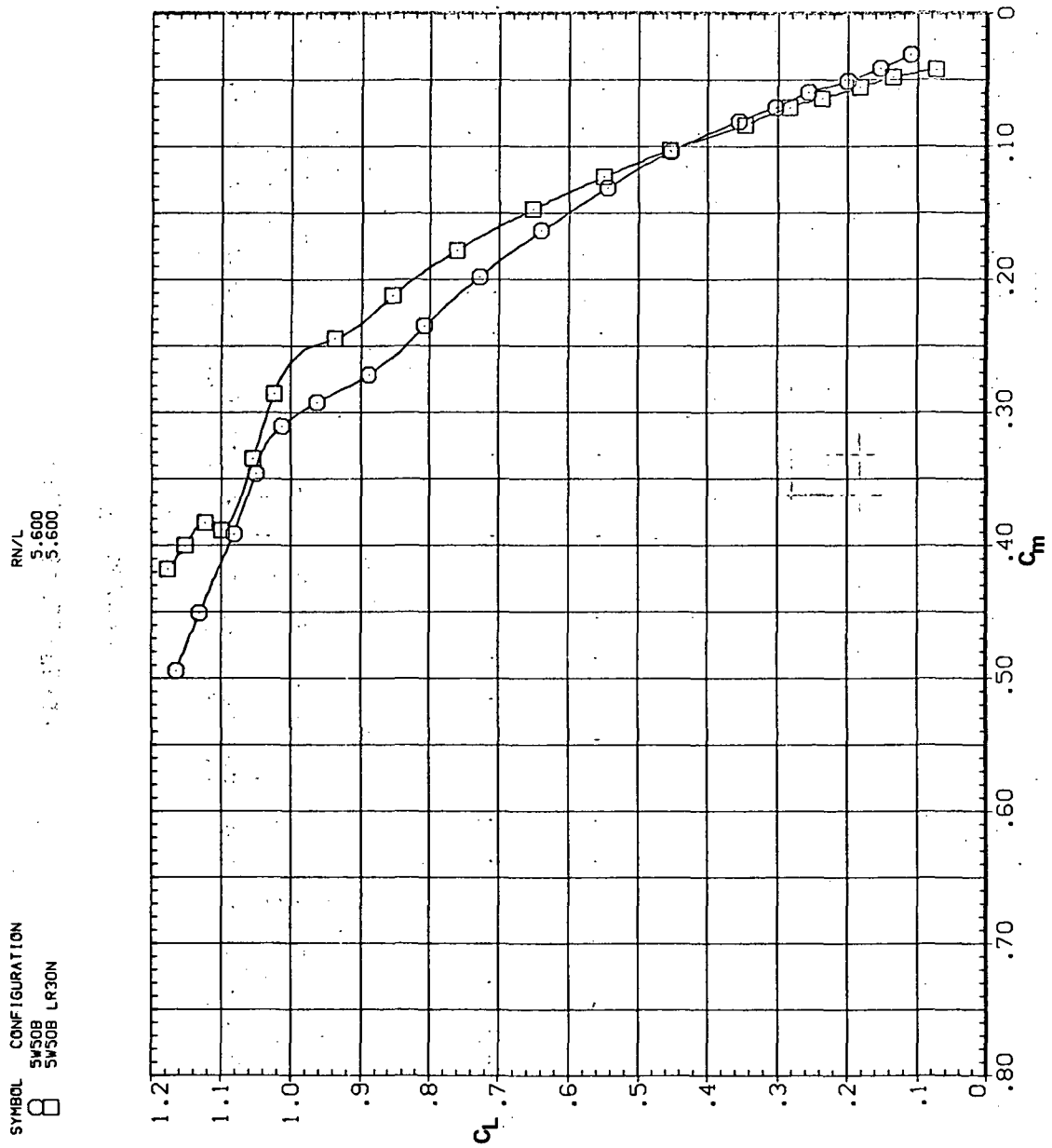
SYMBOL CONFIGURATION      RNL/5.600  
 S550B LR30N



(a)  $C_L$  vs  $\alpha$

Figure 22.—Effect of drooped-nose flaps on the static longitudinal characteristics of the oblique wing: flaps on both wing panels,  $\Lambda = 50^\circ$ ,  $M = 0.25$ .

SYMBOL CONFIGURATION  
 SW50B SW50B LR30N



(b)  $C_L$  vs.  $C_m$

Figure 22.—Continued.

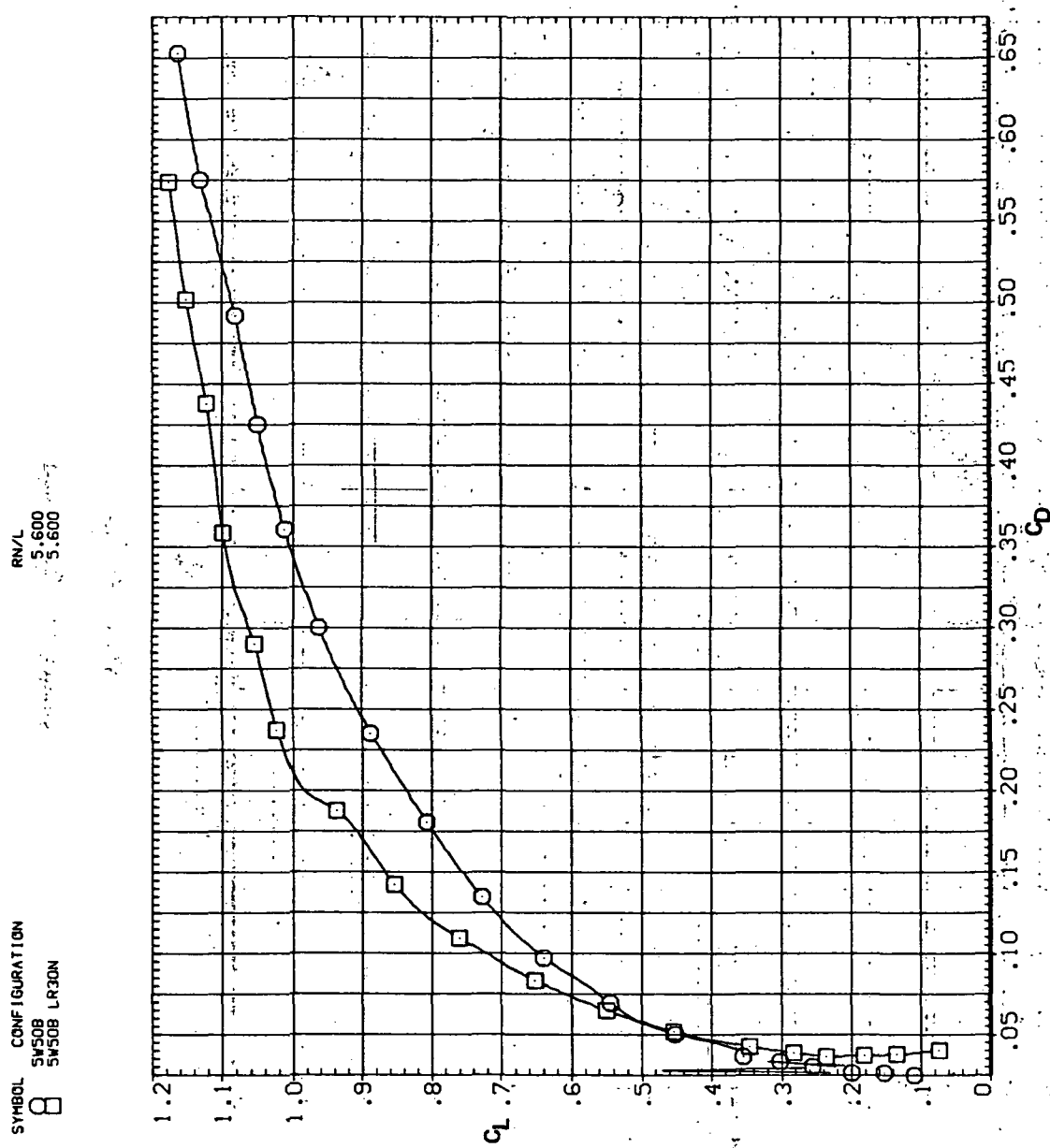


Figure 22.—Continued.  
(c)  $C_L$  vs  $C_D$

SYMBOL CONFIGURATION  
□ 5508  
□ 5508 LR30N

RN/L  
8.200  
8.200

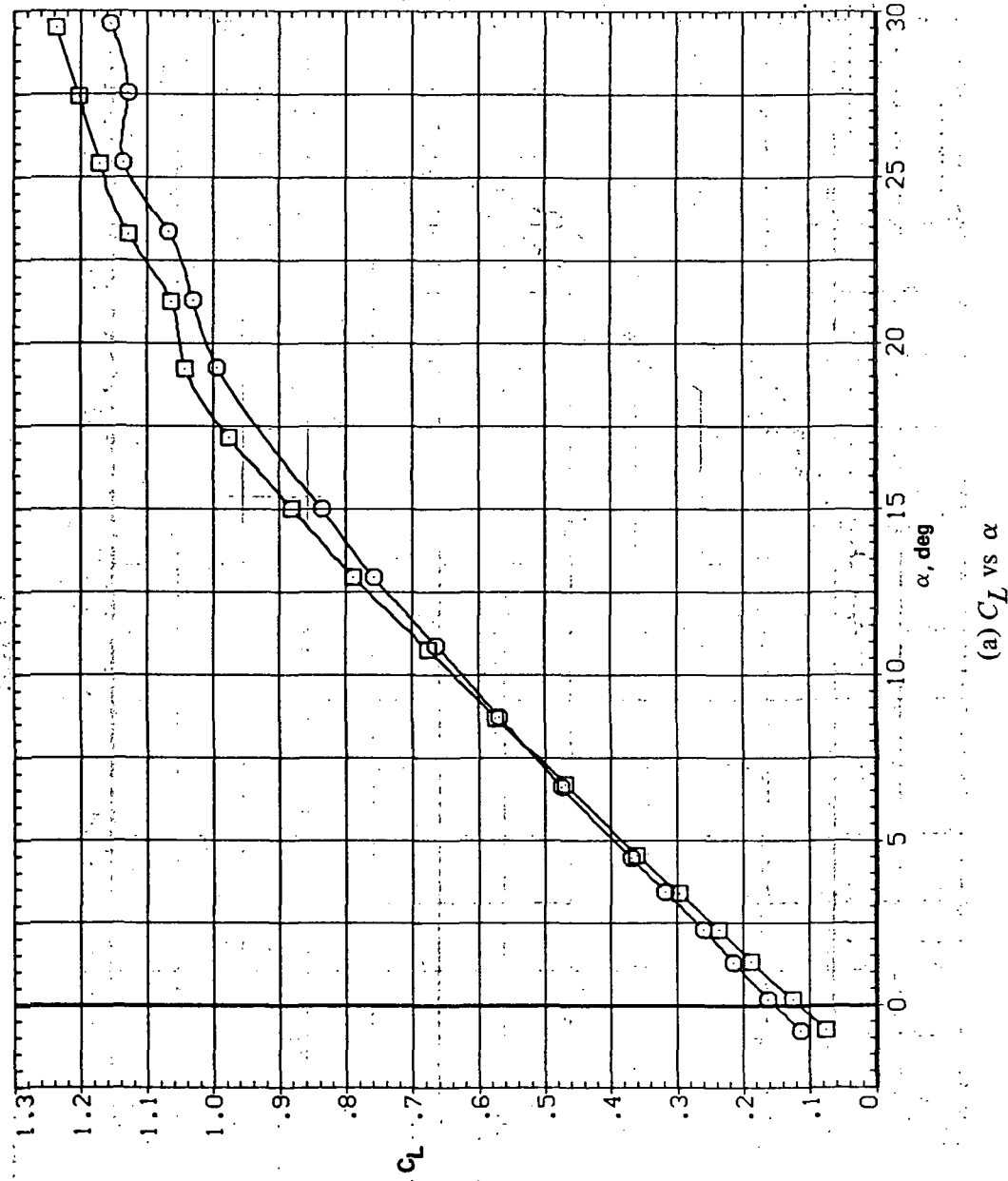
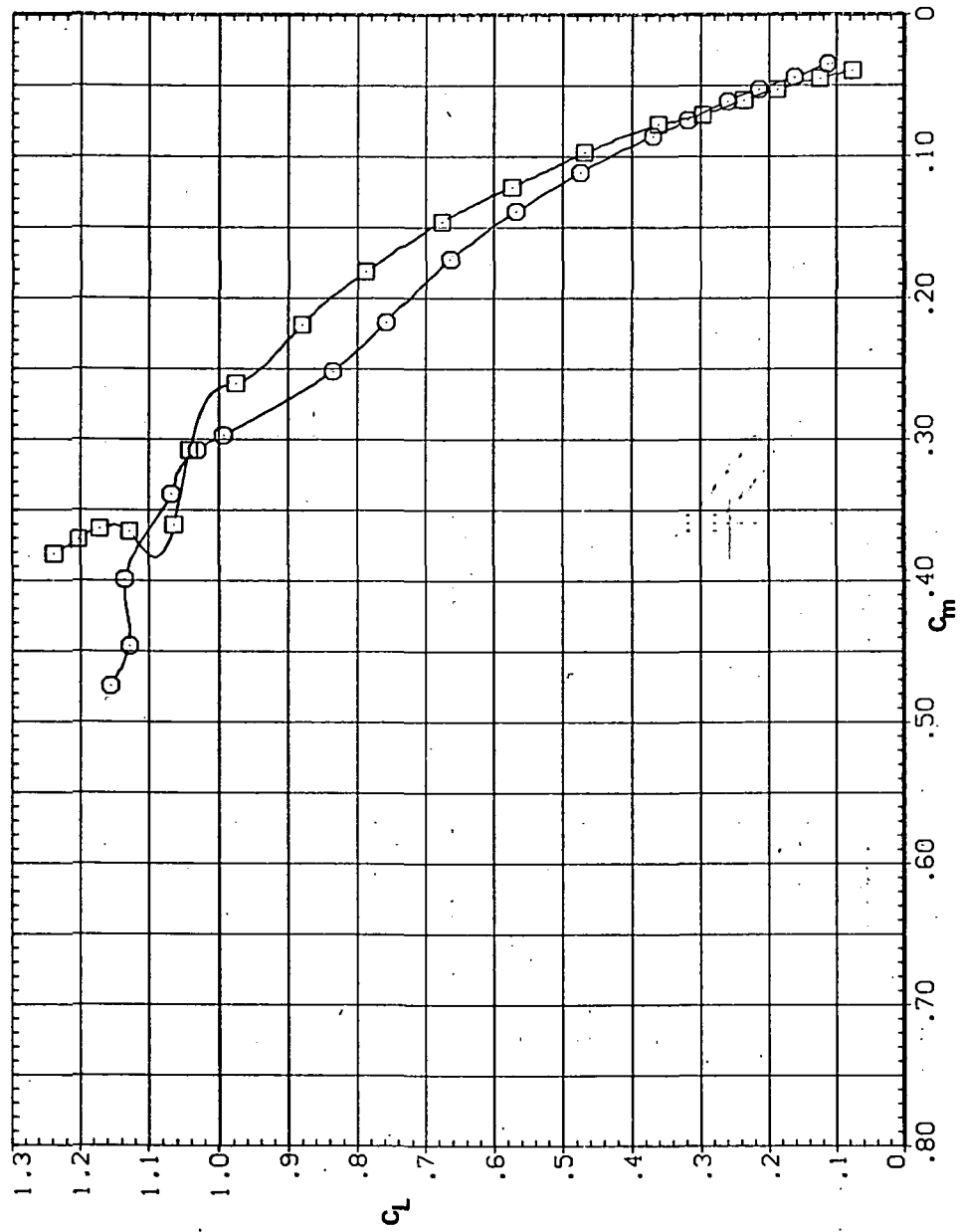


Figure 23.— Effect of drooped-nose flaps on the static longitudinal characteristics of the oblique wing: flaps on both wing panels,  $\Lambda = 50^\circ$ ,  $M = 0.4$ .

TABLE 1  
 SYMBOL CONFIGURATION  
 SW508 SW508 LR30N  
 RNL 8.200 8.200

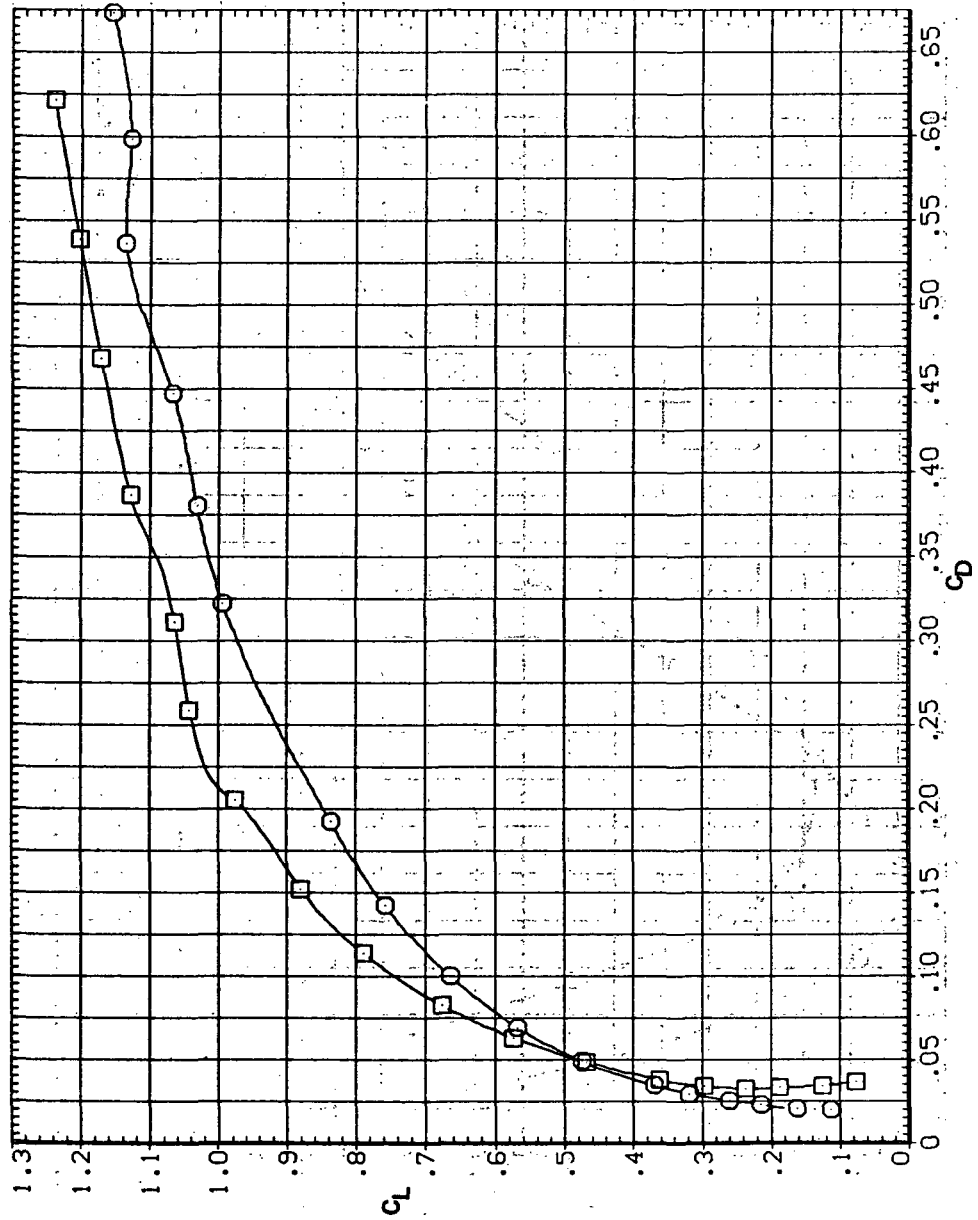


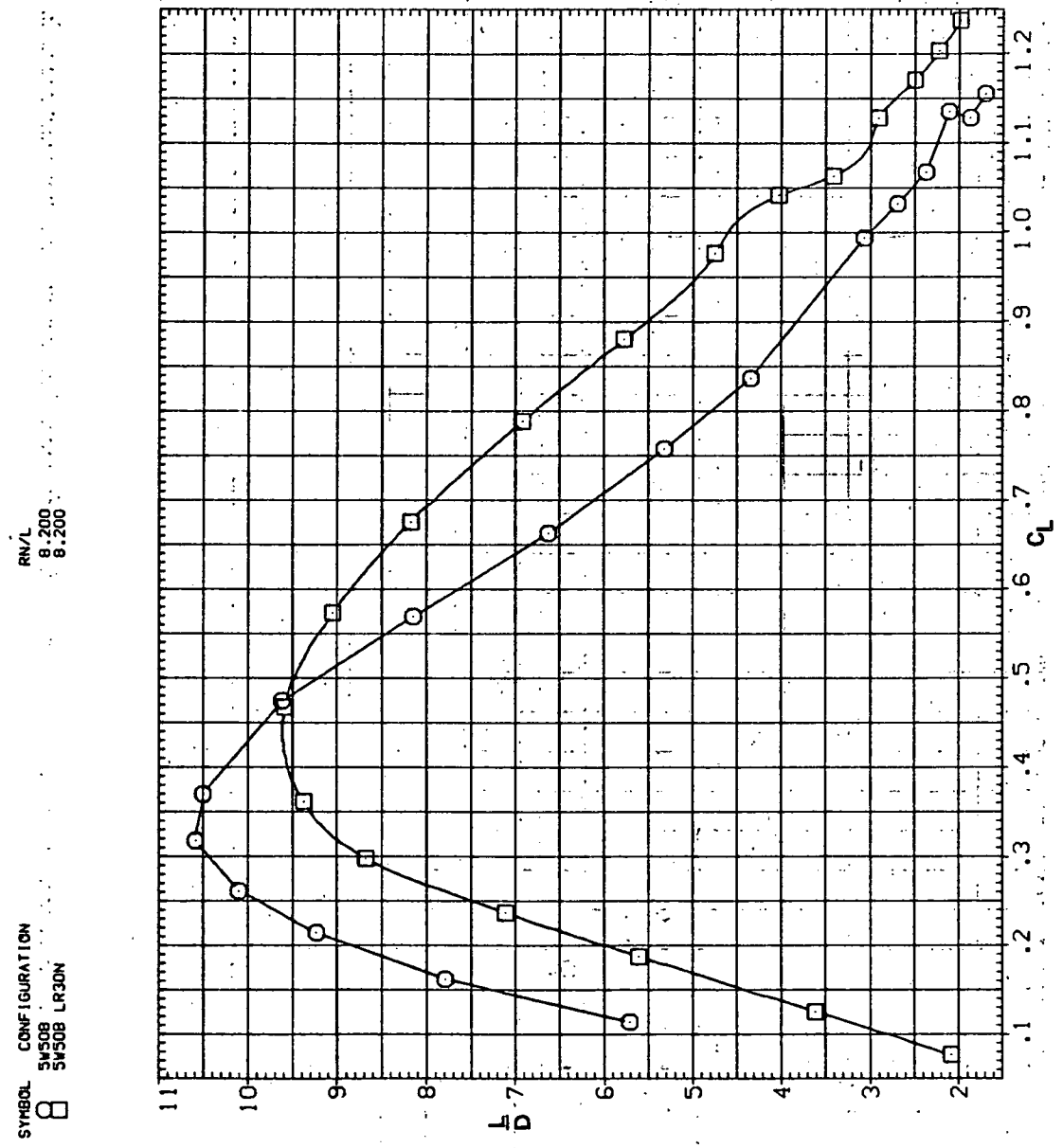
(b)  $C_L$  vs  $C_m$

Figure 23.—Continued.

SYMBOL CONFIGURATION  
SW508 SW508 LR30N

RN/IC  
8.200  
8.200

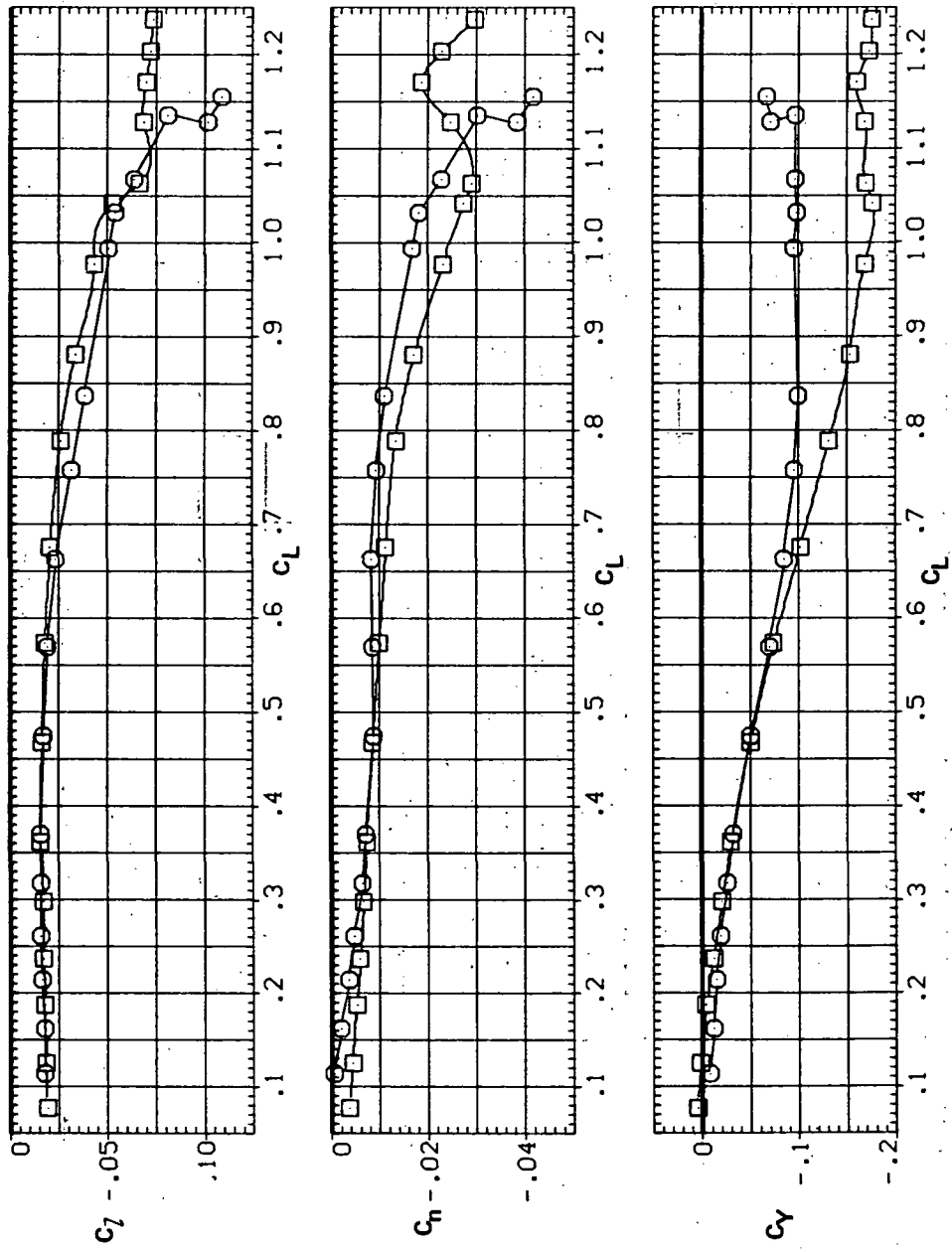




(d)  $L/D$  vs  $C_L$

Figure 23.—Continued.

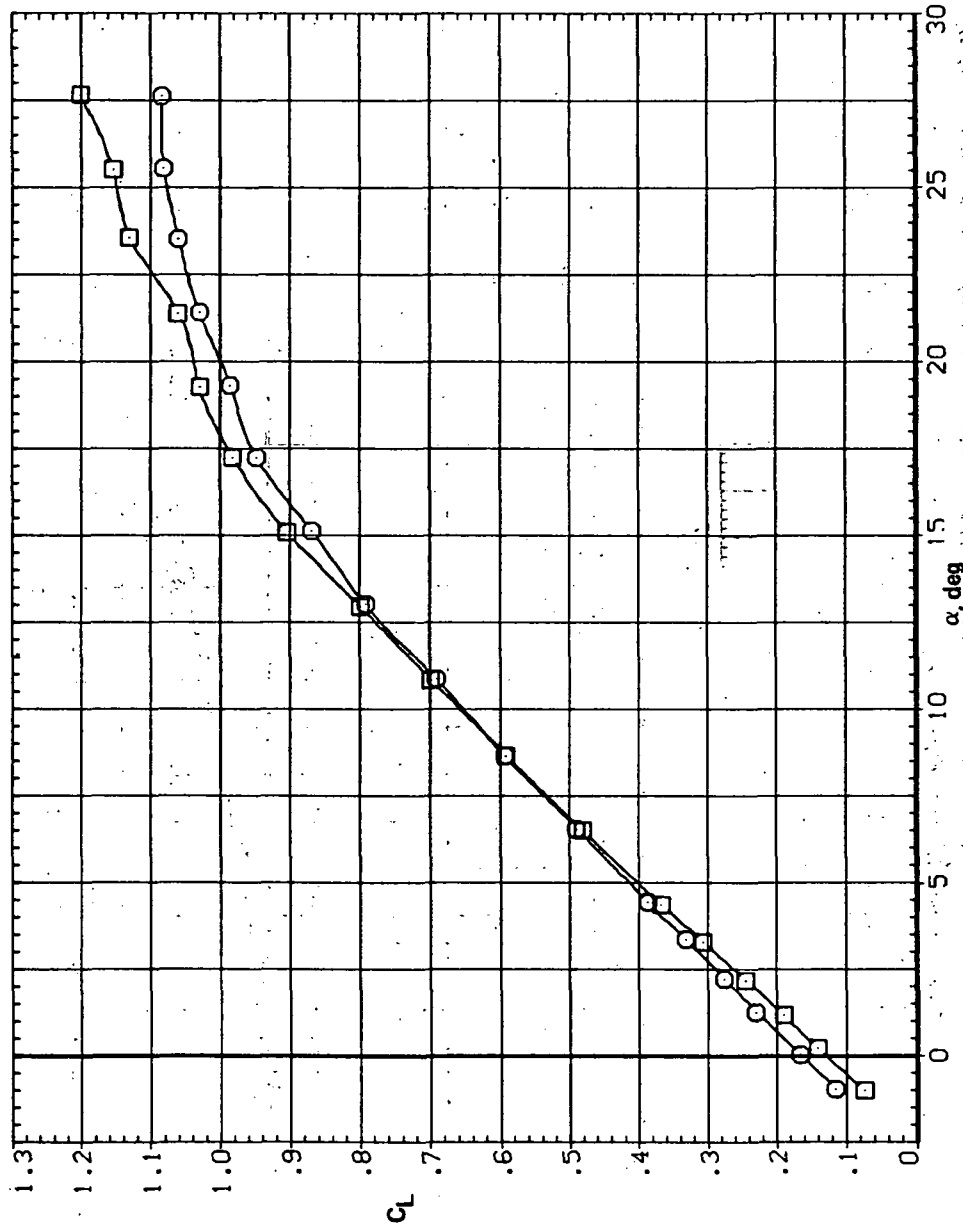
TABLE 1  
 SYMBOL CONFIGURATION  $R_N/L$   
 8 5950B LR30N 8.200  
 8 5950B LR30N 8.200



(e)  $C_L$ ,  $C_D$ , and  $C_Y$  vs.  $C_L$

Figure 23.—Concluded.

SYMBOL CONFIGURATION  
□ RNL 8.200  
○ SW508 8.200  
□ SW508 LR30N



(a)  $C_L$  vs  $\alpha$

Figure 24.— Effect of drooped-nose flaps on the static longitudinal characteristics of the oblique wing: flaps on both wing panels,  $\Lambda = 50^\circ$ ,  $M = 0.6$ .

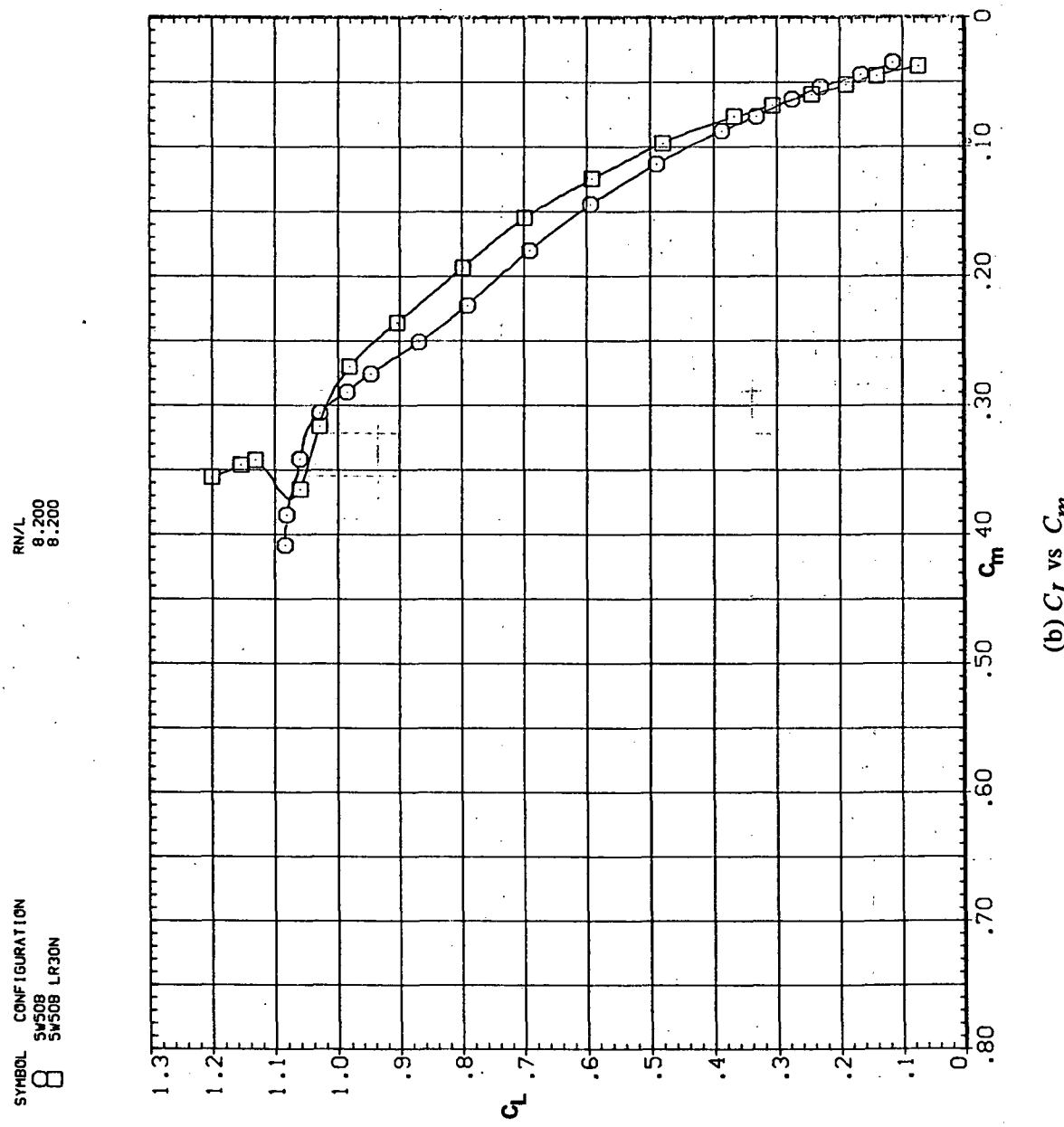
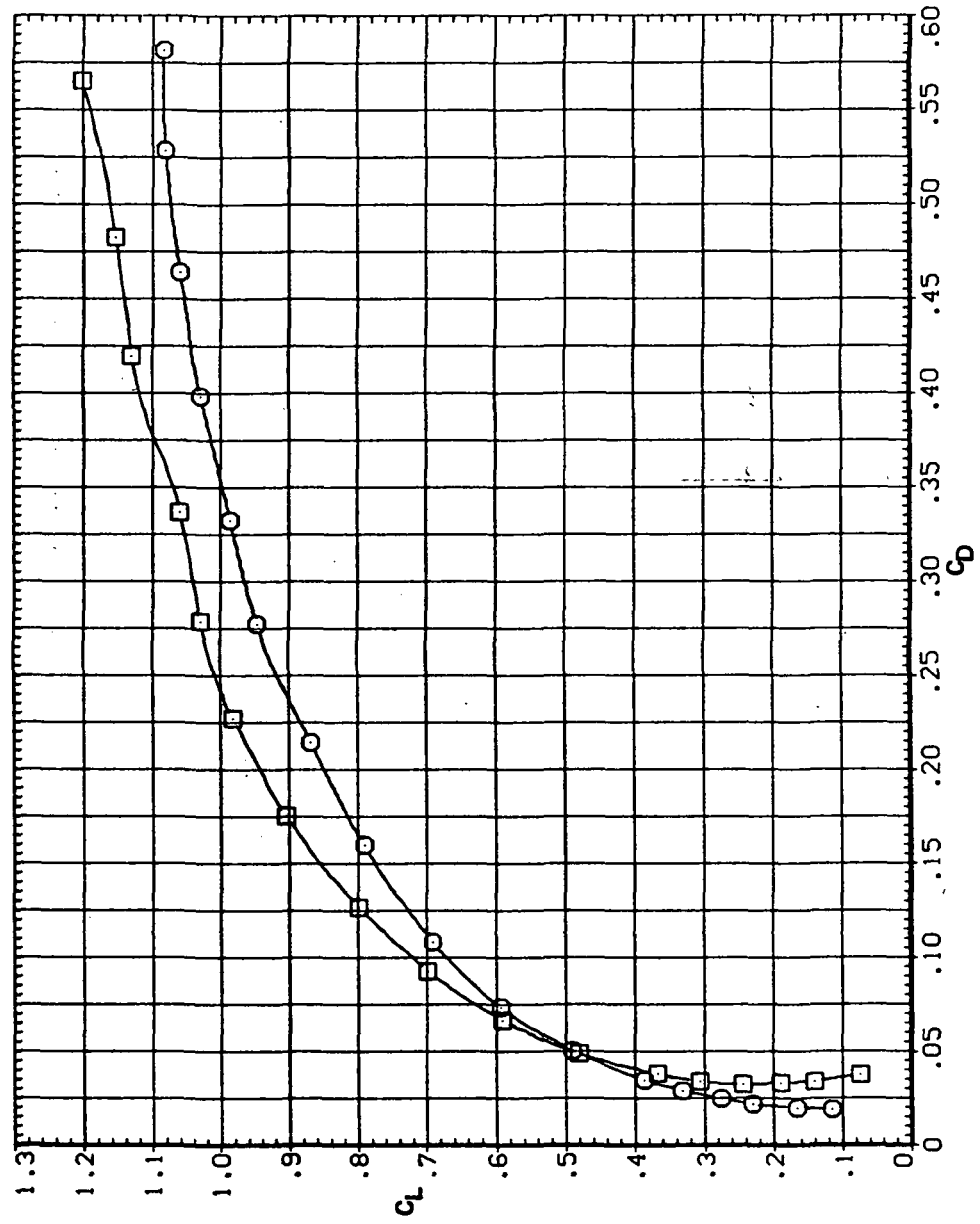


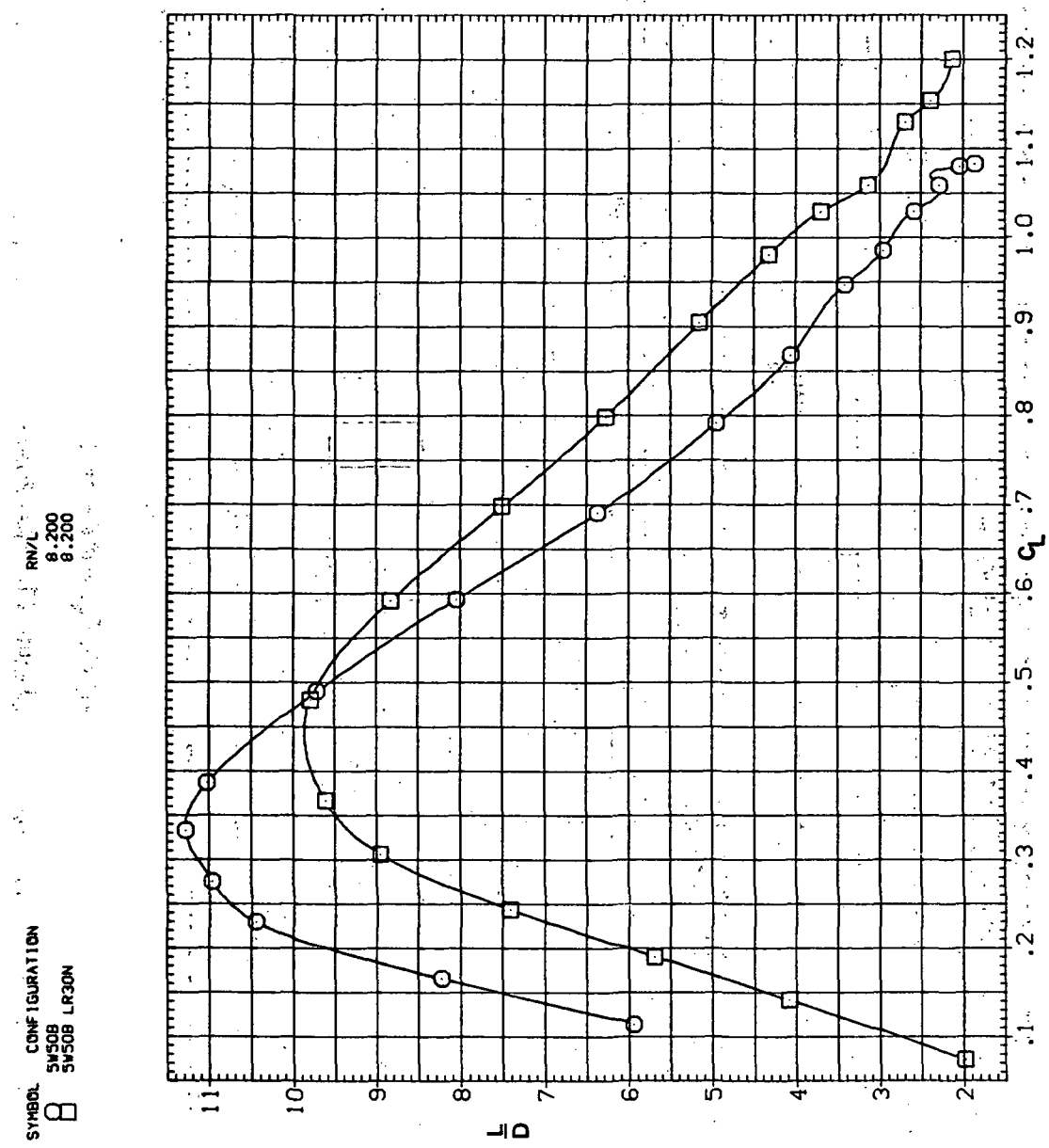
Figure 24.—Continued.

Symbol      Configuration  
 $\square$       5W508 LR30W  
 $\circ$       5W508 8.200



(c)  $C_L$  vs  $C_D$

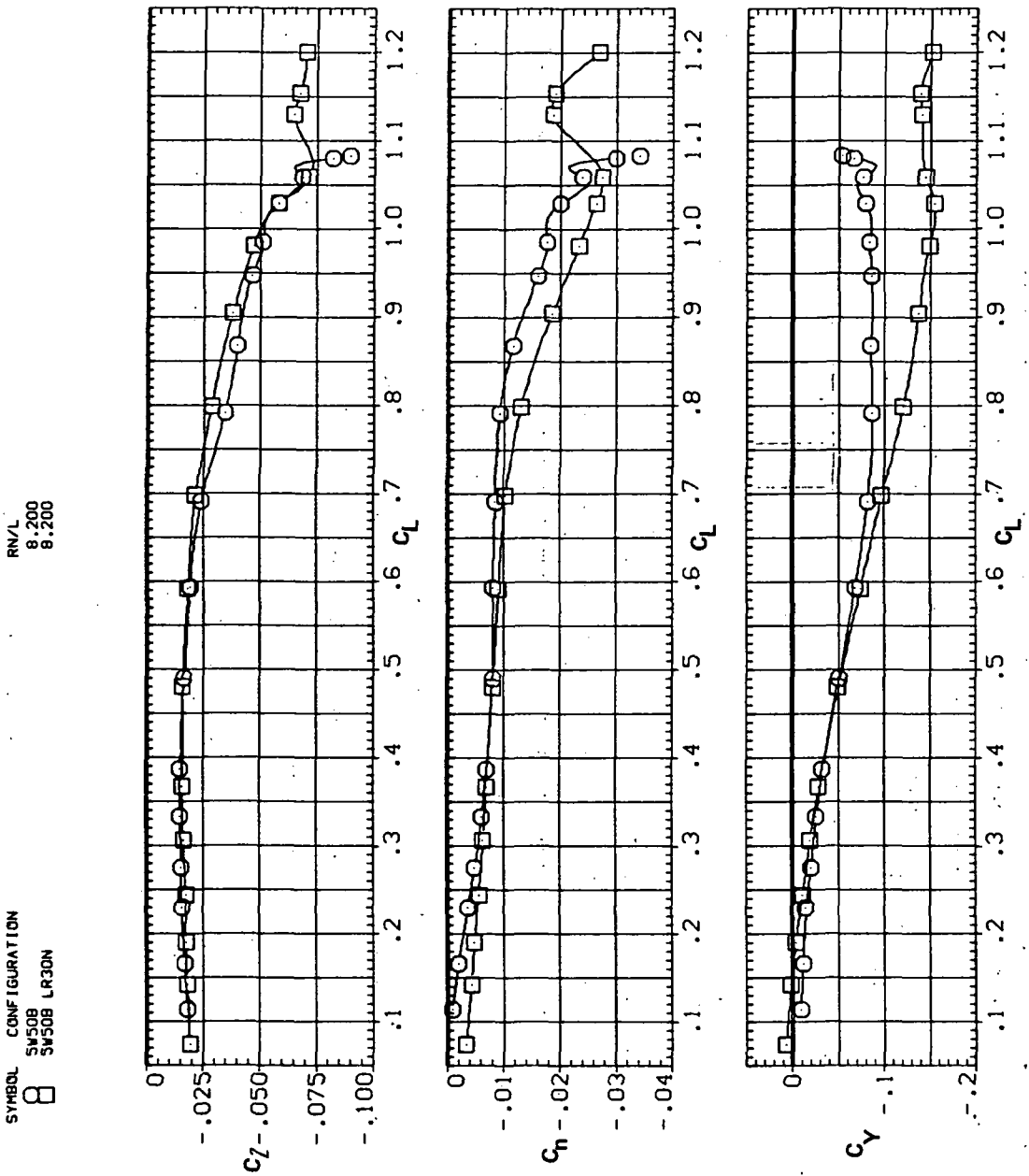
Figure 24.— Continued.



(d)  $L/D$  vs  $C_L$

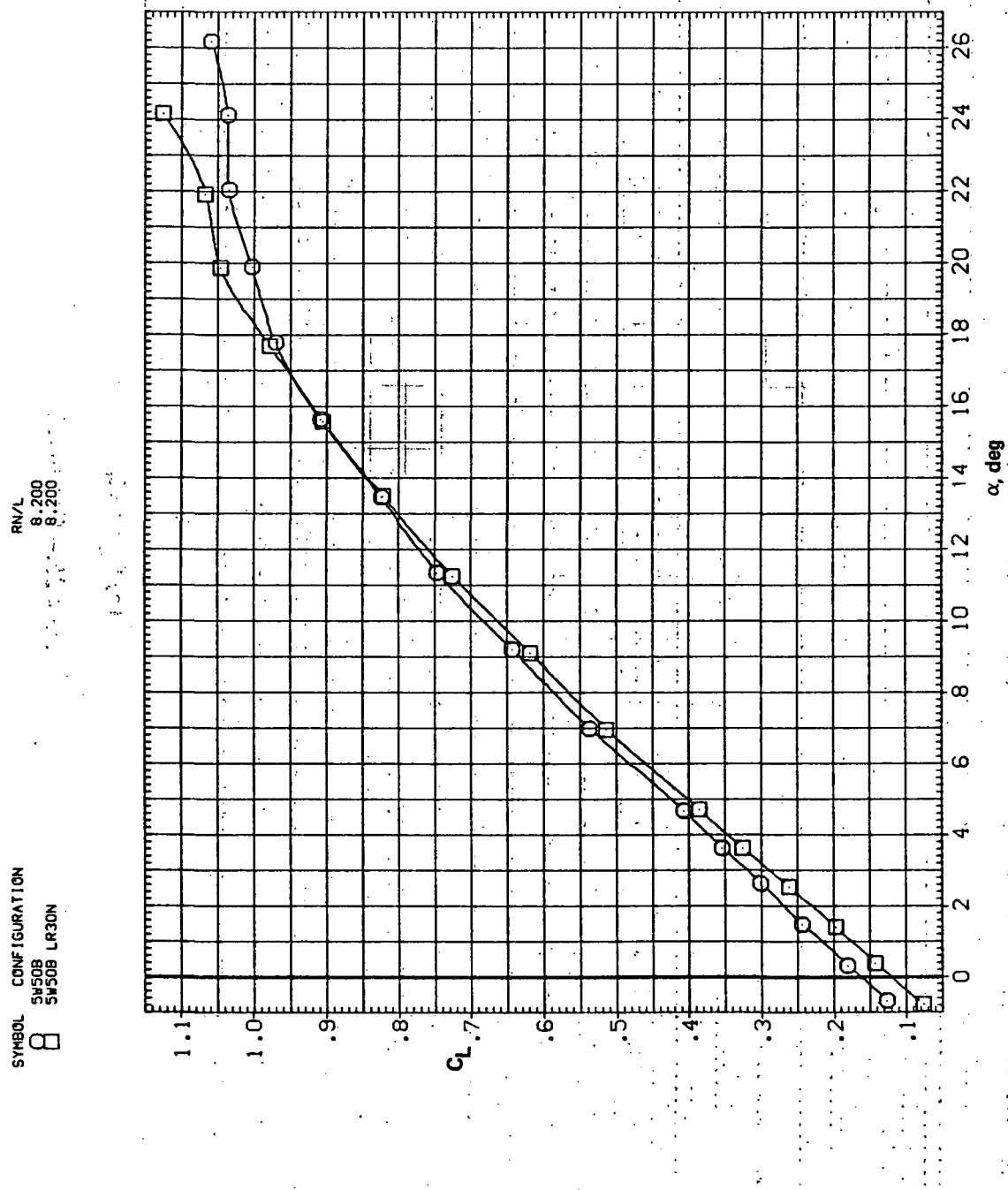
Figure 24.—Continued.

SYMBOL CONFIGURATION  
□ SW508 SW308 LR30N



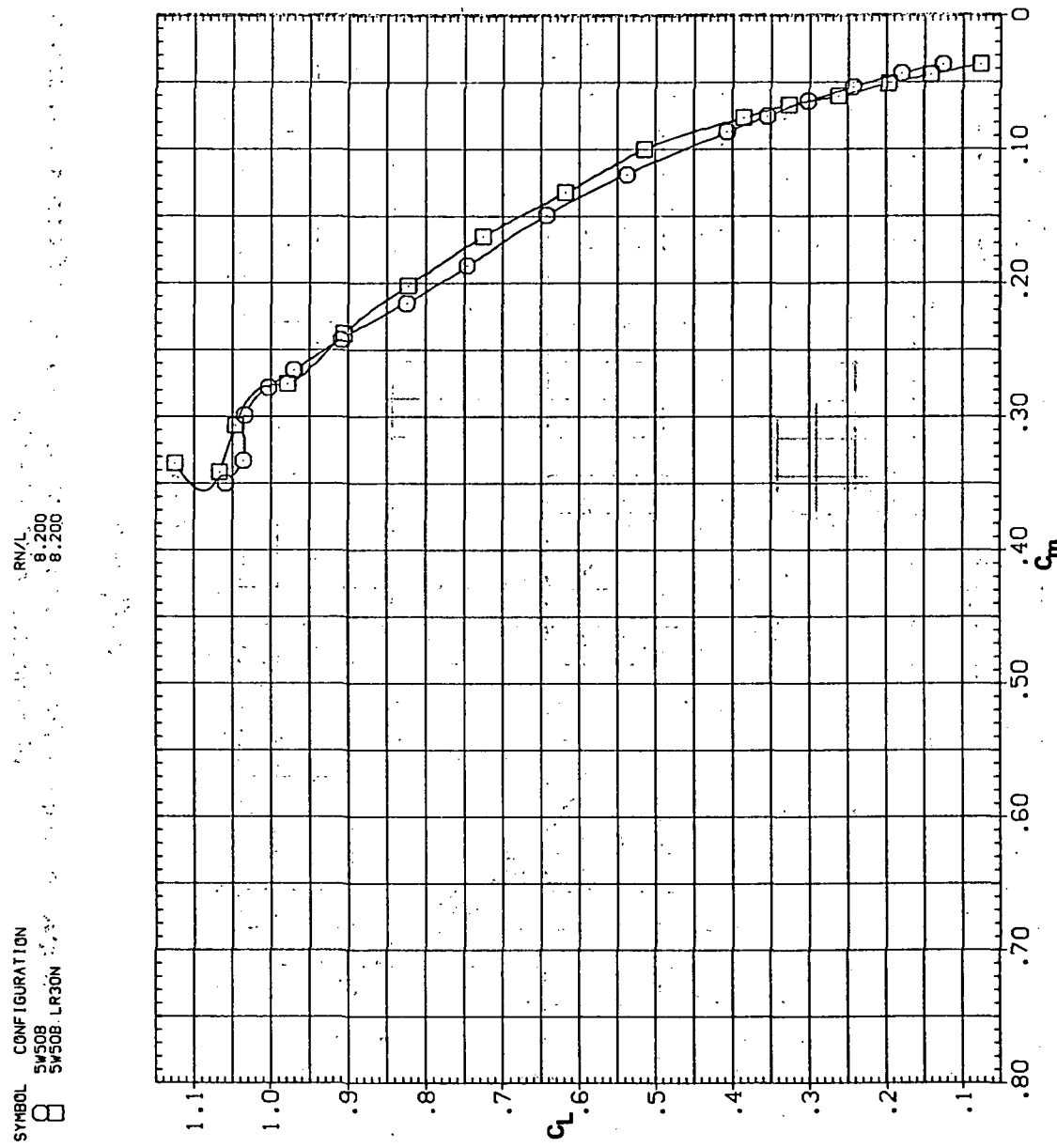
(e)  $C_L$ ,  $C_D$ , and  $C_Y$  vs  $C_L$

Figure 24.—Concluded.



(a)  $C_L$  vs  $\alpha$

Figure 25.—Effect of drooped-nose flaps on the static longitudinal characteristics of the oblique wing: flaps on both wing panels,  $\Lambda = 50^\circ$ ,  $M = 0.8$ .



(b)  $C_L$  vs  $C_m$

Figure 25.—Continued.

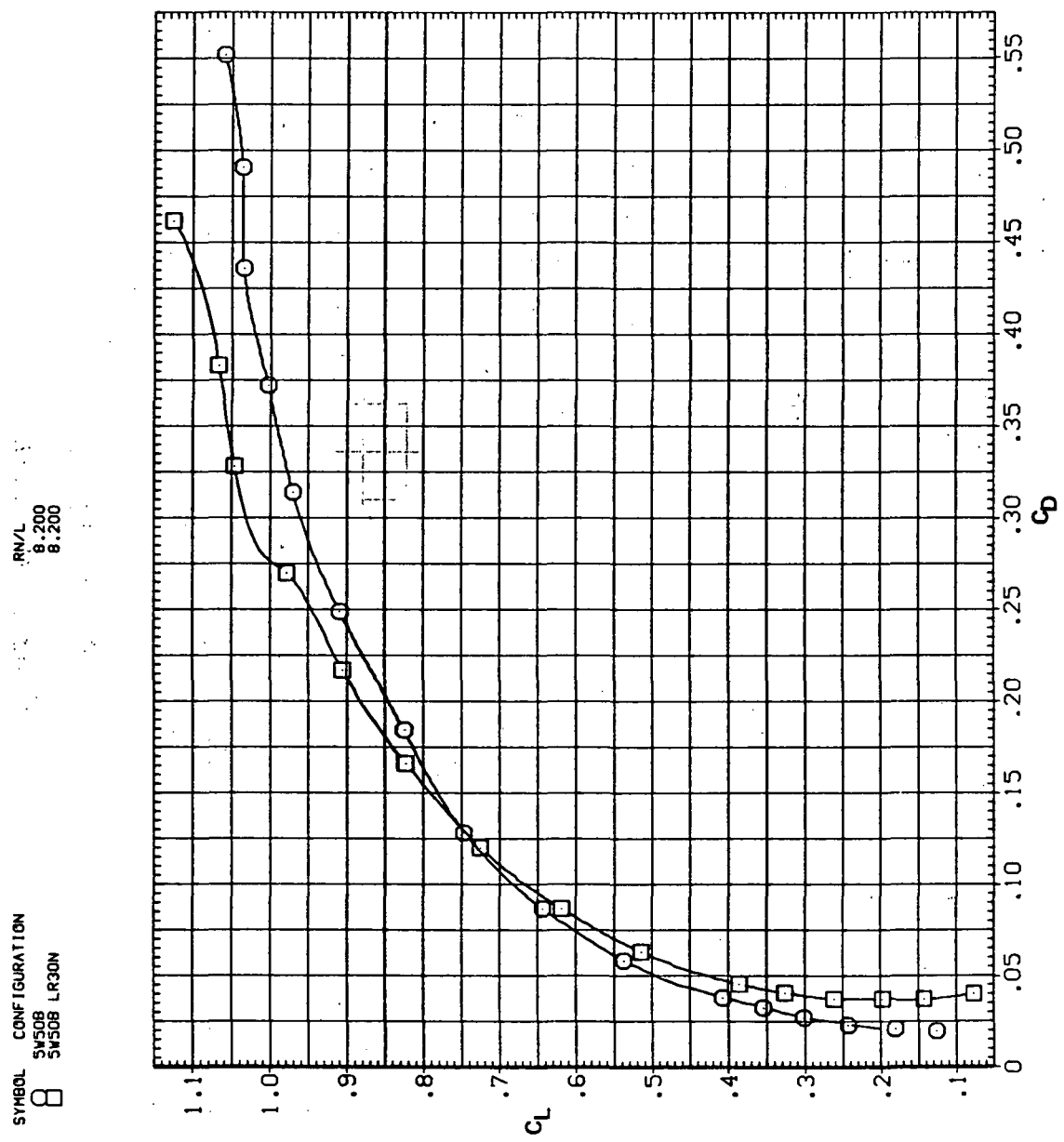
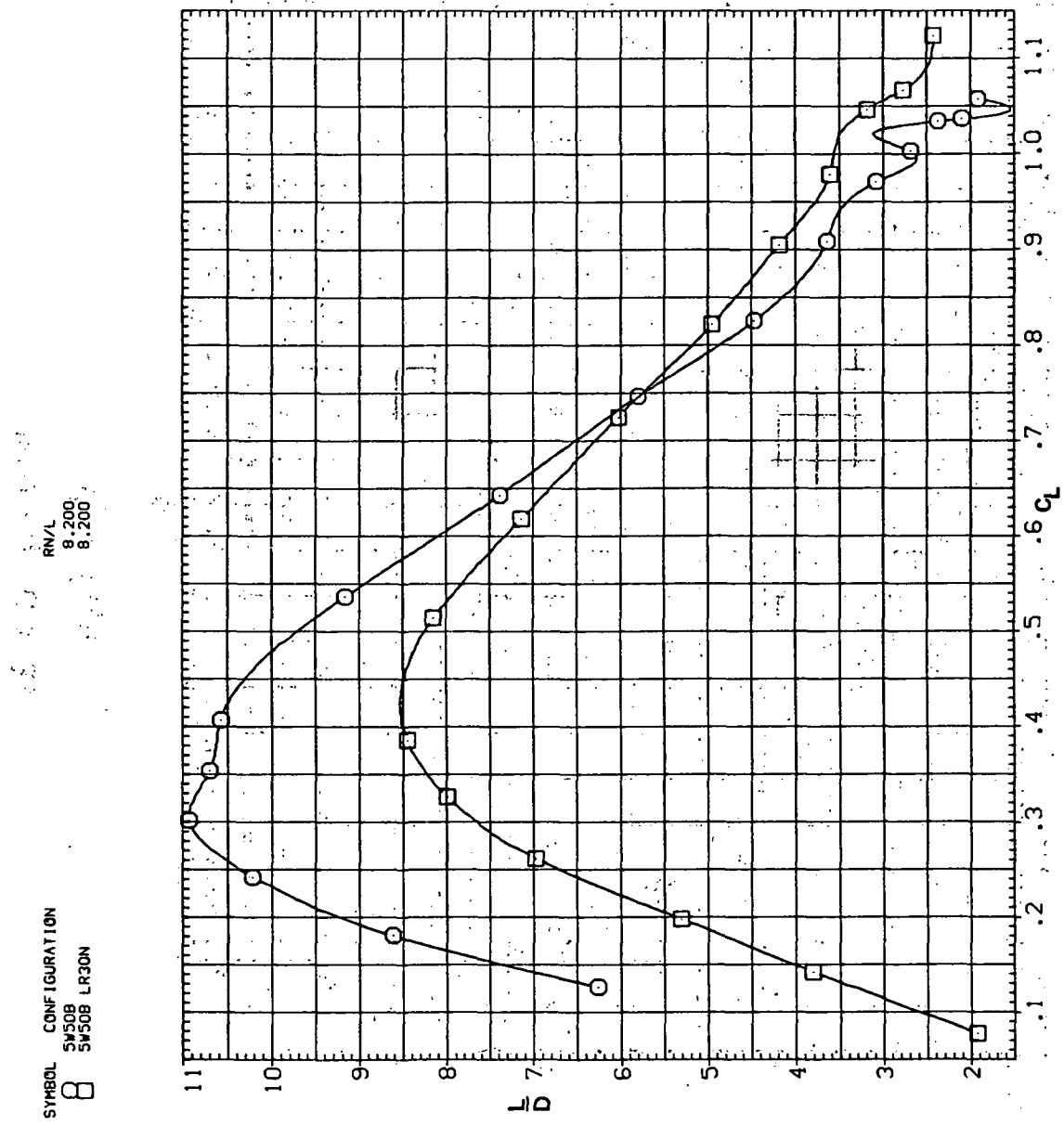


Figure 25.—Continued.



(d)  $L/D$  vs.  $C_L$

Figure 25.—Continued.

SYMBOL CONFIGURATION  
 SW50B SW50B LR30N

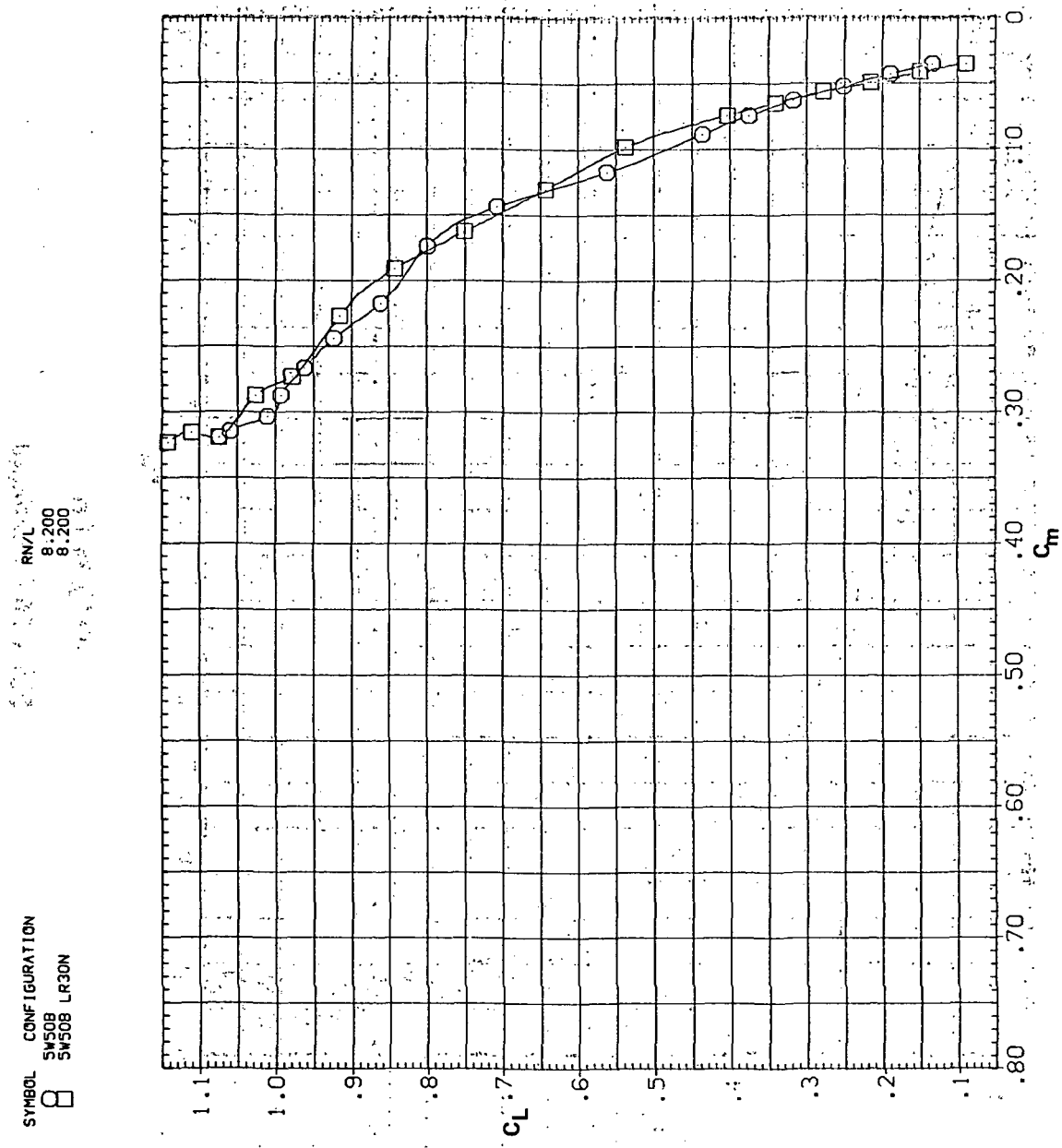
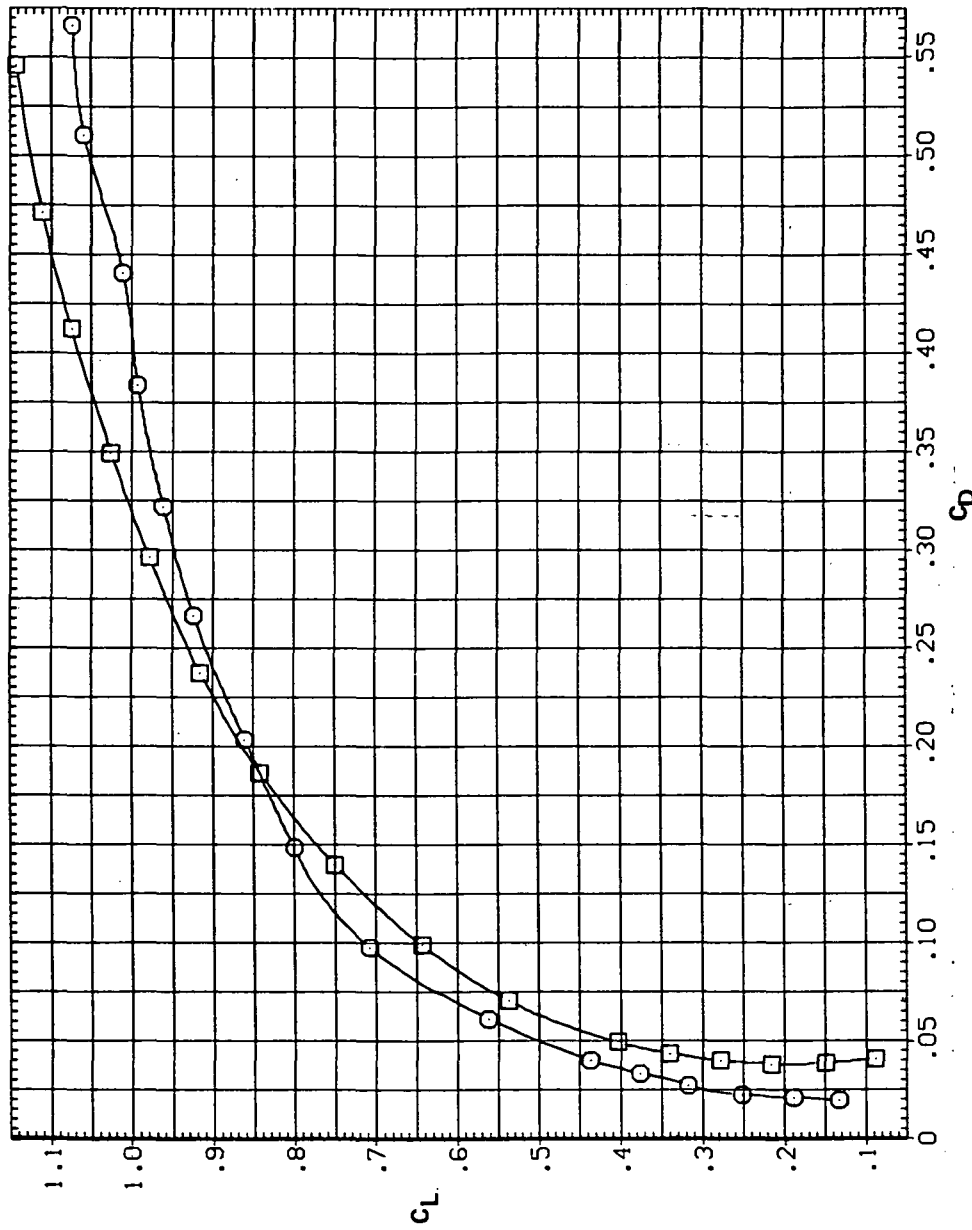
(b)  $C_L$  vs  $C_m$ 

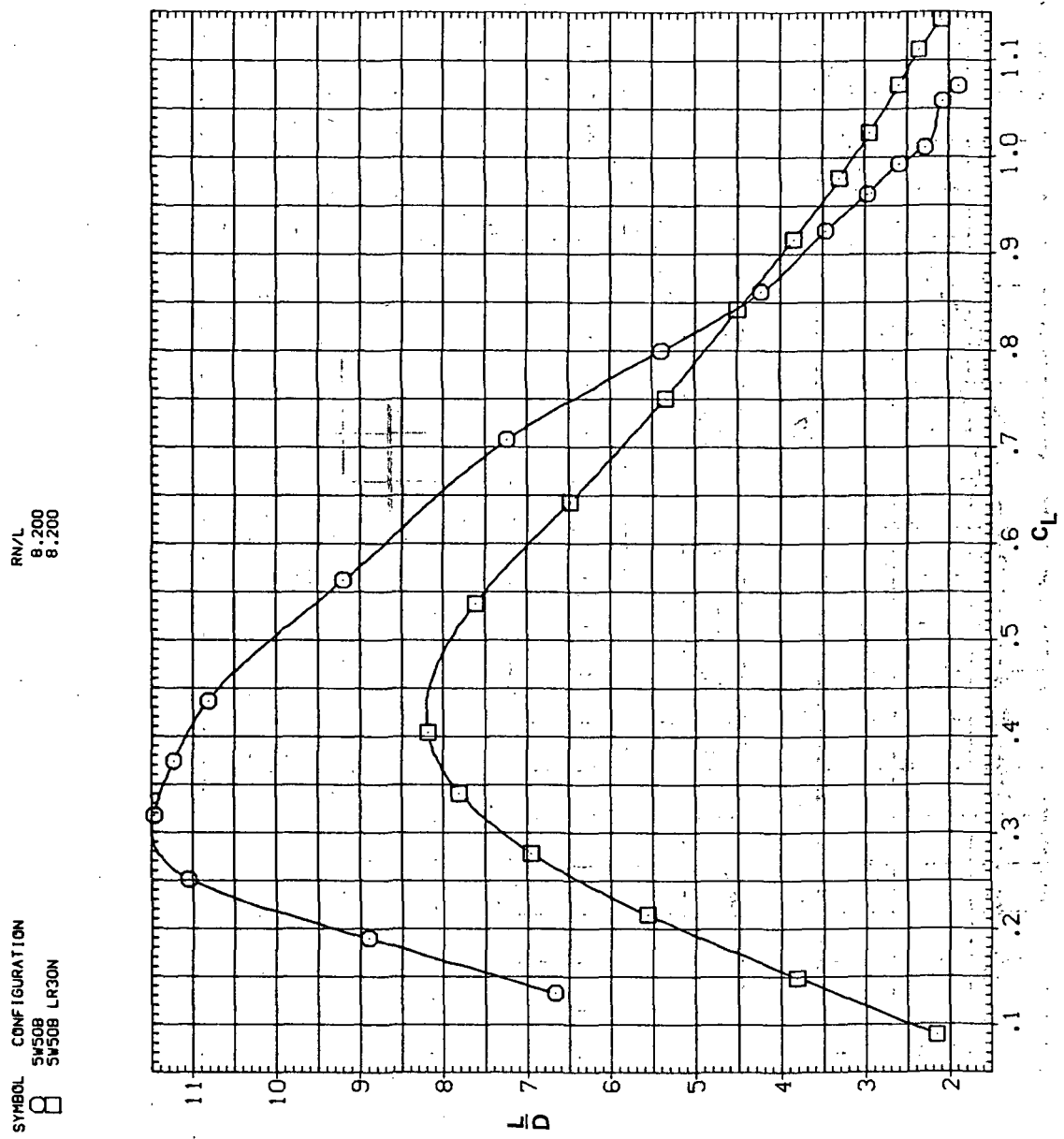
Figure 26.—Continued.

SYMBOL CONFIGURATION  
□ SW508  
○ SW508 LR30N



(c)  $C_L$  vs  $C_D$

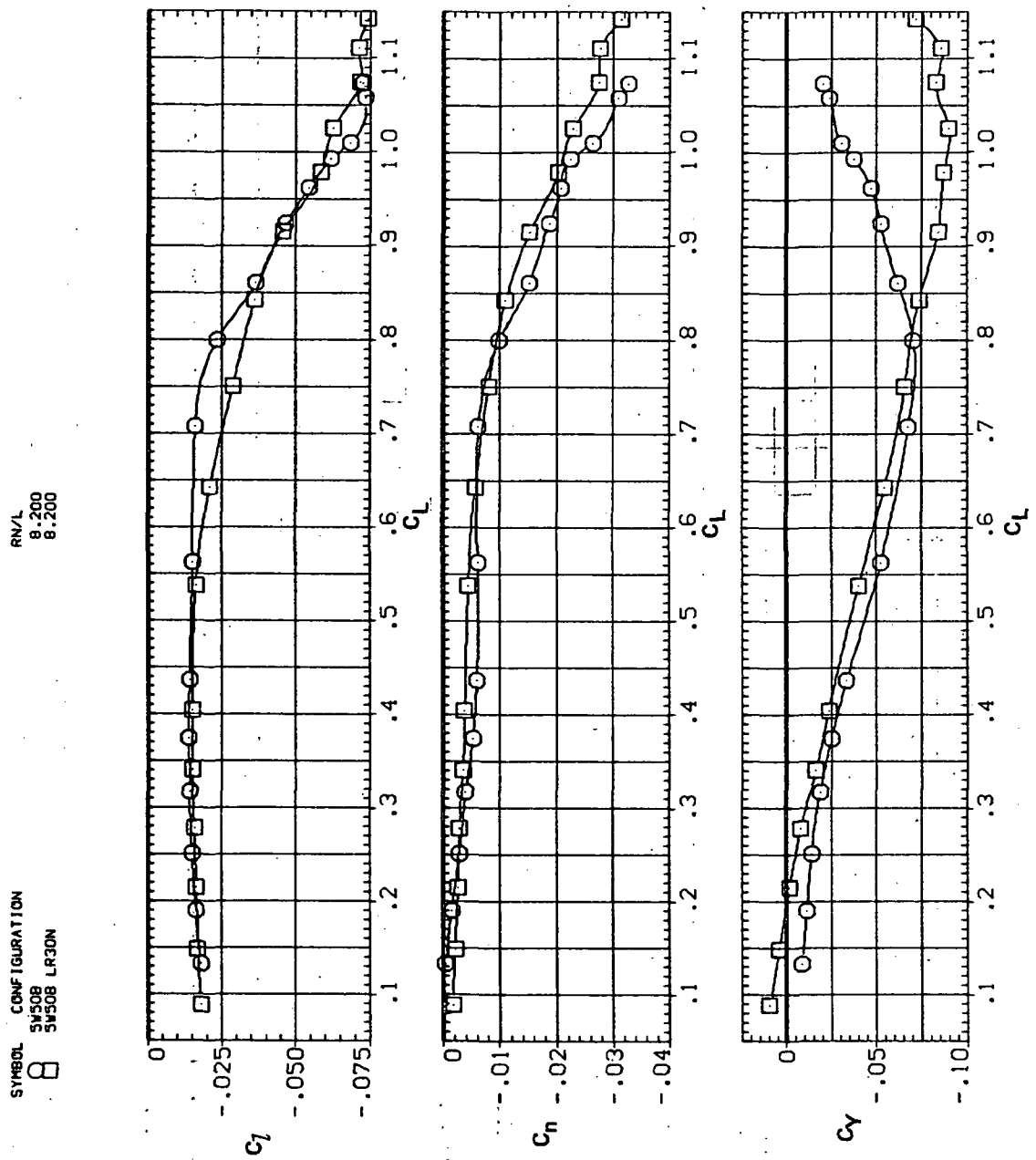
Figure 26.—Continued.



(d)  $L/D$  vs  $C_L$

Figure 26.—Continued.

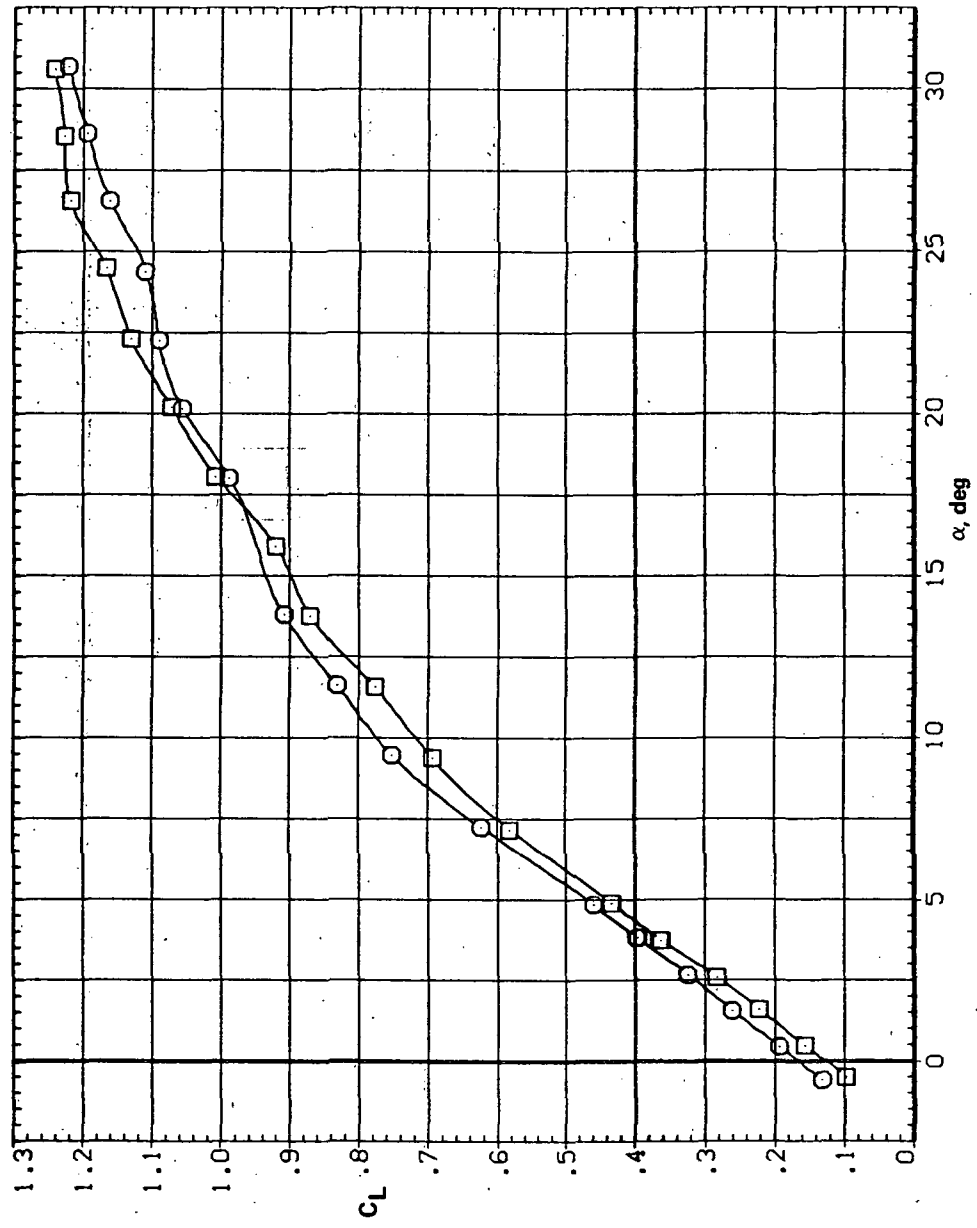
SYMBOL CONFIGURATION  
□ SV508  
○ SV508 LR30N



(e)  $C_q$ ,  $C_n$ , and  $C_y$  vs  $C_L$

Figure 26.— Concluded.

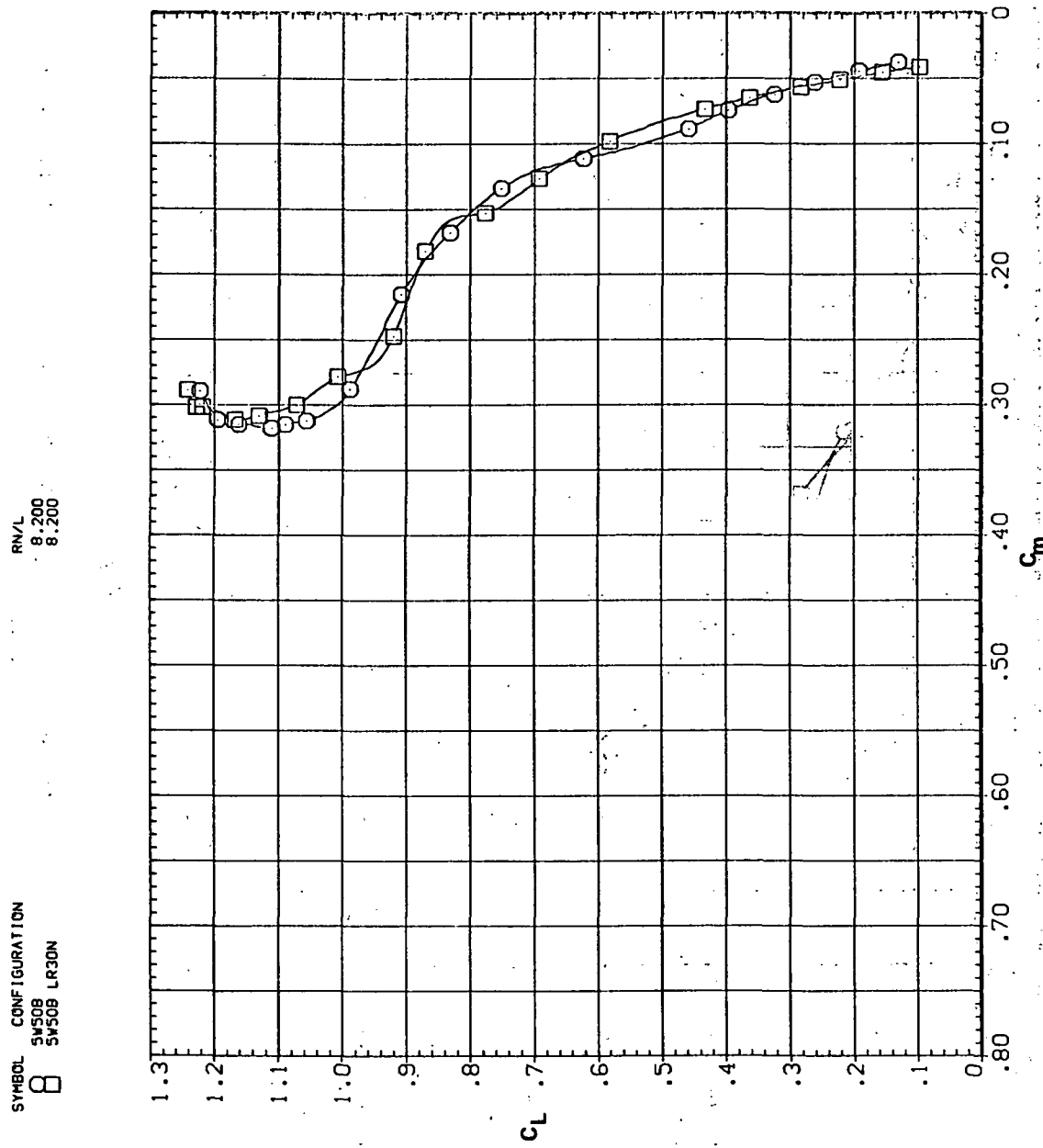
SYMBOL CONFIGURATION  
□ SW50B  
○ SW50B LR30N  
■ RN/L  
 8.200  
 8.200



(a)  $C_L$  vs  $\alpha$

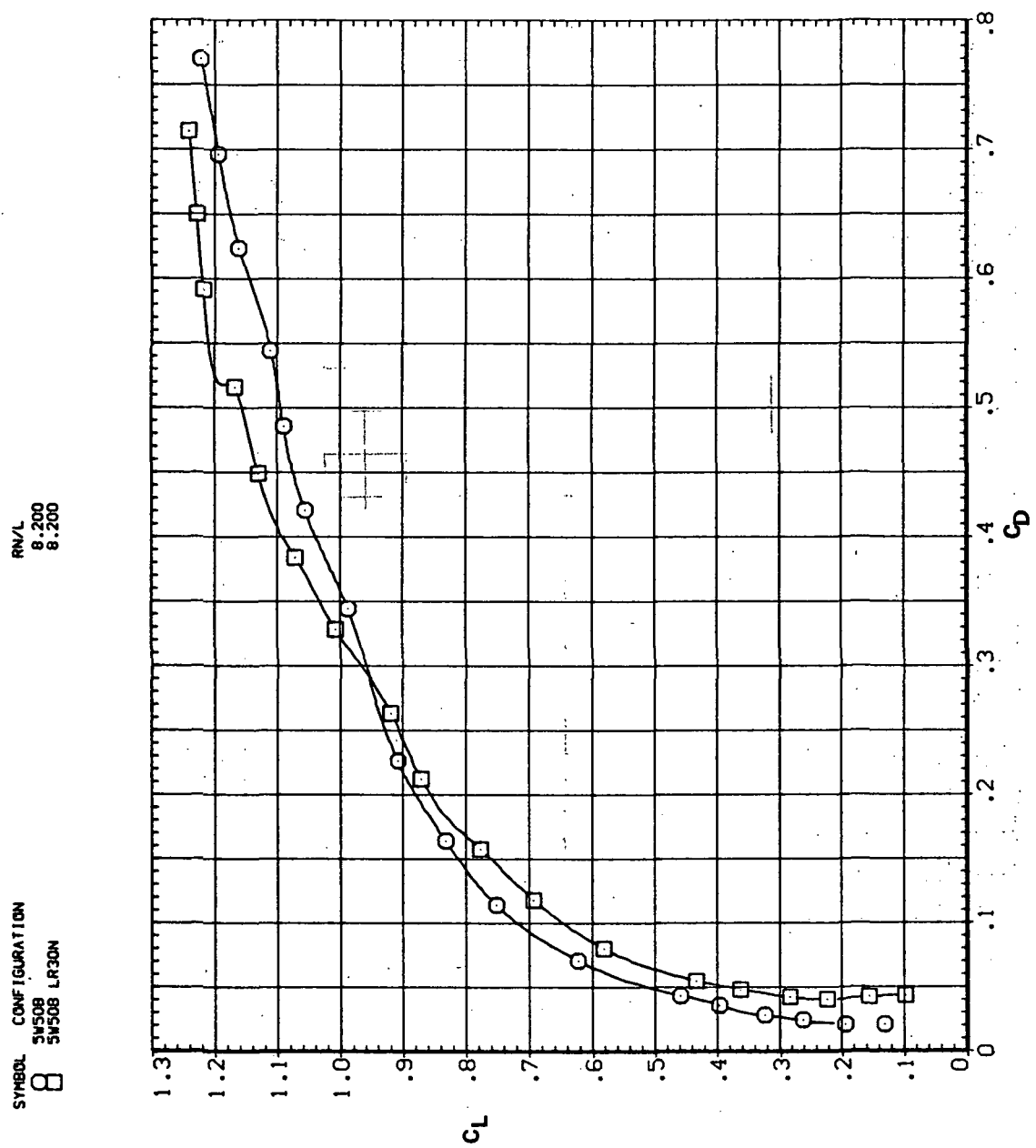
Figure 27.—Effect of drooped-nose flaps on the static longitudinal characteristics of the oblique wing: flaps on both wing panels,  $\Lambda = 50^\circ$ ,  $M = 0.95$ .

SYMBOL CONFIGURATION  
□ SW508 SW508 LR30N



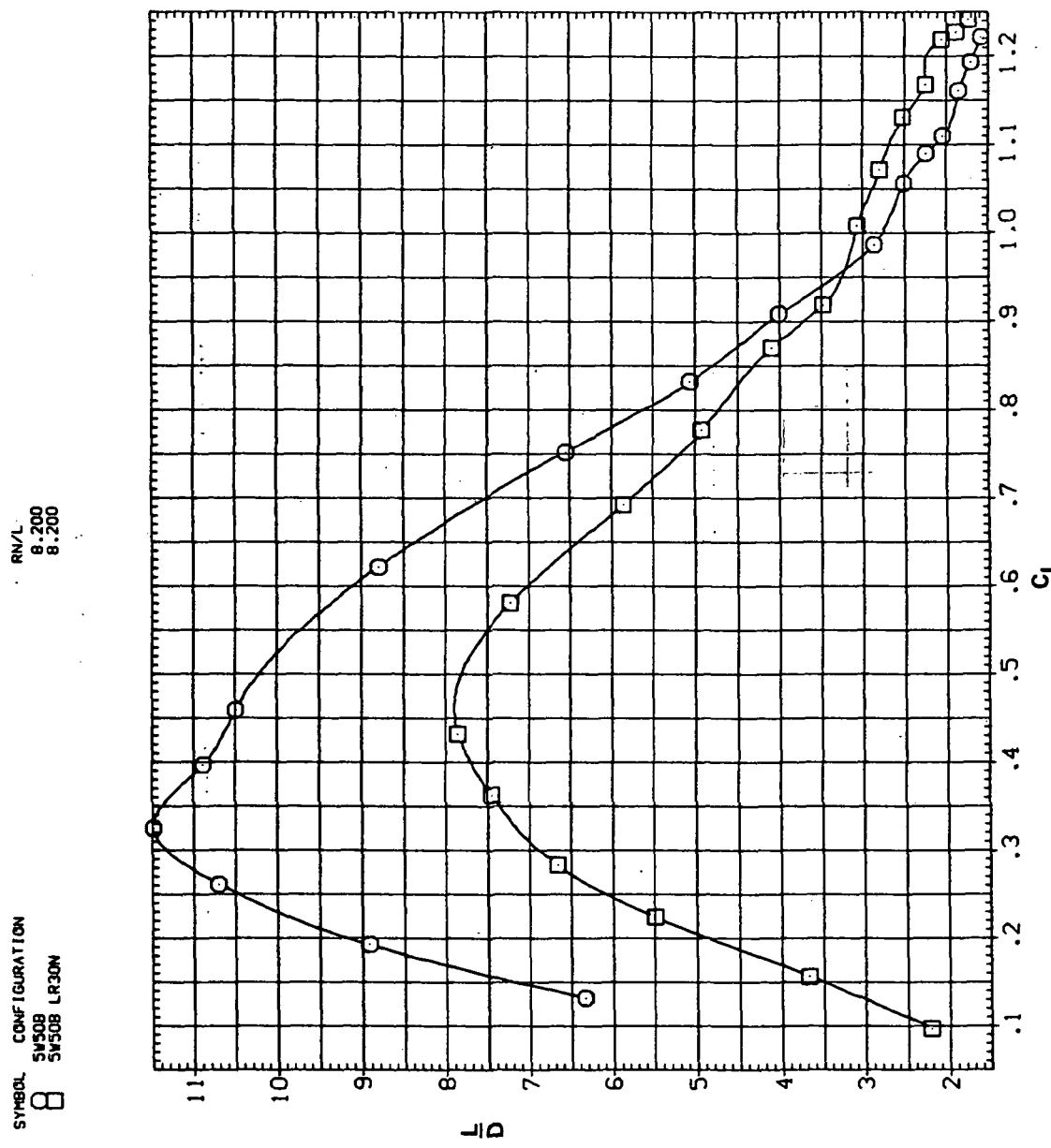
(b)  $C_L$  vs  $C_m$

Figure 27.—Continued.



(c)  $C_L$  vs  $C_D$

Figure 27.—Continued.

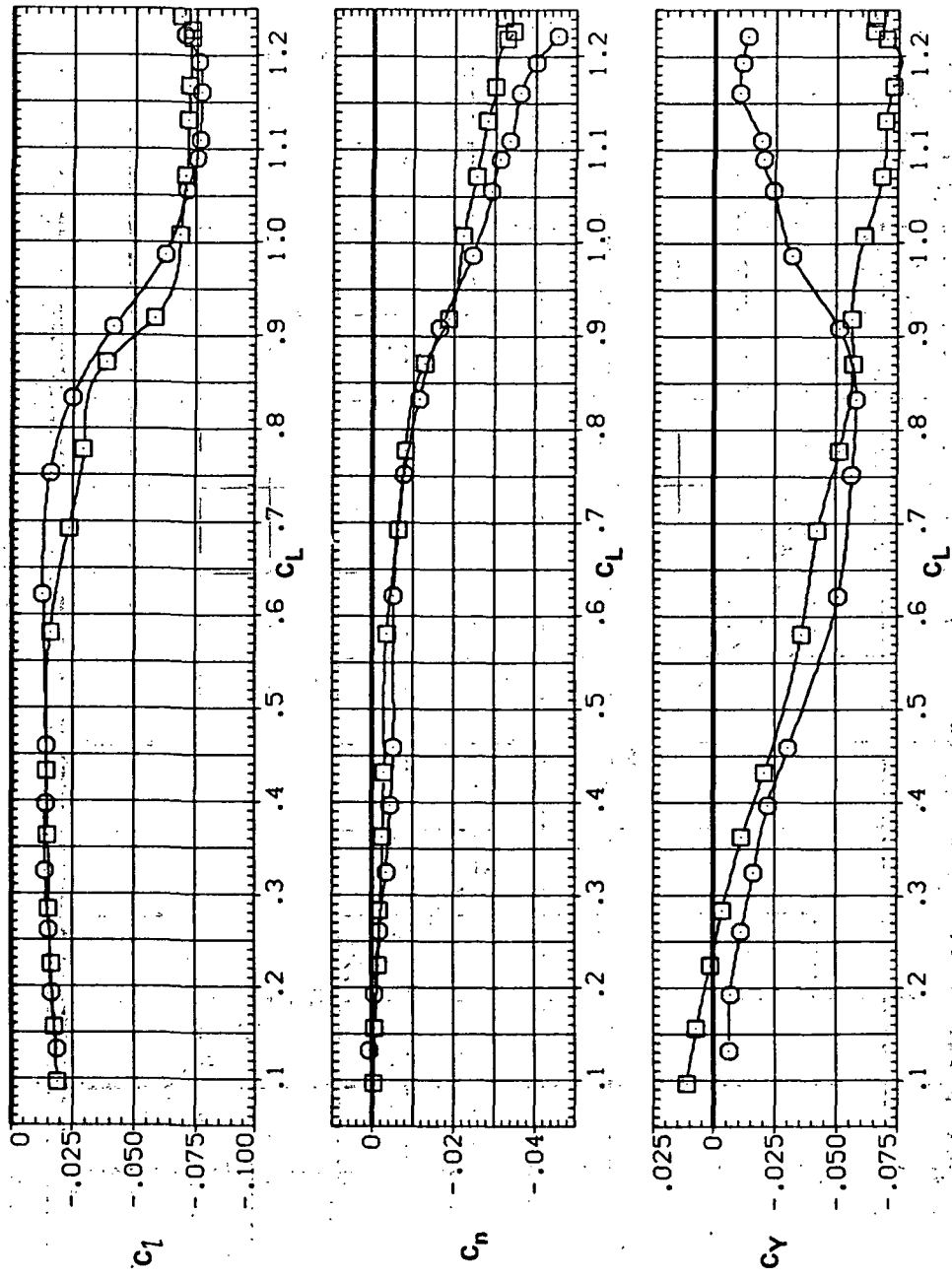


(d)  $L/D$  vs  $C_L$

Figure 27.—Continued.

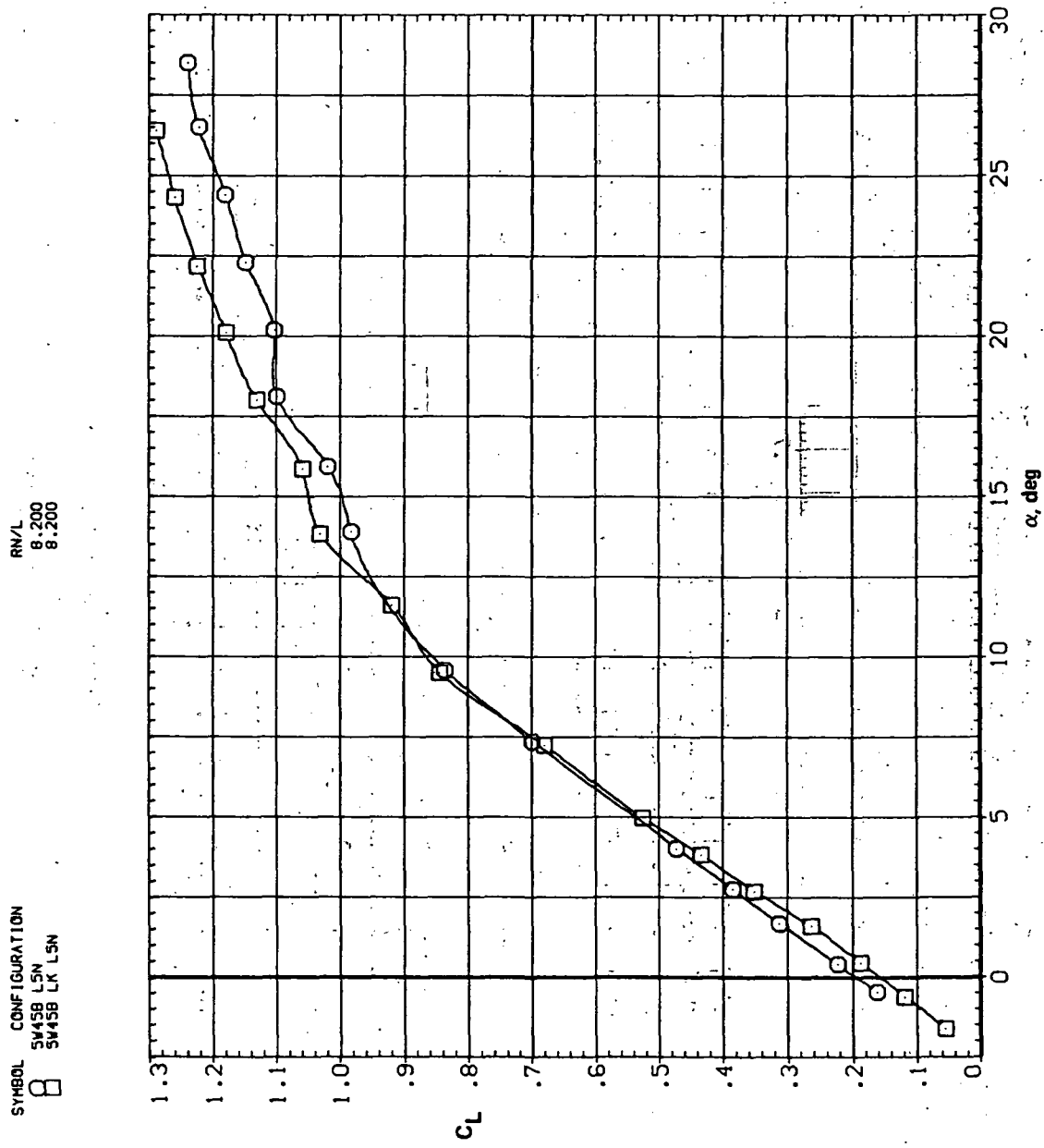
SYMBOL: CONFIGURATION: 8  
S1508 S1508 LR30N

R/N/L: 8.200



(e)  $C_l$ ,  $C_n$ , and  $C_Y$  vs  $C_L$

Figure 27.—Concluded.

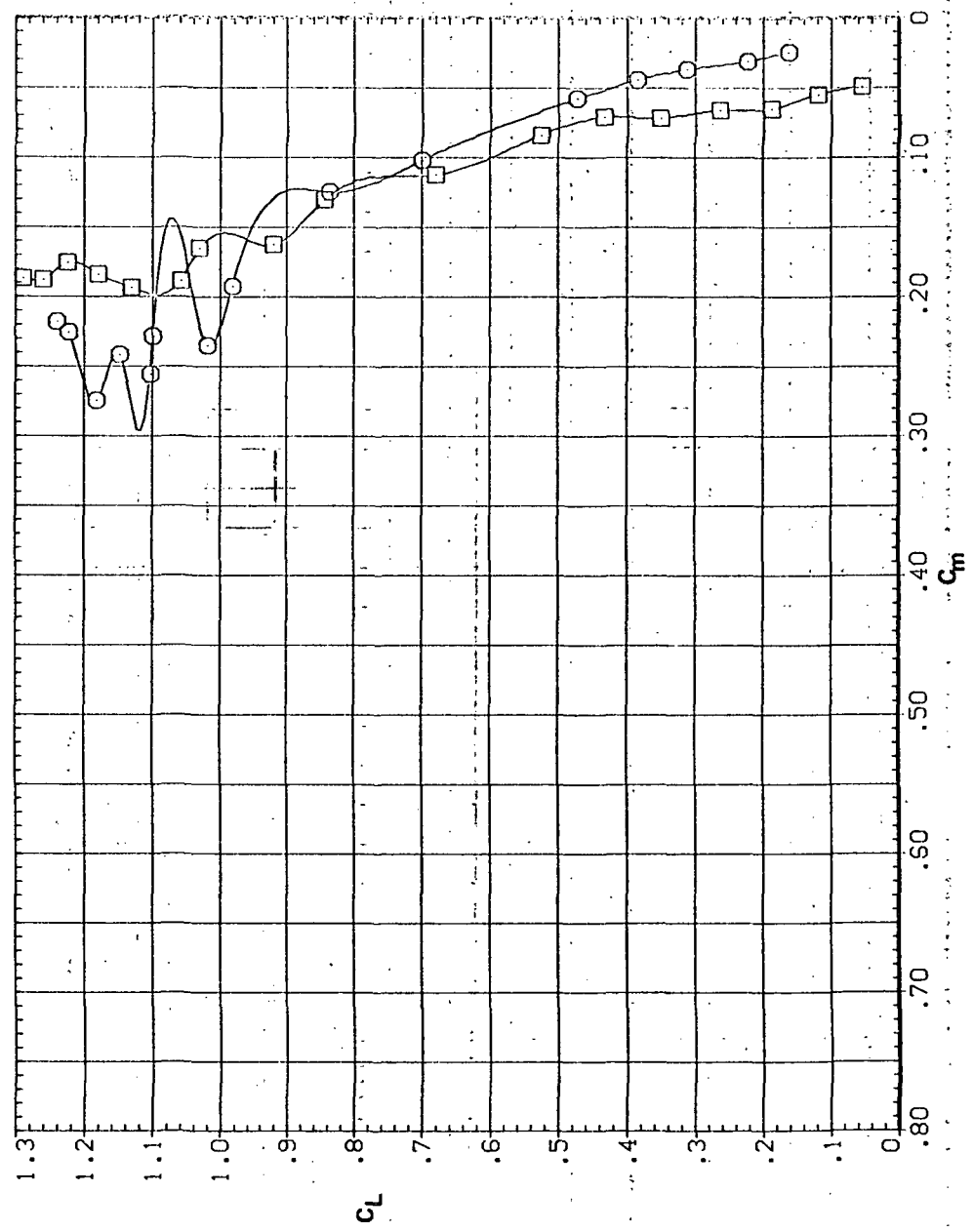


(a)  $C_L$  vs  $\alpha$

Figure 28.— Effect of Krüger-nose flaps on the static longitudinal characteristics of the oblique wing equipped with drooped-nose flaps: flaps on downstream wing panel only,  $\Lambda = 45^\circ$ ,  $M = 0.95$ .

SYMBOL CONFIGURATION  
□ SW45B L5N  
□ SW45B LK L5N

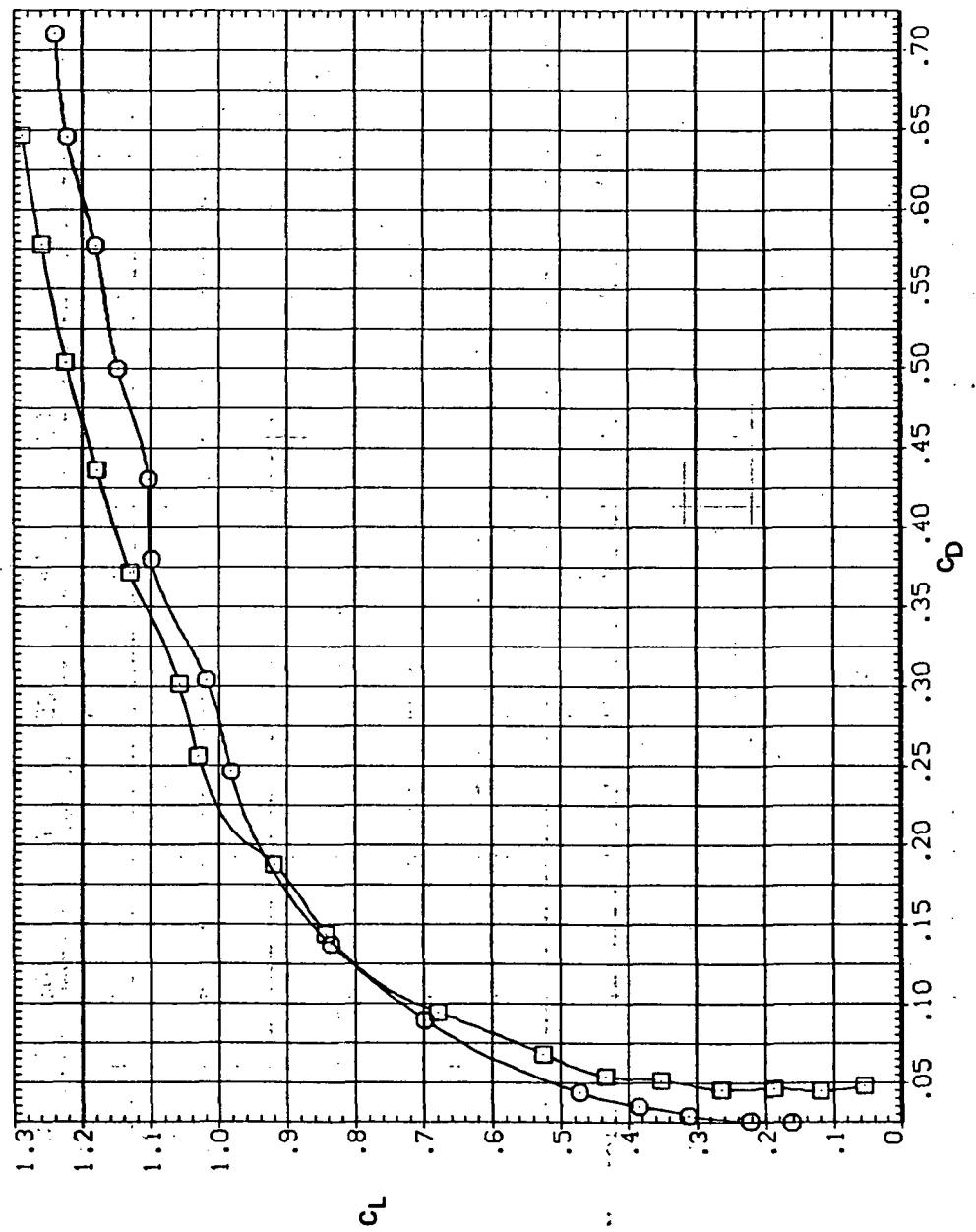
RN/L  
 8.200  
 8.200



(b)  $C_L$  vs  $C_m$

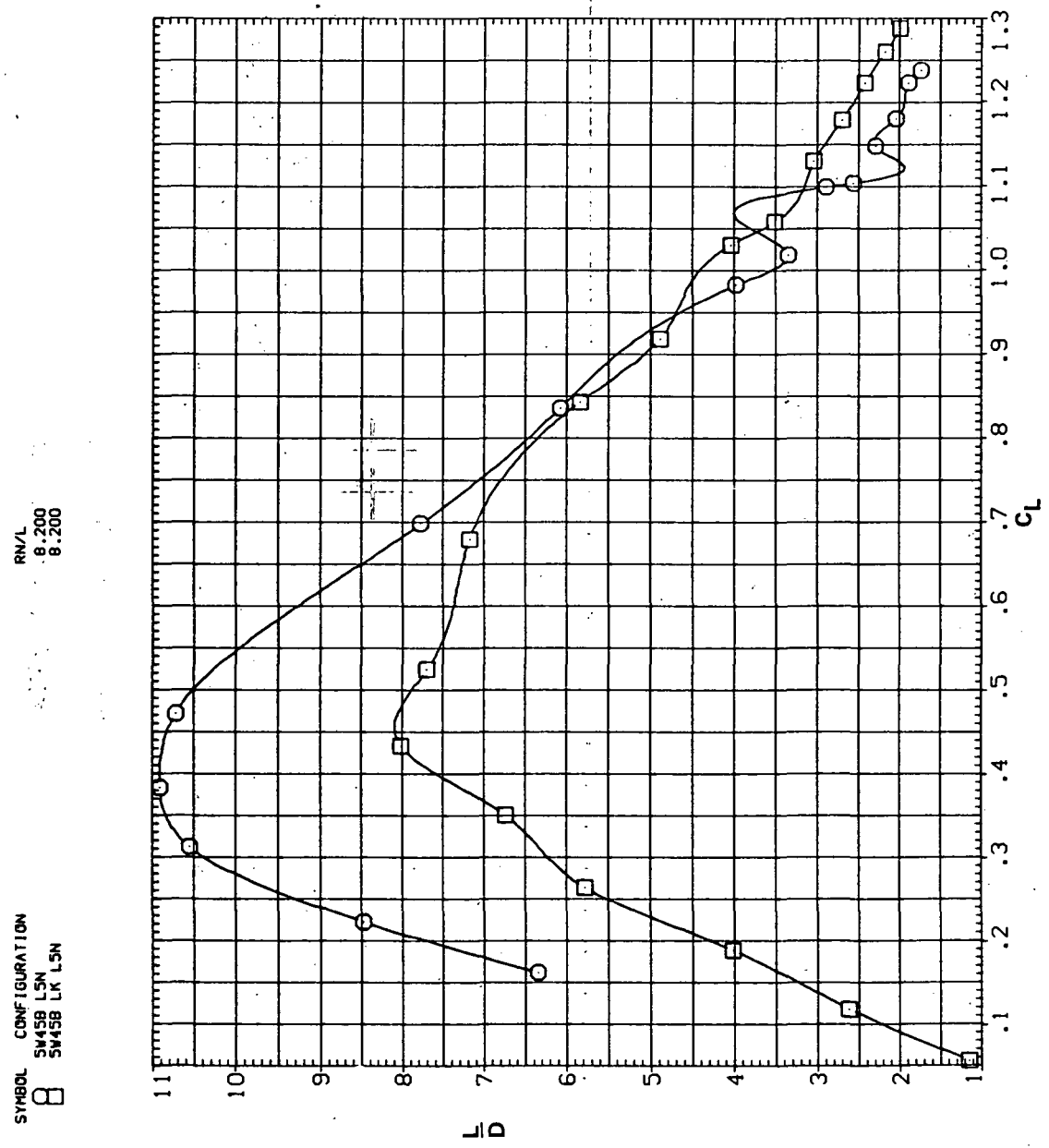
Figure 28.—Continued.

SYMBOL CONFIGURATION  
○ SW458 LSN  
□ SW458 LK LSN



(c)  $C_L$  vs  $C_D$

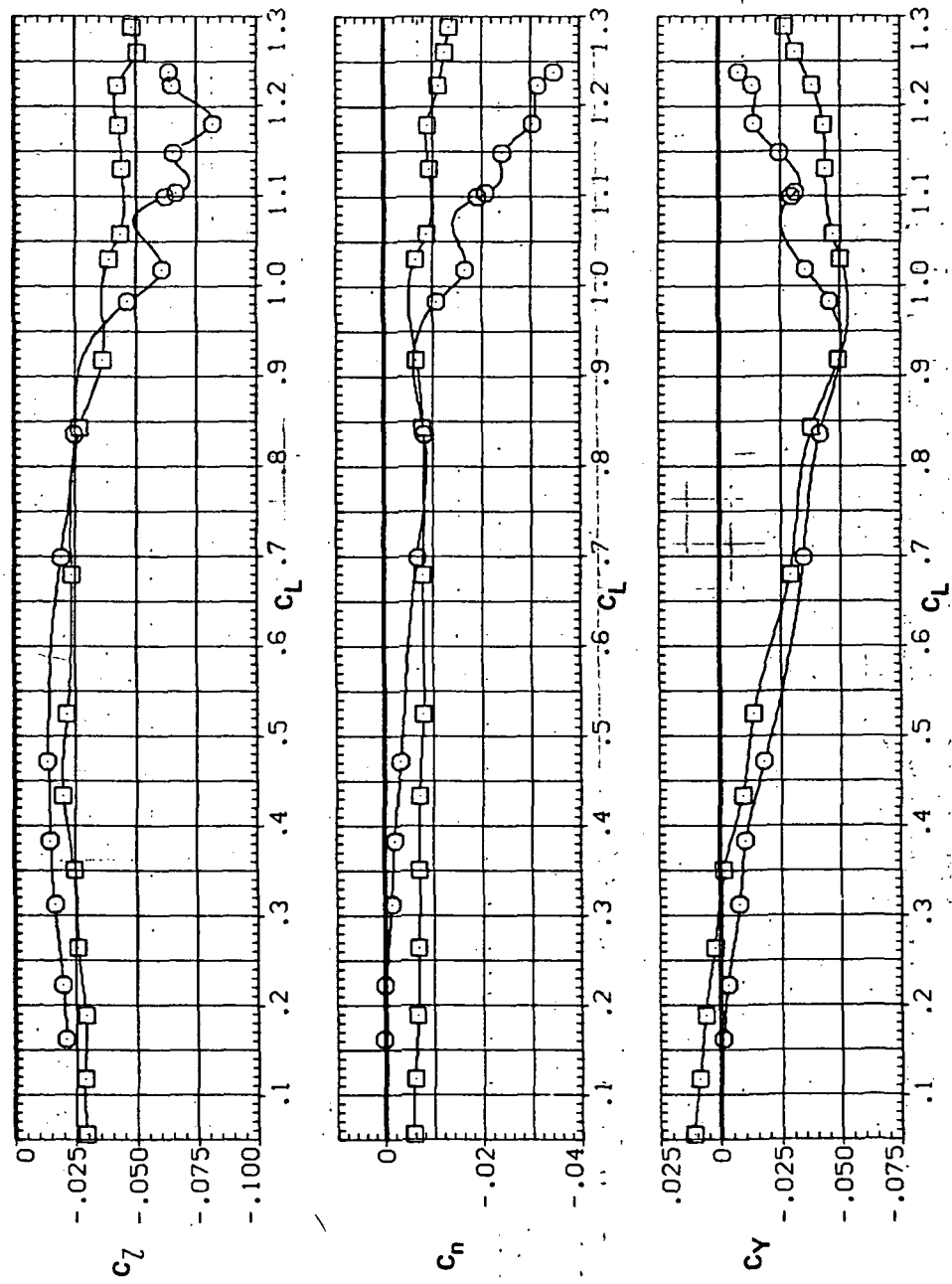
Figure 28.—Continued.



(d)  $L/D$  vs  $C_L$

Figure 28.—Continued.

SYMBOL CONFIGURATION  
 RNL  
 SW58 LSN  
 SW458 LK LSN



\*U.S. GOVERNMENT PRINTING OFFICE: 1976 - 735-004/3

(e)  $C_L$ ,  $C_n$ , and  $C_Y$  vs  $C_L$

Figure 28.—Concluded.

NATIONAL AERONAUTICS AND SPACE ADMINISTRATION  
WASHINGTON, D.C. 20546

OFFICIAL BUSINESS  
PENALTY FOR PRIVATE USE \$300

**SPECIAL FOURTH-CLASS RATE  
BOOK**

POSTAGE AND FEES PAID  
NATIONAL AERONAUTICS AND  
SPACE ADMINISTRATION  
451



POSTMASTER : If Undeliverable (Section 158  
Postal Manual) Do Not Return

*"The aeronautical and space activities of the United States shall be conducted so as to contribute . . . to the expansion of human knowledge of phenomena in the atmosphere and space. The Administration shall provide for the widest practicable and appropriate dissemination of information concerning its activities and the results thereof."*

—NATIONAL AERONAUTICS AND SPACE ACT OF 1958

## NASA SCIENTIFIC AND TECHNICAL PUBLICATIONS

**TECHNICAL REPORTS:** Scientific and technical information considered important, complete, and a lasting contribution to existing knowledge.

**TECHNICAL NOTES:** Information less broad in scope but nevertheless of importance as a contribution to existing knowledge.

**TECHNICAL MEMORANDUMS:** Information receiving limited distribution because of preliminary data, security classification, or other reasons. Also includes conference proceedings with either limited or unlimited distribution.

**CONTRACTOR REPORTS:** Scientific and technical information generated under a NASA contract or grant and considered an important contribution to existing knowledge.

**TECHNICAL TRANSLATIONS:** Information published in a foreign language considered to merit NASA distribution in English.

**SPECIAL PUBLICATIONS:** Information derived from or of value to NASA activities. Publications include final reports of major projects, monographs, data compilations, handbooks, sourcebooks, and special bibliographies.

**TECHNOLOGY UTILIZATION PUBLICATIONS:** Information on technology used by NASA that may be of particular interest in commercial and other non-aerospace applications. Publications include Tech Briefs, Technology Utilization Reports and Technology Surveys.

*Details on the availability of these publications may be obtained from:*

**SCIENTIFIC AND TECHNICAL INFORMATION OFFICE**

**NATIONAL AERONAUTICS AND SPACE ADMINISTRATION**

Washington, D.C. 20546